



**STRUCTURAL SYSTEMS  
RESEARCH PROJECT**

Report No.  
SSRP-2001/22

**EFFECT OF PILE DIAMETER ON  
THE MODULUS OF SUB-GRADE  
REACTION**

by

**TEERAWUT JUIRNARONGRIT  
SCOTT A. ASHFORD**

Final Report Submitted to Caltrans under Contract No. 59A0051

May 2005

Department of Structural Engineering  
University of California, San Diego  
La Jolla, California 92093-0085

University of California, San Diego  
Department of Structural Engineering  
Structural Systems Research Project

Report No. SSRR-2001/22

## **Effect of Pile Diameter on the Modulus of Sub-Grade Reaction**

by

**Teerawut Juirnarongrit**

*Graduate Student Researcher*

**Scott A. Ashford**

*Assistant Professor of Geotechnical Engineering*

Final Report Submitted to Caltrans under Contract No. 59A0051

Department of Structural Engineering  
University of California, San Diego  
La Jolla, California 92093-0085

May 2005

THIS PAGE LEFT BLANK

1. Report No. SSRP-2001/22		2. Government Accession No.		3. Recipient's Catalog No.	
4. Title and Subtitle Effect of Pile Diameter on the Modulus of Subgrade Reaction				5. Report Date December 2001	
				6. Performing Organization Code	
7. Author(s) Teerawut Juirnarongrit and Scott A. Ashford				8. Performing Organization Report No. UCSD / SSRP-2001/22	
9. Performing Organization Name and Address Department of Structural Engineering School of Engineering University of California, San Diego La Jolla, California 92093-0085				10. Work Unit No. (TRAIS)	
				11. Contract or Grant No. 59A0051	
12. Sponsoring Agency Name and Address California Department of Transportation Engineering Service Center 1801 30 <sup>th</sup> St., West Building MS-9 Sacramento, California 95807				13. Type of Report and Period Covered Final Report -	
				14. Sponsoring Agency Code	
15. Supplementary Notes Prepared in cooperation with the State of California Department of Transportation.					
16. Abstract  <p>Integral pile shaft-columns have been increasingly used for bridge foundations in California because of the economical construction of large diameter Cast-In-Drilled-Hole (CIDH) piles. The current design method of piles against lateral loading involves the use of Winkler's spring concept with the standard nonlinear p-y curves. However, the accuracy of using these p-y curves for large pile diameters is questionable because they were developed based on relatively small pile diameters. This research study focused on an evaluation of the pile diameter effect on p-y curves through analytical and experimental programs. Furthermore, an assessment of inelastic performance of CIDH piles under cyclic loading was conducted.</p> <p>Instrumented CIDH piles with diameters ranging from 0.4 m to 1.2 m were installed in dense weakly cemented sand, and both vibration tests and lateral load tests were carried out. Data from the tests for each pile diameter were used to back-calculate p-y curves. It was found that the pile diameter has insignificant effect on the p-y curves at the displacement level below the ultimate soil resistance. Beyond this range, the ultimate soil resistance increases as the pile diameter increases. Based on the characteristics of back-calculated p-y curves, a methodology to develop p-y curves for weakly cemented sand is proposed.</p> <p>Using the standard p-y curves currently available in the literature underestimates the soil resistance in weakly cemented sand for small diameter piles, but tends to overestimate the soil resistance to large diameter piles. Therefore, the use of these standard p-y curves for large diameter piles in weakly cemented sand should be used with caution.</p> <p>Finally, results from the cyclic lateral pile load tests show that even low to medium levels of transverse reinforcement (0.6%) can provide adequate seismic performance due to the effect of soil confinement retarding the concrete spalling.</p>					
17. Key Words			18. Distribution Statement Unlimited		
19. Security Classification (of this report) Unclassified		20. Security Classification (of this page) Unclassified		21. No. of Pages	22. Price

THIS PAGE LEFT BLANK

## **DISCLAIMER**

The opinions, recommendations and conclusions contained within this report are solely those of the authors, and do not necessarily reflect the views of the California Department of Transportation.

THIS PAGE LEFT BLANK

## **ACKNOWLEDGMENTS**

The research described in this report was funded by the California Department of Transportation (CALTRANS) under contract number 59A0051. Special thanks are due to Anderson Drilling Company, for the donation of their services for installation of CIDH piles. Their support is gratefully acknowledged.

THIS PAGE LEFT BLANK

## ABSTRACT

Integral pile shaft-columns have been increasingly used for bridge foundations in California because of the economical construction of large diameter Cast-In-Drilled-Hole (CIDH) piles. The current design method of piles against lateral loading involves the use of Winkler's spring concept with the standard nonlinear p-y curves. However, the accuracy of using these p-y curves for large pile diameters is questionable because they were developed based on relatively small pile diameters. This research study focused on an evaluation of the pile diameter effect on p-y curves through analytical and experimental programs. Furthermore, an assessment of inelastic performance of CIDH piles under cyclic loading was conducted.

Instrumented CIDH piles with diameters ranging from 0.4 m to 1.2 m were installed in dense weakly cemented sand, and both vibration tests and lateral load tests were carried out. Data from the tests for each pile diameter were used to back-calculate p-y curves. It was found that the pile diameter has insignificant effect on the p-y curves at the displacement level below the ultimate soil resistance. Beyond this range, the ultimate soil resistance increases as the pile diameter increases. Based on the characteristics of back-calculated p-y curves, a methodology to develop p-y curves for weakly cemented sand is proposed.

Using the standard p-y curves currently available in the literature underestimates the soil resistance in weakly cemented sand for small diameter piles, but tends to overestimate the soil resistance to large diameter piles. Therefore, the use of these standard p-y curves for large diameter piles in weakly cemented sand should be used with caution.

Finally, results from the cyclic lateral pile load tests show that even low to medium levels of transverse reinforcement (0.6%) can provide adequate seismic performance due to the effect of soil confinement retarding the concrete spalling.

## Table of Contents

DISCLAIMER .....	iii
ACKNOWLEDGMENTS .....	iv
ABSTRACT.....	v
Table of Contents.....	vii
List of Figures.....	xii
List of Tables .....	xxv
Chapter 1 INTRODUCTION .....	1
1.1 Objectives of Research .....	3
1.2 Organization of Report .....	4
Chapter 2 LITERATURE REVIEW .....	7
2.1 Introduction.....	7
2.2 Methods in Predicting Lateral Pile Responses.....	9
2.2.1 Elastic Continuum using Boundary Element Method .....	9
2.2.2 Modified Boundary Element Analyses.....	11
2.2.3 Finite Elements for Soil .....	12
2.2.4 Winkler Method and the Concept of $p$ - $y$ Curves .....	13
2.2.4.1 Concept of $p$ - $y$ Curves .....	16
2.2.4.2 Soft Clay $p$ - $y$ Curves.....	18
2.2.4.3 Stiff Clay $p$ - $y$ Curves below Water Table.....	18
2.2.4.4 Stiff Clay $p$ - $y$ Curves above Water Table.....	19
2.2.4.5 Sand $p$ - $y$ Curves .....	19
2.2.4.6 API Sand $p$ - $y$ Curves.....	20
2.2.4.7 $p$ - $y$ Curves for $c$ - $\phi$ Soils .....	21
2.2.4.8 Hyperbolic Soil Model.....	22
2.2.4.9 Effect of Pile Diameter on $p$ - $y$ Curves.....	23
2.2.4.10 Development of $p$ - $y$ Curves for Layered Soils .....	26
2.2.5 Other Methods .....	27

2.2.5.1	Equivalent Cantilever Approach.....	27
2.2.5.2	Strain Wedge Approach.....	29
2.3	Full-Scale Pile Testing on Single Piles.....	31
2.4	Inelastic Behavior of Concrete Piles.....	34
2.5	Typical Behavior of Cemented Soil.....	34
Chapter 3 EVALUATION OF PILE DIAMETER EFFECT USING 3-D FINITE		
ELEMENT METHOD.....		
3.1	Description of Finite Element Model .....	67
3.2	Linear Elastic Soil Model .....	68
3.3	Elasto-Plastic Soil Model.....	72
3.4	Limitation of 3-D Finite Element Model .....	74
3.5	Summary .....	74
Chapter 4 FULL-SCALE TESTING.....		
4.1	Site Description.....	87
4.2	Description of Test Piles.....	90
4.2.1	Pile Geometry and Section Reinforcement Details .....	90
4.2.2	Instrumentation of Test Piles .....	92
4.3	Vibration Testing .....	94
4.3.1	Description of Instrumentation .....	94
4.3.1.1	Accelerometers .....	94
4.3.1.2	Modal Hammer PCB 086 C50.....	95
4.3.1.3	Mass Shaker .....	95
4.3.1.4	Recording and Data Processing Instruments .....	96
4.3.2	Testing Procedure .....	97
4.3.2.1	Ambient Vibration Test .....	97
4.3.2.2	Impact Vibration Test .....	97
4.3.2.3	Forced Vibration Test .....	98
4.3.3	Testing Program.....	98
4.4	Lateral Load Testing.....	98

4.4.1	Test Setup.....	99
4.4.2	Data Acquisition System.....	99
4.4.3	Testing Program and Testing Procedure.....	100
4.4.3.1	Lateral Load Test 1 .....	101
4.4.3.2	Lateral Load Test 2 .....	102
4.4.3.3	Lateral Load Test 3 .....	103
4.4.3.4	Lateral Load Test 4 .....	103
4.5	Summary .....	104
Chapter 5	TEST RESULTS.....	141
5.1	Vibration Testing .....	141
5.1.1	Natural Frequency.....	141
5.1.1.1	Ambient Vibration Test .....	141
5.1.1.2	Impact Vibration Test .....	142
5.1.1.3	Forced Vibration Test .....	143
5.1.2	Damping Ratio .....	145
5.1.2.1	Impact Vibration Test .....	145
5.1.2.2	Forced Vibration Test .....	145
5.1.3	Mode Shape .....	146
5.2	Lateral Load Testing.....	147
5.2.1	Lateral Load Test No. 1 .....	147
5.2.1.1	Load-Displacement Curves.....	147
5.2.1.2	Longitudinal Strain Gauge Data .....	148
5.2.1.3	Transverse Strain Gauge Data .....	149
5.2.1.4	Observed Pile Performance.....	149
5.2.2	Lateral Load Test No. 2 .....	150
5.2.2.1	Load-Displacement Curves.....	150
5.2.2.2	Longitudinal Strain Gauge Data .....	150
5.2.2.3	Observed Pile Performance.....	150
5.2.3	Lateral Load Test No. 3 .....	151

5.2.3.1	Load-Displacement Curves.....	151
5.2.3.2	Longitudinal Strain Gauge Data .....	151
5.2.3.3	Observed Pile Performance.....	151
5.2.4	Lateral Load Test No. 4 .....	152
5.2.4.1	Load-Displacement Curves.....	152
5.2.4.2	Longitudinal Strain Gauge Data .....	152
5.2.4.3	Observed Pile Performance.....	152
5.2.5	Comparison of Location of Maximum Moment.....	153
5.2.6	Observed Inelastic Behavior of CIDH Piles .....	153
5.3	Summary .....	154
Chapter 6	ANALYSIS OF TEST RESULTS.....	191
6.1	Pile Diameter Effect on Initial Modulus of Subgrade Reaction .....	191
6.1.1	Method of Analysis.....	192
6.1.2	Results of Analyses.....	195
6.1.3	Analysis of Damping .....	197
6.2	Pile Diameter Effect on $p$ - $y$ Curves .....	199
6.2.1	Method for Back-Calculating $p$ - $y$ Curves.....	200
6.2.2	Back-Calculated $p$ - $y$ Curves for CIDH Piles .....	203
6.2.2.1	0.4-m $p$ - $y$ Curves.....	203
6.2.2.2	0.6-m $p$ - $y$ Curves.....	203
6.2.2.3	0.9-m $p$ - $y$ Curves.....	204
6.2.2.4	1.2-m $p$ - $y$ Curves.....	204
6.2.3	Comparison of $p$ - $y$ Curves for Different Pile Diameters .....	205
6.3	Proposed Methodology to Construct $p$ - $y$ Curves for Weakly Cemented Sand 207	
6.4	Limitation of Proposed $p$ - $y$ Curves for Design.....	208
6.5	Effect of External Confinement from Soil on Bending Behavior.....	209
6.6	Commentary on Effect of External Confinement from Soil on Shear Capacity of CIDH Pile .....	211

6.7	Summary .....	213
Chapter 7 IMPLEMENTATION OF EXISTING $p$ - $y$ CURVES FOR WEAKLY		
CEMENTED SAND..... 259		
7.1	$p$ - $y$ Curves for Sand .....	260
7.2	$p$ - $y$ Curves for $c$ - $\phi$ Soil.....	264
7.2.1	Cemented Sand $p$ - $y$ Curves (Ismael 1990) .....	264
7.2.2	$p$ - $y$ Curves for Silt (Reese and Van Impe 2001).....	265
7.2.3	Comparison of Capability of Various $p$ - $y$ Curves.....	266
7.3	Summary .....	267
Chapter 8 SUMMARY AND CONCLUSIONS ..... 287		
8.1	Summary .....	287
8.2	Conclusions.....	287
APPENDIX A..... 289		
APPENDIX B..... 300		
APPENDIX C..... 303		
REFERENCES ..... 308		

THIS PAGE LEFT BLANK

## List of Figures

Figure 1.1 Integral Pile-Shaft Column and Moment Profile.....	2
Figure 2.1 Influence Factors for Determination of Lateral Pile Responses for the Case of Constant Soil Modulus (after Poulos, 1971).....	51
Figure 2.2 Implementation of Winkler Spring Concept for Laterally Loaded Pile Problem.....	52
Figure 2.3 Definition of $p$ - $y$ Concept with a) Pile at Rest; b) Pile after Load Applied (after Dunnavant, 1986).....	52
Figure 2.4 Typical Family of $p$ - $y$ Curves Response to Lateral Loading (after Dunnavant, 1986).....	53
Figure 2.5 Methodology in Developing $p$ - $y$ Curves (Reese and Van Impe, 2001) .....	53
Figure 2.6 Characteristic Shape of $p$ - $y$ Curve for Soft Clay a) Static Loading; b) Cyclic Loading (after Matlock, 1970).....	54
Figure 2.7 Characteristic Shape of $p$ - $y$ Curve for Stiff Clay below Water Table for a) Static Loading; b) Cyclic Loading; c) Value of Constant A (after Reese <i>et al.</i> , 1975) .....	55
Figure 2.8 Characteristic Shape of $p$ - $y$ Curve for Stiff Clay above Water Table for a) Static Loading; b) Cyclic Loading (Welch and Reese 1972; Reese and Welch, 1975) .....	56
Figure 2.9 Characteristic Shapes of $p$ - $y$ Curves for Sand (Reese <i>et al.</i> , 1974).....	57
Figure 2.10 Sand Failure Modes in Laterally Loaded Pile Problem a) Assumed Passive Wedge Failure; b) Assumed Lateral Flow Failure (after Reese <i>et al.</i> , 1974) .....	57
Figure 2.11 Values of Coefficients Used for Developing $p$ - $y$ Curves for Sand a) Coefficient A; b) Coefficient B (after Reese <i>et al.</i> , 1974).....	58
Figure 2.12 Charts Used for Developing API Sand $p$ - $y$ Curves (API, 1987).....	58
Figure 2.13 Characteristic Shape of $p$ - $y$ Curve for Cemented Sand (after Ismael, 1990) .....	59

Figure 2.14 Characteristic Shape of $p$ - $y$ Curve for $c$ - $\phi$ Soil (Reese and Van Impe, 2001)	59
Figure 2.15 Initial Subgrade Reaction Constant (Reese and Van Impe, 2001) a) Values of $k_c$ , and b) Values of $k_\phi$	60
Figure 2.16 Hyperbolic Soil Model (after Carter, 1984)	60
Figure 2.17 Comparison of Ratio of Predicted to Measured Pile Head Deflections based on Two Different Concepts on Pile Diameter Effect (After Ling, 1988)	61
Figure 2.18 Influence of Pile Diameters on Dimensions of Bulb Pressure (Terzaghi, 1955)	61
Figure 2.19 Typical Determination of Equivalent Depths in a Layered Soil Profile (Georgiadis, 1983)	62
Figure 2.20 Concept of Equivalent Cantilever Beam Method (Chai and Hutchinson, 1999)	63
Figure 2.21 Design Chart for Determining Depth of Fixity (Budek, 1997)	63
Figure 2.22 Concept of Strain Wedge Model for Analyzing Lateral Load Pile Problem (Ashour and Norris, 1998)	64
Figure 2.23 Distribution of Soil-Pile Reaction along Deflected Pile (Ashour and Norris, 1998)	64
Figure 2.24 Force-Displacement Hysteretic Loops for Pile Shaft Test a) without External Confinement, b) with External Confinement (Budek, 1997)	65
Figure 2.25 Typical Stress-Strain Curves for Cemented Sand (After Clough <i>et al.</i> , 1981); a) Strongly Cemented, b) Weakly Cemented, c) Artificially-Cemented (4% Cement), d) Artificially-Cemented (2% Cement)	66
Figure 3.1 Finite Element Mesh for Pile Diameter Effect Study	76
Figure 3.2 Typical Results of Compression Stress ( $\sigma_x$ ) and Displacement in Soil in Laterally Loaded Pile Problem	77
Figure 3.3 Comparison of Pile Head Displacement obtained from 3D FEM and Elastic Solution	78

Figure 3.4 Effect of Pile Diameter on Pile Responses (a) Moment , and (b) Displacement.....	79
Figure 3.5 Normalized Pile Head Displacement against Normalized Pile Diameter .....	80
Figure 3.6 Comparison of Pile Responses obtained form 3D FEM and LPILE (a) Moment , and (b) Displacement.....	81
Figure 3.7 Displacement at Pile Head against Modulus of Subgrade Reaction .....	82
Figure 3.8 Normalized Pile Head Displacement against Normalized Modulus of Subgrade Reaction .....	82
Figure 3.9 Comparison of Two Different Concepts on Pile Diameter Effect on Modulus of Subgrade Reaction with Results from 3D FEM .....	83
Figure 3.10 Effect of Pile Diameter on Lateral Pile Responses (a) Pile Head Displacement, and (b) Ratio of Maximum Moment to Yield Moment .....	84
Figure 3.11 Comparison of Moment Profiles for Linear and Nonlinear Analyses.....	85
Figure 3.12 Comparison of Normalized Pile Head Displacement against Normalized Pile Diameter for Linear and Nonlinear Analyses.....	86
Figure 4.1 Location Map of UCSD East Campus Test Site .....	111
Figure 4.2 Topographic Map of UCSD East Campus Test Site .....	112
Figure 4.3 Geologic Map of UCSD East Campus Test Site (Elliot 1988) .....	113
Figure 4.4 Location Map of Subsurface Exploration.....	114
Figure 4.5 Soil Boring Log for Test Site (Borehole BH-1) .....	115
Figure 4.6 Soil Boring Log for Test Site (Borehole BH-2) .....	118
Figure 4.7 Soil Condition at Test Site Including (a) Corrected SPT-N-Values, and (b) Shear Wave Velocity Profile .....	121
Figure 4.8 Additional Locations of Soil Investigation Extracted from Available Soil Reports .....	122
Figure 4.9 Pile Cross Section.....	123
Figure 4.10 Steel Stress-Strain Curves for 0.6-m and 0.9-m Piles .....	124
Figure 4.11 Steel Stress- Strain Curves for 0.4-m and 1.2-m Piles .....	125
Figure 4.12 Sequence of CIDH Pile Installation .....	126

Figure 4.13	Construction of Reinforcement for Load Stub .....	127
Figure 4.14	Completion of Form Works for Load Stubs.....	127
Figure 4.15	Installation of Tiltmeters into Inclinator Casing.....	128
Figure 4.16	Locations of Crossbow Accelerometers for the 0.4-m and 1.2-m CIDH Piles in Forced Vibration Test.....	129
Figure 4.17	Modal Hammer Used for Impact Vibration Test .....	130
Figure 4.18	Eccentric Mass Shaker .....	131
Figure 4.19	Aluminum Buckets with Two Aluminum Plates on Each of Them.....	131
Figure 4.20	Relationship between Dynamic Force and Excitation Frequency for Different Masses of Aluminum Buckets.....	132
Figure 4.21	Modal Hammer Striking on Load Stub to Generate Initial Velocity to 0.6-m CIDH Pile for Impact Vibration Test.....	133
Figure 4.22	Mass Shaker Mounted on Top of Load Stub of 0.6-m CIDH Pile to Generate Harmonic Force Excitation to the Pile .....	133
Figure 4.23	Lateral Pile Load Test Sequence .....	134
Figure 4.24	Lateral Load Test Set-up and Locations of Instruments (Test No.1) .....	135
Figure 4.25	Lateral Load Test Set-up and Locations of Instruments (Test No.2) .....	136
Figure 4.26	Lateral Load Test Set-up and Locations of Instruments (Test No.3) .....	137
Figure 4.27	Lateral Load Test Set-up and Locations of Instruments (Test No.4) .....	138
Figure 4.28	Test Setup for Lateral Load Test No.1 .....	139
Figure 4.29	UCSD Data Acquisition System .....	139
Figure 5.1	Power Spectra for 0.4-m CIDH Pile from Ambient Vibration Tests (E-W Direction) .....	159
Figure 5.2	Power Spectra for 0.6-m CIDH Pile from Ambient Vibration Tests (E-W Direction) .....	159
Figure 5.3	Power Spectra for 0.9-m CIDH Pile from Ambient Vibration Tests (E-W Direction) .....	160
Figure 5.4	Comparison of Power Spectra for Various Pile Diameters from Ambient Vibration Tests (E-W Direction) .....	160

Figure 5.5	Frequency Response Functions for 0.4-m CIDH Pile from Impact Vibration Tests (E-W Direction).....	161
Figure 5.6	Frequency Response Functions for 0.6-m CIDH Pile from Impact Vibration Tests (E-W Direction).....	161
Figure 5.7	Frequency Response Functions for 0.9-m CIDH Pile from Impact Vibration Tests (E-W Direction).....	162
Figure 5.8	Frequency Response Functions for 1.2-m CIDH Pile (No.1) from Impact Vibration Tests (E-W Direction) .....	162
Figure 5.9	Frequency Response Functions for 1.2-m CIDH Pile (No.2) from Impact Vibration Tests (E-W Direction) .....	163
Figure 5.10	Comparison of Frequency Response Functions for Various Pile Diameters from Impact Vibration Tests (E-W Direction).....	163
Figure 5.11	Frequency Response Curves for 0.4-m Pile from Forced Vibration Tests	164
Figure 5.12	Frequency Response Curves for 0.6-m Pile from Forced Vibration Tests	164
Figure 5.13	Frequency Response Curves for 0.6-m Pile from Forced Vibration Tests (after Pile Experienced Highest Amplitude of Excitation Force).....	165
Figure 5.14	Frequency Response Curves for 0.9-m Pile from Forced Vibration Tests	165
Figure 5.15	Frequency Response Curves for 0.9-m Pile from Forced Vibration Tests (after Pile Experienced Highest Amplitude of Excitation Force).....	166
Figure 5.16	Frequency Response Curves for 1.2-m Pile (No.1) from Forced Vibration Tests .....	166
Figure 5.17	Frequency Response Curves for 1.2-m Pile (No.1) from Forced Vibration Tests (after Pile Experienced Highest Amplitude of Excitation Force) .....	167
Figure 5.18	Frequency Response Curves for 1.2-m Pile (No.2) from Forced Vibration Tests .....	167
Figure 5.19	Frequency Response Curves for 1.2-m Pile (No.2) from Forced Vibration Tests (after Pile Experienced Highest Amplitude of Excitation Force) .....	168
Figure 5.20	Comparison of Frequency Response Curves for Various Pile Diameters from Forced Vibration Tests.....	168

Figure 5.21 Acceleration vs. Time for CIDH Piles from Impact Vibration Tests (E-W Direction) .....	169
Figure 5.22 Comparison of Damping Ratio Obtained from Impact and Forced Vibration Tests .....	170
Figure 5.23 Relationship between Mass of Bucket and Damping Ratio for Various Pile Diameters .....	170
Figure 5.24 Mode Shape of Each Pile .....	171
Figure 5.25 Static Load-Displacement Curves for 0.6-m and 0.9-m CIDH Piles before Correction .....	172
Figure 5.26 Static Load-Displacement Curves of 0.9-m Pile Obtained from Phase I and Phase II.....	172
Figure 5.27 Static Load-Displacement Curves for 0.6-m and 0.9-m CIDH Piles after Correction .....	173
Figure 5.28 Cyclic Load-Displacement Curve for 0.6-m CIDH Pile after Correction.	173
Figure 5.29 Strain Distribution in Longitudinal Reinforcement for 0.6-m CIDH Pile.	174
Figure 5.30 Strain Distribution in Transverse Reinforcement for 0.6-m CIDH Pile....	175
Figure 5.31 Rupture of Spiral Reinforcement and 3 Longitudinal Bars in A Direction	176
Figure 5.32 Rupture of 2 Longitudinal Bars in C Direction .....	176
Figure 5.33 Severe Damage of 0.6-m CIDH Pile between Depths 0 m and 0.6 m .....	177
Figure 5.34 Crack Patterns along 0.6-m CIDH Pile .....	177
Figure 5.35 Static Load Displacement Curves for 0.9-m and 1.2-m CIDH Piles.....	178
Figure 5.36 Cyclic Load-Displacement Curve for 0.9-m CIDH Pile .....	178
Figure 5.37 Strain Distribution in Longitudinal Reinforcement for 0.9-m CIDH Pile.	179
Figure 5.38 Crack Patterns along 0.9-m CIDH Pile at Depths between (a) 0 m and 1.2 m, and (b) 0.9 m and 2.4 m .....	180
Figure 5.39 Static Load Displacement Curve for 0.4-m CIDH Piles .....	181
Figure 5.40 Cyclic Load-Displacement Curve for 0.4-m CIDH Pile .....	181
Figure 5.41 Strain Distribution in Longitudinal Reinforcement for 0.4-m CIDH Pile.	182
Figure 5.42 Rupture of Reinforcing Steels of 0.4-m CIDH Pile at Depth of 0.3 m .....	183

Figure 5.43	Crack Patterns along 0.4-m CIDH Pile at Depths between 0 m and 1.2 m	183
Figure 5.44	Static Load Displacement Curves for 1.2-m CIDH Piles.....	184
Figure 5.45	Cyclic Load-Displacement Curves for 1.2-m CIDH Piles .....	184
Figure 5.46	Strain Distribution in Longitudinal Reinforcement for 1.2-m CIDH Pile (No.1).....	185
Figure 5.47	Strain Distribution in Longitudinal Reinforcement for 1.2-m CIDH Pile (No.2).....	186
Figure 5.48	Crack Patterns along 1.2-m Pile ( No.2) at Depths between (a) 0.75 m and 1.5 m, and (b) 1.5 m and 4.5 m.....	187
Figure 5.49	Normalized Strain vs. Ratio of Depth to Pile Diameter .....	188
Figure 5.50	Cyclic Load-Displacement Curves for a) 0.4-m Pile, b) 0.6-m Pile, c) 0.9-m Pile, and (d) 1.2-m Piles.....	189
Figure 6.1	Numerical Soil-Pile System Model for Simple Two-Layer System .....	216
Figure 6.2	Determination of Shear Wave Velocity Profile (a) Travel Time Plot and (b) Shear Wave Velocity .....	217
Figure 6.3	Ratio of Computed to Measure Natural Frequency vs. Pile Diameter for Simple Two-Layer Soil Profile ( $K_{ind}$ vs. $K_{dep}$ ) .....	218
Figure 6.4	Ratio of Computed to Measure Natural Frequency vs. Pile Diameter for Simple Two-Layer Soil Profile ( $K_{ind}$ vs. $K_{fn}$ ) .....	218
Figure 6.5	Ratio of Computed to Measure Natural Frequency vs. Pile Diameter for Increasing Stiffness with Depth Soil Profile.....	219
Figure 6.6	Ratio of Computed to Measure Natural Frequency vs. Pile Diameter for Increasing Stiffness with Depth Soil Profile (After increasing soil spring stiffnesses) .....	219
Figure 6.7	Comparison of Measured and Computed Damping Ratios.....	220
Figure 6.8	Example of Curvature Calculation from Strain Gauge Data (Extracted Data from 1.2-m CIDH Pile (No-1)).....	221
Figure 6.9	Moment-Curvature Relationships for 0.4-m CIDH Pile (a) Entire Curve, and (b) Before Yielding.....	222

Figure 6.10	Moment-Curvature Relationships for 0.6-m CIDH Pile (a) Entire Curve, and (b) Before Yielding .....	223
Figure 6.11	Moment-Curvature Relationships for 0.9-m CIDH Pile (a) Entire Curve, and (b) Before Yielding .....	224
Figure 6.12	Moment-Curvature Relationships for 1.2-m CIDH Pile (a) Entire Curve, and (b) Before Yielding .....	225
Figure 6.13	Back-Calculated $p$ - $y$ Curves for 0.4-m CIDH Pile .....	226
Figure 6.14	Comparison of Test Results and Analysis Using Back-Calculated $p$ - $y$ Curves for 0.4-m CIDH Pile (a) Load-Displacement Curve, and (b) Moment Profiles .....	227
Figure 6.15	Comparison of Test Results and Analysis Using Back-Calculated $p$ - $y$ Curves for 0.4-m CIDH Pile (a) Rotation Profiles, and (b) Displacement Profiles .....	228
Figure 6.16	Back-Calculated $p$ - $y$ Curves for 0.6-m CIDH Pile .....	229
Figure 6.17	Comparison of Test Results and Analysis Using Back-Calculated $p$ - $y$ Curves for 0.6-m CIDH Pile (a) Load-Displacement Curve, and (b) Moment Profiles .....	230
Figure 6.18	Comparison of Test Results and Analysis Using Back-Calculated $p$ - $y$ Curves for 0.6-m CIDH Pile (a) Rotation Profiles, and (b) Displacement Profiles .....	231
Figure 6.19	Back-Calculated $p$ - $y$ Curves for 0.9-m CIDH Pile .....	232
Figure 6.20	Comparison of Test Results and Analysis Using Back-Calculated $p$ - $y$ Curves for 0.9-m CIDH Pile (a) Load-Displacement Curve, and (b) Moment Profiles .....	233
Figure 6.21	Comparison of Test Results and Analysis Using Back-Calculated $p$ - $y$ Curves for 0.9-m CIDH Pile (a) Rotation Profiles, and (b) Displacement Profiles .....	234
Figure 6.22	Back-Calculated $p$ - $y$ Curves for 1.2-m CIDH Pile (No.1) .....	235

Figure 6.23 Comparison of Test Results and Analysis Using Back-Calculated $p$ - $y$ Curves for 1.2-m CIDH Pile (No.1) (a) Load-Displacement Curve, and (b) Moment Profiles .....	236
Figure 6.24 Comparison of Test Results and Analysis Using Back-Calculated $p$ - $y$ Curves for 1.2-m CIDH Pile (No.1) (a) Rotation Profiles, and (b) Displacement Profiles .....	237
Figure 6.25 Back-Calculated $p$ - $y$ Curves for 1.2-m CIDH Pile (No.2) .....	238
Figure 6.26 Comparison of Test Results and Analysis Using Back-Calculated $p$ - $y$ Curves for 1.2-m CIDH Pile (No.2) (a) Load-Displacement Curve, and (b) Moment Profiles .....	239
Figure 6.27 Comparison of Test Results and Analysis Using Back-Calculated $p$ - $y$ Curves for 1.2-m CIDH Pile (No.2) (a) Rotation Profiles, and (b) Displacement Profiles .....	240
Figure 6.28 Comparison of $p$ - $y$ Curves for Different Pile Diameters at Various Depths .....	241
Figure 6.29 Comparison between Measured and Computed Load-Displacement Curves in Inelastic Range for 0.4-m CIDH Pile.....	242
Figure 6.30 Comparison between Measured and Computed Load-Displacement Curves in Inelastic Range for 0.6-m CIDH Pile.....	242
Figure 6.31 Comparison between Measured and Computed Load-Displacement Curves in Inelastic Range for 0.9-m CIDH Pile.....	243
Figure 6.32 Comparison between Measured and Computed Load-Displacement Curves in Inelastic Range for 1.2-m CIDH Pile (No.1) .....	243
Figure 6.33 Comparison between Measured and Computed Load-Displacement Curves in Inelastic Range for 1.2-m CIDH Pile (No.2) .....	244
Figure 6.34 Proposed Methodology for Constructing $p$ - $y$ Curves for Weakly Cemented Sand.....	245
Figure 6.35 Example of Characteristic of Proposed $p$ - $y$ Curves for 0.4-m Pile at Various Depths .....	246

Figure 6.36	Example of Characteristic of Proposed $p$ - $y$ Curves for Various Pile Diameters at Depth of 0.9 m .....	246
Figure 6.37	Comparison of Test Results and Analysis Using Proposed $p$ - $y$ Curves for 0.4-m CIDH Pile (a) Load-Displacement Curve, and (b) Moment Profiles .....	247
Figure 6.38	Comparison of Test Results and Analysis Using Proposed $p$ - $y$ Curves for 0.6-m CIDH Pile (a) Load-Displacement Curve, and (b) Moment Profiles .....	248
Figure 6.39	Comparison of Test Results and Analysis Using Proposed $p$ - $y$ Curves for 0.9-m CIDH Pile (a) Load-Displacement Curve, and (b) Moment Profiles .....	249
Figure 6.40	Comparison of Test Results and Analysis Using Proposed $p$ - $y$ Curves for 1.2-m CIDH Pile (No.1) (a) Load-Displacement Curve, and (b) Moment Profiles .....	250
Figure 6.41	Modified Moment-Curvature Relationships for Effect of Soil Confinement (a) 0.4-m Pile, and (b) 0.6-m Pile .....	251
Figure 6.42	Comparison between Measured and Computed Load-Displacement Curves using Modified Moment-Curvature Relationship for 0.4-m CIDH Pile.....	252
Figure 6.43	Comparison between Measured and Computed Load-Displacement Curves using Modified Moment-Curvature Relationship for 0.6-m CIDH Pile.....	252
Figure 6.44	Modified Moment-Curvature Relationships for Effect of Soil Confinement (a) 0.9-m Pile, and (b) 1.2-m Pile .....	253
Figure 6.45	Comparison between Measured and Computed Load-Displacement Curves using Modified Moment-Curvature Relationship for 0.9-m CIDH Pile.....	254
Figure 6.46	Comparison between Measured and Computed Load-Displacement Curves using Modified Moment-Curvature Relationship for 1.2-m CIDH Pile (No.1) .....	254
Figure 6.47	Relationship of Equivalent Transverse Reinforcement due to Soil confinement.....	255
Figure 6.48	Results of Lateral Load Test on 0.6-m Pile.....	256
Figure 6.49	Comparison of Theoretical Shear Capacity with Experimentally Observed Shear .....	257

Figure 7.1 Comparison of Back-Calculated $p$ - $y$ Curves with Sand $p$ - $y$ Curves (Reese <i>et al</i> 1974; API 1987) for Depths 0 to 1.5 m .....	268
Figure 7.2 Comparison of Back-Calculated $p$ - $y$ Curves with Sand $p$ - $y$ Curves (Reese <i>et al</i> 1974; API 1987) for Depths 1.8 to 3.3 m .....	269
Figure 7.3 Computed Load-Displacement Curves using Sand $p$ - $y$ Curves (Reese <i>et al</i> 1974; API 1987) Compared to Measured Response (a) 0.4-m Pile, (b) 0.6-m Pile, (c) 0.9-m Pile, and (d) 1.2-m Pile (Pile No.1).....	270
Figure 7.4 Comparison of Load-Displacement Curves using Sand $p$ - $y$ Curves (API 1987) and Proposed $p$ - $y$ Curves for (a) 1.8-m Pile, (b) 2.4-m Pile .....	271
Figure 7.5 Predicted Pile Head Displacement, Maximum Moment, and Depth to Maximum Moment Using Sand $p$ - $y$ Curves (Reese <i>et al.</i> 1974) Compared to Response Obtained Using Back-Calculated $p$ - $y$ Curves for Different Pile Diameters (a) Pile Head Displacement, (b) Maximum Moment, and (c) Depth to Maximum Moment .....	272
Figure 7.6 Predicted Pile Head Displacement, Maximum Moment, and Depth to Maximum Moment Using Sand $p$ - $y$ Curves (API 1987) Compared to Response Obtained Using Back-Calculated $p$ - $y$ Curves for Different Pile Diameters (a) Pile Head Displacement, (b) Maximum Moment, and (c) Depth to Maximum Moment .....	273
Figure 7.7 Comparison of Back-Calculated $p$ - $y$ Curves with Cemented Sand $p$ - $y$ Curves (Ismael 1990) for Depths 0 to 1.5 m .....	274
Figure 7.8 Comparison of Back-Calculated $p$ - $y$ Curves with Cemented Sand $p$ - $y$ Curves (Ismael 1990) for Depths 1.8 to 3.3 m .....	275
Figure 7.9 Computed Load-Displacement Curves using Cemented Sand $p$ - $y$ Curves (Ismael 1990) Compared to Measured Response (a) 0.4-m Pile, (b) 0.6-m Pile, (c) 0.9-m Pile, and (d) 1.2-m Pile (Pile No.1) .....	276
Figure 7.10 Predicted Pile Head Displacement, Maximum Moment, and Depth to Maximum Moment Using Cemented Sand $p$ - $y$ Curves (Ismael 1990) Compared to Response Obtained Using Back-Calculated $p$ - $y$ Curves for Different Pile Diameters	

(a) Pile Head Displacement, (b) Maximum Moment, and (c) Depth to Maximum Moment .....	277
Figure 7.11 Comparison of Back-Calculated $p$ - $y$ Curves with Silt $p$ - $y$ Curves (Reese and Van Impe 2001) for Depths 0 to 1.5 m .....	278
Figure 7.12 Comparison of Back-Calculated $p$ - $y$ Curves with Silt $p$ - $y$ Curves (Reese and Van Impe 2001) for Depths 1.8 to 3.3 m .....	279
Figure 7.13 Computed Load-Displacement Curves using Silt $p$ - $y$ Curves (Reese and Van Impe 2001) Compared to Measured Response (a) 0.4-m Pile, (b) 0.6-m Pile, (c) 0.9-m Pile, and (d) 1.2-m Pile (Pile No.1) .....	280
Figure 7.14 Predicted Pile Head Displacement, Maximum Moment, and Depth to Maximum Moment Using Silt $p$ - $y$ Curves (Reese and Van Impe 2001) Compared to Response Obtained Using Back-Calculated $p$ - $y$ Curves for Different Pile Diameters (a) Pile Head Displacement, (b) Maximum Moment, and (c) Depth to Maximum Moment .....	281
Figure 7.15 Predicted Pile Head Displacement, Maximum Moment, and Depth to Maximum Moment Using Existing $p$ - $y$ Curves Compared to Response Obtained Using Back-Calculated $p$ - $y$ Curves for 0.4-m Pile (a) Pile Head Displacement, (b) Maximum Moment, and (c) Depth to Maximum Moment .....	282
Figure 7.16 Predicted Pile Head Displacement, Maximum Moment, and Depth to Maximum Moment Using Existing $p$ - $y$ Curves Compared to Response Obtained Using Back-Calculated $p$ - $y$ Curves for 0.6-m Pile (a) Pile Head Displacement, (b) Maximum Moment, and (c) Depth to Maximum Moment .....	283
Figure 7.17 Predicted Pile Head Displacement, Maximum Moment, and Depth to Maximum Moment Using Existing $p$ - $y$ Curves Compared to Response Obtained Using Back-Calculated $p$ - $y$ Curves for 0.9-m Pile (a) Pile Head Displacement, (b) Maximum Moment, and (c) Depth to Maximum Moment .....	284
Figure 7.18 Predicted Pile Head Displacement, Maximum Moment, and Depth to Maximum Moment Using Existing $p$ - $y$ Curves Compared to Response Obtained	

Using Back-Calculated $p$ - $y$ Curves for 1.2-m Pile (a) Pile Head Displacement, (b) Maximum Moment, and (c) Depth to Maximum Moment .....	285
Figure A-1 Results of Gradation Analysis (Borehole BH-1).....	290
Figure A-2 Results of Gradation Analysis (Borehole BH-1, Continued).....	291
Figure A-3 Results of Gradation Analysis (Borehole BH-1, Continued).....	292
Figure A-4 Results of Gradation Analysis (Borehole BH-1, Continued).....	293
Figure A-5 Results of Gradation Analysis (Borehole BH-2).....	294
Figure A-6 Results of Gradation Analysis (Borehole BH-2, Continued).....	295
Figure A-7 Results of Gradation Analysis (Borehole BH-2, Continued).....	296
Figure A-8 Results of Gradation Analysis (Borehole BH-2, Continued).....	297
Figure A-9 Results of Gradation Analysis (Borehole BH-2, Continued).....	298
Figure A-10 Results of Gradation Analysis (Borehole BH-2, Continued).....	299

THIS PAGE LEFT BLANK

## List of Tables

Table 2.1 Summary of Elastic Solutions for Laterally Loaded Pile for the Case of Constant Soil Modulus with Depth (after Poulos, 1971).....	37
Table 2.2 Summary of Elastic Solutions for Laterally Loaded Pile for the Case of Constant Soil Modulus with Depth (after Davies and Budhu, 1986) .....	38
Table 2.3 Summary of Elastic Solutions for Laterally Loaded Pile for the Case of Linearly Increasing Soil Modulus with Depth (after Budhu and Davies, 1988) .....	39
Table 2.4 Summary of Definition and Dimension of Terms Used in Analysis of Laterally Loaded Piles.....	40
Table 2.5 Summary of Solutions for Laterally Loaded Pile due to Horizontal Loading for the Case of Constant Subgrade Reaction (Hetenyi, 1946).....	41
Table 2.6 Summary of Solutions for Laterally Loaded Pile due to Moment Loading for the Case of Constant Subgrade Reaction (Hetenyi, 1946).....	42
Table 2.7 Summary of Procedure in Developing Soft Clay $p$ - $y$ Curves (Matlock, 1970)	43
Table 2.8 Summary of Procedure in Developing Stiff Clay with Free Water $p$ - $y$ Curves (Reese <i>et al.</i> , 1975) .....	44
Table 2.9 Summary of Procedure in Developing Stiff Clay with No Free Water $p$ - $y$ Curves (Welch and Reese, 1972;and Reese and Welch, 1975) .....	45
Table 2.10 Summary of Procedure in Developing Sand $p$ - $y$ Curves (Reese <i>et al.</i> , 1974)	46
Table 2.11 Summary of Procedure in Developing API Sand $p$ - $y$ Curves (API, 1987)....	47
Table 2.12 Summary of Procedure in Developing Cemented Sand $p$ - $y$ Curves (Ismael, 1990) .....	48
Table 2.13 Summary of Procedure in Developing Silt $p$ - $y$ Curves (Reese and Van Impe, 2001) .....	49
Table 2.14 Summary of Case Histories of Laterally Loaded Single Piles.....	50
Table 4.1 Minimum Transverse Reinforcement Required by Bridge Design Specifications (Caltrans 2000).....	105
Table 4.2 Summary of Average Concrete Strengths for CIDH Piles .....	105

Table 4.3	Summary of Locations of Strain Gauges and Tiltmeters for Each Test Pile	106
Table 4.4	Summary of Testing Program for Vibration Testing for 0.4-m CIDH Pile..	107
Table 4.5	Summary of Testing Program for Vibration Testing for 0.6-m CIDH Pile..	108
Table 4.6	Summary of Testing Program for Vibration Testing for 0.9-m CIDH Pile.	108
Table 4.7	Summary of Testing Program for Vibration Testing for 1.2-m CIDH Pile (No.1).....	109
Table 4.8	Summary of Testing Program for Vibration Testing for 1.2-m CIDH Pile (No.2).....	110
Table 5.1	Summary of Natural Frequencies of Soil-Pile Systems from Ambient and Impact Vibration Tests.....	156
Table 5.2	Summary of Natural Frequencies and Damping Ratios of Soil-Pile Systems from Forced Vibration Tests.....	157
Table 5.3	Summary of Damping Ratios of Soil-Pile Systems from Impact Vibration Tests .....	158
Table 6.1	Summary of Pile and Soil Properties Used in Natural Frequency Computation for Simple Two-Layer Soil System .....	215
Table 6.2	Summary of Measured and Computed Natural Frequency for Simple 2-Layer System.....	215
Table B.1	Summary of Soil Properties at Charter School Site.....	301
Table B.2	Summary of Soil Properties at East Campus Utilities Plant Test Site .....	302
Table C.1	Summary of Soil Properties at UCSD Cancer Center Building Project .....	304
Table C.2	Summary of Soil Properties at UCSD EBU 3 and EBU 4 Site.....	306
Table C.3	Summary of Soil Properties at Gilman Drive Parking Structure Site .....	307

## Chapter 1 INTRODUCTION

Integral pile shaft-columns (Figure 1.1) have been increasingly used for bridge foundations in California because of comparative economy of construction of large diameter of Cast-In-Drilled-Hole (CIDH) piles compared to driven piles with pile cap footings. In addition, the use of large diameter CIDH pile can solve the problem of adding new structures in confined area, which do not allow either driven piling or large spread footings. The understanding of soil-structure interaction characteristics, particularly lateral pile response, has therefore become a major concern for the design of large diameter CIDH piles.

One of the most widely accepted methods used in analyzing the response of laterally loaded piles is the Winkler spring method in which the soil resistance along the pile is modeled using a series of nonlinear soil springs, widely known as  $p$ - $y$  curves. Most of the existing standard  $p$ - $y$  curves (e.g., for sand, see Reese *et al.*, 1974; for soft clay, see Matlock, 1970; for stiff clay above water table, see Reese and Welch, 1975; and for stiff clay below water table, see Reese *et al.*, 1975) were developed based on results of full-scale lateral load tests on a relatively small range of pile diameters and theory was then extrapolated to use for other diameter sizes. Therefore, the degree of accuracy in predicting the lateral responses for a wide range of pile diameters especially for large pile diameters is still questionable. Furthermore, recent research by Carter (1984) and Ling (1988) showed that the soil response actually appears to become stiffer as the pile diameter increases and suggested that the initial modulus of subgrade reaction, the initial stiffness of  $p$ - $y$  curves, should increase linearly with the pile diameter. This is in conflict with the commonly assumed Terzaghi model (Terzaghi, 1955), in which the modulus of subgrade reaction is considered to be independent of pile diameter. It is therefore essential and beneficial to the engineering profession to evaluate the effect of pile diameter on modulus of subgrade reaction. If the pile diameter has a significant effect on modulus of subgrade reaction, the construction cost of foundations can be substantially decreased when large diameter piles are considered in the design.

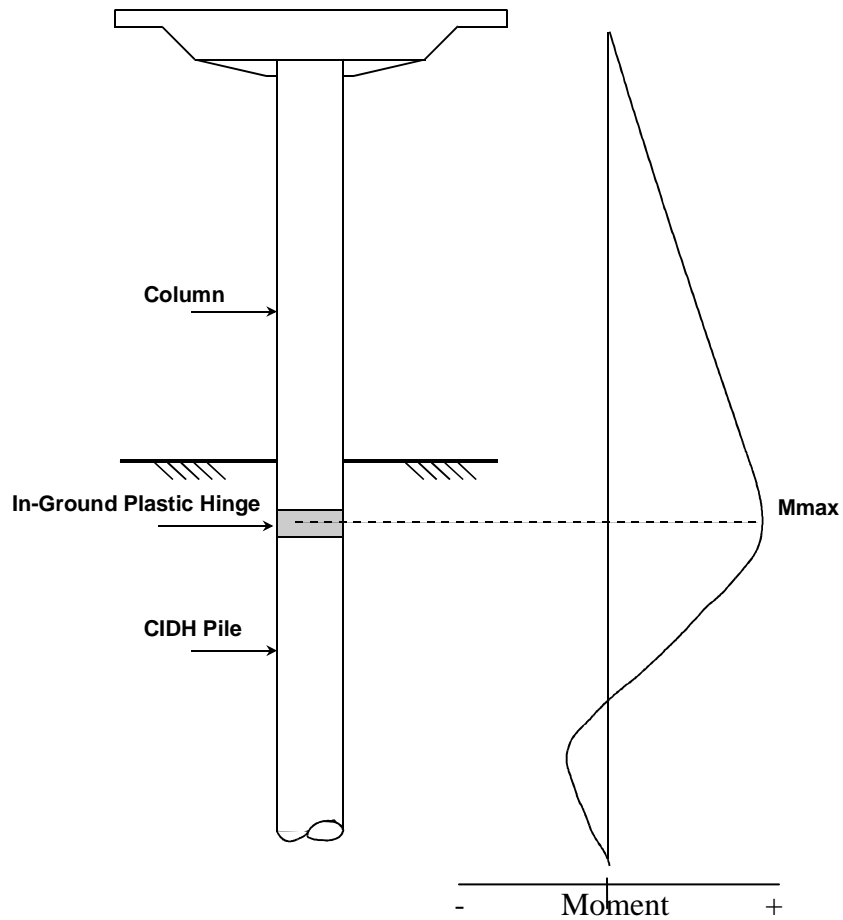


Figure 1.1 Integral Pile-Shaft Column and Moment Profile

It is commonly known that by implementing the integral pile-shaft column, the possibility of an in-ground plastic hinge exists, if the column is continued as a pile shaft extension with the same diameter into the ground (Figure 1.1). Therefore, the understanding of inelastic behavior of the pile becomes another important issue. Several experiments on inelastic behavior of piles have been carried out; however, most of them were tested in the laboratory without soil for confinement. Budek (1997) conducted experiments on the inelastic behavior of CIDH piles by modeling the effect of soil confinement with a series of rubber saddles. The test results indicated that this external confinement, which can be provided by soil, plays a significant role in enhancing the

plastic response of CIDH piles and that only moderate levels of transverse reinforcement are needed for adequate seismic performance. However, the results from full-scale lateral pile load tests in the actual soil are needed to verify the results of the laboratory testing before widely implementing this finding in future design.

## 1.1 Objectives of Research

A research program has been carried out to investigate the effect of pile diameter on modulus of subgrade reaction, as well as the inelastic performance of CIDH piles using the full-scale lateral pile load test. Specifically, the objectives of this research study can be summarized as follows:

1. To study the effect of pile diameter on pile response using both numerical analyses via the 3-D finite element approach and the results from full-scale lateral load tests on different diameters of CIDH piles.
2. To develop the methodology for constructing the  $p$ - $y$  curves for dense weakly cemented sand, taking the pile diameter effects into account.
3. To evaluate the seismic performance of CIDH piles due to the effect of external confinement from soil.
4. To evaluate the capability of existing  $p$ - $y$  curves in predicting the responses of laterally loaded piles in weakly cemented sand for a wide range of pile diameters using the results from the full-scale lateral load tests.

To achieve this goal, the 3-D finite element models for soil-pile interaction were first developed to study the pile diameter effect on soil response using both linear and nonlinear soil models. This provided a general understanding of the diameter effect using the available analytical tools before conducting the full-scale experiments. Cast-In-Drilled-Hole (CIDH) piles with diameters ranging from 0.4 m to 1.2 m were then installed and tested at the University of California, San Diego (UCSD). The test site, which consisted of dense weakly cemented sand, was chosen to represent the soil that is

often found along the coast of Southern California. The  $p$ - $y$  curves for this particular type of soil deposit for a wide range of pile diameters have never been developed.

Two different types of testing were performed in this study including vibration testing and lateral load testing. The vibration testing was performed so as to obtain the dynamic properties of soil-pile system and study the responses of the system at small strain levels where the soil properties remain linear elastic. The test results were used in studying the effect of pile diameter on initial modulus of subgrade reaction, the initial stiffness of  $p$ - $y$  curve. The lateral load test under static loading was performed with the aim of developing the  $p$ - $y$  curves for different pile diameters, and therefore the pile diameter effect at larger strain level can be evaluated. The seismic performance of CIDH piles due to the effect of external confinement from the soil were assessed using the results from cyclic lateral pile load tests. Expecting the improvement from the confinement provided by the soil, the amount of transverse reinforcement used in the CIDH pile test specimens was therefore chosen to be less than that suggested by Bridge Design Specification (Caltrans, 2000).

Furthermore, the possibility of the use of various types of existing  $p$ - $y$  curves to predict the pile response in weakly cemented sand was assessed by comparing the computed responses with the measured responses from the results of full-scale lateral load tests

## **1.2 Organization of Report**

The following outlines the organization of this report.

**Chapter 1 Introduction** – Provides a brief description on the significance of research on the effect of pile diameter on modulus of subgrade reaction, a summary of research objectives, and an outline of this report.

**Chapter 2 Literature Review** – Provides a review on current methods available in predicting the lateral pile response with discussions on the advantages and limitations of each method, the concept of  $p$ - $y$  curves and types of  $p$ - $y$  curves currently available, as well as a summary of research on pile diameter effect on  $p$ - $y$  curves. A summary of full-scale lateral pile load tests conducted by several researchers were also given. In addition, a review on the research on the behavior of weakly cemented soil, as well as inelastic behavior of piles, is provided.

**Chapter 3 Evaluation of Pile Diameter Effect Using 3-D Finite Element Method** – Presents the results of a study of pile diameter effect on pile response using 3-D finite element method. Both linear and nonlinear soil models were incorporated in this study.

**Chapter 4 Full-Scale Testing** – Provides geotechnical information about the test site and the description of test piles. The test arrangement, testing programs, and testing procedures on both vibration and lateral load tests are discussed.

**Chapter 5 Test Results** – The dynamic properties of the soil-pile system based on the results of various types of vibration tests are presented and discussed. This is followed by the results of full-scale lateral load tests under both static and cyclic loadings which include the load-displacement curves, and strain gauge data.

**Chapter 6 Analysis of Test Results** – The evaluation of the effect of pile diameter on  $p$ - $y$  curves based on the experimental results are presented. This included the effect of pile diameter on the initial modulus of subgrade reaction using the results from vibration tests. The  $p$ - $y$  curves for each pile diameter were back-calculated using the results from lateral load tests. The  $p$ - $y$  curves for various pile diameters were then compared to provide insight into the effect of pile diameter on  $p$ - $y$  curves. In addition, the methodology to construct the  $p$ - $y$  curves for the soil type tested in this study was

proposed. Finally, the effect of soil confinement in enhancing the inelastic behavior of the piles was quantitatively evaluated.

**Chapter 7 Implementation of Existing  $p$ - $y$  Curves for Weakly Cemented Sand**– Several existing  $p$ - $y$  curves, including sand  $p$ - $y$  curves and cemented sand  $p$ - $y$  curves were used to predict the experimental test results to evaluate its capability in predicting the pile response for a wide range of pile diameters.

**Chapter 8 Summary and Conclusions**– Provides the summary and conclusions of this research study.

## Chapter 2 LITERATURE REVIEW

### 2.1 Introduction

The problem of the laterally loaded pile was originally of particular interest in the offshore industry. Lateral loads from wind and waves are frequently the most critical factor in the design of such structures. Solutions of the general problem also apply to a variety of onshore cases including pile supported earthquake resistance structures, power poles, and pile-supported structures which may be subjected to lateral blast forces or wind forces.

In the design of pile foundations against lateral loading, two criteria must be satisfied: 1) the pile must have an adequate factor of safety against the maximum lateral loading that might be applied to it, and 2) the deflection that occurs due to a working load must be in an acceptable range that superstructure can withstand (Poulos and Davis, 1980). A common procedure used for analysis and design of piles under lateral loading in earthquake engineering is to conduct a pushover analysis to determine the load-displacement relationship of the structure. The design-basis lateral load used for pile design is calculated based upon an appropriate value of spectral displacement at the structure's fundamental-mode period and damping ratio.

Several analytical methods have been proposed that attempt to model lateral pile response, none of which can completely account for all factors that influence lateral soil-pile interaction. The earliest and simplest representation problem was that of a transversely loaded thin elastic beam, supported by a series of linear springs (Winkler spring method) acting along the length of the beam (Winkler, 1867; Hetenyi, 1946; Barber, 1953; Matlock and Reese, 1960; and Davisson and Gill, 1963). Because of the analytical simplicity, this method is widely used in foundation engineering. However, the response of real soil is far from elastic, and nonlinear soil response is the key factor in the behavior of laterally loaded piles. A series of nonlinear soil spring, known as  $p$ - $y$

curves, back-calculated based on the results from full-scale lateral pile load tests were replaced the linear soil springs for a better representation of the actual soil behavior (e.g., Matlock, 1970; Reese *et al.*, 1974; Reese and Welch, 1975; Reese *et al.*, 1975; and Ismael, 1990). The pile nonlinearity also can be easily taken into account by using this method. As a result, it is one of the most acceptable methods currently used in the design of laterally loaded pile. The disadvantage of this method is, however, a neglecting of soil continuity.

Another analysis method considers the soil as an elastic continuum and implements a boundary element analysis to develop the solutions for analyzing the pile response (e.g., Spillers and Stoll, 1964; Poulos, 1971 and 1973; and Banerjee and Davies, 1978). The nonlinearity of soil, such as soil reaching the ultimate bearing capacity, was taken into account by means of modified boundary element analysis (e.g., Banerjee and Davies, 1979; Davies and Budhu, 1986; and Budhu and Davies, 1988). However, these solutions are limited to simple cases, such as a constant soil modulus with depth, a linear increasing soil modulus with depth, and a simple 2-layered soil system. Application for design of a real problem is not as flexible as the Winkler method. Furthermore, the inelastic behavior of pile can not be properly incorporated in this method. As a result, this method is not widely used in design.

Recently, using a finite element method to represent the soil mass seems to become more popular due to the availability of the computational power of computers, as well as the ability to investigate some other aspects that the previous mentioned methods can not account for, such as stress-strain behavior in the soil mass (Desai and Appel, 1976; Randolph, 1981; Kuhlemeyer, 1979; Kooijman, 1989; Brown *et al.*, 1989; Trochanis *et al.*, 1991; and Bransby, 1999). Though the method can be quite versatile, the use has been limited primarily to research. Application of this method in design has rarely been used due to the limitation of current constitutive soil models, as well as the requirement of engineering time in generating the input and interpreting the results.

In this chapter, a summary of methods being used in lateral pile response analyses are reviewed and the pros and cons of each method are discussed. The review is mainly focused on the Winkler spring method, which is widely used in the current design of bridge foundation. This is followed by a review of previous full-scale lateral pile load tests on single piles under static and cyclic loadings. Furthermore, inelastic behavior of the concrete pile based on the laboratory and full-scale testing found in the literatures are presented. Finally, research on the behavior of cemented sand, a soil type considered in this research study, is reviewed.

## **2.2 Methods in Predicting Lateral Pile Responses**

### **2.2.1 Elastic Continuum using Boundary Element Method**

The boundary element method was used extensively between 1960 and 1980 to solve the problem of piles subjected to lateral loading. In this method, the fundamental solution needs to be solved first, which gives the response of a point at the interior of the soil mass as a result of the application of load at another point of the soil mass. Mindlin (1936) presented the solutions of horizontal displacements caused by a horizontal point load within the interior of semi-infinite, elastic, isotropic homogeneous mass. This solution was used by many researchers (e.g., Spillers and Stoll, 1964; Poulos, 1971, Banerjee and Davies, 1978; and Davies and Budhu, 1986) to analyze the response of a pile subjected to lateral loading. All of these analyses are similar in principle; the differences arising largely from details in the assumptions regarding the pile action. The accuracy of the answers is dependent on the number of element subdivided in the pile, particularly sensitive for a very flexible pile case. The analysis of the single pile problem by means of boundary element analysis involves discretizing the pile interface with soil into small elements and equating the displacement of pile and soil at the center of elements. In this process, the soil displacements are obtained through the Mindlin's solution.

For the case of a constant soil modulus with depth, which is usually used to represent the behavior of overconsolidated clay, the solutions of pile response from both free-head and fixed-head piles taken from works by Poulos (1971) are given in Table 2.1. The dimensionless elastic influence factors can be obtained from graphs presented in Figure 2.1. Another solution of lateral pile response in a constant soil modulus with depth was also given by Davies and Budhu (1987) as summarized in Table 2.2. The slight difference in results obtained from both methods is due to the different assumptions being used as well as the number of pile elements considered in the analyses.

The advantage of this approach is that the continuity of the soil is taken into account to develop the solutions of lateral pile response. However, the elastic continuum approach is limited by several factors. Since in reality the soil is irregular and the Young's modulus and Poisson's ratio change with depth, the assumption of a homogeneous isotropic semi-infinite soil is ideal. Some researchers have proposed solutions to account for varying soil stiffness profiles. Poulos (1973) and Banerjee and Davies (1978) proposed solutions for a layered soil. Banerjee and Davies (1978), and Budhu and Davies (1988) provided solutions for soil with linearly increasing soil modulus with depth. This type of soil profile represents the behavior of sand and normally consolidated clay. Work by Budhu and Davies is summarized in Table 2.3.

Though solutions for a variety of soil profiles have been developed, the implementation of this method is not easy and flexible for real problems. In addition, the behavior of the soil under large deflections is highly nonlinear. Therefore, the assumption that the soil is linear elastic is not acceptable. This assumption is reasonable when only the soil deforms with small strain. Furthermore, the application of this method for the earthquake engineering problem is difficult. This method is therefore useful only for a crude estimation or preliminary analysis due to its simplicity of calculation.

### **2.2.2 Modified Boundary Element Analyses**

A modified boundary element analysis is the extension of the boundary element method in an attempt to incorporate an elasto-plastic soil model to account for soil yielding, particularly at the ground surface. The effect of local yield of the soil was first outlined by Spillers and Stoll (1964), in which a limiting lateral pressure is specified for each element of the pile and the analysis ensures that the computed pile-soil pressure does not exceed this limiting value. A similar principle was employed by Poulos (1971) in his study of the effect of local soil yielding on the response of a laterally loaded pile with various distributions of soil pressures with depth.

Banerjee and Davies (1979) used incremental and iterative initial stress or initial strain procedures in which the effect of yielding or slipping are introduced by distributing initial stresses over volume “cells” and distributing initial tractions over slip surfaces, respectively.

Davies and Budhu (1986) proposed a method to predict the behavior of a laterally loaded pile by taking into account soil and pile yielding. The yielding of the soil considered in this study includes bearing capacity failure in the compressive zone, shear failure at the side along the soil-pile interface, and tension failure in the soil. The solutions were suitable for heavily overconsolidated clay where the soil strength profile can be generally assumed to be constant with depth. Budhu and Davies (1988) implemented the same principle as used in a constant modulus with depth to further develop the solutions to use for soft clay and sand where the soil strength linearly increases with depth.

Though researchers have attempted to incorporate the complexity of soil through the use of modified boundary element analyses, such as taking into account soil yielding, layered soil, and various distributions of soil modulus with depth, this type of analysis is still not sufficiently flexible to model the problem of a laterally loaded pile in reality.

Furthermore, the application to the earthquake engineering industry such as dynamic analysis is difficult. Other methods which seem to be more practical in the engineering practice are discussed in the following sections.

### **2.2.3 Finite Elements for Soil**

In recent years, this method has become more extensively used due to the availability of the computational power of computers. The main advantages of this method are that the continuity of soil, as well as the soil nonlinearity, can be taken into account. This is an idealized method for studying the response of laterally loaded piles in the future because this method is very powerful and most of the aspects that other methods can not be investigated can be studied via finite element method such as the stress and strain in the soil mass, influence of gapping, and the effect of construction sequencing. However, its accuracy still depends on the ability to predict the soil properties and also the accuracy of constitutive soil models. The proper constitutive soil models for this type of analyses need to be developed and also verified with the results from full-scale and/or centrifuge testing. Another disadvantage of this method is the high computation time, especially in the case of 3-D analyses. Currently, the finite element method has been predominantly used in research on laterally loaded piles, but the application of this method has rarely been used in the design due to the limitation of current constitutive soil models, as well as the requirement of engineering time in generating the input and interpreting the results.

There are several examples of research on laterally loaded piles using the finite element method. Desai and Appel (1976) developed a 3-D finite element solution for the laterally loaded pile problem. Randolph (1981) and Kuhlemeyer (1979) introduced a more economical method: using the finite element method in conjunction with Fourier techniques. Randolph (1981) conducted a parametric study on the response of laterally loaded piles embedded in the elastic soil continuum with constant and linear increasing

soil modulus with depth. Algebraic expressions fitted to the results from the parametric study to predict lateral pile response were proposed.

Kooijman (1989) and Brown *et al.* (1989) used three-dimensional finite elements to develop  $p$ - $y$  curves. Trochanis *et al.* (1991) examined the effect of nonlinear soil behavior on the axial and lateral pile responses using a three-dimensional finite element analysis. Bransby (1999) implemented a 2-D finite element analysis to find load-transfer relationships for laterally loaded pile and suggested that these curves could be used as  $p$ - $y$  curves in the analysis of laterally loaded piles.

#### **2.2.4 Winkler Method and the Concept of $p$ - $y$ Curves**

The Winkler method, or sometimes known as the *subgrade reaction method*, currently appears to be the most widely used in a design of laterally loaded piles. The method was first introduced by Winkler (1867) to analyze the response of beams on an elastic subgrade by characterizing the soil as a series of independent linearly-elastic soil springs. Since then, this concept has been extensively employed for the laterally loaded pile problem. The concept of this method is graphically illustrated in Figure 2.2.

One of the great advantages of this method over the elastic continuum method is that the idea is easy to program in the finite difference or finite element methods and that the soil nonlinearity and multiple soil layers can be easily taken into account. The concept can be easily implemented in dynamic analysis. In addition, the computational cost is significantly less than the finite element method. However, the obvious disadvantage of this method is the lack of continuity; real soil is at least to some extent continuous.

The term of subgrade reaction indicates the pressure,  $P$ , per unit area of the surface of the contact between a loaded beam or slab and the subgrade on which it rests

and on to which it transfers the loads. The coefficient of subgrade reaction,  $k$ , is the ratio between the soil pressure,  $P$ , at any given point of the surface of contact and the displacement,  $y$ , produced by the load application at that point:

$$k = \frac{P}{y} \quad (2.1)$$

To implement this concept for a laterally loaded pile, the above equation (2.1) has been modified frequently (e.g. Reese and Matlock, 1956; and Davisson and Gill, 1963) as

$$K = \frac{P}{y} \quad (2.2)$$

where  $K$  is the modulus of subgrade reaction ( $F/L^2$ ) and  $p$  is the soil reaction per unit-length of the pile ( $F/L$ ). It should be noted that the dimensions of each variable are given in parentheses. Since these terms are often confused in the literature, they are summarized in Table 2.4 to make this report easier to follow.

With the subgrade reaction concept, the lateral pile response can be obtained by solving the fourth order differential equation as:

$$E_p I_p \frac{d^4 y}{dz^4} + Ky = 0 \quad (2.3)$$

where  $E_p$  is the modulus of elasticity of the pile,  $I_p$  is the moment of inertia of the pile, and  $z$  is depth.

Solutions of Eq. (2.3) can be obtained either analytically or numerically. Analytical solutions are only available in the case of constant modulus of subgrade

reaction with depth. For other subgrade reaction distribution, the solutions are conveniently solved by using the finite difference method.

Hetenyi (1946) provided solutions for a variety of infinite beams on an elastic Winkler subgrade by solving analytically the governing equations. The solutions can be applied to analyze the response of a laterally loaded pile with a constant subgrade reaction. Table 2.5 and Table 2.6 summarize the solutions of lateral pile responses due to the horizontal loading and moment at the pile head, respectively. Barber (1953) provided the solutions to determine the deflections and rotation at the ground surface using the convenient plots for cases of constant soil modulus of subgrade reaction, as well as the linearly increasing soil modulus of subgrade reaction with depth. Several functions of distribution of modulus of subgrade reaction with depth (i.e., polynomial function and power function) have been considered by Matlock and Reese (1960). Matlock and Reese give the solutions for a special case soil profile where the modulus of subgrade reaction has some finite value at the ground surface and continues to increase linearly with depth.

Davisson and Gill (1963) extended the subgrade reaction theory to analyze the behavior of laterally loaded piles in a two-layer soil system for both free and fixed head conditions and provided the results in non-dimensional forms.

The values of modulus of subgrade reaction can be obtained using the in-situ testing, such as the plate loading test. For practical purposes, Terzaghi (1955) recommended the rough estimate values of coefficient of subgrade reaction for stiff clay and sand to be used for analyzing pile response using subgrade theory. He stated that the linear relationship between the soil pressure and displacement was valid for values of the soil pressure that were smaller than about one-half of the bearing stress.

Another method in estimating the modulus of subgrade reaction is the use of the equation proposed by Vesic (1961). Vesic provided a relationship between the modulus of subgrade reaction,  $K$ , used in the Winkler spring problem and the material properties in the elastic continuum problem as

$$K = \frac{0.65E_s}{(1 - \mu_s^2)} \left[ \frac{E_s D^4}{E_p I_p} \right]^{1/12} \quad (2.4)$$

where  $E_s$  = soil modulus of elasticity,  $\mu_s$  = Poisson's ratio of the soil,  $D$  = pile diameter, and  $E_p I_p$  = flexural rigidity of the pile. By knowing the soil modulus of elasticity from the laboratory or field testing, as well as the pile property, the modulus of subgrade reaction can be estimated.

#### 2.2.4.1 Concept of $p$ - $y$ Curves

All of the solutions based on subgrade reaction theory mentioned in the previous sections are valid only for a case of linear soil properties. In reality, the relationship between soil pressure per unit pile length  $p$  and deflection  $y$  is nonlinear. Taking the nonlinearity of soil into account, the linear soil springs are replaced with a series of nonlinear soil springs, which represent the soil resistance-deflection curve so called, “ $p$ - $y$ ” curve. The  $p$ - $y$  curves of the soil have been developed based on the back analysis of the full scale lateral pile load test. This concept was first developed by McClelland and Focht (1958).

The concept of a  $p$ - $y$  curve can be defined graphically as shown in Figure 2.3. It was assumed that the pile was perfectly straight prior to driving and there was no bending of the pile during driving. The soil pressure acting against the pile prior to loading can be reasonably assumed to be uniform, Figure 2.3a. The resultant pressure for this condition is zero. If the pile is loaded with a given lateral deflection as shown in Figure 2.3b, a net

soil reaction will be obtained by the integration of the soil pressures around the pile giving the unbalanced force per unit length of the pile. This process can be repeated in concept for a series of deflections resulting in a series of forces per unit length of pile which may combine to form a  $p$ - $y$  curve. In a similar manner, the sets of  $p$ - $y$  curves along the pile as shown in Figure 2.4 can be obtained. If such a set of curves can be predicted, the yield pile deflection, pile rotation, bending moment, shear, and soil reaction for any load capable of being sustained by the pile can be obtained by solving the beam equation.

The series of  $p$ - $y$  curves greatly depends upon the soil type. The  $p$ - $y$  curves can be obtained experimentally by conducting the full scale testing of instrumented piles in the type of soil deposit interested. Figure 2.5 presents the methodology in developing the  $p$ - $y$  curves. The bending moment diagram along the pile can generally be computed by the product of pile curvatures, which are computed from the measured strain along the pile, with the known pile stiffness. Double differentiation of the bending moment diagram produces the soil reaction curve. The deflection along the pile can be obtained by double integration of the curvature diagram. Therefore, the soil reaction versus the deflection of the pile,  $p$ - $y$  curve, at a given depth can be obtained.

Though the Winkler method neglects soil continuity, a disadvantage to a considerable extent, it has been overcome through calibrating  $p$ - $y$  curves to full-scale test results. However, many factors which influence the behavior of laterally loaded piles have been lumped into the characteristic shape of the  $p$ - $y$  curves and difficult to separate due to the limit number of the full-scale testing. Some of parameters which may have a significant effect on the pile response have not been investigated systematically such as the pile diameter effect, the effect of soil gapping, and the validity of using these  $p$ - $y$  curves for a rigid pile case. Further research on these issues needs to be investigated in order to improve the existing  $p$ - $y$  curves for the wider range of application.

Several researchers have proposed methods to construct  $p$ - $y$  curves for various soil types based upon back-computation from full-scale test results. The following paragraphs presents the brief description of each  $p$ - $y$  curves currently available in the industry. Most of these  $p$ - $y$  curves have been incorporated in the commercial programs in analyzing behavior of laterally loaded pile, such as COM624P (Wang and Reese, 1993), LPILE (Reese *et al.*, 2000), and FLPIER (University of Florida, 1996).

#### 2.2.4.2 Soft Clay $p$ - $y$ Curves

Matlock (1970) conducted full-scale lateral load tests on a 0.3-m diameter instrumented steel pipe pile embedded in soft clay deposit at Lake Austin, Texas. The methodology to develop the  $p$ - $y$  curves was proposed based on the back-computed  $p$ - $y$  curves from the test results. Figure 2.6a presents the characteristic shape of the soft clay  $p$ - $y$  curves for static loading case which can be represented by using cubic parabola relationship as:

$$\frac{p}{p_u} = 0.5 \left( \frac{y}{y_{50}} \right)^{\frac{2}{3}} \quad (2.5)$$

where:  $p_u$  = ultimate soil resistance which is related to the undrained shear strength of the soil as well as a function of depth, and  $y_{50}$  = the soil displacement at one-half of ultimate soil resistance. Figure 2.6b shows characteristic of  $p$ - $y$  curves under cyclic loading. The main difference between static and cyclic loading is that the soil resistance at large strain level is deteriorated due to the effect of cyclic loading. A summary of procedure in developing the soft clay  $p$ - $y$  curves for both static and cyclic loading is given in Table 2.7

#### 2.2.4.3 Stiff Clay $p$ - $y$ Curves below Water Table

Reese *et al.* (1975) performed lateral load tests on two 0.6-m diameter steel pipe piles embedded in stiff clay under water table at Manor, Texas. The characteristic shapes

of these  $p$ - $y$  curves for both static and cyclic loading are presented in Figure 2.7. The shape of the  $p$ - $y$  curve shows a very large loss of soil resistance much more than has been observed elsewhere, probably because the soil at Manor site was expansive and continued to imbibe water as cycling progressed. The use of these  $p$ - $y$  curves will therefore yield a conservative estimate of pile response. The parameters, which control the characteristic shape of the  $p$ - $y$  curves, are similar to those of soft clay  $p$ - $y$  curves as mentioned earlier. Table 2.8 summarizes the methodology for developing the  $p$ - $y$  curves for stiff clay below water table for both static and cyclic loadings.

#### 2.2.4.4 Stiff Clay $p$ - $y$ Curves above Water Table

Welch and Reese (1972) conducted lateral load tests at a site in Houston, Texas with a 0.76-m diameter bored pile and proposed the detailed procedure in constructing  $p$ - $y$  curves in stiff clay above water table. The characteristic shape of  $p$ - $y$  curves are somewhat similar to the  $p$ - $y$  curves for soft clay (Matlock, 1970), but stiffer due to the use of the fourth degree of parabola relationship to represent the curve. Furthermore, unlike stiff clay under water table, no soil softening is observed on the characteristic shape of  $p$ - $y$  curves in stiff clay without water table as presented in Figure 2.8. The soil resistance for cyclic  $p$ - $y$  curves decreases as the number of the cycles of load application increases. Table 2.9 summarizes a procedure in constructing the  $p$ - $y$  curves for this type of soil.

#### 2.2.4.5 Sand $p$ - $y$ Curves

Reese *et al.* (1974) proposed the procedure in constructing the  $p$ - $y$  curves for sand under static and cyclic lateral loadings. The procedure was developed from the results of tests at Mustang Island on two 0.6 m diameter, flexible driven piles embedded in a deposit of submerged, dense, fine sand (Cox *et al.*, 1974). The characteristic shape of the  $p$ - $y$  curve is highly nonlinear and can be described by three straight line portions and a parabolic curve as illustrated in Figure 2.9. The method in developing the  $p$ - $y$  curves involves the estimation of initial modulus of subgrade reaction and ultimate soil

resistance. The suggested values of initial modulus of subgrade reaction for different relative densities of sand are given by Reese *et al.* (1974). This initial straight-line portion of the curves (where  $E_s$  is linearly with deflection) governs for only small deflections. Therefore, the initial slope of the  $p$ - $y$  curve influences analyses for only very small load level.

The ultimate soil resistance near the ground surface is developed based on a wedge type failure theory; whereas, that at some distance below the ground surface was derived based on the flow failure model as presented in Figure 2.10.

It was found that by using the equations for estimating the soil resistance based on the theoretical developed above, the ultimate soil resistance was much smaller than the experimental one. Therefore, Reese *et al.* (1974) modified the ultimate soil resistance by introducing an empirical adjustment factor  $A$  as presented in Figure 2.11a to bring the two quantities into agreement. Since the theory developed to predict the ultimate soil pressure did not match the experimental  $p$ - $y$  curves, extrapolating this method for different soil strengths and/or pile diameters should be investigated.

#### 2.2.4.6 API Sand $p$ - $y$ Curves

The method in developing the  $p$ - $y$  curve based on the procedure proposed by Reese *et al.* (1974) is quite tedious. O'Neill and Murchison (1983) proposed a simplified method for sand  $p$ - $y$  curves, which also yielded the results with relatively good accuracy compared to the original  $p$ - $y$  curves. These modified  $p$ - $y$  curves were accepted by the American Petroleum Institute (API) committee and officially used extensively. In the API method, the sand  $p$ - $y$  curves were simplified using a hyperbolic tangent function to describe the characteristic shape of the  $p$ - $y$  curves as presented in Table 2.11. The lengthy equations for determining the ultimate soil pressure were simplified by the use of three coefficients  $C_1$ ,  $C_2$  and  $C_3$  as a function of the friction angle, which can be simply obtained from the graph as presented in Figure 2.12a. The initial modulus of subgrade

reaction constant was proposed in the graphical form as presented in Figure 2.12b. The experimental adjustment factor  $A$  for the static load test was simplified using a linear equation; therefore, a difference in the empirical adjustment factor  $A$  was expected and therefore resulted in a slight difference in ultimate soil pressure. Table 2.11 presents the step by step in developing the API sand  $p$ - $y$  curves.

#### 2.2.4.7 $p$ - $y$ Curves for $c$ - $\phi$ Soils

Generally, in design, the soil is usually classified into 2 different types, either cohesive or cohesionless soils, since the theories to analyze geotechnical problems were developed based on that concept. This practice sometimes leads to a significantly conservative design in the case of cemented soil or silt, which always neglects the soil resistance from the cohesion component. For the behavior of laterally loaded piles in cemented soil, it is apparent that the cohesion from cementation will increase soil resistance significantly, especially for soil near the ground surface.

Ismael (1990) conducted full-scale lateral load pile tests in medium dense cemented sands on single piles and on small groups under static loading in Kuwait. All 12 tested piles were 0.3 m-diameter reinforced concrete bored piles with the pile lengths of 3 m and 5 m. Two of them were instrumented with electric resistance strain gauges to measure bending moment. Based on drained triaxial test results, the angle of friction and cohesion were  $35^\circ$  and 20 kPa, respectively. It was shown that the predicted load-displacement characteristics based on sand  $p$ - $y$  curves developed by Reese *et al.* (1974) significantly underestimated the experimental response because it ignored the cohesion component. Theoretical parabolic  $p$ - $y$  curves, which accounted for both angle of friction and cohesion component, were then proposed as presented in Figure 2.13. A summary of the procedure used in developing cemented sand  $p$ - $y$  curves is presented in Table 2.12. Using these  $p$ - $y$  curves the predicted responses were in good agreement with the experimental results.

The procedure proposed by Ismael indirectly showed that the cemented soil behaves more like cohesive soil than cohesionless soil because the  $p$ - $y$  curves as presented in Figure 2.13 are approximated by using a cubic parabola as used in the soft clay  $p$ - $y$  curves (Matlock 1970).

In contrast, Reese and Van Impe (2001) believed that the behavior of  $c$ - $\phi$  soils is closer to that of cohesionless soil than of cohesive soil. The procedure to develop  $p$ - $y$  curves for  $c$ - $\phi$  soil was suggested based upon procedure in developing  $p$ - $y$  curves for sand and ideas presented by Ismael (1990). The characteristic shape of  $c$ - $\phi$  soil  $p$ - $y$  curves, which is called silt  $p$ - $y$  curves in LPILE computer program, are different from that obtained from the cemented sand  $p$ - $y$  curves (Ismael, 1990) in which the strain softening appears after reaching its peak strength as presented in Figure 2.14. A summary of developing this type of  $p$ - $y$  curves are given in Table 2.13. It is noted that the silt  $p$ - $y$  curves were developed based on the theoretical basis alone without any validation from the full-scale test results.

#### 2.2.4.8 Hyperbolic Soil Model

Similar to the concept of  $p$ - $y$  curves, Carter (1984) developed the simple hyperbolic soil model ( $P$ - $y$  curves) to represent the characteristics of soil and implemented them in the Winkler method. The difference is that the soil pressure,  $P$ , not the soil resistance per unit length,  $p$ , is used in this soil model. Therefore, to change this soil model to  $p$ - $y$  curves the soil pressure needs to be multiplied by the pile diameter. This simple soil model can be established using only three parameters, including the initial coefficient of subgrade reaction,  $k_o$ , ultimate soil pressure,  $P_{ult}$ , and nonlinearity index  $n$ , as presented in Figure 2.16. The curve of hyperbolic soil model is given as:

$$y = \frac{P}{k_o} \left[ \frac{P_{ult}^n}{(P_{ult}^n - P^n)} \right] \quad (2.6)$$

where  $y$  = soil displacement at any point (L),  $P$  = soil pressure ( $F/L^2$ ),  $n$  = index that controls nonlinearity (1 for sand and 0.2 for clay),  $k_o$  = small strain coefficient of subgrade reaction ( $F/L^3$ ), and  $P_{ult}$  = ultimate soil pressure ( $F/L^2$ ). The main advantage of this method is that one soil model can be used for both cohesive and cohesionless soil cases. Carter (1984) implemented this soil model to predict the results of full scale pile tests and found that a value of  $n = 1$ , seems appropriate for sand and 0.2 for clay. Six series of pile tests analyses by Carter appears to predict the response of piles with a similar level of accuracy that of  $p$ - $y$  curves proposed by Reese *et al.* (1974).

Ling (1988) continued Carter's work by conducting the analysis by using the computer program developed by Carter (1984) to predict the response of full scale pile tests from case histories. Ling found that using the hyperbolic model with the value of  $n = 1$  can predict the response of twenty eight full scale pile tests, both in sand and clay with a reasonable degree of accuracy.

#### 2.2.4.9 Effect of Pile Diameter on $p$ - $y$ Curves

$p$ - $y$  curves have been developed for various soil types which show that different types of soils have their own characteristic shapes. Pile diameter, one of the factors which may significantly influence the behavior of laterally loaded piles, has not yet been systematically investigated. As can be seen from the review of various types of  $p$ - $y$  curves, most of the  $p$ - $y$  curves were developed based on the results of full scale testing on a limited number of piles due to the high cost of full-scale testing. The theory was then developed based on that limited information and then empirically extrapolated to use for other diameters. The degree of accuracy in predicting the pile response for a wide range of pile diameters is therefore of interest.

A few studies on pile diameter effect on clay are available in the literature. No studies have been reported on an investigation of pile diameter on  $p$ - $y$  curves in sand. Reese *et al.* (1975) back-calculated  $p$ - $y$  curves of 0.65-m pile tested at Manor site and used them to predict the behavior of 0.15 m diameter pile. Good agreement of moment comparison between analysis and experiment was found; however, the computed deflection was considerably lower than the measured one. No conclusion could be made on the disagreement.

O'Neill and Dunnavant (1984) and Dunnavant and O'Neill (1985) conducted the laterally loaded piles with diameters of 0.27 m, 1.22 m and 1.83 m in an overconsolidated clay site. They found that the deflection at one half of the ultimate soil pressure ( $y_{50}$ ) is not linearly dependent on pile diameter, with the  $y_{50}$  getting smaller as the pile diameter increases. This means that the pile diameter effect incorporated in the clay  $p$ - $y$  curves is actually less than that observed from the actual behavior. The modification on Matlock's  $p$ - $y$  curves was proposed to match the agreement between measured and computed response.

Stevens and Audibert (1979) collected published case histories on laterally loaded piles in clay and implemented existing  $p$ - $y$  curves proposed by Matlock (1970) and API (1987) to analyze the pile response. They found that the computed to measured deflection ratio is generally greater than 1 and becomes larger with increasing pile diameter. In addition, the computed maximum moment is higher than the observed values as much as 30%. In order to match the test results, Stevens and Audibert (1979) suggested that the pile displacement at 50% of ultimate soil pressure should be proportional to the square root of pile diameter, not a linear function of the pile diameter as originally proposed by Matlock (1970). Again, this finding indicates that the actual pile diameter effect is more than that incorporated in the soft clay  $p$ - $y$  curves.

Ling (1988) performed back analysis of lateral response of pile based on a large number of case histories on full-scale lateral pile load tests by using the hyperbolic soil model proposed by Carter (1984). The results presented in Figure 2.17 show that the ratio of predicted to measured deflection with respect to pile diameter using Terzaghi's concept in which the initial modulus of subgrade reaction is independent of pile diameter underestimate the pile head displacement for pile diameter less than 1 m. However, it tends to overestimate the pile head deflection when the pile diameter larger than 1 m. By making a linear correction to the modulus of subgrade reaction suggested by Carter (1984) and Ling (1988), the ratio between the predicted to measures is very close to 1.0.

Previous reviews show that pile diameter has some effect on the  $p$ - $y$  curves. This contradicts the research by Terzaghi (1955). Terzaghi explained the influence of pile diameter on the coefficient of subgrade reaction by using the concept of a stress bulb to show that the larger pile diameter has a deeper stress influence than the smaller one as presented in Figure 2.18. Therefore, with an equivalent applied pressure, a larger pile diameter encounters greater displacement with simple proportion to the pile diameter resulting in a lower coefficient of subgrade reaction.

$$k_n = \frac{P}{y_n} = \frac{P}{ny_1} = \frac{k_1}{n} \quad (2.7)$$

where  $k_n, k_1$  = coefficient of subgrade reaction for pile diameter  $D$  and  $D_1$ , respectively,  $n = D/D_1$ , and  $p/y_1 = k_1$ . Terzaghi concluded that the coefficient of subgrade reaction is linearly proportional to the inverse of pile diameter. In other words, the modulus of subgrade reaction is independent of pile diameter. Due to the contradiction of pile diameter effect on  $p$ - $y$  curves, more research on this area needs to be continued.

#### 2.2.4.10 Development of $p$ - $y$ Curves for Layered Soils

The  $p$ - $y$  curves mentioned in the preceding sections are applied for homogeneous soil. However, the soil in reality usually consists of several soil layers. Some analytical studies have been performed by Davission and Gill (1963), Khadilkar *et al.* (1973), Naik and Peyrot (1976), and Dordi (1977) for two-layer soils to define pile length, the thickness of the upper layer, and the ratio of stiffness of the upper layer to the stiffness of the lower layer, on pile response. However, these analyses are based on simplified assumptions and do not consider the non-linearity of soil, which is one of the main advantages of the  $p$ - $y$  approach.

Georgiadis (1983) proposed a new approach to develop  $p$ - $y$  curves in a layered soil system. The soil layering is taken into account by computing equivalent depths for each of the underlying layers. The determination is presented schematically in Figure 2.19. The  $p$ - $y$  curves of the first soil layer are determined according to the standard criteria for homogeneous soils. To compute the  $p$ - $y$  curves of the second layer, the equivalent depth  $h_2$  of the top of this layer has to be previously determined. The force  $F_1$  required to induce the soil failure of the pile segment embedded to the bottom of the upper layer is computed by performing an integration of the ultimate resistance,  $p_{ul}$ , of the  $p$ - $y$  curves, over the thickness,  $H_1$ , of the first layer as:

$$F_1 = \int_0^{H_1} p_{ul} dH \quad (2.8)$$

The embedded depth,  $h_2$ , of the same pile in a material having the properties of the second layer is calculated so that the force required to cause failure is equal to  $F_1$ . This depth is the equivalent depth of the top of the second layer and is obtained from the solution of the following equation:

$$F_1 = \int_0^{h_2} p_{u2} dH \quad (2.9)$$

where the  $p_{u2}$  is the ultimate soil resistance of the  $p$ - $y$  curves which is a function of the equivalent depth, the actual overburden pressure and the strength properties of the second layer. When the equivalent depth of the top of the second layer has been determined the  $p$ - $y$  curves of this layer can be computed using the conventional  $p$ - $y$  criteria. The equivalent depth  $h_3$  and the  $p$ - $y$  curves of the third layer are obtained by the same procedure.

The lateral pile response predicted using this new approach and the homogeneous soil  $p$ - $y$  approach for layered soil were compared to field test results obtained from the literature. Excellent agreement was found between the field test results and those predicted by the new method in terms of both maximum bending moment and deflection. The pile response computed by the homogeneous soil properties throughout the entire depth, was found to either overestimate or underestimate the actual pile capacity with respect to the equivalent depth method and the field test results, depending on whether the upper layer is softer or stiffer than the underlying layer, respectively.

## 2.2.5 Other Methods

Besides the methods in analyzing the lateral pile behavior mentioned earlier, several other methods which cannot be categorized into the previous groups, have been summarized in the following sections.

### 2.2.5.1 Equivalent Cantilever Approach

A common method that structural engineers and the California Department of Transportation (Caltrans) often use to analyze the responses of laterally loaded piles is the equivalent cantilever method. In this method, the soil-pile system is replaced by an

equivalent cantilever fully restrained against translation and rotational at the base without surrounding soil as presented in Figure 2.20. The equivalent depth of fixity can be determined by equating the lateral stiffness of the soil-pile system to that of an equivalent fixed-base cantilever. The depth of fixity can be determined by trial and error until the equivalent system has the same displacement with the actual soil-pile system. Design charts based on this concept were developed to facilitate the design engineer to determine the depth of fixity for various soil types as presented in Figure 2.21.

In this method, the displacement ductility of the pile can be estimated as presented below (Budek, 1997).

The yield displacement can be determined as

$$\Delta_y = \frac{\phi_y (L_a + L_f)^2}{3} \quad (2.10)$$

where  $L_a$  = above-ground height,  $L_f$  = equivalent depth of fixity,  $\phi_y$  = yield curvature. The plastic rotation  $\theta_p$  is given by

$$\theta_p = L_p (\phi_u - \phi_y) \quad (2.11)$$

where  $L_p$  = plastic hinge length, and  $\phi_u$  = ultimate curvature.

The plastic displacement at the top of the pile can be written as:

$$\Delta_p = \theta_p (L_a + L_m) \quad (2.12)$$

where  $L_m$  = depth to maximum moment.

The displacement ductility of the pile can be then determined by

$$\mu_{\Delta} = \frac{\Delta_u}{\Delta_y} = 1 + \frac{\Delta_p}{\Delta_y} \quad (2.13)$$

The drawback of this method is that the depth to fixity is determined based on solutions for an elastic pile embedded in elastic soil. This assumption is not appropriate because the behavior of most soils is highly nonlinear. Second, the depth of maximum moment does not occur at the base of the cantilever but at a depth shallower than the equivalent depth to fixity. Third, current design practices usually assume that the depth of maximum moment occurs approximately  $2D$  below the ground surface with a plastic hinge length is equal to the pile diameter  $D$ . This value is based on intuition, without any test evidence or theoretical basis.

Chai and Hutchinson (1999) showed that the depth to maximum moment can be determined by assuming the ultimate soil pressure mobilized by the pile. The plastic hinge length based on the experimental test results of 4 reinforced concrete piles with two different above-ground heights showed that the plastic hinge length was about  $1.2D$  for the piles with an above ground height of  $2D$  and  $1.6D$  for those with an above ground height of  $6D$ .

#### 2.2.5.2 Strain Wedge Approach

Ashour and Norris (1998 and 2000) developed the new approach using a Strain Wedge (SW) model to predict the response of a flexible pile under the lateral loading. The strain wedge model parameters are related to a three-dimensional passive wedge of soil developing in front of the pile as presented in Figure 2.22. The basic purpose of the SW model is to relate stress-strain-strength behavior of the soil in the wedge using a Mohr-Coulomb representation of soil strength to the one dimensional beam on elastic

foundation parameters (BEF). Therefore, the response of the pile under lateral loading can be obtained by solving the fourth order differential equation (Eq. 2.3) with the BEF parameters.

The concept of the strain wedge method is that as the pile deflects, a growing passive wedge develops in front of the pile. The SW model is characterized by base angles  $\Theta_m$  and  $\beta_m$ , the current passive depth,  $h$ , and the spread of the wedge fan angle,  $\varphi_m$  (mobilized friction angle). The soil resistance consists of the horizontal stress change at the passive wedge face,  $\Delta\sigma_h$ , and the side shear,  $\tau$ , as shown in Figure 2.22a. It is assumed that the deflection pattern of the pile is taken to be linear over the controlling depth of the soil near the pile top, resulting in a linearized deflection angle,  $\delta$ , as presented in Figure 2.22b. Changes in the shape and depth of the passive wedge, together with changes in the state of loading and pile deflection, occur with the change in the uniform strain in the developing passive wedge.

An iterative procedure is used to evaluate  $h$  and  $\Theta_m$  under a given head load. As part of this procedure, at each point along the deflected pile, horizontal soil strain in front of the pile is related to stress level,  $SL$ . The horizontal stress,  $\Delta\sigma_h$ , is used to evaluate a passive resultant force, which when combined with a side shear force, yields quantity  $p$  in the  $p$ - $y$  curve. Quantity  $y$  is readily determined from strain,  $\varepsilon$ , and  $\Theta_m$ . Therefore, by varying the pile head load, the corresponding nonlinear  $p$ - $y$  curves can be obtained. The application of this method in the problem of multiple soil layers is also possible as presented in Figure 2.23.

The  $p$ - $y$  curves developed based on this concept show that they are not unique and change not only with soil properties, but also with the pile properties such as the pile stiffness, pile diameter, pile head fixity, and cross section. This is significantly different from the standard  $p$ - $y$  curves, where the  $p$ - $y$  curves are dependent on only the soil properties and pile diameter.

### 2.3 Full-Scale Pile Testing on Single Piles

Numerous full-scale lateral pile load tests (Table 2.14) have been conducted to understand the behavior of soil-structure interaction, varying from small diameter timber and steel pipe piles to large diameter cast-in-place shafts. The tests include static and cyclic loading in various types of soil. The tests were conducted by using the hydraulic jack or actuator to provide the applied force to the pile head. The displacement of the pile was measured using displacement transducers. Some of the tested piles were also instrumented with strain gauges to measure the moment along the pile and thus allow to back-calculated the  $p$ - $y$  curves. For instrumented piles where moment data is available, the data were used to back-calculate the  $p$ - $y$  curves. The method in constructing the  $p$ - $y$  curves for different soil types have been proposed as mentioned earlier. As can be seen from Table 2.14, these  $p$ - $y$  curves were developed based on the limited number of the tests, and then they were extrapolated for use with different soil strengths, and other pile diameters. As a result, the verification of these  $p$ - $y$  curves using further full-scale testing results is still necessary. Some of lateral load tests in the literature were conducted to compare the measured responses with the results from analyses using the available methods for estimating the pile responses, such as elastic continuum, subgrade reaction theory, and  $p$ - $y$  curve methods. Brief descriptions on some of these full-scale lateral tests are discussed below.

Weaver (2001) and Ashford and Rollins (2002) conducted full-scale lateral load tests in liquefied soil using controlled-blast technique at Treasure Island. The  $p$ - $y$  curves of liquefied soil at various excess pore pressure ratios were back-calculated based on the results of instrumented piles. They found that the characteristic shape of the liquefied  $p$ - $y$  curves is dramatically different from standard  $p$ - $y$  curves with the shape of the  $p$ - $y$  curves being concave up. The soil resistance increased as the excess pore water ratios decreased. Furthermore, the pile diameter has an effect on the  $p$ - $y$  curves in liquefied soil with the soil resistance being increased with the pile diameter.

Jayonan *et al.* (2001) conducted field testing on an extensively instrumented large diameter CIDH shaft/column (1.8 m in diameter) at a stiff clay site and developed the  $p$ - $y$  curves from section curvature measurements using the bilinear moment-curvature relationship. He stated that using the nonlinear moment-curvature relationship is an important feature of the results, as previous data reduction routines, by using linear moment-curvature relations, have lumped both shaft and soil nonlinearity into  $p$ - $y$  curves. The finding of this study indicates that the actual  $p$ - $y$  response near the ground surface is considerably stiffer than that predicted by existing models. Use of existing models would result in an underprediction of the failure load for the column and an overprediction of the plastic hinge depth relative to what was measured during the test.

Chai and Hutchinson (1999) investigated inelastic behavior of reinforced concrete piles in loose and dense dry sand with above ground height of  $6D$  and  $2D$  under cyclic lateral loading. A total of four 406 mm diameter reinforced concrete piles with a longitudinal steel of 2.1% and a confining steel ratio of 0.57 and 1.06% were used in test piles. The test piles were constructed as precast units and positioned in a container before the placement of soil. Then the soil was filled and compacted layer by layer using vibratory flat-plate compactor to achieve required soil density by controlling the layer thickness of each lift, number of pass per lift, and amount of input energy from the compactor. The test piles were instrumented with electrical resistance strain gauges along 4 longitudinal steel bars and four principal directions of spiral, curvature rods with linear potentiometer, and inclinometers. The load cell in the actuator, together with linear potentiometers at the pile head, were used to obtain load-displacement characteristics as well as pile head rotations. The test results showed that all four test piles exhibited a ductile behavior even though fairly low transverse reinforcement ratio of about  $\frac{1}{2}$  of that required by the Applied Technology Council (ATC-32) was used. Surprisingly, test results indicated that the maximum lateral force of the soil-pile system was not sensitive to the soil density. However, the depth of maximum moment appeared to decrease with an increase in soil density and an increase in the above ground height. Furthermore, the

kinematic model based on the equivalent fixed base cantilever concept was proposed to simulate the curvature ductility demand. The model was shown to provide a reasonable prediction of ductility demand upon yielding of the pile. No  $p$ - $y$  curves were developed in this study.

Some of the other main findings observed from other lateral pile load tests listed in Table 2.14 are summarized as the following:

1. Vertical pile can provide some resistance against lateral loading.
2. The lateral pile response is dominated by the soil at shallow depth. If the pile length is longer than an effective length, there is no change on the pile response.
3. Cyclic loading causes an increase in total deflection. The first cycle causes significant more cyclic degradation than during the next other cycles. After a large number of cycles of loading, a soil pile system tends to be stabilized.
4. Load displacement curve of laterally loaded pile appears to be highly nonlinear due to the effect of soil nonlinearity.
5. The characteristic of  $p$ - $y$  curves are highly nonlinear, inelastic, and dependent on the soil type.
6. The  $p$ - $y$  curve characteristics appear to be independent of pile-head restraint. (Matlock, 1970).

Though many full-scale testing have been conducted to study the behavior of laterally loaded pile, some important issues have not been yet resolved. These include the effect of pile installation, the behavior of pile in cemented sand, the effect of pile diameter on  $p$ - $y$  curves, and application of  $p$ - $y$  curves for rigid piles. For this reason, further full-scale testing is still needed to provide further insight into behavior of soil-pile interaction and resolve these problems.

## 2.4 Inelastic Behavior of Concrete Piles

For most bridges, the foundation systems are usually designed to remain elastic during an earthquake. However, in many cases the plastic hinging in the members of the foundations system cannot be avoided during severe earthquakes (e.g., using integral pile shaft-column). Research has been conducted to study the inelastic behavior of piles (i.e., Ikeda *et al.*, 1982; Banerjee *et al.*, 1987; Falconer and Park, 1982; Pam *et al.*, 1988; and Muguruma *et al.*, 1987). However, all of these tests were performed on prestressed concrete piles in the laboratory without the soil. Recent research by Budek (1997) showed that external confinement, such as from soil, plays a very significant role in pile shaft response. Budek performed the load test on piles by using a group of neoprene-lined saddles extending 100° around the circumference of shaft, top and bottom, to simulate the lateral confinement by soil. Figure 2.24 presents a comparison of load-displacement curves of the piles with and without the effect of external confinement. It shows that the confining pressure provided by the external confinement can significantly increase the effective confinement on the section and retard localized plastic rotation and that only moderate levels of transverse reinforcement are needed for adequate seismic performance.

## 2.5 Typical Behavior of Cemented Soil

In this research, the full-scale lateral loaded pile tests were conducted in weakly cemented soil. A review of a typical behavior of cemented soil is summarized in the following paragraphs.

Cemented soils are found in many areas in the world. Examples include marine terrace deposits along the Pacific coast of the United States, loess deposits in the mid-west United States and China, and volcanic ash deposits in Japan and Guatemala (Sitar, 1990). Cemented sands are characterized by their ability to stand in very steep natural slopes. The common cementing agents are silica, clays, carbonates, and iron oxides. It

seems that the relatively undisturbed samples of this soil types for laboratory testing is very difficult, and that conventional geotechnical design would usually tend to be conservative and neglect the presence of cementation.

Saxena and Lastrico (1978) studied the behavior of lightly cemented sand under static loading. They found that the at low strain level the soil strength from the cohesion component was predominant whereas the strength from friction component governed the soil behavior at the high strain levels.

Clough *et al.* (1981) investigated behavior of cemented soils to use in a study of investigation of slope behavior in cemented soils. A total of 137 laboratory tests were performed on four samples of naturally occurring cemented soils and on artificially cemented soils fabricated to simulate the natural soil behavior. The artificially cemented soils were used because it is difficult to obtain undisturbed specimens of the sensitive natural slope. Furthermore, the artificially cemented soils allow evaluating the effects of amount of cementing agent and sand density on soil response. The artificially cemented soils were prepared by mixing Type II Portland cement and a uniform sand together with a water content of 8%. It was found from basic properties of four naturally cemented soils that the more well-cemented soils have a significant fraction of fines. The laboratory tests consisted of drained triaxial compression, Brazilian, and simple shear tests. The tests results of naturally cemented soil indicated that the stiffness and peak strength increases with increasing of confining stress. The strongly cemented soil showed the brittle failure behavior at all confinements, while the moderate and weakly cemented soil showed a transitional response from brittle failure to ductile failure as confining pressures increase as presented in Figure 2.25. The volumetric strain increases during shearing, however decreases as confining pressure increases. Although Clough *et al.* concluded that the initial modulus of cemented soil increases with increasing confining pressure, it seemed that the stiffness of initial slope is independent of confining

pressure as presented in Figure 2.25c and Figure 2.25d. Based on the artificially cemented soil test results, the following conclusion can be drawn.

1. The peak strength increases with degree of cementation.
2. The strain at peak strength mobilization decreases with degree of cementation.
3. The volumetric strain increase during shear is concentrated over a small strain range and occurs at a lower strain as degree of cementation increases.
4. The residual strength of cemented sand is close to that of uncemented sand.

Table 2.1 Summary of Elastic Solutions for Laterally Loaded Pile for the Case of Constant Soil Modulus with Depth (after Poulos, 1971)

Pile Response	Free-Head Pile	Fixed-Head Pile
Pile Head Displacement ( $u$ )	$u = I_{UH} \left( \frac{H}{E_s L} \right) + I_{UM} \left( \frac{M}{E_s L^2} \right)$	$u = I_{UF} \left( \frac{H}{E_s L} \right)$
Pile Head Rotation ( $\theta$ )	$\theta = I_{\theta H} \left( \frac{H}{E_s L} \right) + I_{\theta M} \left( \frac{M}{E_s L^3} \right)$	0
Maximum Moment ( $M_z$ ) <sub>max</sub> for Free-Head Pile or Fixing Moment at Pile Head ( $M_f$ ) for Fixed-Head Pile	From Figure 2.1	From Figure 2.1

Note:

$$K_R = \frac{E_p I_p}{E_s L^4}$$

- where:  $D$  = Pile diameter  
 $E_p$  = Modulus of elasticity of pile  
 $E_s$  = Soil modulus  
 $H$  = Applied horizontal force at ground level  
 $I_p$  = Moment of inertia of pile  
 $I_{UH}, I_{UM}, I_{\theta H}, I_{\theta M}, I_{UF}$  = Dimensionless Elastic influence factors (from Figure 2.1)  
 $K_R$  = Pile flexibility factor,  
 $L$  = Pile length  
 $M$  = Moment at ground level  
 $\nu_s$  = Poisson's ratio

Table 2.2 Summary of Elastic Solutions for Laterally Loaded Pile for the Case of Constant Soil Modulus with Depth (after Davies and Budhu, 1986)

Pile Response	Free-Head Pile	Fixed-Head Pile
Pile Head Displacement ( $u$ )	$u = I_{UH} \frac{H}{E_s D} + I_{UM} \frac{M}{E_s D^2}$ <p>where <math>I_{UH} = 1.3K^{-2/11}</math></p> $I_{UM} = I_{\theta H} = 2.2K^{-2/11}$	$u = I_{FH} \frac{H}{E_s D}$ <p>where <math>I_{FH} = 0.80K^{-2/11}</math></p>
Pile Head Rotation ( $\theta$ )	$\theta = I_{\theta H} \frac{H}{E_s D^2} + I_{\theta M} \frac{M}{E_s D^3}$ <p>where <math>I_{\theta M} = 9.2K^{-8/11}</math></p>	0
Maximum Moment ( $M_M$ ) for Free-Head Pile or Fixing Moment at Pile Head ( $M^F$ ) for Fixed-Head Pile	$M_M = I_{MH} HD$ <p>where <math>I_{MH} = 0.12K^{3/11}</math></p>	$M^F = -I_{MF} HD$ <p>where <math>I_{MF} = 0.24K^{3/11}</math></p>
Location of Maximum Moment ( $L_M$ )	$L_M = 0.20DK^{4/11}$	--

Note:

$$K = E_p / E_s$$

where:  $D$  = Pile diameter  
 $E_p$  = Modulus of elasticity of pile  
 $E_s$  = Soil modulus  
 $H$  = Applied horizontal force at ground level  
 $I_{UH}, I_{UM}, I_{\theta H}, I_{\theta M}, I_{MH}, I_{MF}$  = Compliance factor  
 $K$  = Pile stiffness ratio  
 $L$  = Pile length  
 $M$  = Moment at ground level

Table 2.3 Summary of Elastic Solutions for Laterally Loaded Pile for the Case of Linearly Increasing Soil Modulus with Depth (after Budhu and Davies, 1988)

Pile Response	Free-Head Pile	Fixed-Head Pile
Pile Head Displacement ( $u$ )	$u = I_{UH} \frac{H}{mD^2} + I_{UM} \frac{M}{mD^3}$ <p>where <math>I_{UH} = 3.2K^{-3/9}</math></p> $I_{UM} = I_{\theta H} = 5.0K^{-5/9}$	$u = I_{FH} \frac{H}{mD^2}$ <p>where <math>I_{FH} = 1.4K^{-3/9}</math></p>
Pile Head Rotation ( $\theta$ )	$\theta = I_{\theta H} \frac{H}{mD^3} + I_{\theta M} \frac{M}{mD^4}$ <p>where <math>I_{\theta M} = 13.6K^{-7/9}</math></p>	0
Maximum Moment ( $M_M$ ) for Free-Head Pile or Fixing Moment at Pile Head ( $M^F$ ) for Fixed-Head Pile	$M_M = I_{MH} HD$ <p>where <math>I_{MH} = 0.3K^{2/9}</math></p>	$M^F = -I_{MF} HD$ <p>where <math>I_{MF} = 0.4K^{2/9}</math></p>
Location of Maximum Moment ( $L_M$ )	$L_M = 0.53DK^{2/9}$	--

Note:

$$K = E_p / mD$$

$$E_s = mz$$

where:  $D$  = Pile diameter  
 $E_p$  = Modulus of elasticity of pile  
 $E_s$  = Soil modulus  
 $H$  = Applied horizontal force at ground level  
 $I_{UH}, I_{UM}, I_{\theta H}, I_{\theta M}, I_{MH}, I_{MF}$  = Compliance factor  
 $K$  = Pile stiffness ratio  
 $L$  = Pile length  
 $m$  = Constant (Rate of increasing soil modulus with depth)  
 $M$  = Moment at ground level

Table 2.4 Summary of Definition and Dimension of Terms Used in Analysis of Laterally Loaded Piles

Description	Symbol	Definition	Dimension
Soil resistance per unit length	$p$		F/L
Pile deflection	$y$		L
Pile diameter	$D$		L
Spring spacing	$\Delta L$		L
Spring force	$F$	$F = p * \Delta L$	F
Soil pressure	$P$	$P = p/D$	F/L <sup>2</sup>
Modulus of subgrade reaction	$K$	$K = p/y$	F/L <sup>2</sup>
Soil spring stiffness	$K_s$	$K_s = F/y,$ $K_s = K * \Delta L$	F/L
Coefficient of subgrade reaction	$k$	$k = P/y, k = K/D$	F/L <sup>3</sup>

Table 2.5 Summary of Solutions for Laterally Loaded Pile due to Horizontal Loading for the Case of Constant Subgrade Reaction (Hetenyi, 1946)

Pile Response	Due to Horizontal Loading, $H$
Pile Displacement ( $u$ )	$u = \left( \frac{2H\beta}{k_h D} \right) \left( \frac{\sinh \beta L \cos \beta z \cosh \beta(L-z) - \sin \beta L \cosh \beta(L-z)}{\sinh^2 \beta L - \sin^2 \beta L} \right)$
Pile Rotation ( $\theta$ )	$\theta = \left( \frac{2H\beta^2}{k_h D} \right) \left( \frac{1}{\sinh^2 \beta L - \sin^2 \beta L} \right) \left( \sinh \beta L [\sin \beta z \cosh \beta(L-z) + \cos \beta z \sinh \beta(L-z)] + \sin \beta L [\sinh \beta z \cos \beta(L-z) + \cosh \beta z \sin \beta(L-z)] \right)$
Shear Force ( $Q$ )	$Q = - \left( \frac{H}{\sinh^2 \beta L - \sin^2 \beta L} \right) \left( \sinh \beta L [\cos \beta z \sinh \beta(L-z) - \sin \beta z \cosh \beta(L-z)] - \sin \beta L [\cosh \beta z \sin \beta(L-z) - \sinh \beta z \cos \beta(L-z)] \right)$
Moment ( $M$ )	$M = - \left( \frac{H}{\beta} \right) \left[ \frac{\sinh \beta L \sin \beta z \sinh \beta(L-z) - \sin \beta L \sinh \beta z \sin \beta(L-z)}{\sinh^2 \beta L - \sin^2 \beta L} \right]$

where :  $\beta = \left( \frac{k_h D}{4E_p I_p} \right)^{1/4}$

- $D$  = Pile Diameter
- $E_p I_p$  = Pile Stiffness
- $k_h$  = Coefficient of Subgrade Reaction
- $z$  = Depth

Table 2.6 Summary of Solutions for Laterally Loaded Pile due to Moment Loading for the Case of Constant Subgrade Reaction (Hetenyi, 1946)

Pile Response	Due to Moment Loading, $M_0$
Pile Displacement ( $u$ )	$u = \frac{2M_0\beta^2}{k_h D} \left( \frac{1}{\sinh^2 \beta L - \sin^2 \beta L} \right)$ $\left( \sinh \beta L [\cosh \beta(L-z) \sin \beta z - \sinh \beta(L-z) \cos \beta z] \right.$ $\left. + \sin \beta L [\sinh \beta z \cos \beta(L-z) - \cosh \beta z \sin \beta(z-L)] \right)$
Pile Rotation ( $\theta$ )	$\theta = \left( \frac{4M_0\beta^3}{k_h D} \right)$ $\left[ \frac{\sinh \beta L \cosh \beta(L-z) \cos \beta z + \sin \beta L \cosh \beta z \cos \beta(L-z)}{\sinh^2 \beta L - \sin^2 \beta L} \right]$
Shear Force ( $Q$ )	$M = \frac{M_0}{\sinh^2 \beta L - \sin^2 \beta L} \left( \begin{array}{l} \sinh \beta L \left[ \begin{array}{l} \sinh \beta(L-z) \cos \beta z + \\ \cosh \beta(L-z) \sin \beta z \end{array} \right] \\ - \sin \beta L \left[ \begin{array}{l} \sinh \beta z \cos \beta(L-z) + \\ \cosh \beta z \sin \beta(L-z) \end{array} \right] \end{array} \right)$
Moment ( $M$ )	$Q = \frac{-2M_0\beta}{\sinh^2 \beta L - \sin^2 \beta L} \left[ \begin{array}{l} \sin \beta L \sin \beta(L-z) \sin \beta z + \\ \sin \beta L \sinh \beta z \sin \beta(L-z) \end{array} \right]$

where :  $\beta = \left( \frac{k_h D}{4E_p I_p} \right)^{1/4}$

- $D$  = Pile Diameter  
 $E_p I_p$  = Pile Stiffness  
 $k_h$  = Coefficient of Subgrade Reaction  
 $z$  = Depth

Table 2.7 Summary of Procedure in Developing Soft Clay  $p$ - $y$  Curves (Matlock, 1970)

**Static Loading**

1. Compute Ultimate Soil Resistance, $p_u$ (Using the smaller values)	$p_u = \left[ 3 + \frac{\gamma'}{c_u} z + \frac{J}{D} z \right] c_u D$ $p_u = 9c_u D$
2. Compute Deflection at One-Half the Ultimate Soil Resistance, $y_{50}$	$y_{50} = 2.5\varepsilon_{50} D$
3. Develop $p$ - $y$ Curves using the following Expression	$\frac{p}{p_{ult}} = 0.5 \left( \frac{y}{y_{50}} \right)^{1/3}$

**Cyclic Loading**

1. Develop $p$ - $y$ Curves	Construct $p$ - $y$ curves in the same manner as for static loading for values of $p$ less than $0.72 p_u$
2. Determine Transition Depth, $z_r$	$z_r = \frac{6c_u D}{(\gamma' D + Jc_u)}$
3. If the depth is greater than or equal $z_r$	$p = 0.72 p_u \text{ for } y > 3y_{50}$
4. If the depth is less than $z_r$	$p = 0.72 p_{ult} \quad \text{at } y = 3y_{50} \text{ and}$ $p = 0.72 p_{ult} \left( \frac{z}{z_r} \right) \quad \text{at } y = 15y_{50}$

where:  $c_u$  = Undrained Shear Strength  
 $D$  = Pile Diameter  
 $J$  = Constant (0.5 for Soft Clay and 0.25 for Medium Clay)  
 $p_u$  = Ultimate Soil Resistance  
 $y_{50}$  = Deflection at One-Haft the Ultimate Soil Resistance  
 $z$  = Depth  
 $z_r$  = Transition Depth  
 $\gamma'$  = Effective Soil Unit Weight  
 $\varepsilon_{50}$  = Strain at One-Haft the Ultimate Soil Resistance  
 0.020 for soft clay, 0.010 for medium clay, and 0.005 for stiff clay

Table 2.8 Summary of Procedure in Developing Stiff Clay with Free Water  $p$ - $y$  Curves (Reese *et al.*, 1975)

<b>Static Loading</b>	
1. Compute Ultimate Soil Resistance, $p_u$ (Using the smaller values)	$p_{ut} = 2c_a D + \gamma' D z + 2.83c_a z$ (Wedge Failure) $p_{ud} = 11c_u D$ (Flow Failure)
2. Establish Initial Straight Line Portion	$p = (k_s z)y$ for Static, $p = (k_c z)y$ for Cyclic
3. Develop $p$ - $y$ Curves using the following Expression	$p = 0.5 p_u \left( \frac{y}{y_{50}} \right)^{0.5}$ , $y_{50} = \epsilon_{50} D$
4. Develop the Second Parabolic Portion of the $p$ - $y$ Curves (from $A_s y_{50}$ to $6A_s y_{50}$ )	$p = 0.5 p_u \left( \frac{y}{y_{50}} \right)^{0.5} - 0.055 p_u \left( \frac{y - A_s y_{50}}{A_s y_{50}} \right)^{1.25}$
5. Establish Straight-Line Portion (from $6A_s y_{50}$ to $18A_s y_{50}$ )	$p = 0.5 p_u (6A_s)^{0.5} - 0.411 p_u - \frac{0.0625}{y_{50}} p_u (y - 6A_s y_{50})$
6. Establish Final Straight-Line Portion (beyond $18A_s y_{50}$ )	$p = 0.5 p_u (6A_s)^{0.5} - 0.411 p_u - 0.75 p_u A_s$

### **Cyclic Loading**

1. Follow Step 1 to 3 of Static Case	Follow Step 1 to 3 of Static Case
2. Establish Parabolic Portion (up to $0.6 y_p$ )	$p = A_c p_u \left[ 1 - \left  \frac{y - 0.45 y_p}{0.45 y_p} \right ^{2.5} \right]$ , $y_p = 4.1 A_c y_{50}$
3. Establish Straight-Line Portion (from $0.6 y_p$ to $1.8 y_p$ )	$p = 0.936 A_c p_u - \frac{0.085}{y_{50}} p_u (y - 0.6 y_p)$
4. Establish Final Straight-Line Portion (beyond $1.8 A_s y_{50}$ )	$p = 0.936 A_c p_u - \frac{0.102}{y_{50}} p_u y_p$

where:  $A_s, A_c$  = Constants (from Figure 2.7c)  
 $c_a$  = Average Undrained Shear Strength over Depth  $z$   
 $c_u$  = Undrained Shear Strength  
 $D$  = Pile Diameter  
 $k_s, k_c$  = Initial Subgrade Reaction Constant for Static and Cyclic Loading  
 $y_{50}$  = Deflection at One-Haft the Ultimate Soil Resistance  
 $z$  = Depth  
 $\epsilon_{50}$  = Strain at One-Haft the Ultimate Soil Resistance (0.004-0.007)  
 $\gamma'$  = Effective Soil Unit Weight

Table 2.9 Summary of Procedure in Developing Stiff Clay with No Free Water  $p$ - $y$  Curves (Welch and Reese, 1972;and Reese and Welch, 1975)

### Static Loading

1. Compute Ultimate Soil Resistance, $p_u$ (Using the smaller values)	$p_u = \left[ 3 + \frac{\gamma'}{c_u} z + \frac{J}{D} z \right] c_u D$ $p_u = 9c_u D$
2. Compute Deflection at One-Half the Ultimate Soil Resistance, $y_{50}$	$y_{50} = 2.5\varepsilon_{50} D$
3. Develop $p$ - $y$ Curves using the following Expression	$\frac{p}{p_u} = 0.5 \left( \frac{y}{y_{50}} \right)^{1/4} \quad \text{for } y \leq 16y_{50}$ $p = p_u \quad \text{for } y > 16y_{50}$

### Cyclic Loading

1. Develop $p$ - $y$ Curves for Static Loading	Follow Step 1 to 3
2. Determine Parameter Describing Effect of Repeated Loading, $C$	$C = 9.6 \left( \frac{p}{p_u} \right)^4$
3. Determine $y$ for Cyclic Loading, $y_c$	$y_c = y_s + y_{50} C \log N$

where:  $c_u$  = Undrained Shear Strength  
 $D$  = Pile Diameter  
 $J$  = Constant = 0.5  
 $N$  = Number of Cycles  
 $p_{ult}$  = Ultimate Soil Resistance  
 $y_{50}$  = Deflection at One-Haft the Ultimate Soil Resistance  
 $y_c$  = Deflection under  $N$ -Cycles of Load  
 $y_s$  = Deflection under Short-Term Static  
 $z$  = Depth  
 $\varepsilon_{50}$  = Strain at One-Haft the Ultimate Soil Resistance  
 0.020 for soft clay, 0.010 for medium clay, and 0.005 for stiff clay  
 $\gamma'$  = Effective Soil Unit Weight

Table 2.10 Summary of Procedure in Developing Sand  $p$ - $y$  Curves (Reese *et al.*, 1974)

1. Preliminary Computation	$\alpha = \frac{\phi}{2}, \beta = 45 + \frac{\phi}{2}, K_0 = 0.4, K_a = \tan^2\left(45 - \frac{\phi}{2}\right)$
2. Theoretical Ultimate Soil Resistance due to Wedge Failure, $p_{st}$	$p_{st} = \gamma' z \left[ \frac{K_0 z \tan \phi \sin \beta}{\tan(\beta - \phi) \cos \alpha} + \frac{\tan \beta}{\tan(\beta - \phi)} (D + z \tan \beta \tan \alpha) \right] + K_0 z \tan \beta (\tan \phi \sin \beta - \tan \alpha) - K_a D$
3. Theoretical Ultimate Soil Resistance due to Flow Failure, $p_{sd}$	$p_{sd} = K_a D \gamma' z (\tan^8 \beta - 1) + K_0 D \gamma' z \tan \phi \tan^4 \beta$
4. Govern Theoretical Ultimate Soil Resistance, $p_s$	$p_s = \text{the smaller of the values given from step 2 and 3}$
5. Ultimate Soil Resistance, $p_u$	$p_u = \bar{A}_s p_s$ for static loading or $p_u = \bar{A}_c p_s$ for cyclic loading
6. Soil Pressure at D/60	$p_m = B_s p_s$ for static loading or $p_m = B_c p_s$ for cyclic loading
7. Establish Initial Straight Line Portion	$p = (kz)y$
8. Establish Parabolic Section of $p$ - $y$ Curves	$p = \bar{C} y^{1/n}, m = \frac{p_u - p_m}{y_u - y_m}, n = \frac{p_m}{m y_m}, \bar{C} = \frac{p_m}{y_m^{1/n}}, y_k = \left( \frac{\bar{C}}{kz} \right)^{n-1}$

where:  $\bar{A}_s, \bar{A}_c =$  Adjustment Coefficient for Static and Cyclic  $p$ - $y$  Curves from Figure 2.9a

$B_s, B_c =$  Nondimensional Coefficient for Static and Cyclic  $p$ - $y$  Curves from Figure 2.9b

$D =$  Pile Diameter

$k =$  Initial Subgrade Reaction Constant (MN/m<sup>3</sup>)

Loose Sand (Submerge/above water)	5.4/ 6.8
Medium Dense Sand	16.3/ 24.4
Dense Sand	34/ 61

$p_{sd} =$  Theoretical Ultimate Soil Resistance due to Flow Failure

$p_{st} =$  Theoretical Ultimate Soil Resistance due to Wedge Failure

$p_s =$  Govern Ultimate Soil Resistance

$p_u =$  Ultimate Soil Resistance

$z =$  Depth

$\phi =$  Friction Angle

$\gamma' =$  Effective Soil Unit Weight for Soil under Water

Table 2.11 Summary of Procedure in Developing API Sand  $p$ - $y$  Curves (API, 1987)

1. Theoretical Ultimate Soil Resistance due to Wedge Failure, $p_{st}$	$p_{st} = (C_1 z + C_2 D) \gamma' z$
2. Theoretical Ultimate Soil Resistance due to Flow Failure, $p_{sd}$	$p_{sd} = C_3 D \gamma' z$
3. Govern Theoretical Ultimate Soil Resistance, $p_s$	$p_s$ = the smaller of the values given from step 2 and 3
4. Determine Adjustment Coefficient for Static and Cyclic Loading	$\bar{A}_s = \left( 3.0 - 0.8 \frac{z}{D} \right) \geq 0.9 \text{ for static lading}$ $\bar{A}_c = 0.9 \text{ for cyclic loading}$
5. Develop Characteristic Shape of $p$ - $y$ Curves	$p = \bar{A} p_s \tanh \left( \frac{kz}{\bar{A} p_u} y \right)$

where:  $\bar{A}_s, \bar{A}_c$  = Adjustment Coefficient for Static and Cyclic  $p$ - $y$  Curves  
 $C_1, C_2, C_3$  = Coefficients from Figure 2.12a  
 $D$  = Pile Diameter  
 $k$  = Initial Subgrade Reaction Constant (MN/m<sup>3</sup>)  
 from Figure 2.12b  
 $p_{sd}$  = Theoretical Ultimate Soil Resistance due to Flow Failure  
 $p_{st}$  = Theoretical Ultimate Soil Resistance due to Wedge Failure  
 $p_s$  = Govern Ultimate Soil Resistance  
 $p_u$  = Ultimate Soil Resistance  
 $z$  = Depth  
 $\phi$  = Friction Angle  
 $\gamma'$  = Effective Soil Unit Weight for Soil under Water

Table 2.12 Summary of Procedure in Developing Cemented Sand  $p$ - $y$  Curves (Ismael, 1990)

1. Ultimate Soil Resistance, $p_u$	$p_u = C_p \sigma_p D$
2. Correction Factor, $C_p$	$C_p = 1.5$ for $\phi \leq 15^\circ$ $C_p = \frac{\phi}{10}$ for $\phi > 15^\circ$
3. Passive Earth Pressure, $\sigma_p$	$\sigma_p = 2c \tan\left(45 + \frac{\phi}{2}\right) + \sigma_v \tan^2\left(45 + \frac{\phi}{2}\right)$
4. Characteristic Shape of $p$ - $y$ Curves	$\frac{p}{p_u} = 0.5 \left(\frac{y}{y_{50}}\right)^{1/3}$
5. Pile Deflection at which $p = 0.5p_u$ , $y_{50}$	$y_{50} = 2.5\varepsilon_c D$

where:

$c$	=	Soil Cohesion
$C_p$	=	Correction Factor for Small Width of Pile
$D$	=	Pile Diameter
$p_u$	=	Ultimate Soil Resistance
$y_{50}$	=	Pile Deflection at $p = 0.5p_u$
$\phi$	=	Soil Friction Angle
$\sigma_p$	=	Passive Earth Pressure
$\sigma_v$	=	Effective Vertical Stress
$\varepsilon_c$	=	Strain at $(\sigma_1 - \sigma_3) = 0.5(\sigma_1 - \sigma_3)_u$
$(\sigma_1 - \sigma_3)_u$	=	Ultimate Principal Stress Difference in Triaxial Test
$\sigma_1$	=	Major Principal Stress
$\sigma_3$	=	Minor Principal Stress

Table 2.13 Summary of Procedure in Developing Silt  $p$ - $y$  Curves (Reese and Van Impe, 2001)

1. Preliminary Computation	$\alpha = \frac{\phi}{2}, \beta = 45 + \frac{\phi}{2}, K_0 = 0.4, K_a = \tan^2\left(45 - \frac{\phi}{2}\right)$
2. Ultimate Soil Resistance, $p_u$	$p_u = \overline{A}_s p_{u\phi} + p_{uc}$ for Static $p_{ult} = \overline{A}_c p_{ult\phi} + p_{ultc}$ for Cyclic
2. Friction Component, $p_{u\phi}$ (The smaller values from these 2 Eqs.)	$p_{u\phi} = \gamma' z \left[ \frac{K_o \tan \phi \sin \beta}{\tan(\beta - \phi) \cos \alpha} + \frac{\tan \beta}{\tan(\beta - \phi)} (D + z \tan \beta \tan \alpha) \right]$ $+ \gamma' z [K_o z \tan \beta (\tan \phi \sin \beta - \tan \alpha) - K_a D]$ $p_{u\phi} = K_a D \gamma' z (\tan^8 \beta - 1) + K_o D \gamma' z \tan \phi \tan^4 \beta$
3. Cohesion Component, $p_{uc}$ (The smaller values from these 2 Eqs.)	$p_{uc} = \left( 3 + \frac{\gamma'}{c} z + \frac{J}{D} z \right) c D$ $p_{uc} = 9cD$
4. Soil Pressure at $D/60$	$p_m = B_s p_s$ for Static Loading or $p_m = B_c p_s$ for Cyclic Loading
5. Establish Initial Straight Line Portion	$p = (k_{py} z) y, k_{py} = k_c + k_\phi$ $k_c$ from Figure 2.15b
6. Establish Parabolic Section of $p$ - $y$ Curves	$p = \overline{C} y^{1/n}, m = \frac{p_u - p_m}{y_u - y_m}, n = \frac{p_m}{m y_m}, \overline{C} = \frac{p_m}{y_m^{1/n}}, y_k = \left( \frac{\overline{C}}{k_{py} z} \right)^{n-1}$

where:

$c$	=	Soil Cohesion
$D$	=	Pile Diameter
$J$	=	Constant
$k_c, k_f$	=	Initial Subgrade Reaction Constant from Cohesion and Friction Components, Respectively (from Figure 2.15)
$p_s$	=	Govern Ultimate Soil Resistance (from Step 4 of Table 2.4)
$k_{py}$	=	Initial Subgrade Reaction Constant
$p_u$	=	Ultimate Soil Resistance
$p_\phi$	=	Ultimate Soil Resistance from Friction Component
$p_c$	=	Ultimate Soil Resistance from Cohesion Component
$z$	=	Depth
$\phi$	=	Friction Angle
$\gamma'$	=	Effective Soil Unit Weight

Table 2.14 Summary of Case Histories of Laterally Loaded Single Piles

No.	Reference (Year)	Pile Type	Pile Dia.	Pile Length	Soil Condition	Loading	Moment Data	Summary of Work
1	Ashford and Rollins (2002), Weaver (2001)	1 Steel Pipe Pile 2 CIPSS Piles	0.3 m 0.6m-0.9m	11.6 m 13.6 m-14.3 m	Liquefied Sand	Static/Cyclic	Yes	Back-calculated p-y Curves
2	Jayman et al. (2001)	1 Drilled Shaft	1.8-m	12.2 m	Silty Clay	Cyclic	Yes	Back-calculated p-y Curves Study includes Examination of Pile and Develop Kinematic Model for Analyze Behavior of Laterally Loaded Pile
3	Chai and Hutchinson (1999)	4 Concrete Piles	0.4m	5.4m	Loose and Dense Sand	Cyclic	Yes	Compare with LPILE and Propose Methodology for Developing p-y Curves
4	Ismail (1990)	12 Bored Piles	0.3 m	3m-5m	Medium Dense Cemented Sand	Static	Yes	Comparison with COM624
5	Narumbe and Feng (1980)	4 Drilled Shaft	1.2m-2.4m	16.2m-21.6m	Stiff and Clay	Static/Cyclic	Yes	Back-calculated p-y Curves and Proposed Modification on Clay p-y Curves
6	Dunavant and O'Neill (1989)	2 Steel Pipe Piles 1 Drilled Shaft	0.27m-1.2m 1.66 m	11.4m-11.8 m 11.4 m	Submerged Clay	Static/Cyclic	Yes	Compared with Pressuremeter Test Results
7	Little and Elnad (1988)	4 Drilled Shafts 1 Square Prestress Pile 1 Steel Pipe Pile	0.9m-1m 0.5 m 0.6 m	29.1m-36.4 m 29.4 m 36 m	Medium Dense Sand	Static/Cyclic	No	
8	Monson (1988)	1 Steel Pipe Pile	0.29 m	12.7 m	Stiff Clay and Compacted Sand	Static/Cyclic	No	Back-Calculated p-y Curves and Compared to Standard p-y Curves
9	Tucker and Elnad (1988)	2 HP-Piles	H14x73	20.1 m	Medium to Dense Sand	Static/Cyclic	No	Comparison with LPILE and Pressuremeter Test Results
10	Long and Reese (1984)	2 CIPSS Piles	1.22 m	13.1 m	Dense Sand to Stiff Clay	Static/Cyclic	Yes	Comparison with COM624
11	Blustian et al. (1991)	7 Drilled Shafts	0.6m-1.2m	5.2m-5.5m	Medium to Dense Sand	Static/Cyclic	No	Compared with Bromis, LPILE and Elastic Continuum Methods
12	Reese et al. (1974)	2 Steel Pipe Pile	0.6 m	21 m	Submerged Dense Sand	Static/Cyclic	Yes	Propose Method to develop p-y Curves
13	Reese et al. (1975)	2 Steel Pipe Pile	0.6 m	15.2 m	Stiff Clay below Water Table	Static/Cyclic	Yes	Propose Method to develop p-y Curves
14	Weich and Reese (1972), Reese and Welch (1975)	1 Drilled Shaft	0.76 m	13 m	Stiff Clay above Water Table	Static/Cyclic	Yes	Propose Method to develop p-y Curves
15	Alizadeh and Davison (1970)	3 Pipe Piles 4 HP-Piles	0.40.5 m	12.6m-16.5m	Medium Dense Sand w/ Ground Water Table	Static/Cyclic	Yes	
16	Mattlock (1970)	1 Steel Pipe Pile 3 Concrete Piles	0.3 m	12.6 m	Soft Clay	Static/Cyclic	Yes	Compared with Subgrade Reaction Theory -- Generalized Solution (Mattlock and Reese 1960) Propose Method to develop p-y Curves
17	Alizadeh (1969)	4 Timber Piles	0.3m	13.2m	Sand, Gravel, Clay	Static/Cyclic	Yes	Comparison with Subgrade Reaction Theory (Dawson and Gill (1963), Reese and Mattlock (1965))
18	Dawson and Saffley (1969)	4 Drilled Shafts	1.2m	4.3m-14.4m	Medium Dense Sand w/ Ground Water Table	Static/Cyclic	Yes	Reported Test Data and Discussion
19	McNulty (1966)	3 Taper Concrete Piles	0.6 m	4.2m-6.1 m	Medium Dense Silty Sand	Static	No	Reported Test Data and Discussion
20	McClelland and Focht (1966)	1 Steel Pipe Pile	0.6 m	22.6 m	Soft Clay	Static/Dynamic	Yes	Back-calculated p-y Curves

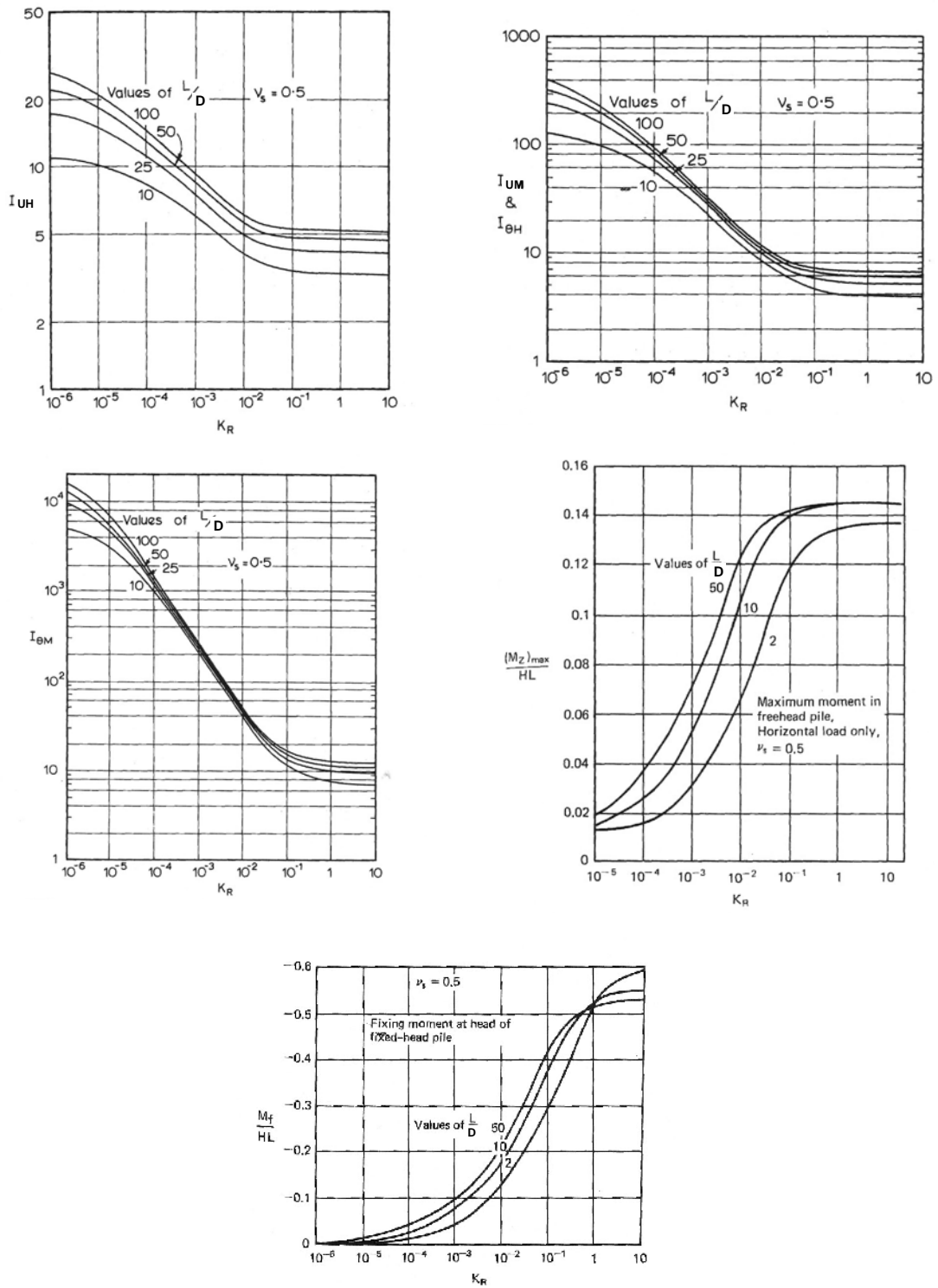


Figure 2.1 Influence Factors for Determination of Lateral Pile Responses for the Case of Constant Soil Modulus (after Poulos, 1971)

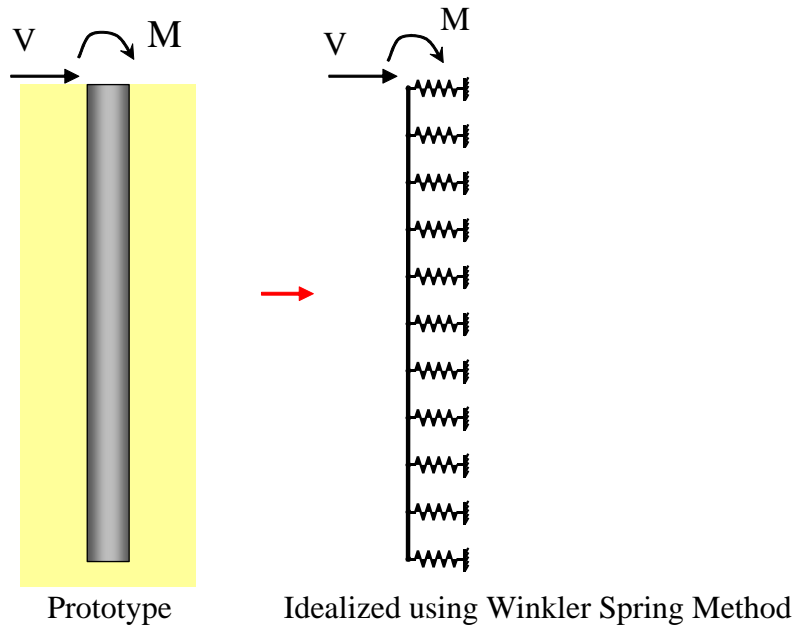


Figure 2.2 Implementation of Winkler Spring Concept for Laterally Loaded Pile Problem

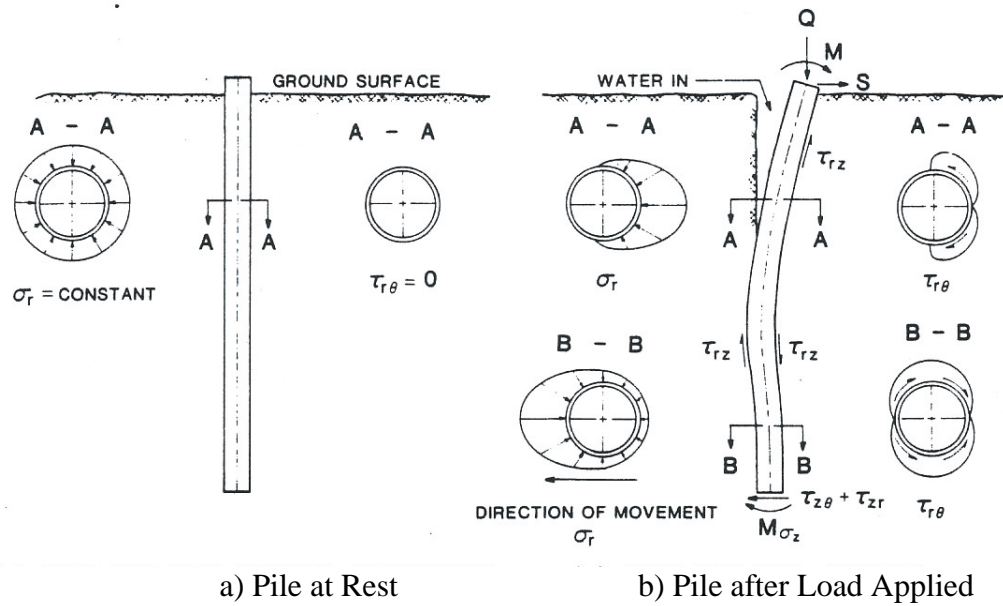


Figure 2.3 Definition of  $p$ - $y$  Concept with a) Pile at Rest; b) Pile after Load Applied (after Dunnavant, 1986)

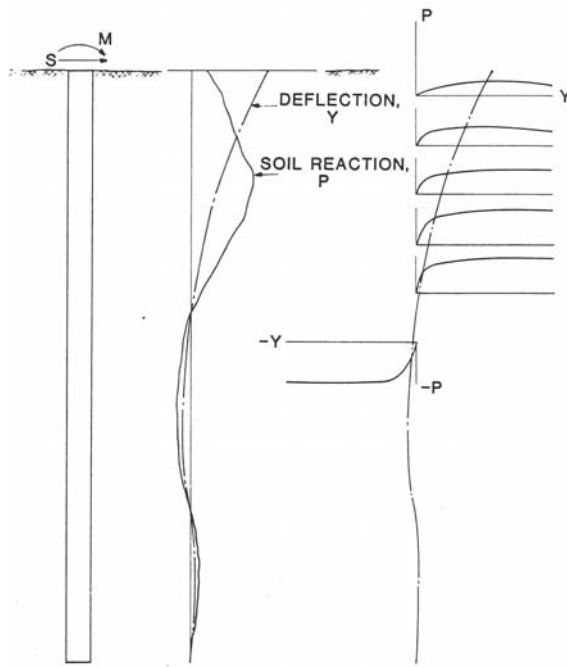


Figure 2.4 Typical Family of  $p$ - $y$  Curves Response to Lateral Loading (after Dunnavant, 1986)

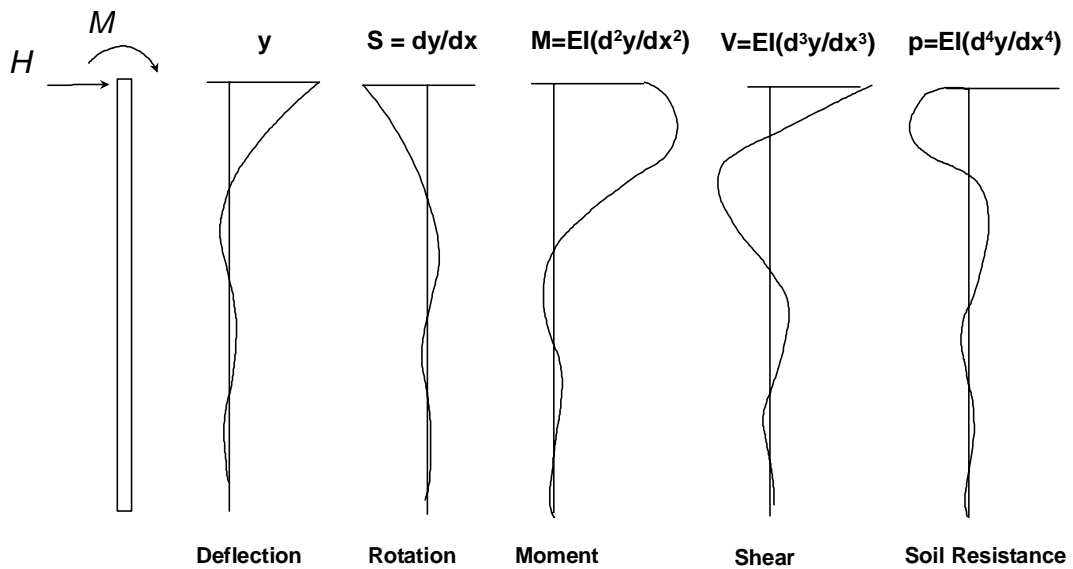


Figure 2.5 Methodology in Developing  $p$ - $y$  Curves (Reese and Van Impe, 2001)

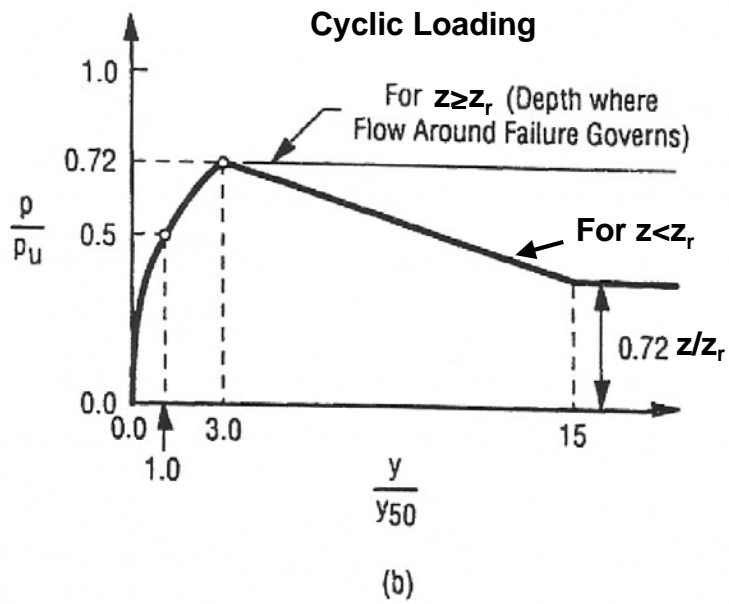
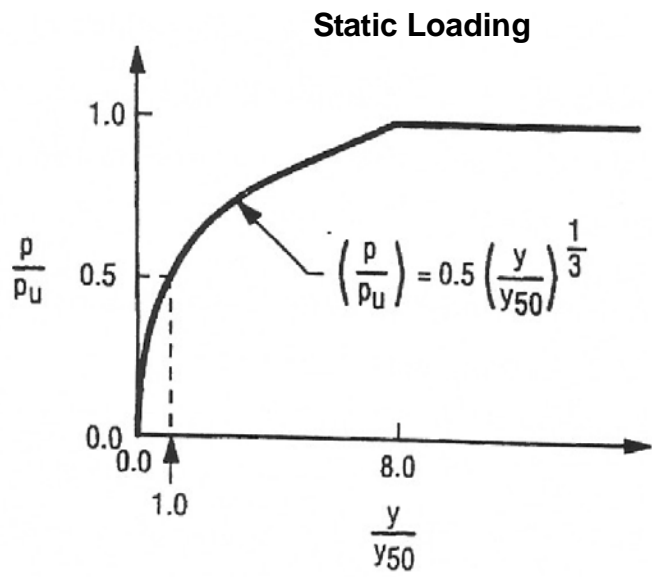
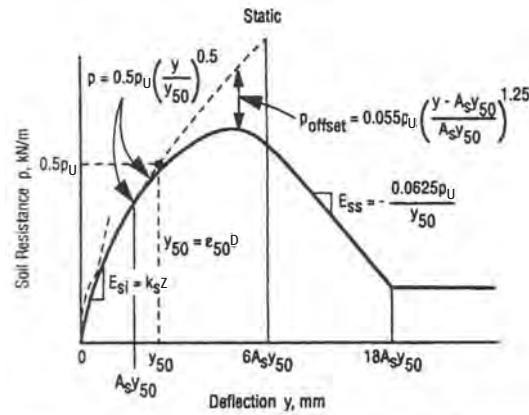
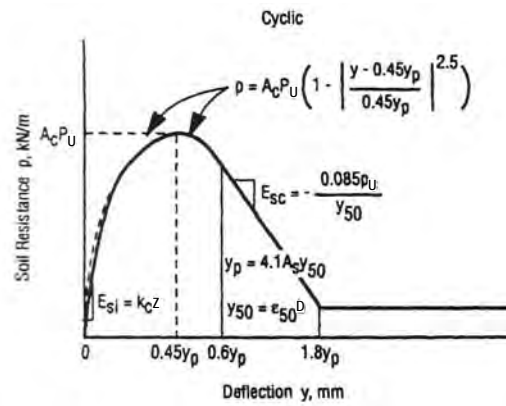


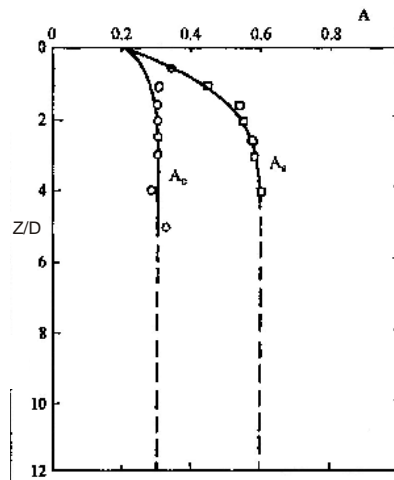
Figure 2.6 Characteristic Shape of  $p$ - $y$  Curve for Soft Clay a) Static Loading; b) Cyclic Loading (after Matlock, 1970)



a) Static Loading

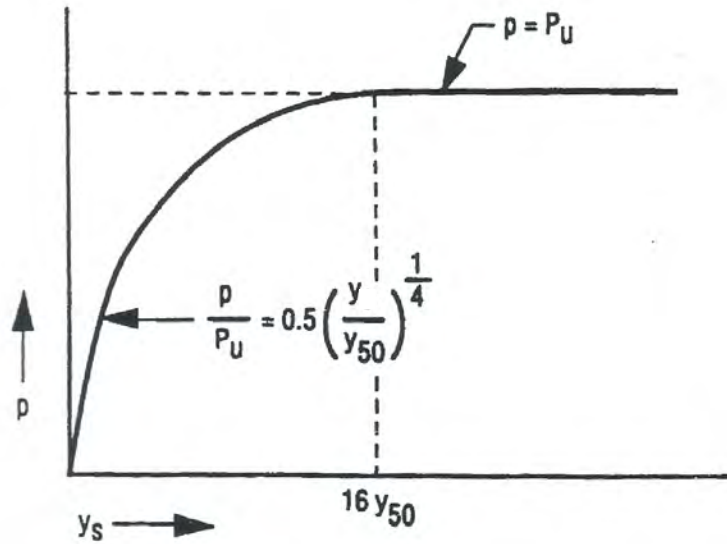


b) Cyclic Loading

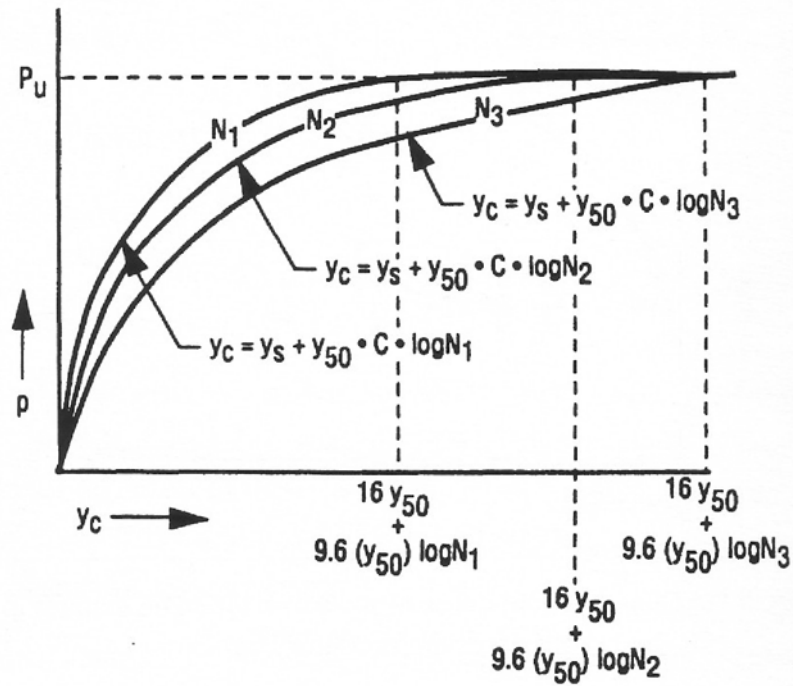


c) Value of Constant A

Figure 2.7 Characteristic Shape of  $p$ - $y$  Curve for Stiff Clay below Water Table for a) Static Loading; b) Cyclic Loading; c) Value of Constant A (after Reese *et al.*, 1975)



a) Static Loading



b) Cyclic Loading

Figure 2.8 Characteristic Shape of  $p$ - $y$  Curve for Stiff Clay above Water Table for a) Static Loading; b) Cyclic Loading (Welch and Reese 1972; Reese and Welch, 1975)

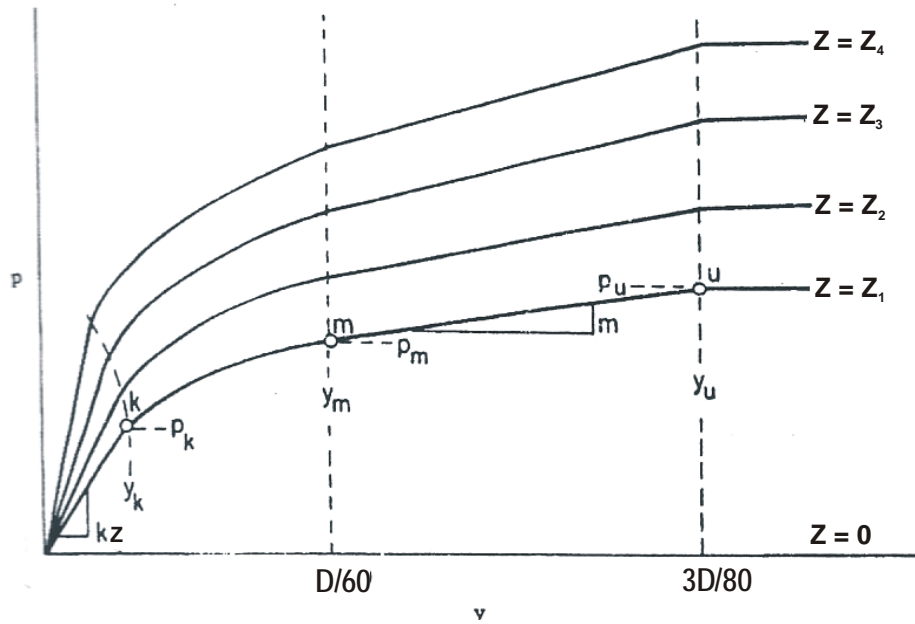
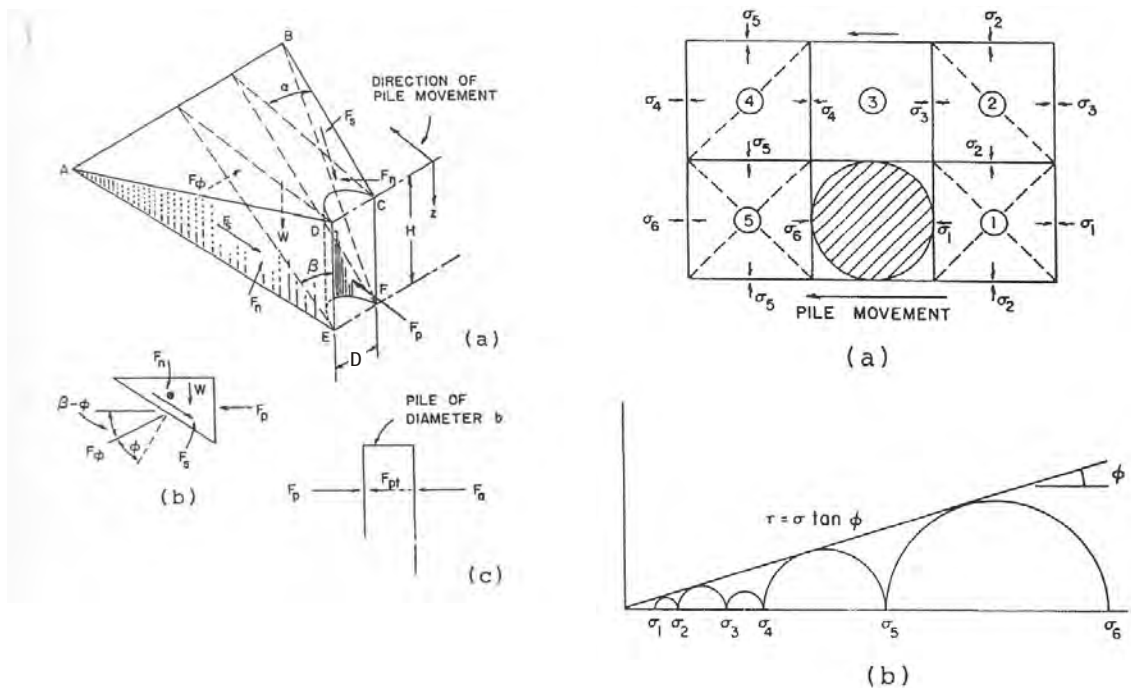


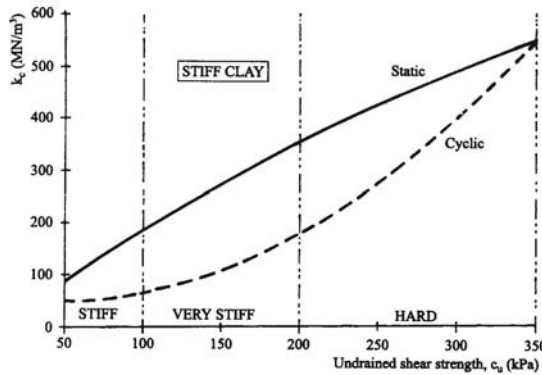
Figure 2.9 Characteristic Shapes of  $p$ - $y$  Curves for Sand (Reese *et al.*, 1974)



a) Assumed Passive Wedge Failure

b) Assumed Lateral Flow Failure

Figure 2.10 Sand Failure Modes in Laterally Loaded Pile Problem a) Assumed Passive Wedge Failure; b) Assumed Lateral Flow Failure (after Reese *et al.*, 1974)



a) Values of  $k_c$

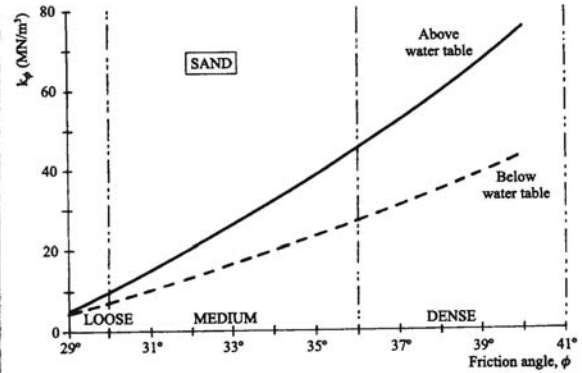


Figure 3.31. Values of  $k_\phi$  for sand.

b) Values of  $k_\phi$   
 loading from Figure 3.30 is 90,000 kN/m<sup>2</sup> (at beginning of curve). The recommended value of  $k_\phi$  from Figure 3.31 is 38 MN/m<sup>3</sup>, yielding a value for  $k_{py}$  of 128,00 kN/m<sup>3</sup>.  
 4. Establish the parabolic section of the  $p$ - $y$  curve,

$$n = \bar{c}_u^{1/n}$$

(3.68)

Figure 2.15 Initial Subgrade Reaction Constant (Reese and Van Impe, 2001) a) Values of  $k_c$ , and b) Values of  $k_\phi$

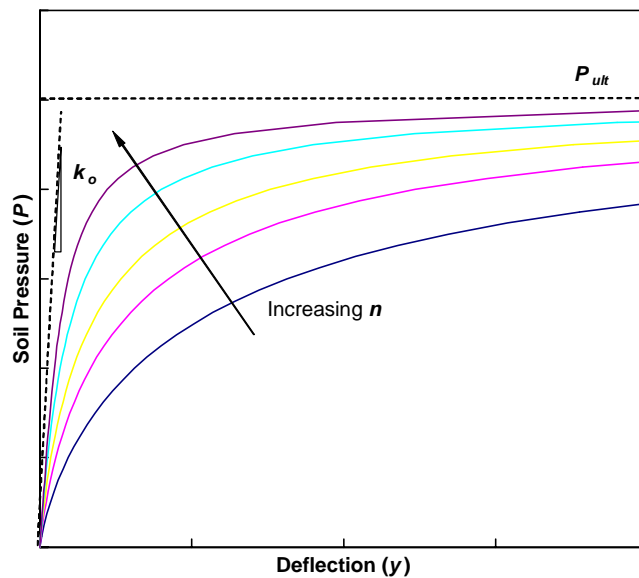
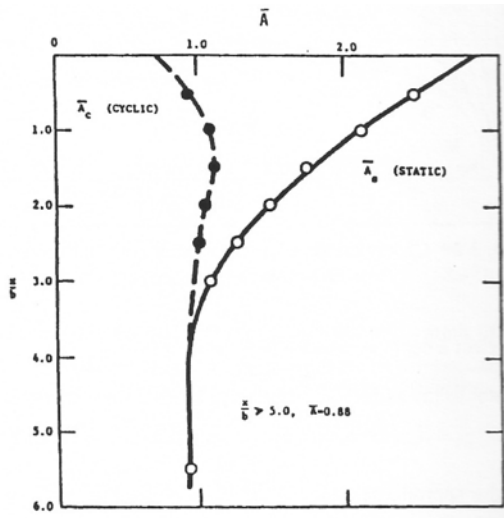
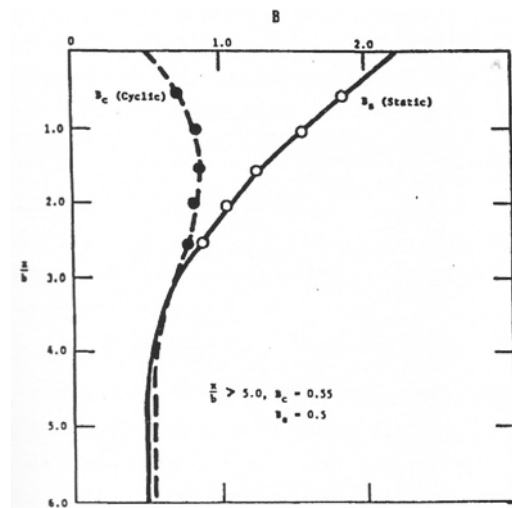


Figure 2.16 Hyperbolic Soil Model (after Carter, 1984)

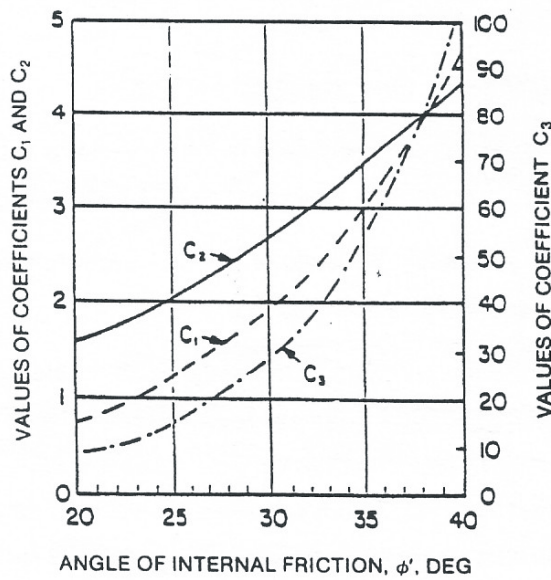


a) Coefficient A

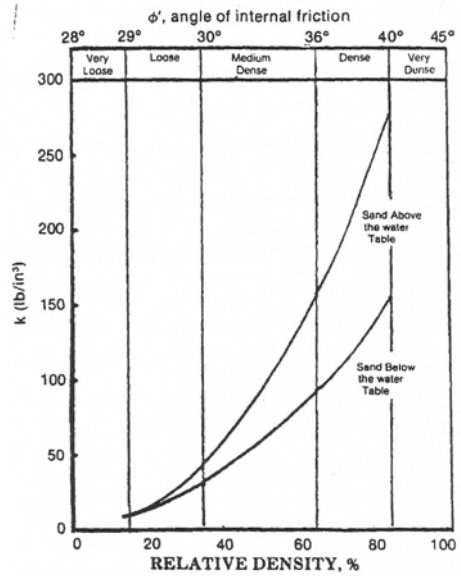


b) Coefficient B

Figure 2.11 Values of Coefficients Used for Developing  $p$ - $y$  Curves for Sand a) Coefficient A; b) Coefficient B (after Reese *et al.*, 1974)



a) Coefficients as Function of  $\phi$  for API Sand



b) Initial Modulus of Subgrade Reaction for API Sand

Figure 2.12 Charts Used for Developing API Sand  $p$ - $y$  Curves (API, 1987)

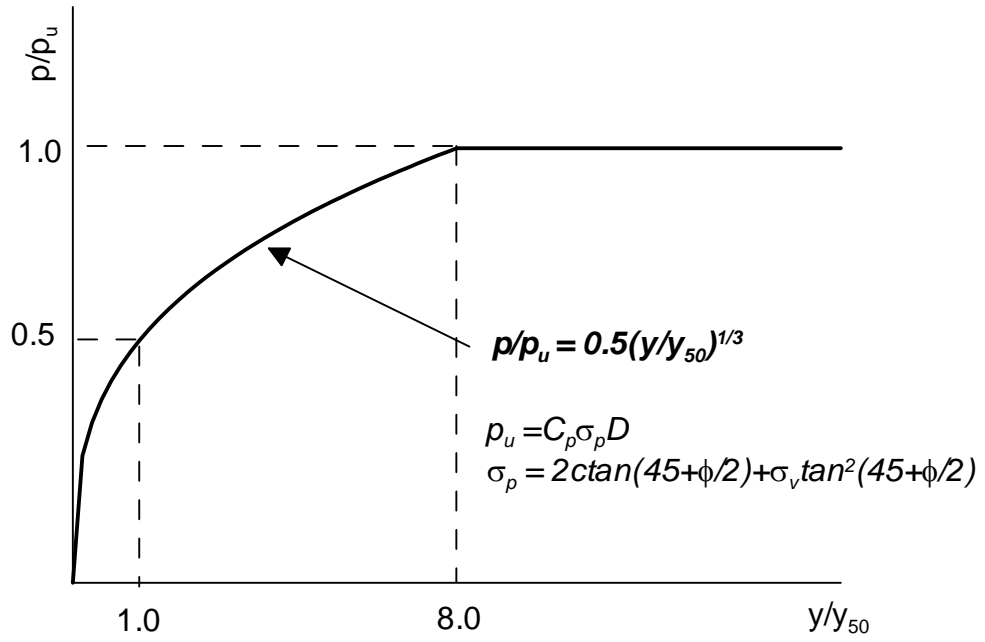


Figure 2.13 Characteristic Shape of  $p$ - $y$  Curve for Cemented Sand (after Ismael, 1990)

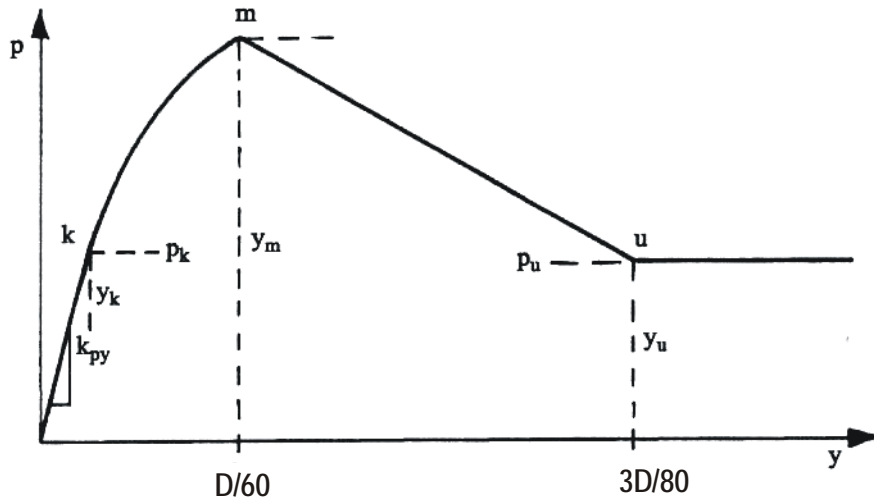


Figure 2.14 Characteristic Shape of  $p$ - $y$  Curve for  $c$ - $\phi$  Soil (Reese and Van Impe, 2001)

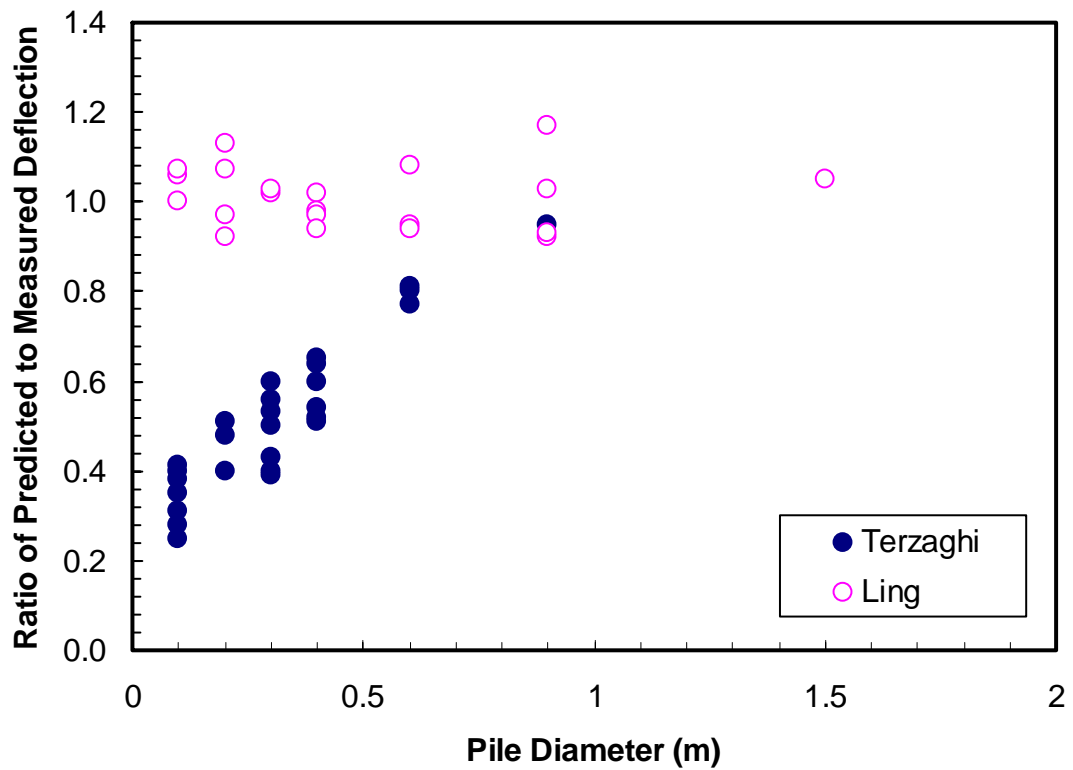


Figure 2.17 Comparison of Ratio of Predicted to Measured Pile Head Deflections based on Two Different Concepts on Pile Diameter Effect (After Ling, 1988)

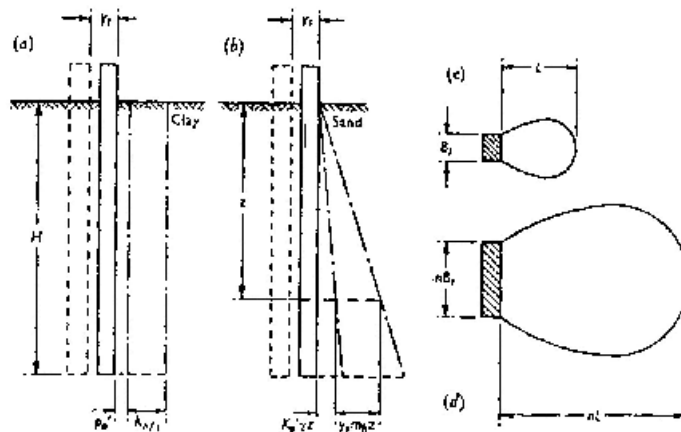


Figure 2.18 Influence of Pile Diameters on Dimensions of Bulb Pressure (Terzaghi, 1955)

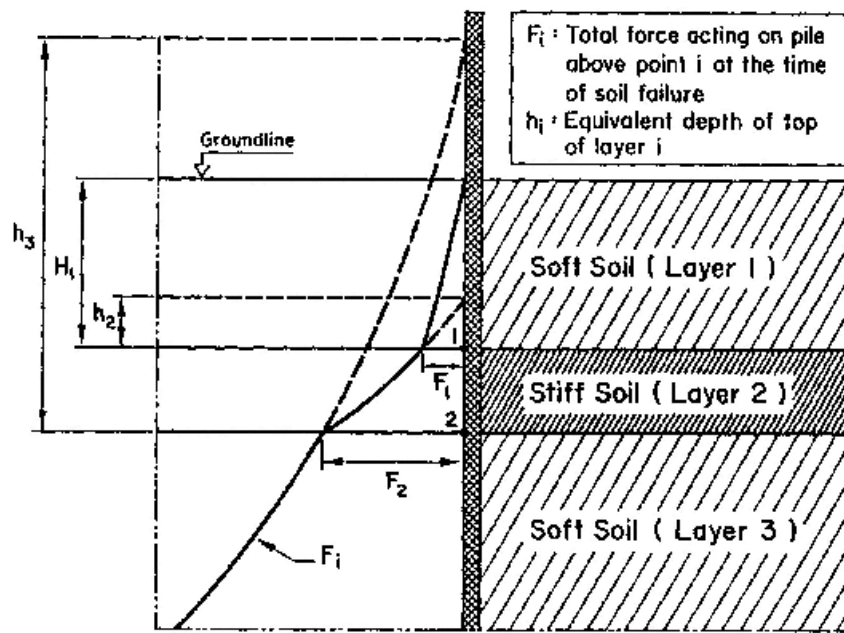


Figure 2.19 Typical Determination of Equivalent Depths in a Layered Soil Profile (Georgiadis, 1983)

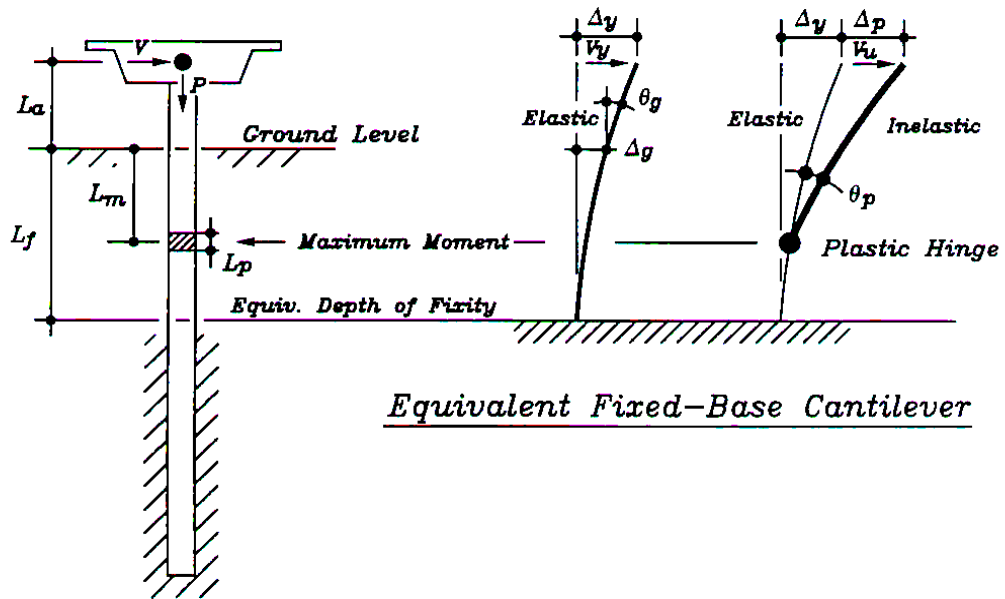


Figure 2.20 Concept of Equivalent Cantilever Beam Method (Chai and Hutchinson, 1999)

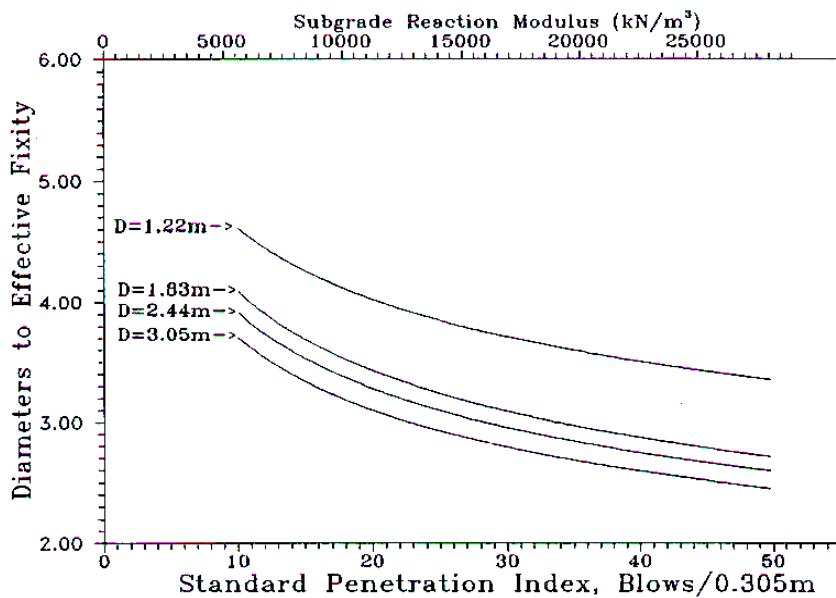


Figure 2.21 Design Chart for Determining Depth of Fixity (Budek, 1997)

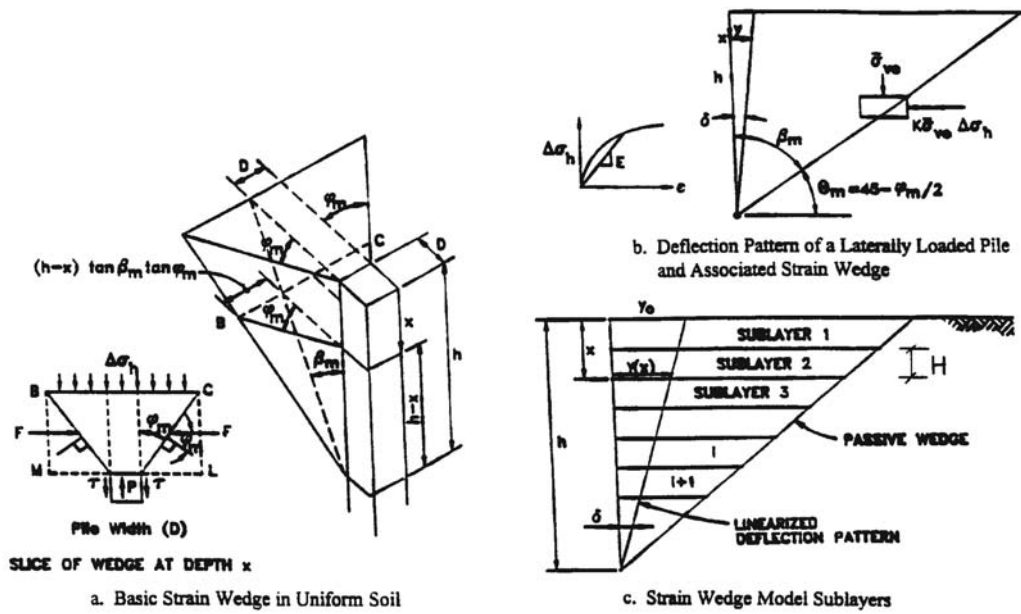


Figure 2.22 Concept of Strain Wedge Model for Analyzing Lateral Load Pile Problem (Ashour and Norris, 1998)

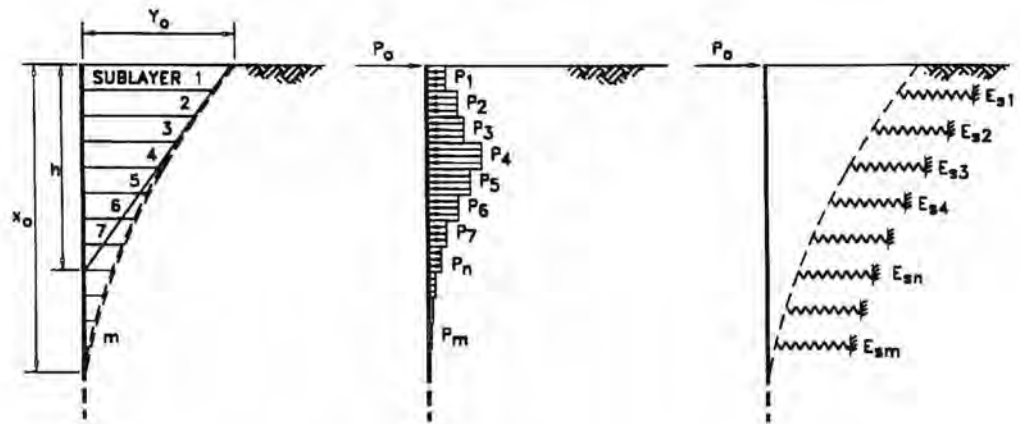
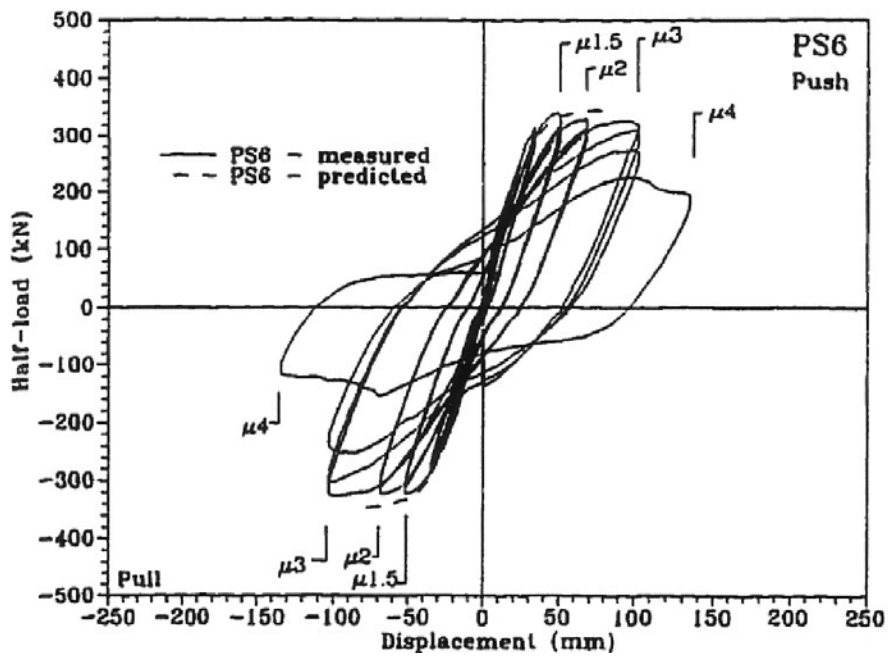
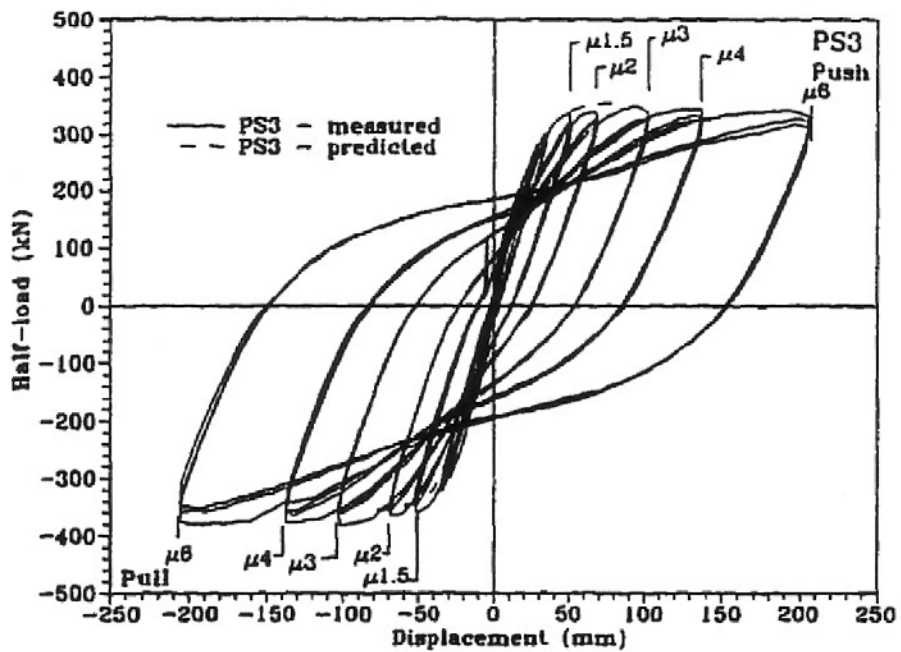


Figure 2.23 Distribution of Soil-Pile Reaction along Deflected Pile (Ashour and Norris, 1998)

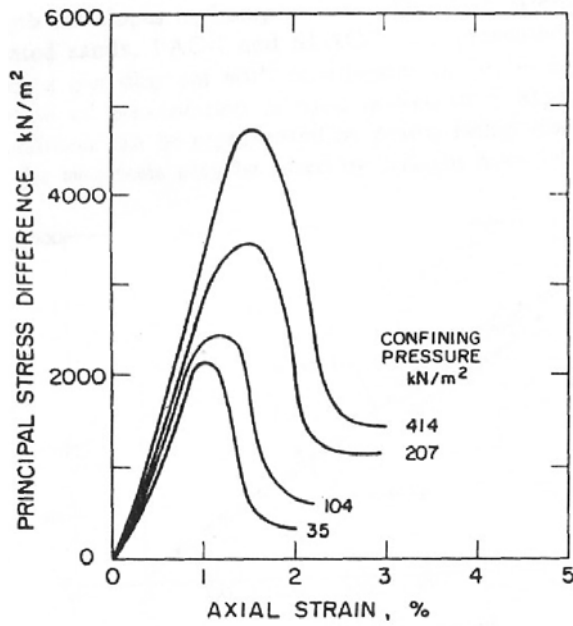


a) without External Confinement

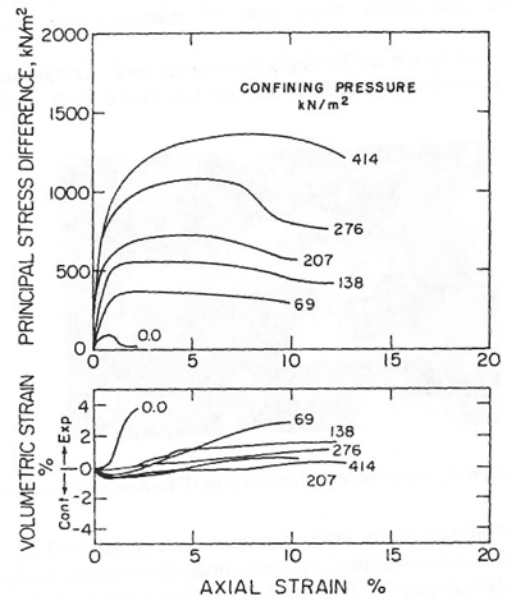


b) with External Confinement

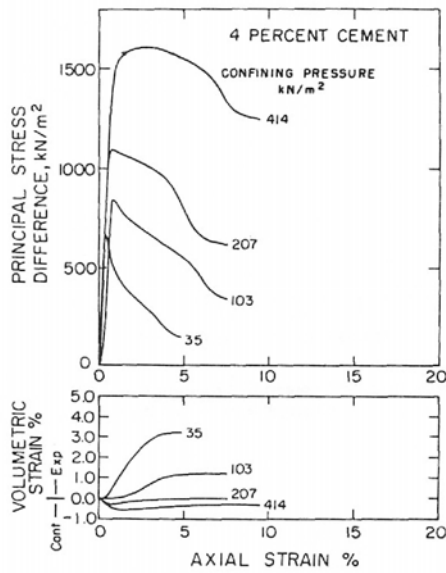
Figure 2.24 Force-Displacement Hysteretic Loops for Pile Shaft Test a) without External Confinement, b) with External Confinement (Budek, 1997)



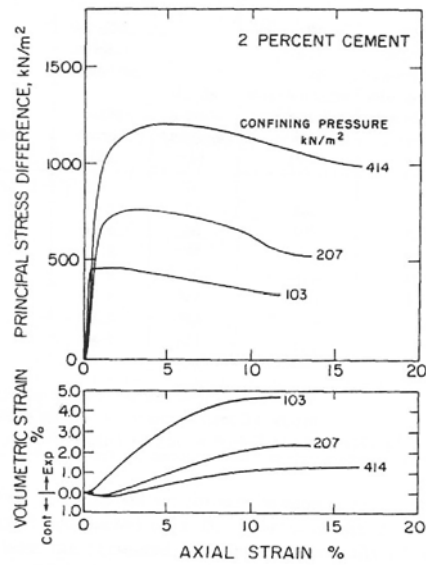
a) Strongly Cemented Sand (from Natural Soil Samples)



b) Weakly Cemented Sand (from Natural Soil Samples)



c) Artificially-Cemented Sand (4% Cement)



d) Artificially-Cemented Sand (2% Cement)

Figure 2.25 Typical Stress-Strain Curves for Cemented Sand (After Clough *et al.*, 1981); a) Strongly Cemented, b) Weakly Cemented, c) Artificially-Cemented (4% Cement), d) Artificially-Cemented (2% Cement)

THIS PAGE LEFT BLANK

## Chapter 3 EVALUATION OF PILE DIAMETER EFFECT USING 3-D FINITE ELEMENT METHOD

In this chapter, the effect of pile diameter on lateral pile response using the finite element method is discussed. Since the pile diameter effect is a geometrical problem in three-dimensional space, 3-D finite element analyses were required to complete the objective of this study. The Finite Element Analysis Program, FEAP (Taylor 1998), was used for this parametric study. Two models, including linear elastic and elasto-plastic soil models, were considered in the analyses to study the variation in the effect of pile diameter when the behavior of soil changes from linear to nonlinear. The conclusions drawn from these tests are useful in interpreting the influence of pile diameter in the experimental phase.

### 3.1 Description of Finite Element Model

The 3-D finite element method was used to study the effect of pile diameter on pile response. The finite element mesh model for this problem is illustrated in Figure 3.1. 8-node hexahedron (brick) solid elements were used to model the soil and the pile was modeled by using a series of beam elements. Rigid link elements were used to connect the pile to the soil elements. The rigid links were modeled using beam elements with very large flexural rigidity,  $EI$ , (i.e. 1,000 times the  $EI$  of the pile) such that they can transfer the load to the soil with the plane section of the pile before and after being subjected to the bending moment remaining plane. The advantage of symmetry was used to decrease the number of degree-of-freedom, thus decreasing the computational time. In this study, the model was based upon a 0.6-m steel pipe pile with a wall thickness of 10 mm and a nominal length of 20.3 m embedded in stiff overconsolidated clay. For each case in this study, the pile was chosen to be long enough to act as a “long pile” (i.e., the lateral pile response was independent of depth). The  $EI$  of the pile was computed as  $1.58 \times 10^5$  kN-m<sup>2</sup> and the Young's modulus of the soil,  $E_s$ , was  $1.38 \times 10^4$  kN/m<sup>2</sup> with

Poisson's ratio of 0.45. To study the pile diameter effect on the pile response, the  $EI$  of the pile, the pile length, as well as the Young's modulus of the soil were kept constant throughout the analyses, while only the pile diameter was changed. Pile diameters in this study ranged from 0.15 m to 1.07 m, such that largest pile diameter was 7 times larger than the smallest one. The boundary of the soil was chosen to be far enough away to minimize boundary effects (about 20 m from the center of the pile). Roller supports were used as a boundary condition along 4 different vertical planes, while pinned supports were used as a boundary condition at the bottom of the mesh. In all cases, the pile was subjected to a horizontal point load of 890 kN applied at the pile head. To check the validity of each model, the mesh was verified by comparing the displacement at the pile head with the solutions from the boundary element method based on elastic continuum theory (Davies and Budhu 1986) until the error was less than 10%. These meshes were later used for further analyses. The comparison of results based on the 3-D finite element approach and elastic solution will be presented in the following section.

### **3.2 Linear Elastic Soil Model**

The results of 3-D finite element analyses for different pile diameters are presented in this section. Typical contours of horizontal stress ( $x-x$ ) and horizontal deformation in the soil mass due to the pile subjected to lateral loading are presented in Figure 3.2. A stress concentration occurs in the soil adjacent to the pile, and the stress becomes smaller as the distance from the pile increases. It should be noted that only compression stress contours are presented in the figure for clarity. The same stress pattern, but in tension, occurs on the other side due to symmetry. As the pile is subjected to lateral load, the soil in front of the pile moves upward to form a passive wedge. Based on the horizontal displacement contour, it can be expected that the failure plane of the wedge is a curve as opposed to a traditional assumption that the failure plane of a wedge is a straight line. The pile head deflection for different pile diameters using a linear elastic soil model is presented in Figure 3.3. The results based on the solution from the

elastic continuum theory using the boundary element method proposed by Davies and Budhu (1986) are in good agreement with those obtained from 3-D FEM indicating the 3-D mesh used in these analyses is reasonably adequate to model the soil-pile interaction, especially for the next analyses where the soil model will be changed from linear to nonlinear.

It is clearly seen from Figure 3.3 that the pile diameter has some effect on the response of laterally loaded pile. With the  $EI$  of the pile and stiffness of the soil being constant, increasing the pile diameter decreases the pile head deflection. This is due to the fact that a pile with larger diameter mobilizes more soil and hence achieves higher lateral resistance. The pile diameter effect on moment distribution is shown in Figure 3.4a. As the pile diameter increases, the maximum moment becomes lower and the location of maximum moment moves closer to the ground surface. The effect of pile diameter on pile deflection profile is also shown in Figure 3.4b.

Figure 3.5 presents the relationship between normalized pile head deflection ( $u/u_{ref}$ ) and normalized pile diameter ( $D/D_{ref}$ ): where  $u$  is the pile head displacement,  $u_{ref}$  is the reference pile head displacement (i.e., in this case the pile head displacement of the smallest pile was used as a reference displacement),  $D$  is the pile diameter, and  $D_{ref}$  is the reference diameter. Figure 3.5 shows that in order to decrease the pile head displacement two times, the pile diameter needs to be increased by approximately 10 times. For linear elastic case, the pile diameter appears to have insignificant effect on the pile response. The relationship between normalized pile head displacement ( $u/u_{ref}$ ) and normalized pile diameter ( $D/D_{ref}$ ) based on curve fitting is given as follows:

$$\frac{u}{u_{ref}} = \left( \frac{D}{D_{ref}} \right)^{-0.273} \quad (3.1)$$

The similar relationship as shown in Eq. (3.1) can also be derived from the solutions provided by Davies and Budhu (1986).

The input soil parameters used in the 3-D finite element analyses were Young's modulus and Poisson's ratio. These parameters are not directly related to the modulus of subgrade reaction used in the 1-D problem (i.e. Beam on Winkler's spring problem). In order to evaluate the effect of pile diameter on the modulus of subgrade reaction (i.e. soil spring resistance), a pile with a series of Winkler springs was analyzed by varying the spring stiffness. LPILE (Reese *et al.* 2000), a computer program for analyzing lateral pile response using Beam on Winkler's spring concept, was used. It was assumed that the Beam on Winkler spring method can reproduce the same response of laterally loaded pile as the 3D-finite element without any significant error, though the Winkler method neglects the soil continuity. Using the same pile stiffness as the previous study and varying the soil springs until the pile head deflection matched with the deflection obtained from the 3-D analyses for the 0.30-m pile, the moment and displacement profiles obtained from these different types of analyses were compared, as presented in Figure 3.6. The agreement of moment and displacement profiles obtained from the different methods is very good, confirming that the above assumption is reasonable. The pile head displacements with varying modulus of subgrade reaction at different  $EI$  were then calculated as presented in Figure 3.7. The normalized pile head displacement plotted against normalized modulus of subgrade reaction is presented in Figure 3.8, which shows that the normalized pile head displacement is independent of  $EI$ . The relationship between normalized pile head displacement and normalized modulus of subgrade reaction ( $K/K_{ref}$ ) can be written as:

$$\frac{u}{u_{ref}} = \left( \frac{K}{K_{ref}} \right)^{-0.75} \quad (3.2)$$

By equating the normalized pile head displacement from Eq. (3.1) based on the 3-D finite element analyses and Eq. (3.2) based on the subgrade reaction theory, the relationship between pile diameter and modulus of subgrade reaction can be obtained as:

$$\frac{K}{K_{ref}} = \left( \frac{D}{D_{ref}} \right)^{0.364} \quad (3.3)$$

The relationship based on the above expression is graphically illustrated in Figure 3.9 together with two different concepts regarding pile diameter effect on modulus of subgrade reaction. It is observed that Terzaghi's concept (1955), in which the modulus of subgrade reaction is independent of pile diameter, is conservative. However, the modulus of subgrade reaction derived from Carter's concept (1984) is too large for the linear elastic case.

Eq. (3.3) implies that in order to double the modulus of subgrade reaction, the pile diameter needs to be increased by about 7 times. If the pile diameter is doubled, the modulus of subgrade reaction will increase by only 30%. In reality, increasing the pile diameter also increases the stiffness of the pile ( $EI$ ). If the pile is a solid circular section, increasing the pile diameter by 2 times increases the pile stiffness by 16 times. Figure 3.10 presents a comparison of pile response (i.e., pile head displacement and ratio of maximum moment to yield moment) due to the change of pile diameter. It can be seen that the pile diameter has more effect on the pile head displacement than the maximum moment. Increasing pile diameter by 10 times decreases the pile head displacement by 50%, while the maximum moment was decreased by only 20%. It is noted that the yield moment,  $M_y$ , of the reference pile was assumed to be the same as the maximum moment occurred in that pile, and thus the yield stress of this material,  $\sigma_y$ , could be computed using the basic strength of materials (i.e.,  $M_y = \frac{\pi D^3}{32} \sigma_y$ ). The yield moment for other pile diameters was then calculated in the same fashion. The improvement of lateral pile

response due to the effect of increasing soil modulus of subgrade reaction with the pile diameter is significantly less than that due to the change in pile stiffness ( $EI$ ) with pile diameter, particularly for the ratio of the maximum moment to the yield moment. Furthermore, the improvement of the pile response due to the combined effect of both soil and pile is insignificant compared with the case when considered only the effect from the increase of pile stiffness. In other words, for the linear elastic case, increasing pile diameter increases the lateral soil resistance (i.e., the modulus of subgrade reaction), resulting in the improvement of lateral pile response. However, this effect is overshadowed by a significant improvement of pile stiffness as the pile diameter increases.

According to the results of the linear elastic case, pile diameter has a small effect on pile response when considering only the effect from the soil. It is interesting to pursue the study of pile diameter effect using the same mesh, but changing the soil properties from linear to the elasto-plastic soil model. This will allow us to understand the trend of pile diameter effect on the response of laterally loaded piles due to the effect of soil nonlinearity.

### **3.3 Elasto-Plastic Soil Model**

The meshes from the previous analyses were reused in this section by modifying the soil properties from a linear material to an elasto-plastic material with hardening, using 3-D J2 plasticity model with von-Mises yield criterion and a linear hardening law (Taylor 1998). This model was used because it was the only 3-D nonlinear model available in FEAP. The same modulus and Poisson's ratio of the soil from previous study were incorporated with nonlinear parameters used for specifying the yielding and hardening portion of the soil. The yield shear stress for the soil in this case was  $34.5 \text{ kN/m}^2$  and the kinematic hardening modulus was  $275.8 \text{ kN/m}^2$ . Though the soil properties used in the analyses were not directly related to the typical soil parameters

used in geotechnical engineering (i.e., friction angle and cohesion), the analyses is useful for indicating how the pile diameter effect changes due to the nonlinearity of the soil. Extensive studies were conducted to determine the optimal number of time steps and iterations to ensure that the solution converged before conducting the study. It was found that with 40 time steps and 10 iterations, the solution had sufficient accuracy, and that was used throughout the analyses.

Figure 3.11 presents the comparison of moment profiles for both linear and nonlinear cases for different pile diameters with a horizontal pile head load of 890 kN. It is seen that the maximum moment became larger and its location became deeper when the nonlinear soil properties were used. The maximum moment and its location for the nonlinear case follows the same trend as the linear case in which the maximum moment increased and its location moved toward the ground surface as the pile diameter increased. Figure 3.12 presents the normalized pile head displacement ( $u/u_{ref}$ ) against normalized pile diameter ( $D/D_{ref}$ ) for nonlinear and linear cases at different horizontal loads. It indicates that the effect of pile diameter becomes more significant when the soil behavior changes from linear to nonlinear. The pile diameter effect depends on the loading level. Increasing the pile head horizontal load yields greater nonlinearity and thus increases the pile diameter effect on pile response. In addition, it can be expected that the pile diameter effect depends upon the degree of nonlinearity of the soil. The higher degree of soil nonlinearity, the greater the pile diameter effect on the soil-pile response.

As the soil in its nature is nonlinear, it is worthwhile to evaluate the influence of pile diameter on the response of lateral load pile in real soil. To accomplish this, a series of full-scale lateral load tests on CIDH piles were carried out and are discussed in the following chapters. The details of test setup and test results will be given in the next chapters.

### **3.4 Limitation of 3-D Finite Element Model**

Due to the simplicity of the 3-D finite element model used in this study, some other important aspects could not be incorporated, which may have significant contributions to the effect of pile diameter on the pile response. These include soil-pile separation, friction between the soil and pile, and the effect of soil confinement. Further research in this area with a better 3-D model, that allows incorporation of these important aspects, is important to provide better understanding on the effect of pile diameter on the pile response. The results of full-scale lateral pile load tests are, however, needed as a baseline to calibrate the finite element model. Once the model has been verified with the experimental test results, the investigation of other aspects can then be studied.

### **3.5 Summary**

The 3-D finite element method was used to model the soil-pile structure interaction problem to evaluate the effect of pile diameter on pile responses. Both linear and nonlinear soil model was considered in the analyses. Though the pile diameters were varied, the pile stiffnesses were kept to be constant throughout the analyses. Results from the analyses shows that pile diameter has some effect on the pile response (i.e. pile head displacement and moment distribution). Increasing the pile diameter appears to decrease the pile head displacement, the maximum moment, as well as lower the depth to maximum moment. However, pile diameter effect on the pile response seems to be very small when considering the effect of increasing pile stiffness with the pile diameter. In addition, the nonlinearity of the soil increases the effect of pile diameter on the pile response.

Though results from the analyses provide insight into pile diameter effect on the pile response to some extent, the simple model used in the analyses could not cover all aspects which are actually present in the actual behavior of the soil-pile interaction.

Therefore, the full-scale testing on different diameters of CIDH piles was carried out to investigate pile diameter effect experimentally as presented in the following chapters.

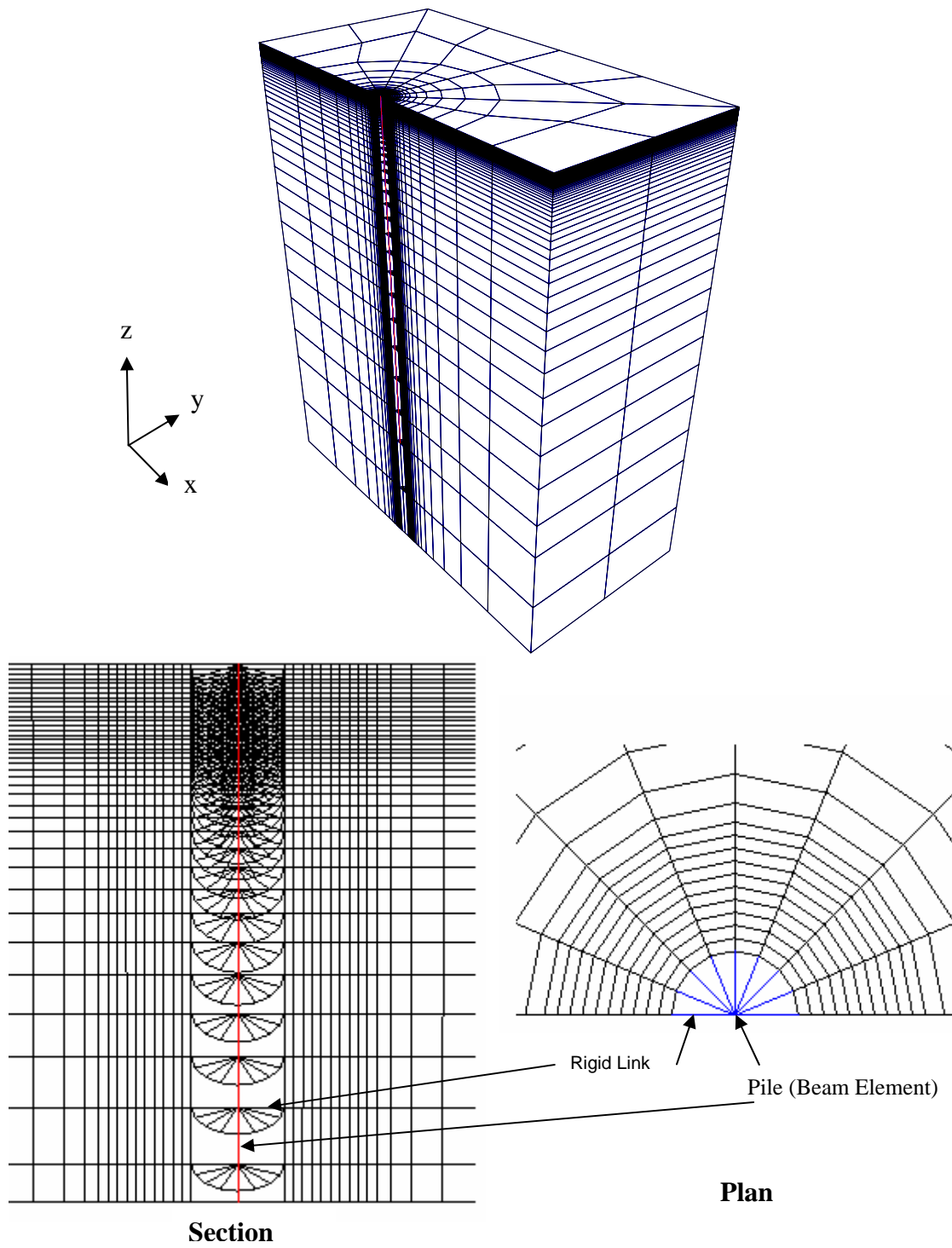


Figure 3.1 Finite Element Mesh for Pile Diameter Effect Study

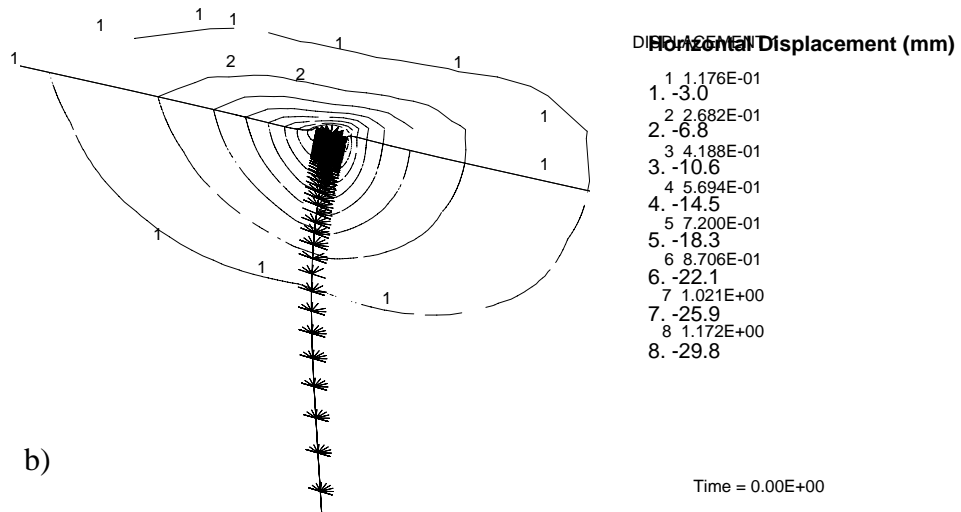
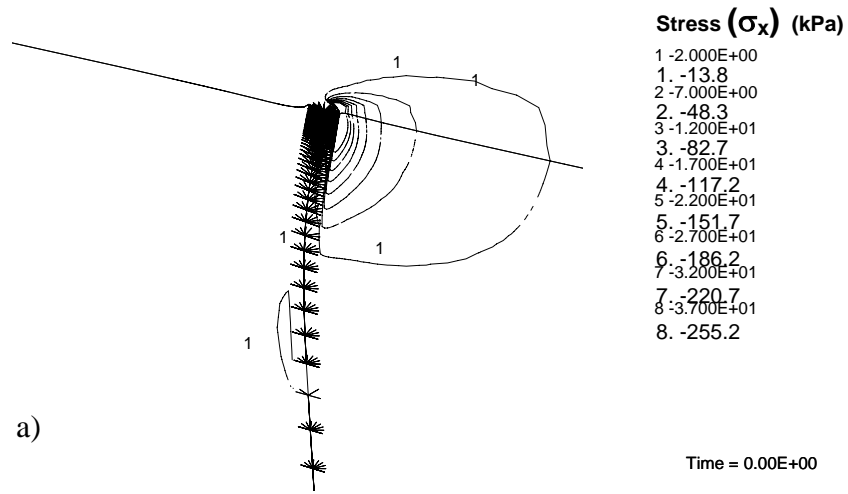


Figure 3.2 Typical Results of Compression Stress ( $\sigma_x$ ) and Displacement in Soil in Laterally Loaded Pile Problem

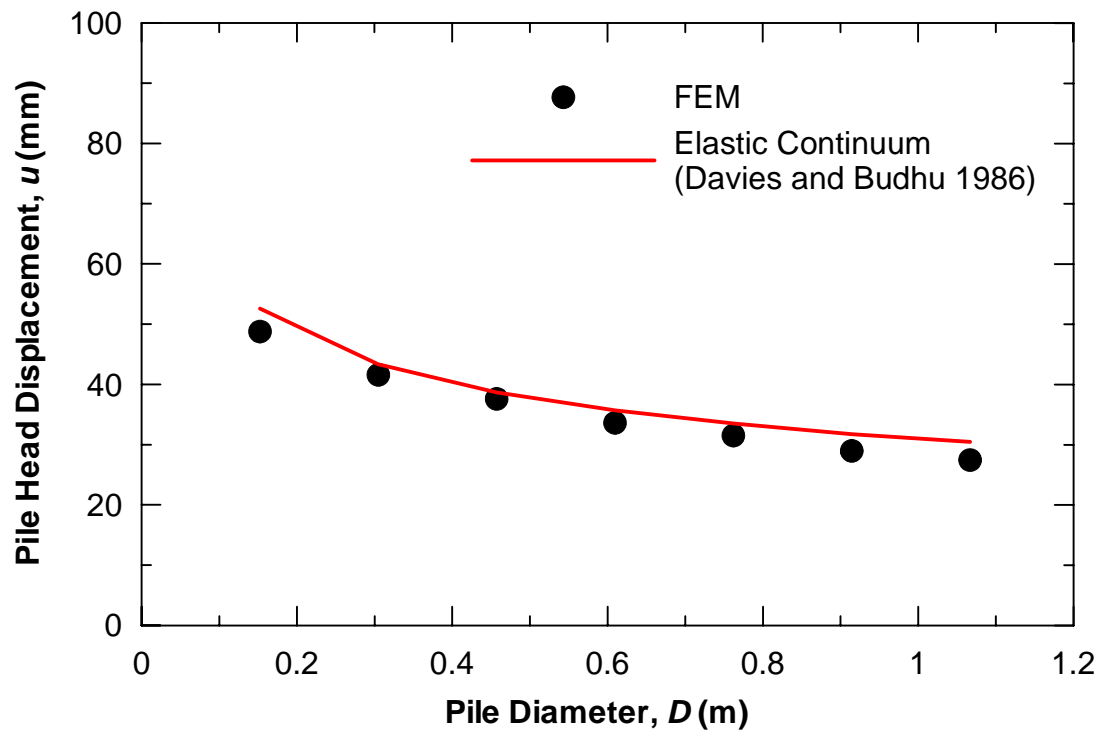


Figure 3.3 Comparison of Pile Head Displacement obtained from 3D FEM and Elastic Solution

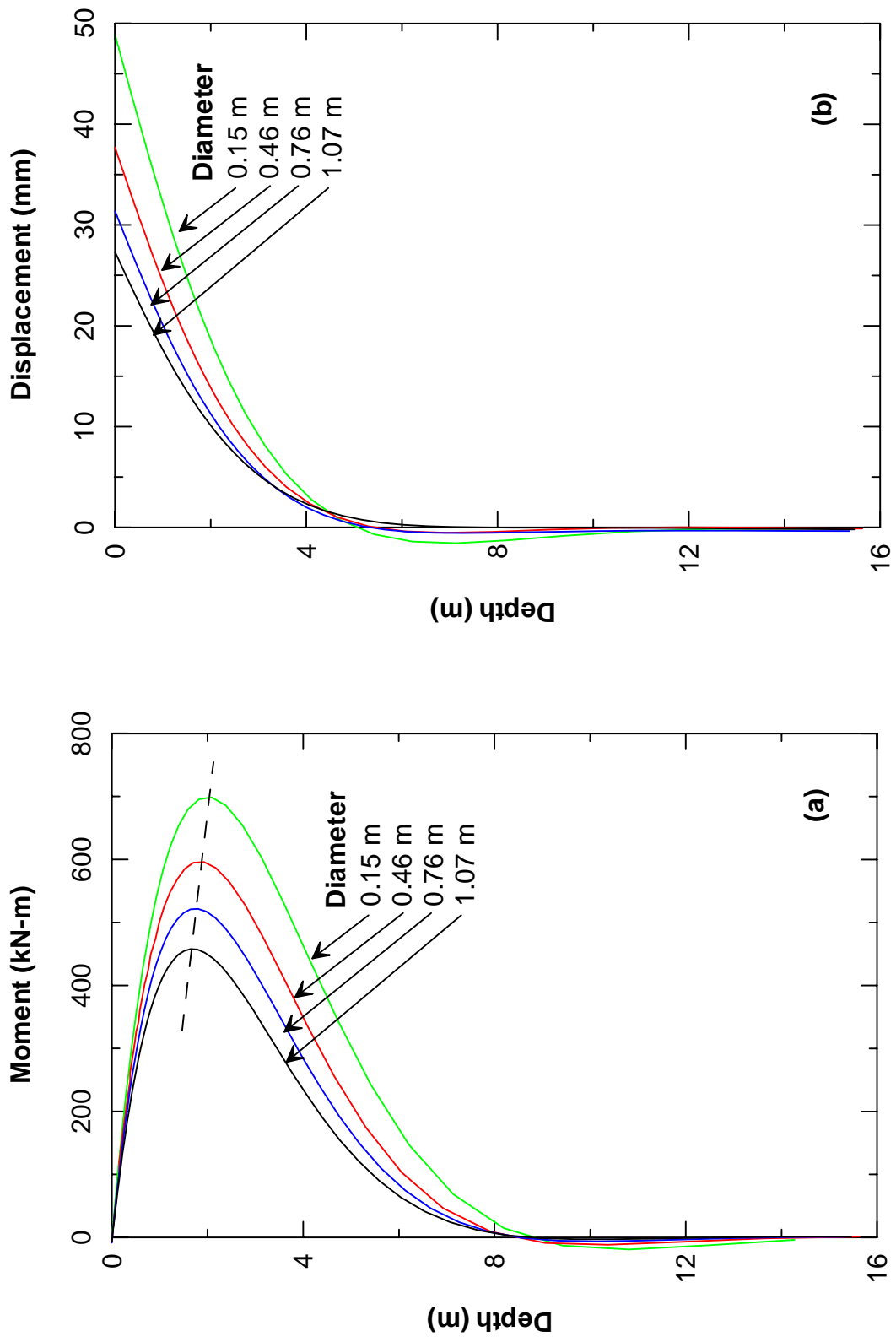


Figure 3.4 Effect of Pile Diameter on Pile Responses (a) Moment , and (b) Displacement

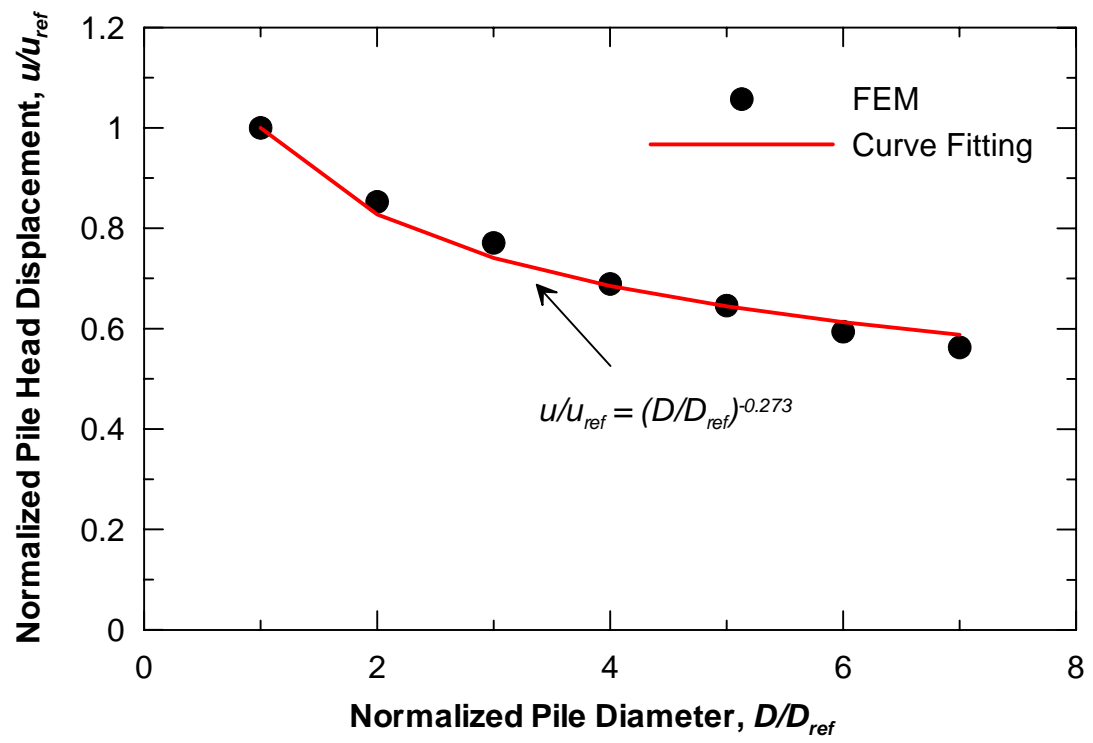


Figure 3.5 Normalized Pile Head Displacement against Normalized Pile Diameter

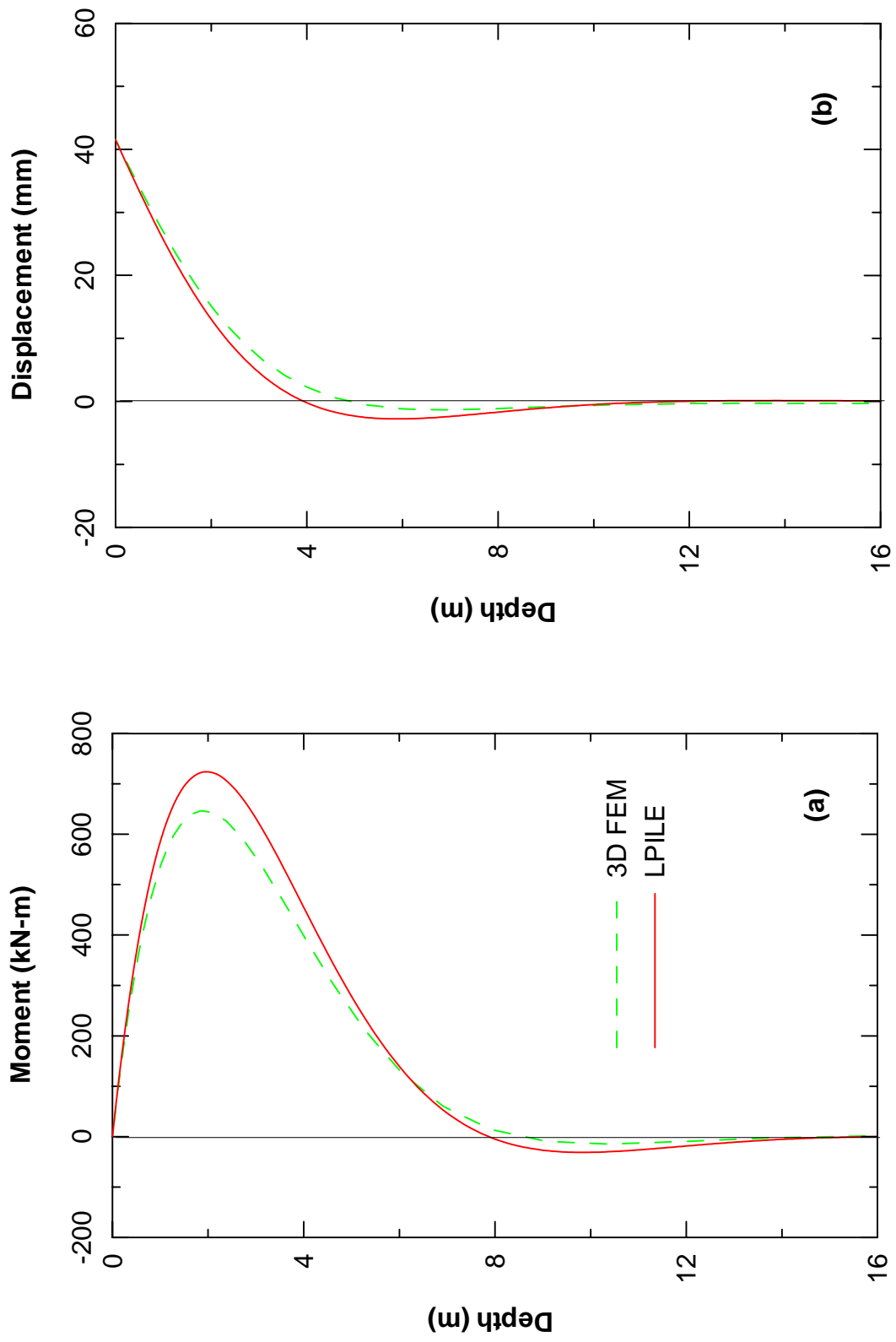


Figure 3.6 Comparison of Pile Responses obtained from 3D FEM and LPILE (a) Moment, and (b) Displacement

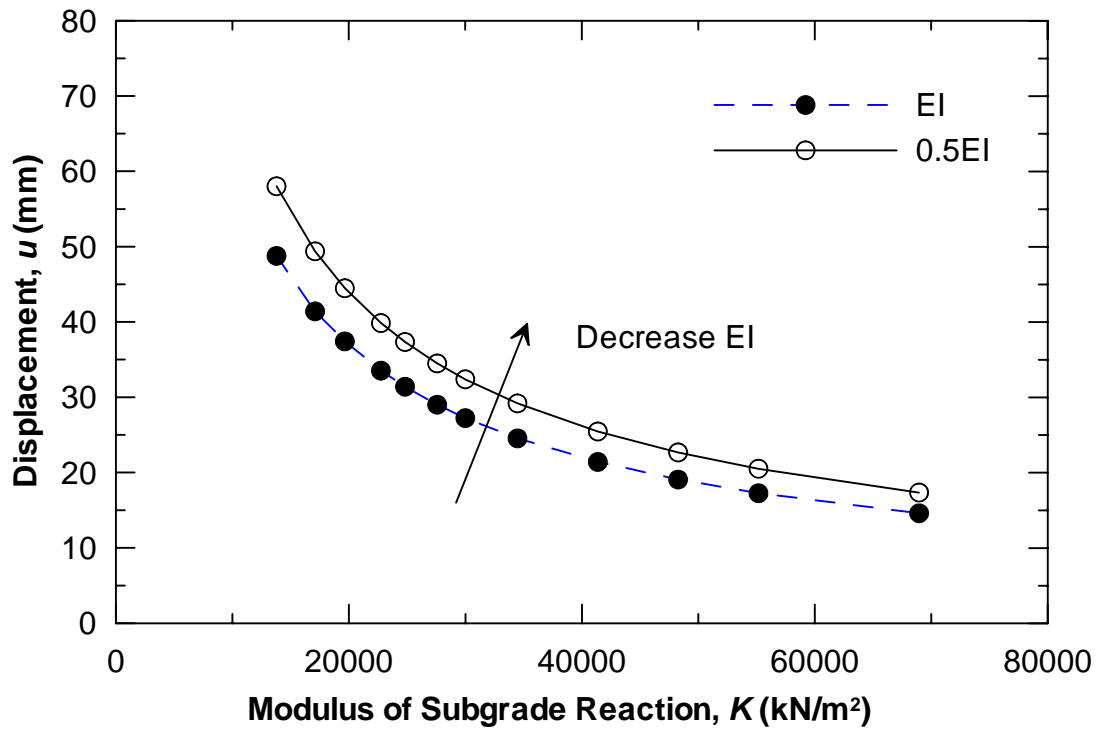


Figure 3.7 Displacement at Pile Head against Modulus of Subgrade Reaction

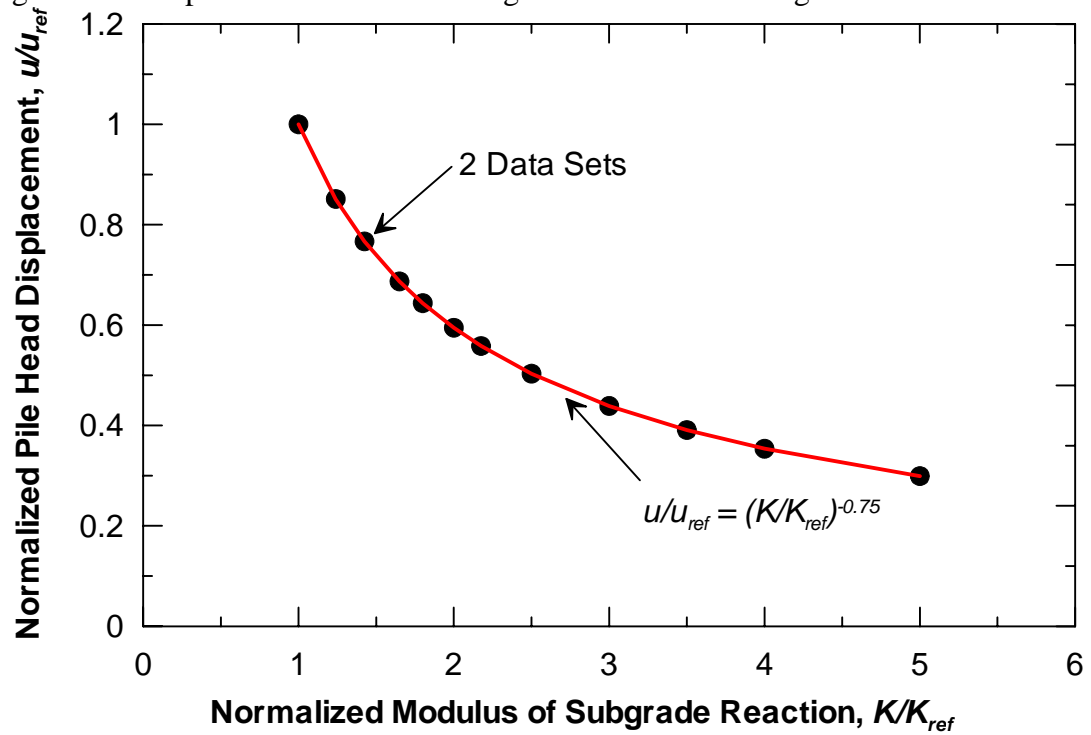


Figure 3.8 Normalized Pile Head Displacement against Normalized Modulus of Subgrade Reaction

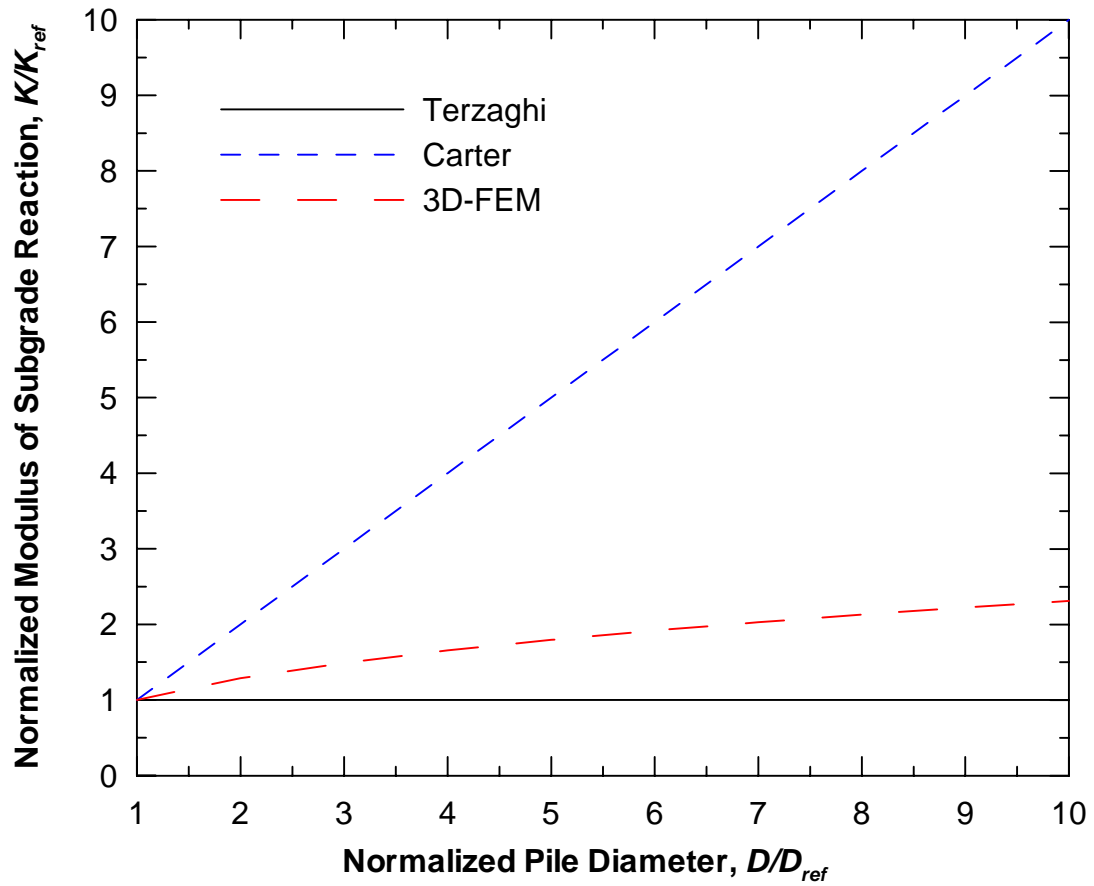


Figure 3.9 Comparison of Two Different Concepts on Pile Diameter Effect on Modulus of Subgrade Reaction with Results from 3-D FEM

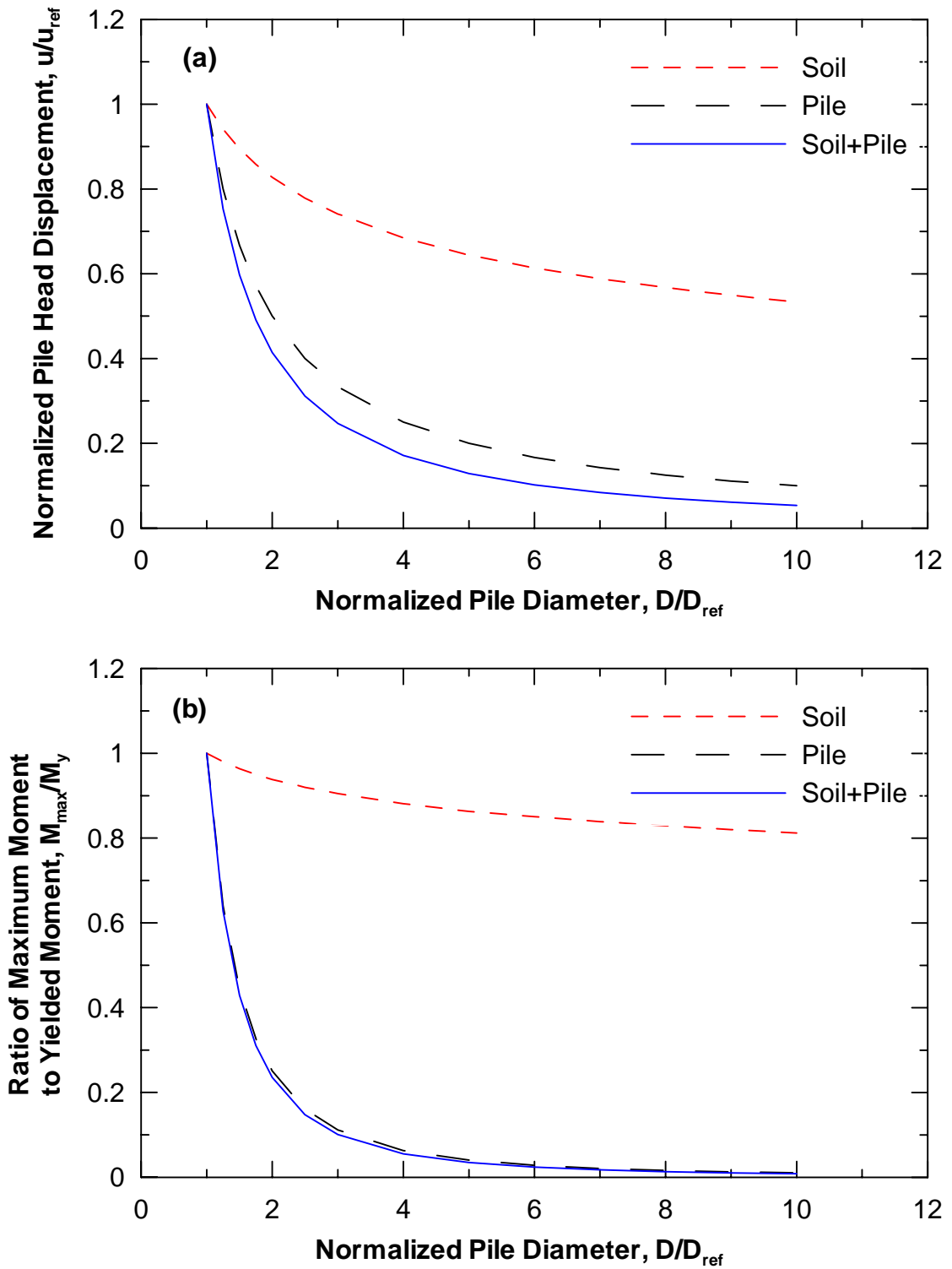


Figure 3.10 Effect of Pile Diameter on Lateral Pile Responses (a) Pile Head Displacement, and (b) Ratio of Maximum Moment to Yield Moment

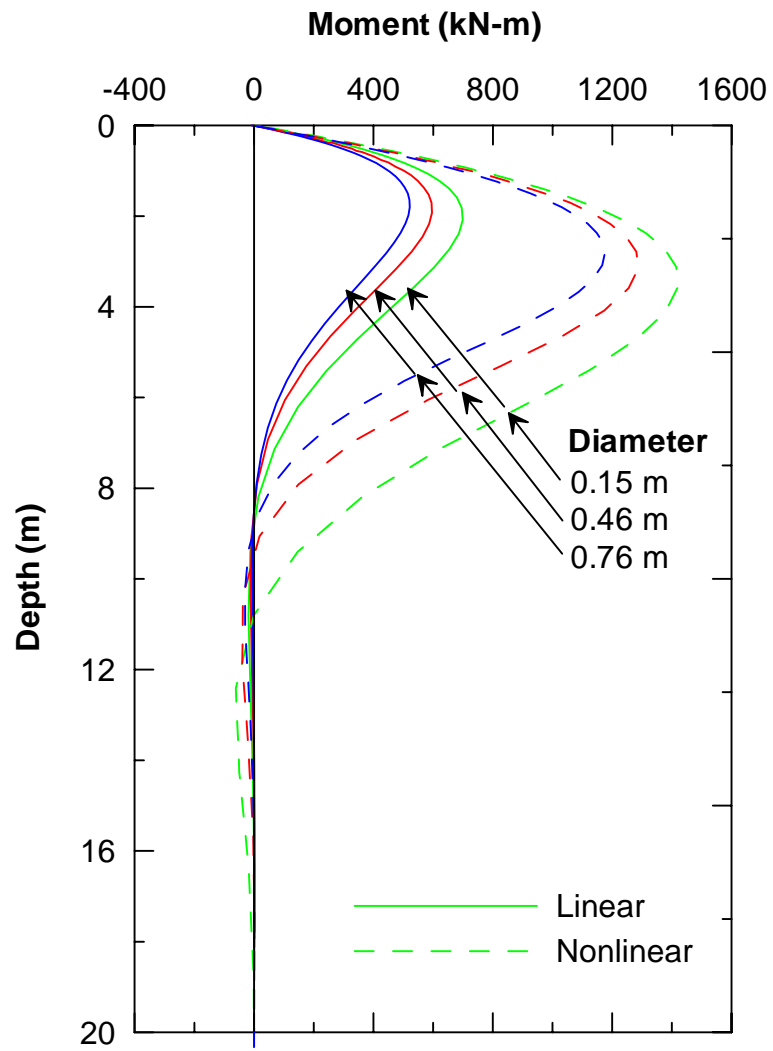


Figure 3.11 Comparison of Moment Profiles for Linear and Nonlinear Analyses

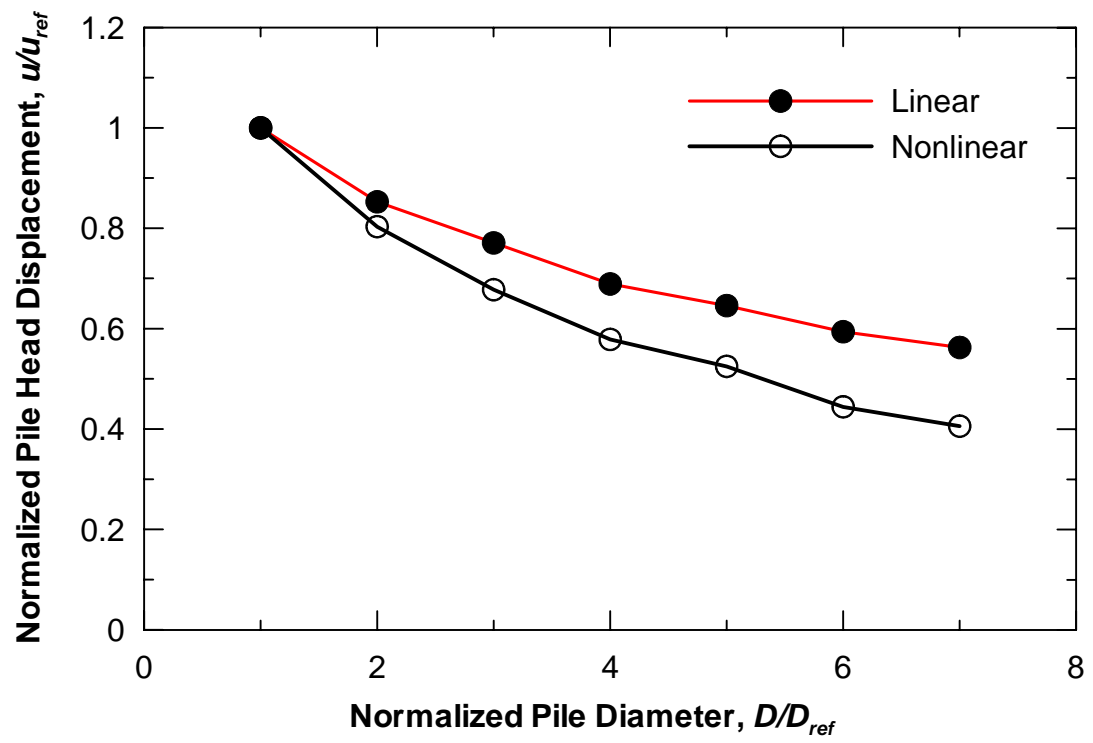


Figure 3.12 Comparison of Normalized Pile Head Displacement against Normalized Pile Diameter for Linear and Nonlinear Analyses

## **Chapter 4 FULL-SCALE TESTING**

The results of the 3-D finite element analyses in the previous chapter showed that the effect of pile diameter on pile response increases as the soil behavior changes from linear to nonlinear. The motivation from the analytical results leads to further investigation on the pile diameter effect in real soil where the nonlinearity is expected by its nature. Full-scale testing programs including vibration and lateral load testing were carried out to fulfill the aim of this study. The results from the vibration tests were used to study the behavior of soil-pile interaction at small strain, as well as to evaluate the pile diameter effect when the soil is linearly elastic. The results from the full-scale lateral load test were used to assess the pile diameter effect at larger strain levels where the soil behavior becomes nonlinear, as well as to evaluate the seismic performance of CIDH piles.

In this chapter, the site characterization is first discussed to give an overview of the site conditions and the strength characteristic of the soil at the test site. This is followed by the pile description which includes the pile geometry, reinforcement details, and pile instrumentation. Finally, the testing procedure and testing programs for both vibration and lateral load tests on CIDH piles are described.

### **4.1 Site Description**

The test site is located immediately east of Interstate 5 at the University of California, San Diego, known as UCSD East Campus. It is located southwest of Parking Lot 702 and southeast of a baseball field. The location map of the UCSD East Campus test site is shown in Figure 4.1. The test site is relatively flat, and is bounded on north and west by moderate to steep canyon slopes. The test specimens were located within the test site to avoid any slope effects. The topographic map of this site is presented in Figure 4.2.

According to available geologic literature (GEOCON, 1986 and Elliot, 1988), the soil formation of UCSD East campus property is underlain by the Eocene-aged Scripps Formation, the Pleistocene-aged Linda Vista Formation and four types of surficial deposits consisting of alluvium, colluvium, topsoil and landslide deposits. The Scripps Formation, a marine sedimentary deposit, generally consists of light brown and gray, weakly cemented silty sand interbedded with sandy siltstone, with clay beds and seams. Very hard cemented concretions occur frequently within this formation. The Linda Vista Formation, a non-marine and marginal marine sedimentary deposit, overlies the Scripps Formation. It consists of very dense, reddish-brown, cemented, clayey sand and occasional cobble conglomerates. The colluvial/ alluvial deposits are typically composed of loose, porous, silty clay/ clayey sand that have accumulated near the base of slopes or along canyon bottoms. The topsoil consists of loose, silty, dark grayish-brown, fine sands as well as clayey sands. Quaternary landslide deposits typically consisting of slide scarps and hummocky slide mass topography are commonly observed in the field, on topographic maps and stereographic aerial photographs. Though all these soils are found on East Campus, only the Scripps Formation is present at the test site as indicated in the geologic map in Figure 4.3.

Apart from the available literatures, a subsurface exploration was conducted to obtain more geotechnical information of the test site. The exploration work was started on September 2, 1998 and was completed on September 3, 1998. Two boreholes were drilled to depths of 20 m and 24 m by means of a percussion drilling method. The ground water table was not encountered during the soil investigation. The locations of both boreholes are presented in Figure 4.4. The Standard Penetration Test (SPT) was carried out to determine the strength characteristics of the soil. Soil samples were also collected at several depths by using split-spoon samplers for soil classification. Gradation analysis tests (ASTM 1998) using the wet-sieve method (ASTM D1140-97) were performed on the soil samples to determine the soil types as given in Appendix-A. Soil at this site consists of light brown and gray to dark brown, medium dense to very

dense cemented clayey to silty sand. According to the unified soil classification system: ASTM D2487-93 (ASTM 1998), the soil was classified as SC and SM. The corrected SPT N-values,  $(N_1)_{60}$ -values, varied from 16 to approximately 50 for the first 6 m. Below this layer, the  $(N_1)_{60}$ -values exceed 50. The SPT N-values were corrected based upon a hammer type and release system, sampler configuration, short rod lengths, and overburden stresses. Lenses and seams of siltstone and sandstone were found at various depths. Clay and silt (CL and ML) beds were also encountered. The soil boring log of each borehole is shown in Figure 4.5 and Figure 4.6. The corrected SPT N-value profile is presented in Figure 4.7a. In addition, the shear wave velocity profile was measured using the seismic down-hole technique. The travel-time curve together with calculated shear wave velocity is presented in Figure 4.7b. This type of stepped profile is common in weakly cemented sands (e.g. Ashford and Sitar 1994).

By the nature of weakly cemented sand, undisturbed soil samples are extremely difficult to obtain. The typical procedure used in California to characterize the shear strength of this particular type of soil is penetration resistance using the Modified California sampler. Direct shear tests on the driven samples are also occasionally conducted to evaluate the shear strength, but represent somewhat the lower bound values due to significant degree of soil disturbance during the sampling. In order to further understand the characteristics of the weakly cemented sand from the Scripps formation, additional soil data was extracted from available soil reports conducted at UCSD by local geotechnical engineering firms. The locations of soil investigation sites are presented in Figure 4.8, each site having three to eleven borings. Sites B-1 and B-2 were located in the direct vicinity of the test site. The blow count values using California sampler of the Scripps formation are more than 50, representing very dense sand. A summary of the blow counts of each borehole is given in Appendix B. Direct shear tests on driven soil samples were also conducted with cohesion ranging from approximately  $15 \text{ kN/m}^2$  to  $55 \text{ kN/m}^2$  and the angle of friction varying between 30 degrees and 32 degrees. The dry density of this formation ranged from  $14.6 \text{ kN/m}^3$  to  $19.2 \text{ kN/m}^3$  with an average value of

17.1 kN/m<sup>3</sup>. The moisture content varied between 5.4 % and 20.6% with an average value of 10.4%. A summary of soil properties are provided in Appendix B. The same soil formation also exists in several other locations on the UCSD campus. The soil properties of this formation at some locations further away from the test sites (i.e., site C-1, C-2, and C-3 in Figure 4.8) are summarized in Appendix C. Similar soil characteristics were observed with blow count values of more than 50. The results from direct shear tests show that soil cohesion ranged from approximately 36 kN/m<sup>2</sup> to 53 kN/m<sup>2</sup>, and the friction angle varied between 20 degrees and 34 degrees. The dry density varied between 13.0 kN/m<sup>3</sup> and 19.2 kN/m<sup>3</sup> with an average value of 16.4 kN/m<sup>3</sup>. The average moisture content is 15.8%.

In summary, the Scripps formation has the SPT N-values of more than 50, as a result the friction angle of 45 degree is suggested. The average dry unit weight of 17 kN/m<sup>3</sup> appears to be reasonable for this type of soil deposit with the water content of about 12%. Comparing the strength characteristic of this formation obtained from the subsurface investigation at the test site and data obtained from the local geotechnical firms, the soil condition at the test site appears to represent the lower bound soil strength of this formation.

## **4.2 Description of Test Piles**

### **4.2.1 Pile Geometry and Section Reinforcement Details**

Four different diameters of CIDH piles were designed and installed at the UCSD test site ranging in diameter from 0.4 m to 1.2 m. The 0.4-m CIDH pile was 4.5 m long and all others were 12 m long, though all acted as “long piles” (i.e., the piles were long enough that the lateral response was independent of depth.). A longitudinal reinforcement of 2% (i.e. volumetric ratio of longitudinal steel) and a transverse reinforcement of 0.6% (i.e. volumetric ratio of transverse steel) were used. The concrete cover of each pile was approximately 50 mm. The section reinforcement details of each

pile are presented in Figure 4.9. The reinforcing steel of the 0.4-m CIDH pile comprised 13- 15.9 mm (#5) bars with 9.5 mm (#3) spiral spaced at 152 mm intervals. The 0.6-m CIDH pile consisted of 15-22.2 mm (#7) with 9.5 mm (#3) spiral spaced at 89 mm intervals. The reinforcing steel of the 0.9-m CIDH pile consisted of 26- 25.4 mm (#8) bars with 12.7 mm (#4) spiral spaced at 102 mm intervals. The reinforcing steel of the 1.2-m CIDH piles contained 28- 32.3 mm (#10) bars with 15.9 mm (#5) spiral spaced at 121 mm intervals. A total of three specimens of each bar diameter were tested. The stress-strain curves from the tensile tests for each bar size are summarized in Figure 4.10 and Figure 4.11. The amount of transverse reinforcement was chosen to be lower than that specified in Caltrans Bridge Design Specifications, BDS (Caltrans 2000) because the effect of soil confinement in enhancing the inelastic behavior of CIDH piles was expected. According to Article 8.18.2.2.2 in BDS, the minimum ratio of spiral reinforcement in potential plastic hinge zone  $\rho_s$  shall not be less than:

for column 0.9 m or less

$$\rho_s = 0.45 \left( \frac{A_g}{A_c} - 1 \right) \frac{f_c'}{f_y} \left( 0.5 + 1.25 \frac{P_e}{f_c' A_g} \right) \quad (4.1)$$

or

for column larger than 0.9 m

$$\rho_s = 0.12 \frac{f_c'}{f_y} \left( 0.5 + 1.25 \frac{P_e}{f_c' A_g} \right) \quad (4.2)$$

But not less than the value given by

$$\rho_s = 0.45 \left( \frac{A_g}{A_c} - 1 \right) \frac{f_c'}{f_y} \quad (4.3)$$

where  $f'_c$  = concrete compression strength,  $f_y$  = yield strength of the spiral but cannot exceed 414 MPa,  $P_e$  = axial load,  $A_g$  = area of gross section, and  $A_c$  = area of core section.

According to this specification and the material properties of the pile, the minimum transverse reinforcement for each pile was calculated as summarized in Table 4.1. It should be noted that the amount of transverse reinforcement ratios compared to those recommended by BDS varied from 22% for the 0.4-m pile to 85% for the 1.2-m pile.

The piles were built and installed in two different periods. The 0.6-m and 0.9-m piles were installed in September 1998 (Phase I). The remaining piles were installed in September 2000 (Phase II). The piles were installed by using the Cast-In-Drilled-Hole (CIDH) method. The ground was drilled with a required diameter to a specified depth. After that, the instrumented steel cage was lowered into the drilled hole. The drilled hole was then filled with concrete. Figure 4.12 present sequence of an installation of a CIDH pile. The pile shaft above the ground and load stubs were constructed and cast approximately one month after the pile installation. Figure 4.13 and Figure 4.14 present the preparation and construction of load stubs. The target compressive strength at 28 days of each pile was  $f'_c = 24.1$  MPa. However, the actual compressive strengths were higher. The average compressive strength of concrete for each pile is given in Table 4.2.

#### **4.2.2 Instrumentation of Test Piles**

In this section, the instrumentation of test piles for lateral load testing is described, while that for vibration testing will be given in the following section. Several types of instrumentation (i.e., strain gauges, tiltmeters, load cells, and linear potentiometers) were installed on each pile specimen to measure pile responses under lateral loading. Strain gauges were instrumented along four longitudinal bars of each pile to obtain the bending moment along the pile. For the 0.6-m and 0.9-m piles, two instrumented longitudinal bars were approximately aligned with the loading direction and

the other two were perpendicular to the loading direction. However, the locations of instrumented strain gauge bars were modified for piles constructed in Phase II (i.e., 0.4-m and 1.2-m piles) to provide more information in estimating the pile curvature. Two instrumented longitudinal bars were aligned approximately with the loading direction. The other two were evenly spaced between them. The locations of strain gauge bars for each pile are presented in Figure 4.9. Strain gauges were attached along the pile length with closer spacing for the upper portion and wider spacing for the lower portion. The locations of strain gauges for each pile are summarized in Table 4.3. Furthermore, strain gauges were also attached along the spiral of the 0.6-m and 0.9-m CIDH piles for the first 3m below the ground surface to measure shear strain in the piles. The directions of these strain gauges were similar to bending strain gauge direction.

A series of tiltmeters were installed along the pile to monitor pile rotation during lateral load testing. They were used for computing the pile deflection as well as backing up the strain gauge data. For the 0.6-m and 0.9-m piles (Phase I), the tiltmeters were installed by tightening them with the reinforcing steel at depths of 0 m, 0.9m, 1.8m and 2.7 m. As a result, they could not be reused after the test. Considering the cost and the amount of tiltmeters required for each test, a system was specially designed and fabricated such that tiltmeters could be inserted into the inclinometer tube. With this design the tiltmeter can be pulled out after the lateral load test and reused for the next tests. Figure 4.15 shows a method in installing tiltmeters in the inclinometer casing. This type of system was used for the 0.4-m and 1.2-m piles in Phase II. A summary of locations of tiltmeters for each pile is given in Table 4.3. The other instrumentation, including linear potentiometers and load cells for providing the load-displacement curves, is discussed in the test setup for lateral load testing section because their locations depend on the configuration of each test setup.

### **4.3 Vibration Testing**

Prior to the lateral load testing, extensive vibration tests were conducted to determine the dynamic properties of the soil-pile system (i.e., natural frequency, damping, and mode shape) and to evaluate the pile diameter effect at a small strain level where the soil and the pile can be considered as a linear elastic material. Various types of vibration tests including ambient, impact, and forced vibration tests were carried out prior to conducting the lateral load test. These vibration tests were intended to determine the dynamic properties of the soil-pile system at small strain. In this section, the descriptions of instrumentation and data acquisition system are provided. This is followed by the descriptions of the testing procedure as well as the testing program.

#### **4.3.1 Description of Instrumentation**

##### **4.3.1.1 Accelerometers**

Two different types of accelerometers were used for the vibration testing. The PCB Model 393 C accelerometer is a very sensitive and robust accelerometer and it is suitable for most types of vibration testing, especially for very small vibration tests. The PCB accelerometer has a frequency range between 0.025 and 800 Hz, an amplitude range of  $\pm 2.5g$ , and a resolution of 0.0001g. They were attached on the load stub in N-S and E-W direction to measure the pile response during vibration.

The crossbow Model LF series accelerometer has an amplitude range of  $\pm 2g$  with a resolution of 0.0012g. The crossbow accelerometers LF series were only used for the forced vibration test at resonant frequency because they are small and therefore could be inserted into the pile via inclinometer tubes to measure the response of the pile at its resonant frequency, thus allowing it to obtain the mode shape. A series of the crossbow accelerometers were inserted into the inclinometer tube by means of attaching them to the inclinometer accessories. The locations of the accelerometers for the forced vibration

tests at a resonant frequency of the 0.4-m and 1.2-m CIDH piles are presented in Figure 4.16.

#### 4.3.1.2 Modal Hammer PCB 086 C50

The modal hammer PCB 086 C50 (Figure 4.17) was used to excite the pile to measure the dynamic properties of soil-pile system in the impact test. The hammer weighs 5.4 kg and has a head diameter of 75 mm. The hammer includes a series of four removable rubber tips for modifying the amplitude of the applied force and the frequency range of excitation.

#### 4.3.1.3 Mass Shaker

An eccentric mass shaker was used for the forced vibration test to generate sinusoidal dynamic force to the piles. The mass shaker (Figure 4.18) used in this study was initially designed and constructed at RPI (Van Laak and Elgamal 1991) based on the original Hudson (1964) design. Originally, the shaker was designed to provide up to 22 kN of horizontal shaking force within a frequency range of 0.5-30 Hz. To achieve this wide range of operating frequencies without exceeding the shaker-load capacity, both mass and eccentricity of the counter rotating elements are designed to be conveniently changed during testing by adding lead plates in the counter rotating steel buckets up to 10 Hz (Hudson 1964), or by replacing these buckets with eccentric steel masses (15.1 kg each) in the operational range of 10-30 Hz (Van Laak and Elgamal 1991). Though the shaker has the capability to handle a wide range of frequency interest, the amplitude of the dynamic force produced by the shaker with available types of buckets appeared to be too large for the test piles and could have caused significant disturbance to the soil-pile system before lateral load testing. The eccentric aluminum buckets (Figure 4.19) based on the original design of steel buckets were therefore designed and constructed to decrease the level of dynamic force produced by the shaker. The aluminum buckets were designed in such a way that the amplitude of dynamic force can be varied up to 4

different levels by adding the aluminum plates to the buckets (i.e., empty bucket (0.65 kg), one aluminum plate (1.46 kg), two aluminum plates (2.06 kg), and a full bucket (2.65 kg)). The relationship between amplitude of dynamic force and frequency excitation at different bucket masses is presented in Figure 4.20. A DC motor and electronic controller was used to drive the eccentric masses. The rotational speed of the shaker was verified to remain stable at any specified frequency within a 0.0625 Hz range.

#### 4.3.1.4 Recording and Data Processing Instruments

The HP 3566A dynamic analyzer was used to collect and process the data during testing. With this system, processing dynamic data in both time and frequency domains can be performed (e.g., power spectrum, frequency response, time/linear spectrum, and etc.). The description of the analyzer and signal conditioner is briefly provided.

##### HP Analyzer

The HP 3566A is an expandable analyzer that characterizes signals in both time and frequency domains. The analyzer uses an MS-DOS operating software and Microsoft Windows based user interface. The HP 3566A has 16 channels and a maximum frequency bandwidth of 12.8 kHz on each channel. Its specialty is multi-channel measurements and monitoring at low frequencies. The HP 3566A measurement hardware consists of a HP 35650A mainframe containing the following modules:

- 1 HP 35651C HP-IB/signal processor module
- 2 HP 35655A 8-channel input modules
- 1 HP 35653C source module

##### Signal Conditioner

The model 583 multi-channel signal conditioner is designed for powering piezoelectric sensors and provides an effective method for managing large numbers of sensor channels. The model used in this study has 16 channels.

## **4.3.2 Testing Procedure**

### **4.3.2.1 Ambient Vibration Test**

The naturally occurring vibration of the test piles embedded in the soil caused by wind and other environmental factors were measured during the ambient vibration test to yield the natural frequencies of the soil-pile systems. A power spectrum measurement was chosen to obtain the values of frequency components because the signal analyzer allowed for averaging the results of many runs, thus smoothing out the signal. In this case, a total of 100 runs were used for each test. The ambient vibration tests were performed on all piles. However, for the 1.2-m diameter pile where the magnitude of vibration was approximately noise level and the peak representing the natural frequency of the system could not be observed therefore the results of the ambient vibration test for the 1.2-m piles will not be presented. In some tests, an additional mass (220 kg) from the mass shaker was added to the system by mounting it on the load stub so as to decrease the natural frequency of the system.

### **4.3.2.2 Impact Vibration Test**

Frequency response measurement was used for the impact vibration test, which shows the ratio of the measured output to the input stimulus. The load stub was hit by a modal hammer with a load cell and a rubber tip to generate an initial velocity to the pile (Figure 4.21). The response under a free vibration of the pile was recorded using accelerometers. In this case, the input stimulus is the force that was applied to the load stub and the output is the acceleration of the load stub. A total of 10 hits per test were conducted for averaging the signal. The locations of accelerometers for this test were similar to those of ambient vibration test.

#### 4.3.2.3 Forced Vibration Test

For the forced vibration test, a mass shaker (harmonic oscillator) was mounted on the top of the pile to generate the sinusoidal excitation force (Figure 4.22). A series of frequency sweeps using sinusoidal excitation were performed. The pile was excited at a specific frequency until the steady-state response was attained and the pile response was recorded. The frequency of excitation was then increased and the process was repeated to obtain the response curve of which the resonant frequency of the system can be determined from its peak. For each set of resonant frequency test, the harmonic forced vibration tests were repeated at least 3 times to ensure that the constant of resonant frequency was obtained. The pile was then shaken at the resonant frequency and data from several crossbow accelerometers as well as strain gauges along the piles were recorded. With this data, the mode shape of the system can be computed. The effect of the level of dynamic force to the natural frequency of the system was also studied by adding more aluminum plates to the buckets resulting in an increase in the amplitude of excitation.

#### 4.3.3 Testing Program

In general, the testing program for vibration tests for each pile was essentially the same. The ambient and impact vibration tests were first performed before the forced vibration test to obtain the natural frequency of soil-pile system under undisturbed soil condition. Subsequently, the forced vibration test was conducted to obtain the dynamic properties at a higher strain level. A summary of testing program for vibration testing for each pile is given in Table 4.4 through Table 4.8.

#### 4.4 Lateral Load Testing

After the completion of vibration tests, a series of lateral load tests were performed under both static and cyclic loading to study pile diameter effect on  $p$ - $y$  curves

as well as evaluate inelastic behavior of CIDH piles with the effect of soil confinement. In this section, the test setup, testing program and testing procedure of each test are described.

#### **4.4.1 Test Setup**

A total of 4 lateral load tests were carried out. The first lateral load test was conducted in December 1999 (Phase I). The others were conducted in November 2000 (Phase II). The testing sequence is illustrated in Figure 4.23. One or two 2200-kN hydraulic actuators were connected between two piles to provide the lateral load to the test specimens. The larger pile served as a reaction pile to test the smaller one. The load acting on the specimen was measured by load cells in the actuator. Several string-activated linear potentiometers were attached to each pile to monitor pile displacements as well as load-displacement curves. The locations of string-activated linear potentiometers for each test are presented in Figure 4.24 through Figure 4.27 together with the locations of the other instruments (i.e., strain gauges and tiltmeters), which were connected to a data acquisition system. Figure 4.28 presented a photograph of lateral load test setup for the 0.6-m CIDH pile against the 0.9-m CIDH pile.

#### **4.4.2 Data Acquisition System**

Data from various instruments was collected through a high-speed data acquisition system with the LabVIEW computer software (National Instrument 1998) to acquire and manipulate the data during the test. The system was housed inside the UCSD mobile field testing laboratory as presented in Figure 4.29. The system consisted of a SCXI signal conditioner manufactured by National Instruments, and a DaqBoard to convert the conditioned analog signal into a corresponding digit number with a maximum scan rate of 100 kHz. The SCXI conditioner consisted of 4 SCXI 1001 chassis, 4 SCXI 1120 modules, 44 SCXI 1121 modules, 4 SCXI 1320 terminal blocks, and 44 SCXI 1321 terminal blocks having a capability to handle up to a total of 200 channels. The SCXI

1001 is a rugged, compact 12-slot chassis that is able to house the SCXI modules. The SCXI-1120 module is the 8 channel isolation amplifiers used for acquiring and changing the raw transducer signal (i.e., tiltmeter, load cell, and linear potentiometers) into a standardized voltage output. The SCXI-1121, which can also offer excitation sources for each channel, was used to acquire and manipulate the signal from strain gauges. The SCXI-1320 and 1321 terminal blocks provide a convenient method for connecting and disconnecting the signal to the SCXI modules.

#### **4.4.3 Testing Program and Testing Procedure**

The lateral load testing procedure for each pile was essentially the same. The sequence of a lateral load test can be divided into 3 categories: static load test, cyclic load test before idealized yield, and cyclic load test after idealized yield. The standard testing procedures are given as the following:

First, the static load test was performed to obtain the load-displacement information under static loading so as to develop  $p$ - $y$  curves for each pile. The loading procedure was conducted in general accordance with ASTM standard (ASTM 1998) with standard loading procedure: ASTM D3966-90. The test pile was pushed against the reaction pile until the load reached a target level. Then, the load was maintained for either 10 minutes or 20 minutes depending on the load level to allow the pile displacement to stabilize before the next step of loading. Afterward, the next load increment was applied and the same procedure was repeated. The specimen was loaded to 12.5%, 25%, 37.5%, 50%, 62.5%, 75% and 85% of the idealized yield load. After that, the pile was unloaded to 75%, 50% and 25% of yield load, and at each unloading step, the load was maintained for 10 minutes. The pile was then unloaded to zero. After a completion of the lateral static load test, the test pile was pulled back to its original position and then the cyclic load test was started. It should be noted that due to the error of estimation of the yield load based on the available  $p$ - $y$  curves, the actual loading scheme for each test was slightly different from the planning stage.

Second, the cyclic load test before the idealized yield of the pile was performed to study the strength degradation of pile-soil system due to an increase of number of load cycles. The pile was cycled 25 times at each step of loading for the 0.6-m pile. For the other piles, the number of cycles was decreased to 10 times because test results from the 0.6-m pile indicated that after the 5<sup>th</sup> cycle, no strength degradation was observed. The pile was loaded to the displacements at  $\pm 12.5\%$ ,  $\pm 25\%$ ,  $\pm 37.5\%$ ,  $\pm 50\%$ ,  $\pm 62.5\%$ ,  $\pm 75\%$ ,  $\pm 87.5\%$  and  $\pm 100\%$  of the idealized yield load. The displacement at the idealized yield load was estimated based on the test results from the static test. A ramp rate between 0.64 mm/s and 2.5 mm/s was applied during the test.

Finally, the cyclic load test was conducted after the idealized yield of the pile in order to study seismic pile performance. The pile was cycled 3 times to approximately  $\pm 150\%$ ,  $\pm 200\%$ ,  $\pm 250\%$ ,  $\pm 300\%$ ,  $\pm 400\%$ ,  $\pm 500\%$  and  $\pm 600\%$  of displacement at idealized yield corresponding to a displacement ductility of 1.5, 2.0, 2.5, 3.0, 4.0, 5.0 and 6.0, respectively. Since the actuator capacity in the pull direction was limited to only 980 kN, some displacement targets in the pull direction could not be achieved. Furthermore, it should be noted that there were some problems in controlling the actuator during lateral load test no.4, making the actual procedure slightly different from the planning stage. Details of test procedure of individual tests are given as the following:

#### 4.4.3.1 Lateral Load Test 1

The detail of the static test of the 0.6-m pile was different from the standard procedure given above. Unlike the other tests in which the piles were tested under load control, the test on the 0.6-m pile was conducted under displacement control. The load-displacement relationship for the 0.6-m diameter CIDH pile was first analyzed using the FLPIER computer program (University of Florida 1996) to develop the loading scheme that was implemented in the testing procedure. Based on the prediction, the displacement at the ground surface at idealized yield of the pile was approximately 3.2 mm with the ultimate load capacity around 250 kN. However, due to the uncertainty of soil and

material properties, as well as the doubt in accuracy in implementing the existing sand  $p$ - $y$  curves (Reese *et al.* 1974) for weakly cemented sand, the displacement of 25.4 mm was chosen to be the displacement at idealized yield. It was implemented in this way to decrease the risk in yielding the pile during the static test. The lateral load testing was conducted by pulling towards each other until it reached a specified displacement. The specimen was loaded to approximately +12.5%, +25%, +50%, +75% and +100% of the computed idealized yield displacement. At each step of loading, the load was maintained for 10 minutes to allow the displacements of the piles to be stabilized. The load was maintained for 20 minutes at the last loading step. Subsequently, the load was decreased to +50%, +25% and 0% of the computed idealized yield displacement.

To study the strength degradation of the pile-soil system due to an increase of number of load cycles, the pile was cycled 25 times at each step of loading. The pile was loaded to  $\pm 6.25\%$ ,  $\pm 12.5\%$ ,  $\pm 25\%$ ,  $\pm 50\%$ ,  $\pm 75\%$  and  $\pm 100\%$  of the computed displacement at idealized yield.

The 0.6-m diameter pile was then cycled 3 times to  $\pm 150\%$ ,  $\pm 200\%$ ,  $\pm 300\%$ ,  $\pm 400\%$ ,  $\pm 600\%$  of displacement at computed idealized yield to evaluate the seismic performance of the pile. An increase in the displacement of the pile was continued until the 0.6-m diameter pile reached failure.

#### 4.4.3.2 Lateral Load Test 2

The procedure of static load test was the same as the standard procedure given above. However, the actual yield load was lower than the predicted one (i.e., 1690 kN) causing the pile to yield at 75 % of the predicted yield load (i.e. 1112 kN). It was found that the actuator load measured in the first test should be reduced by 25% likely due to the human error. More details are discussed in the next chapter. Since the pile was yielded before the target load, the static loading procedure was adjusted by unloading from 75% to 50%, 25% and 0% of predicted yield load with maintaining the load for 10

minutes at each step. After that, the pile was pulled back to the original position and the cyclic load test was started by following the standard cyclic loading procedure as mentioned above. The pile was tested until the displacement of the pile head reached the capacity of a linear potentiometer.

#### 4.4.3.3 Lateral Load Test 3

The prediction of the load-displacement curve was made before the test in order to estimate the yield load and the yield displacement using the results from the previous test. The predicted yield load was 160 kN. The static test was first performed using standard procedure as discussed above. Based on the load-displacement curve obtained from the static test, the yield displacement was estimated for the cyclic loading scheme. The pile was tested under cyclic loading until the pile failed.

#### 4.4.3.4 Lateral Load Test 4

The results of the vibration test showed that at the end of the forced vibration test, the natural frequency of the 1.2-m pile (No.1) was slightly lower than that of 1.2-m pile (No.2). Therefore, it was expected that the stiffness of pile No.2 was slightly larger than that of pile No.1. The test arrangement was then prepared in such a way that pile No.1 was treated as a test pile and pile No.2 was treated as a reaction pile. The displacement at the loading point of pile No.1 was initially used to control the testing. The yield load was predicted as 2290 kN. Initially, the stiffness of pile No.1 was lower than No.2, as expected. However, beyond 25 mm of the displacement of pile No.1, its stiffness became higher than the other one. This was due to the fact that pile No.2 was located close to the natural slope. Therefore the soil resistance at a large displacement level was lower due to the smaller soil confining pressure. During the cyclic loading at 75% of displacement at the yield load of pile No.1, there was a problem in controlling the actuator. The actuator moved beyond the displacement target (i.e., 61 mm) by 20 mm causing considerable movement to pile No.2 (i.e., 380 mm). The test was then immediately stopped and the

controlled location of displacement was switched from pile No.1 to pile No.2. Then, the cyclic load test was continued until it reached the capacity of linear potentiometer.

#### **4.5 Summary**

A total of 5 instrumented CIDH piles with diameter varying between 0.4 m and 1.2 m were installed at the UCSD test site to study the pile diameter effect on the  $p$ - $y$  curves as well as to evaluate the effect of soil confinement in enhancing the inelastic pile performance. The steel reinforcing of each pile consisted of 2% of longitudinal reinforcement and 0.6% of transverse reinforcement. The amount of transverse reinforcement used in this study is below that suggested in the BDS. Based on the subsurface investigation results, the soil conditions at test site consisted of dense to very dense weakly cemented sand without the presence of water table. Two types of testing were conducted in this experimental study, including the vibration and full-scale lateral load testing. The vibration tests consisted of ambient, impact, and forced vibration tests with aiming at determining the dynamic properties of soil-pile system and utilizing the test results to evaluate pile diameter effect at a very small strain level. This was followed by the full-scale lateral load tests on CIDH piles under static and cyclic loadings. The static load test results were used for back-calculating the  $p$ - $y$  curves and evaluated the pile diameter effect. The cyclic lateral load tests were carried out to investigate the inelastic performance of CIDH piles. The test results of each test are presented in the next chapter.

Table 4.1 Minimum Transverse Reinforcement Required by Bride Design Specifications (Caltrans 2000)

Pile Diameter, $D$ (m)	$f_c'$ (Mpa)	$f_y$ (Mpa)	$\rho_s$ min (%)
0.4	31.9	450	2.7
0.6	41.4	447	2.0
0.9	42.1	432	1.2
1.2	34.5	450	0.7

Note: Since  $f_y$  for all sizes of pile diameter is more than 414 Mpa, the value of 414 Mpa was used to determine the minimum transverse reinforcement.  $f_c'$  was obtained from compression tests on concrete cylinders as summarized in Table 3.2.

Table 4.2 Summary of Average Concrete Strengths for CIDH Piles

Pile Diameter (m)	Average Compressive Strength $f_{c(ave)}$ (Mpa)			Curing Time Corresponding to Test Day (days)
	7 days	28 days	Test Day	
0.4	16.6	24.3	31.9	137
0.6	19.3	28.1	41.4	425
0.9	18.2	26.9	42.1	809
1.2	18.8	24.9	34.5	137

Table 4.3 Summary of Locations of Strain Gauges and Tiltmeters for Each Test Pile

Depth (m)	Strain Gauge				Tiltmeter			
	0.4-m Pile	0.6-m Pile	0.9-m Pile	1.2-m Piles	0.4-m Pile	0.6-m Pile	0.9-m Pile	1.2-m Piles
0.00	●	●	●	●	●	●	●	●
0.15	●							
0.30	●	●	●	●	●			●
0.46	●							
0.61	●	●	●	●	●			●
0.76	●							
0.91	●	●	●	●	●			●
1.07	●							
1.22	●	●	●	●	●			
1.52	●	●	●	●	●			●
1.83	●	●	●	●	●			
2.13	●	●	●	●	●			●
2.44	●	●	●	●	●			
2.74	●	●	●	●	●			●
3.05	●	●	●	●		●	●	
3.35								
3.66		●	●	●				●
3.96								
4.27		●	●	●				
4.57								●
4.88		●	●	●				
5.18								
5.49		●	●	●				●
5.79								
6.10		●	●	●		●	●	
6.40								●
6.71				●				
7.01								
7.32		●	●	●				●
7.62								
7.92								
8.23				●				
8.53		●	●					
8.84								
9.14				●		●	●	
9.45								
9.75		●	●					
10.06								
10.36								
10.67				●				
10.97		●	●					
11.28								
11.58								
11.89								
12.19								

Table 4.4 Summary of Testing Program for Vibration Testing for 0.4-m CIDH Pile

Date	Descriptions	Types of Vibration Testing		
		Ambient	Impact	Forced
	<b>0.4-m CIDH Pile</b>			
9/27/00	Undisturbed Soil Condition (Without Mass Shaker)	●	●	
10/9/00	Undisturbed Soil Condition (With Mass Shaker)	●	●	
	Forced Vibration with Empty Bucket (0.65 kg)-Test 1			●
	After Forced Vibration Test 1	●	●	
	Forced Vibration with Empty Bucket (0.65 kg)-Test 2			●
	After Forced Vibration Test 2	●	●	
10/10/00	Forced Vibration with Empty Bucket (0.65 kg)-Test 3			●
	After Forced Vibration Test 3	●	●	
	Forced Vibration with Empty Bucket (0.65 kg)-Test 4			●
	After Forced Vibration Test 4	●	●	
10/11/00	Forced Vibration with Empty Bucket (0.65 kg)-Test 5			●
	After Forced Vibration Test 5	●	●	
10/13/00	Without Mass Shaker	●	●	

Table 4.5 Summary of Testing Program for Vibration Testing for 0.6-m CIDH Pile

Date	Descriptions	Types of Vibration Testing		
		Ambient	Impact	Forced
	<b>0.6-m CIDH Pile</b>			
9/28/99	Undisturbed Soil Condition (Without Mass Shaker)	●	●	
11/4/99	Undisturbed Soil Condition (With Mass Shaker)	●	●	
	Forced Vibration with Empty Bucket (0.65 kg)-Test 1			●
11/5/99	Forced Vibration with Empty Bucket (0.65 kg)-Test 2-4			●
11/12/99	Forced Vibration with Empty Bucket (0.65 kg)-Test 5-13			●
11/17/99	Forced Vibration with One Plate (1.46 kg) -Test 1-6			●
	Forced Vibration with Two Plates (2.06 kg) -Test 1-5			●
11/18/99	After Forced Vibration Test	●	●	
	Forced Vibration with Empty Bucket (0.65 kg) -Test 14			●
	Forced Vibration with One Plate (1.46 kg) -Test 7			●
	Forced Vibration with Two Plates (2.06 kg) - Test 6			●
12/7/99	Immediately After Lateral Load Test	●	●	

Table 4. 6 Summary of Testing Program for Vibration Testing for 0.9-m CIDH Pile

Date	Descriptions	Types of Vibration Testing		
		Ambient	Impact	Forced
	<b>0.9-m CIDH Pile</b>			
9/28/99	Undisturbed Soil Condition (Without Mass Shaker)	●	●	
10/24/99	Forced Vibration with One Plate (1.46 kg) - Test 1			●
10/25/99	Forced Vibration with One Plate (1.46 kg) - Test 2-4			●
10/28/99	Forced Vibration with Full Bucket (2.65 kg)- Test 1-2			●
	Forced Vibration with Empty Bucket (0.65 kg)-Test 1			●
11/4/99	After Forced Vibration Test	●	●	
12/7/99	Immediately After Lateral Load Test	●	●	
12/16/99	Forced Vibration with Full Bucket (2.65 kg)- Test 3-5			●
03/1/99	2.5 Months after Lateral Load Test	●	●	

Table 4.7 Summary of Testing Program for Vibration Testing for 1.2-m CIDH Pile (No.1)

Date	Descriptions	Types of Vibration Testing		
		Ambient	Impact	Forced
	<b>1.2-m CIDH Pile (No.1)</b>			
9/27/00	Undisturbed Soil Condition (Without Mass Shaker)	●	●	
10/12/00	Undisturbed Soil Condition (With Mass Shaker)	●	●	
10/14/00	Forced Vibration with Empty Bucket (0.65 kg)- Test 1			●
	Forced Vibration with Empty Bucket (0.65 kg)- Test 2			●
	Forced Vibration with Empty Bucket (0.65 kg)- Test 3			●
	After Forced Vibration Test 3		●	
10/15/00	Forced Vibration with One Plate (1.46 kg) - Test 1			●
	Forced Vibration with One Plate (1.46 kg) - Test 2			●
	Forced Vibration with One Plate (1.46 kg) - Test 3			●
	After Forced Vibration Test 3		●	
	Forced Vibration with Two Plates (2.06 kg) -Test 1			●
	Forced Vibration with Two Plates (2.06 kg) -Test 2			●
	Forced Vibration with Two Plates (2.06 kg) -Test 3			●
	After Forced Vibration Test 3		●	
	Forced Vibration with Full Bucket (2.65 kg)- Test 1			●
	Forced Vibration with Full Bucket (2.65 kg)- Test 2			●
	Forced Vibration with Full Bucket (2.65 kg)- Test 3			●
	After Forced Vibration Test 3		●	
10/16/00	Forced Vibration with Two Plates (2.06 kg)			●
	Forced Vibration with One Plate (1.46 kg)			●
	Forced Vibration with Empty Bucket (0.65 kg)			●
10/17/00	Without Mass Shaker		●	

Table 4.8 Summary of Testing Program for Vibration Testing for 1.2-m CIDH Pile (No.2)

Date	Descriptions	Types of Vibration Testing		
		Ambient	Impact	Forced
	<b>1.2-m CIDH Pile (No.2)</b>			
9/27/00	Undisturbed Soil Condition (Without Mass Shaker)	●	●	
10/17/00	Undisturbed Soil Condition (With Mass Shaker)		●	
10/17/00	Forced Vibration with Empty Bucket (0.65 kg)- Test 1			●
	Forced Vibration with Empty Bucket (0.65 kg)- Test 2			●
	Forced Vibration with Empty Bucket (0.65 kg)- Test 3			●
	After Forced Vibration Test 3		●	
	Forced Vibration with One Plate (1.46 kg) - Test 1			●
	Forced Vibration with One Plate (1.46 kg) - Test 2			●
	Forced Vibration with One Plate (1.46 kg) - Test 3			●
	After Forced Vibration Test 3		●	
10/18/00	Forced Vibration with Two Plates (2.06 kg) -Test 1			●
	Forced Vibration with Two Plates (2.06 kg) -Test 2			●
	Forced Vibration with Two Plates (2.06 kg) -Test 3			●
	After Forced Vibration Test 3		●	
	Forced Vibration with Full Bucket (2.65 kg)- Test 1			●
	Forced Vibration with Full Bucket (2.65 kg)- Test 2			●
	Forced Vibration with Full Bucket (2.65 kg)- Test 3			●
	After Forced Vibration Test 3		●	
	Forced Vibration with Two Plates (2.06 kg)			●
	Forced Vibration with One Plate (1.46 kg)			●
	Forced Vibration with Empty Bucket (0.65 kg)			●

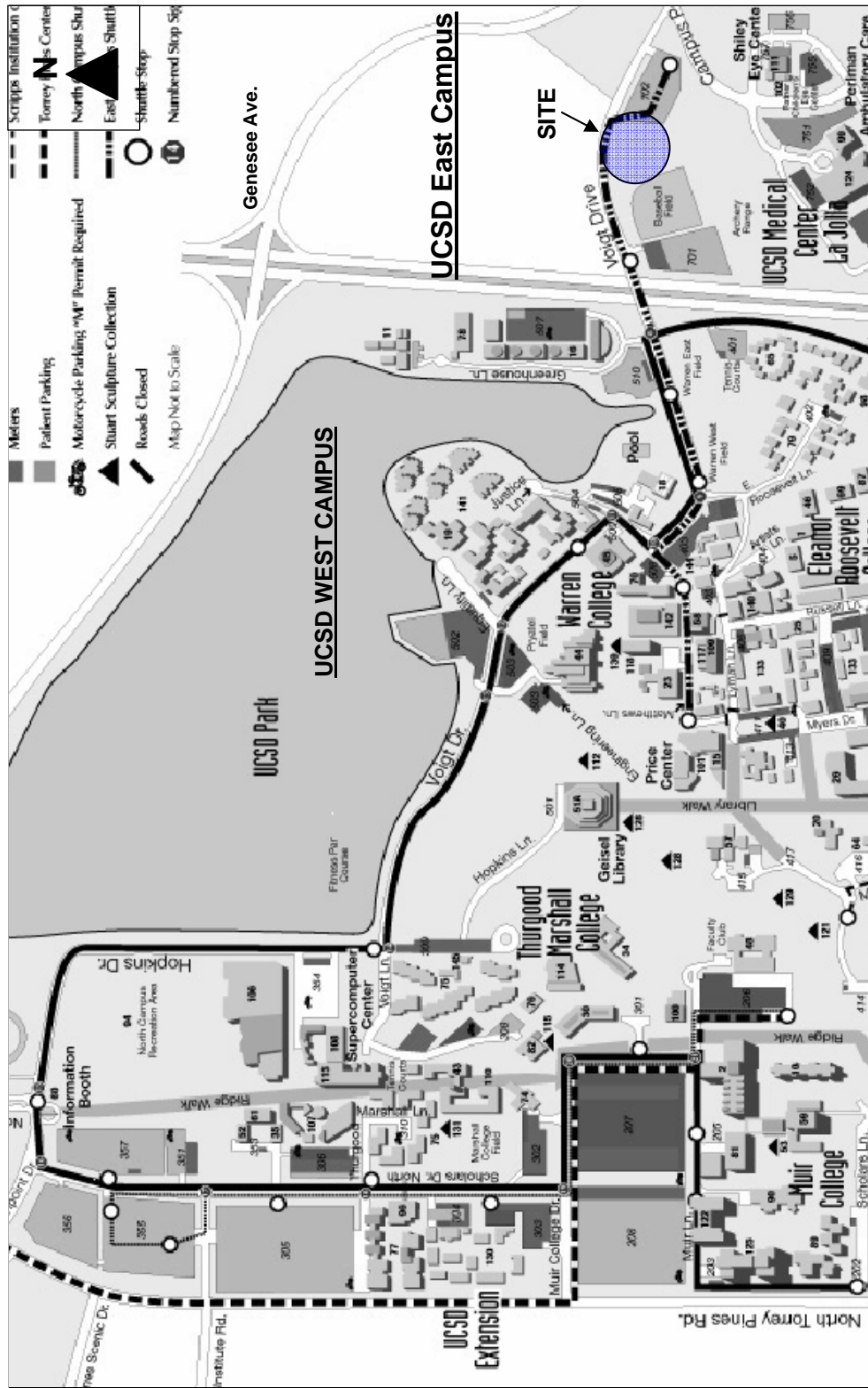


Figure 4.1 Location Map of UCSD East Campus Test Site

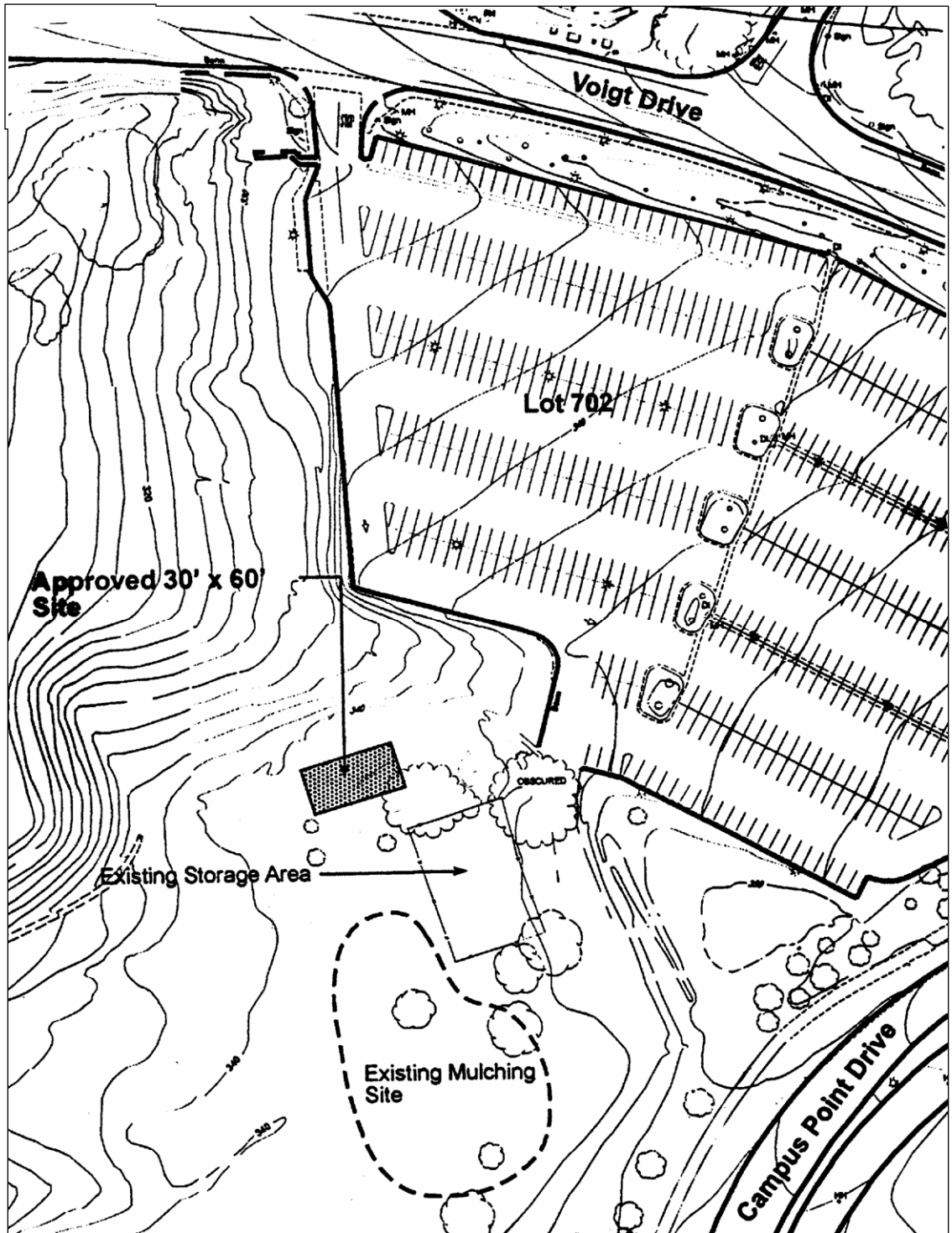


Figure 4.2 Topographic Map of UCSD East Campus Test Site

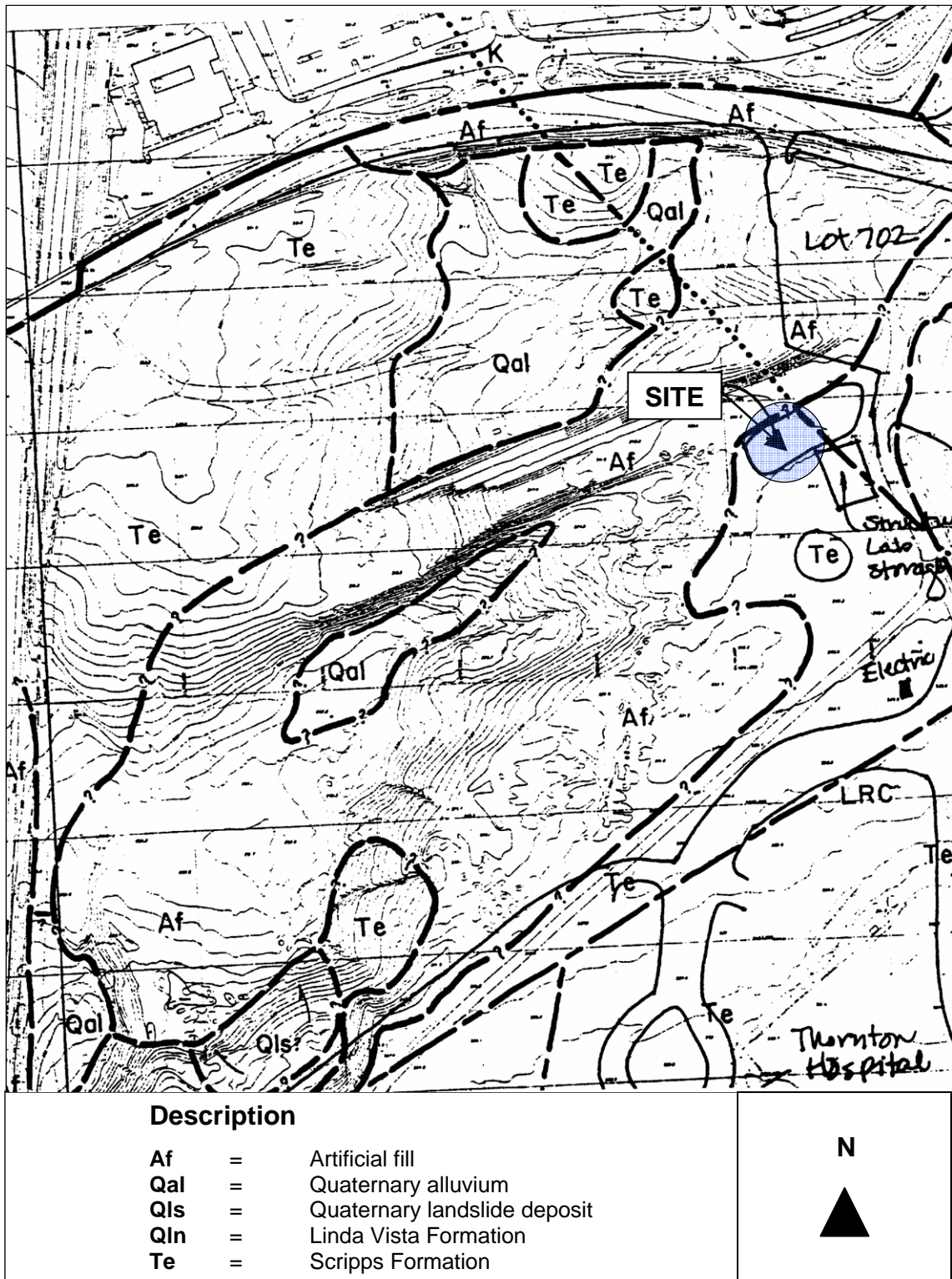


Figure 4.3 Geologic Map of UCSD East Campus Test Site (Elliot 1988)

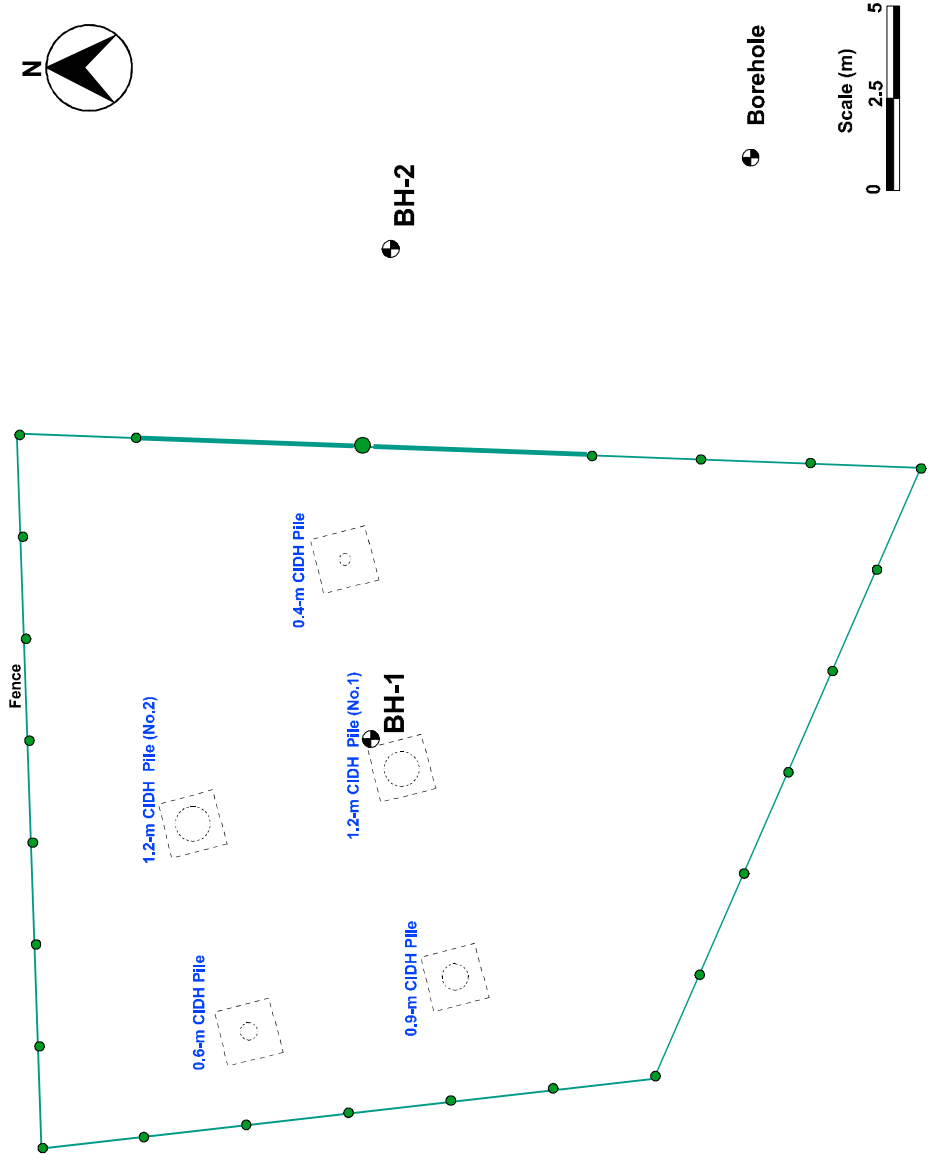


Figure 4.4 Location Map of Subsurface Exploration

	<b>Soil Boring Log</b>			
	Project Number	SSRCA06	Boring Number	BH-1
	Logger	T. Weaver	Sheet	1 of 3

Project	Caltrans	Elevation	103.4 m
Location	East Campus Test Site	Water Levels	Not encountered
Drilling Method and Equipment	Percussion Hammer	Starting Date	09/02/98 (8:30 AM)
Drilling Contractor	Tri County Drilling/ Dennis	Finishing Date	09/02/98 (7:50 PM)

Depth Below Surface (ft)	Sample			Standard Penetration Test Results  6"-6"-6" (N)	Soil Description  Soil Name, USCS Group Symbol, Color, Moisture Content, Relative Density or Consistency, Soil Structure, Mineralogy	Comments  Depth of Casing, Drilling Rate, Drilling Fluid Loss, Tests and Instrumentation
	Interval	Number and Type	Recovery (ft)			
5						8:55 Using Automatic Safety Hammer for SPT
(2m)	18"	S-1	12"	12-9-10 (19)	Silty SAND (SM), light brown, dry, medium dense	8:57 Using SPT with Liners
10						9:05
(4m)	18"	S-2	14"	10-9-15 (24)	Silty SAND (SM), light brown with hematite stains, dry, medium dense	
15						9:10 9:15
(6m)	18"	S-3	18"	12-20-23 (43)	Clayey SAND (SC), dark brown, moist, dense	
20						9:20
(8m)	18"	S-4	18"	13-21-18 (39)	Silty SAND (SM), light to dark brown, moist, dense	Driller says hit swelling layer @ 19' that blocked the hole
25						9:40
(8m)	12"	S-5	12"	7-44	Silty SAND (SM), light brown with hematite stains, slightly moist, dense	
30						

Figure 4.5 Soil Boring Log for Test Site (Borehole BH-1)

	<b>Soil Boring Log</b>			
	Project Number	SSRCA06	Boring Number	BH-1
	Logger	T. Weaver	Sheet	2 of 3

Project	Caltrans	Elevation	103.4 m
Location	East Campus Test Site	Water Levels	Not encountered
Drilling Method and Equipment	Percussion Hammer	Starting Date	09/02/98 (8:30 AM)
Drilling Contractor	Tri County Drilling/ Dennis	Finishing Date	09/02/98 (7:50 PM)

Depth Below Surface (ft)	Sample			Standard Penetration Test Results  6"-6"-6" (N)	Soil Description  Soil Name, USCS Group Symbol, Color, Moisture Content, Relative Density or Consistency, Soil Structure, Mineralogy	Comments  Depth of Casing, Drilling Rate, Drilling Fluid Loss, Tests and Instrumentation
	Interval	Number and Type	Recovery (ft)			
10m 35	8"	S-6	6"	51	Clayey SAND (SC), light brown, slightly moist, very dense	With Liners 9:50 9:55
	6"	S-7	6"	45-8 (5.7")		
12m 40	10"	S-8	6"	52 <sup>+</sup>	Clayey SAND (SC), light brown with olive and hematite stains, slightly moist, very dense	10:35
	6"	S-9	6"	50		
14m 50	6"	S-10	6"	51	SILTSTONE, grey with hematite stains, slightly moist	11:17
	0.4"	S-11	0.4"			
16m 55						12:30
18m 60						Using 50+ ft of Hex Rod for SPT, 2" Diameter Switching to Augers, cannot get percussion to penetrate 55 ft

Figure 4.5 Soil Boring Log for Test Site (Borehole BH-1, continued)

	<b>Soil Boring Log</b>			
	<b>Project Number</b>	SSRCA06	<b>Boring Number</b>	BH-1
	<b>Logger</b>	T. Weaver	<b>Sheet</b>	3 of 3

<b>Project</b>	Caltrans	<b>Elevation</b>	103.4 m
<b>Location</b>	East Campus Test Site	<b>Water Levels</b>	Not encountered
<b>Drilling Method and Equipment</b>	Percussion Hammer	<b>Starting Date</b>	09/02/98 (8:30 AM)
<b>Drilling Contractor</b>	Tri County Drilling/ Dennis	<b>Finishing Date</b>	09/02/98 (7:50 PM)

Depth Below Surface (ft)	Sample			Standard Penetration Test Results  6"-6"-6" (N)	Soil Description  Soil Name, USCS Group Symbol, Color, Moisture Content, Relative Density or Consistency, Soil Structure, Mineralogy	Comments  Depth of Casing, Drilling Rate, Drilling Fluid Loss, Tests and Instrumentation
	Interval	Number and Type	Recovery (ft)			
65	6"	S-12	6"	50	Silty SAND (SM) grey, dry, very dense	Use Auger to Penetrate to Depth of 65 ft
66						Auger 40 ft, 4:35
67						45ft, 4:50
68						50ft, 5:00
69						55ft, 5:10
70	60ft, 5:45					
75						
80						
85						
90						

Figure 4.5 Soil Boring Log for Test Site (Borehole BH-1, continued)

	<b>Soil Boring Log</b>			
	Project Number	SSRCA06	Boring Number	BH-2
	Logger	T. Weaver	Sheet	1 of 3

Project	Caltrans	Elevation	103.4 m
Location	East Campus Test Site	Water Levels	Not encountered
Drilling Method and Equipment	Percussion Hammer	Starting Date	09/03/98 (8:20 AM)
Drilling Contractor	Tri County Drilling/ Dennis	Finishing Date	09/03/98 (1:10 PM)

Depth Below Surface (ft)	Sample			Standard Penetration Test Results	Soil Description	Comments
	Interval	Number and Type	Recovery (ft)			
				6"-6"-6" (N)	Soil Name, USCS Group Symbol, Color, Moisture Content, Relative Density or Consistency, Soil Structure, Mineralogy	Depth of Casing, Drilling Rate, Drilling Fluid Loss, Tests and Instrumentation
5	(2m) 18"	S-1	12"	6-8-10 (18)	Clayey SAND (SC), light brown with hematite stains, dry, medium dense	8:21
10						
15	(4m) 11"	S-2	18"	5-6-5 (11)	Silty SAND (SM), dark brown, slightly moist, medium dense	8:26
20						
25	(6m) 11"	S-3	11"	31-43 (5")	Silty SAND (SM), light brown with some black grains and hematite strains, slightly moist, very dense	8:35
30						
30	(8m) 12"	S-4	10"	30-51 (5")	Silty SAND (SM), light brown with some black grains and hematite strains, slightly moist, very dense	8:45
30						
30	(8m) 12"	S-5	8"	30-51 (5")	Silty SAND (SM), light brown with some black grains and hematite strains, slightly moist, very dense	8:55
30						

Figure 4.6 Soil Boring Log for Test Site (Borehole BH-2)

	<b>Soil Boring Log</b>			
	<b>Project Number</b>	SSRCA06	<b>Boring Number</b>	BH-2
	<b>Logger</b>	T. Weaver	<b>Sheet</b>	2 of 3

<b>Project</b>	Caltrans	<b>Elevation</b>	103.4 m
<b>Location</b>	East Campus Test Site	<b>Water Levels</b>	Not encountered
<b>Drilling Method and Equipment</b>	Percussion Hammer	<b>Starting Date</b>	09/03/98 (8:20 AM)
<b>Drilling Contractor</b>	Tri County Drilling/ Dennis	<b>Finishing Date</b>	09/03/98 (1:10 PM)

Depth Below Surface (ft)	Sample			Standard Penetration Test Results  6"-6"-6" (N)	Soil Description  Soil Name, USCS Group Symbol, Color, Moisture Content, Relative Density or Consistency, Soil Structure, Mineralogy	Comments  Depth of Casing, Drilling Rate, Drilling Fluid Loss, Tests and Instrumentation
	Interval	Number and Type	Recovery (ft)			
10m	9"	S-6	6"	27-50 (3")	Silty SAND (SM), light grey with some black grains and hematite strains, slightly moist, very dense	9:07
35	12"	S-7	12"	21-54	Silty SAND (SM), light grey with some black grains and hematite strains, slightly moist, very dense (found lenses of grey siltstone near top of recovery)	9:22
12m 40	18"	S-8	18"	20-27-36 (63)	Sandy SILT (ML), grey with hematite stains, slightly moist, hard, flaky grains	9:35
45	17.5"	S-9	17.5"	12-28-52 (5.5")	Sandy SILT (ML), grey with hematite stains, slightly moist, hard ( found sand lense)	9:49
14m 50	11"	S-10	11"	42-50	Silty SAND (SM) to SILT with sand (ML), reddish brown to grey with hematite stains, slightly moist, very dense	10:02
16m 55	11"	S-11	11"	20-51	SILT with sand (ML), grey with hematite stains, slightly moist, hard	10:20 10:30
18m 60						

Figure 4.6 Soil Boring Log for Test Site (Borehole BH-2, continued)

	<b>Soil Boring Log</b>			
	<b>Project Number</b>	SSRCA06	<b>Boring Number</b>	BH-2
	<b>Logger</b>	T. Weaver	<b>Sheet</b>	3 of 3

<b>Project</b>	Caltrans	<b>Elevation</b>	103.4 m
<b>Location</b>	East Campus Test Site	<b>Water Levels</b>	Not encountered
<b>Drilling Method and Equipment</b>	Percussion Hammer	<b>Starting Date</b>	09/03/98 (8:20 AM)
<b>Drilling Contractor</b>	Tri County Drilling/ Dennis	<b>Finishing Date</b>	09/03/98 (1:10 PM)

Depth Below Surface (ft)	Sample			Standard Penetration Test Results  6"-6"-6" (N)	Soil Description  Soil Name, USCS Group Symbol, Color, Moisture Content, Relative Density or Consistency, Soil Structure, Mineralogy	Comments  Depth of Casing, Drilling Rate, Drilling Fluid Loss, Tests and Instrumentation
	Interval	Number and Type	Recovery (ft)			
65	6"	S-12	6"	52	Clayey SAND (SC), light brown with hematite stains, slightly moist, very dense	10:43
						10:50
20m 70	15"	S-13	15"	32-46-50 (3")	Silty SAND (SM), reddish brown with hematite stains, slightly moist, very dense	11:00
						12:10
22m 75	9"	S-14	9"	39-50	CLAY with sand (CL), greyish brown, slightly moist, hard	11:20
						11:30
24m 80	7"	S-15	6"	11-50	Clayey SAND (SC), brown with very little hematite stains, dry, very dense	11:50
26m 85	6"		0"	50 (6")	No Sample	1:00
90						

Figure 4.6 Soil Boring Log for Test Site (Borehole BH-2, continued)

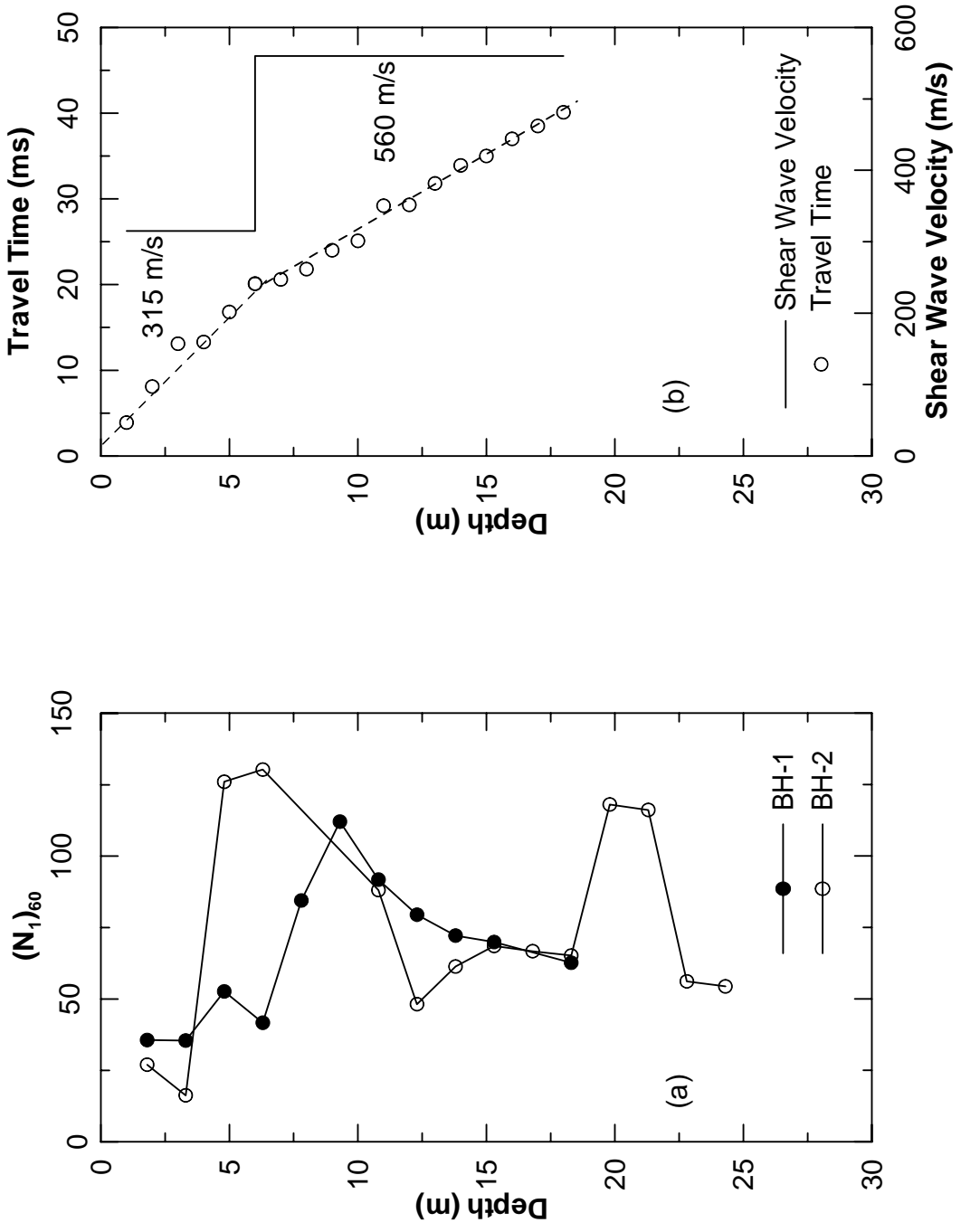


Figure 4.7 Soil Condition at Test Site Including (a) Corrected SPT-N-Values, and (b) Shear Wave Velocity Profile



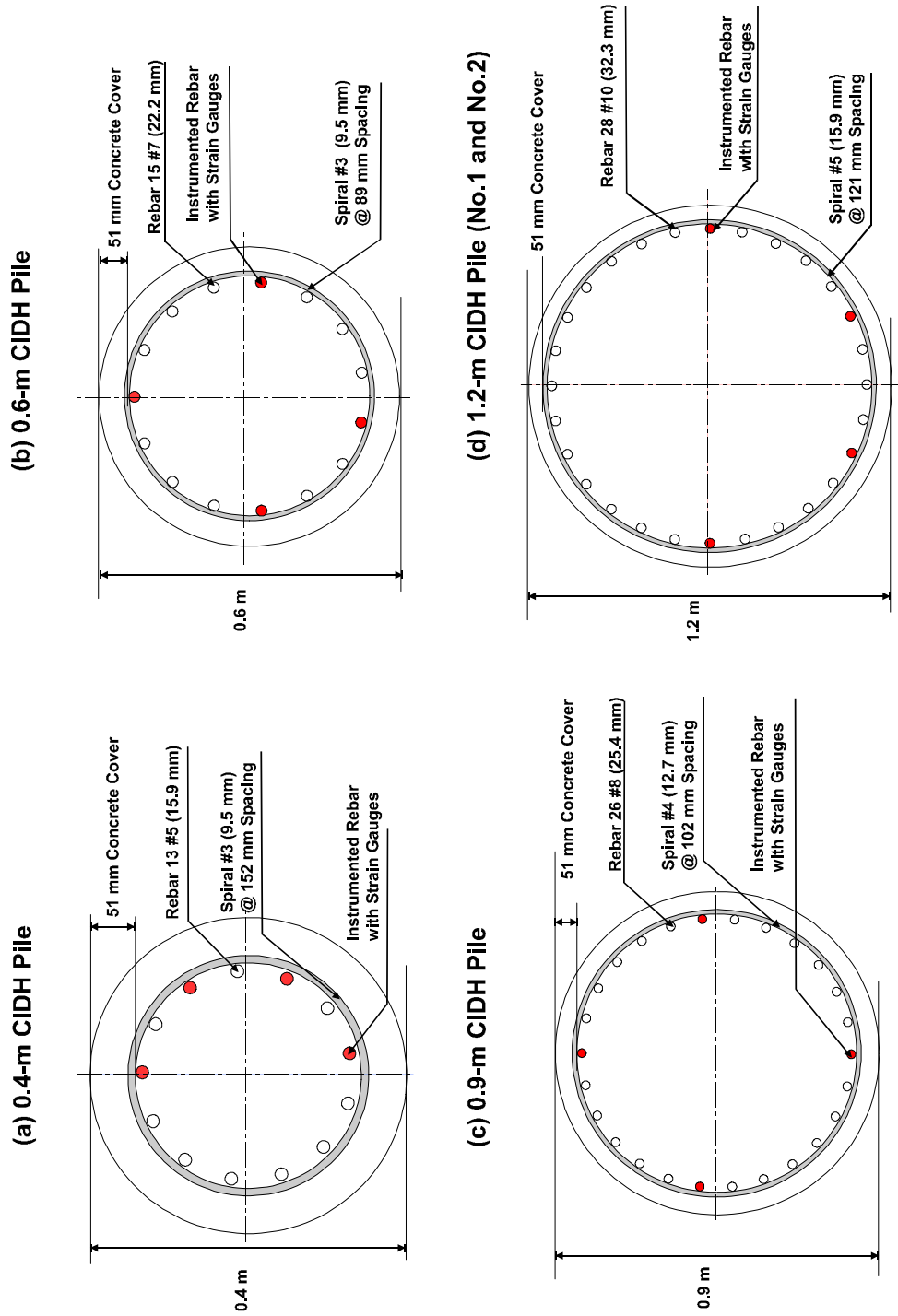


Figure 4.9 Pile Cross Section

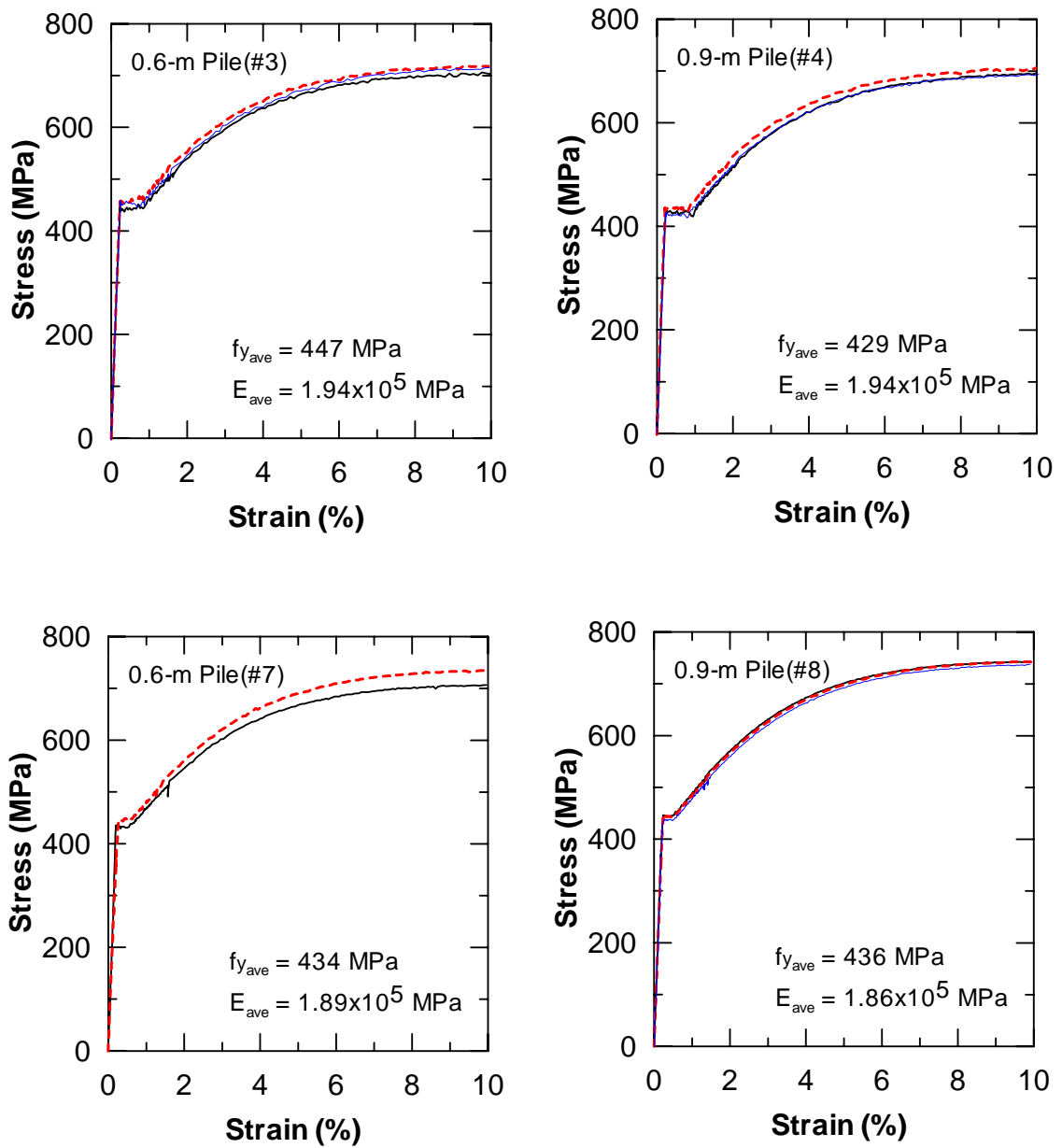


Figure 4.10 Steel Stress-Strain Curves for 0.6-m and 0.9-m Piles

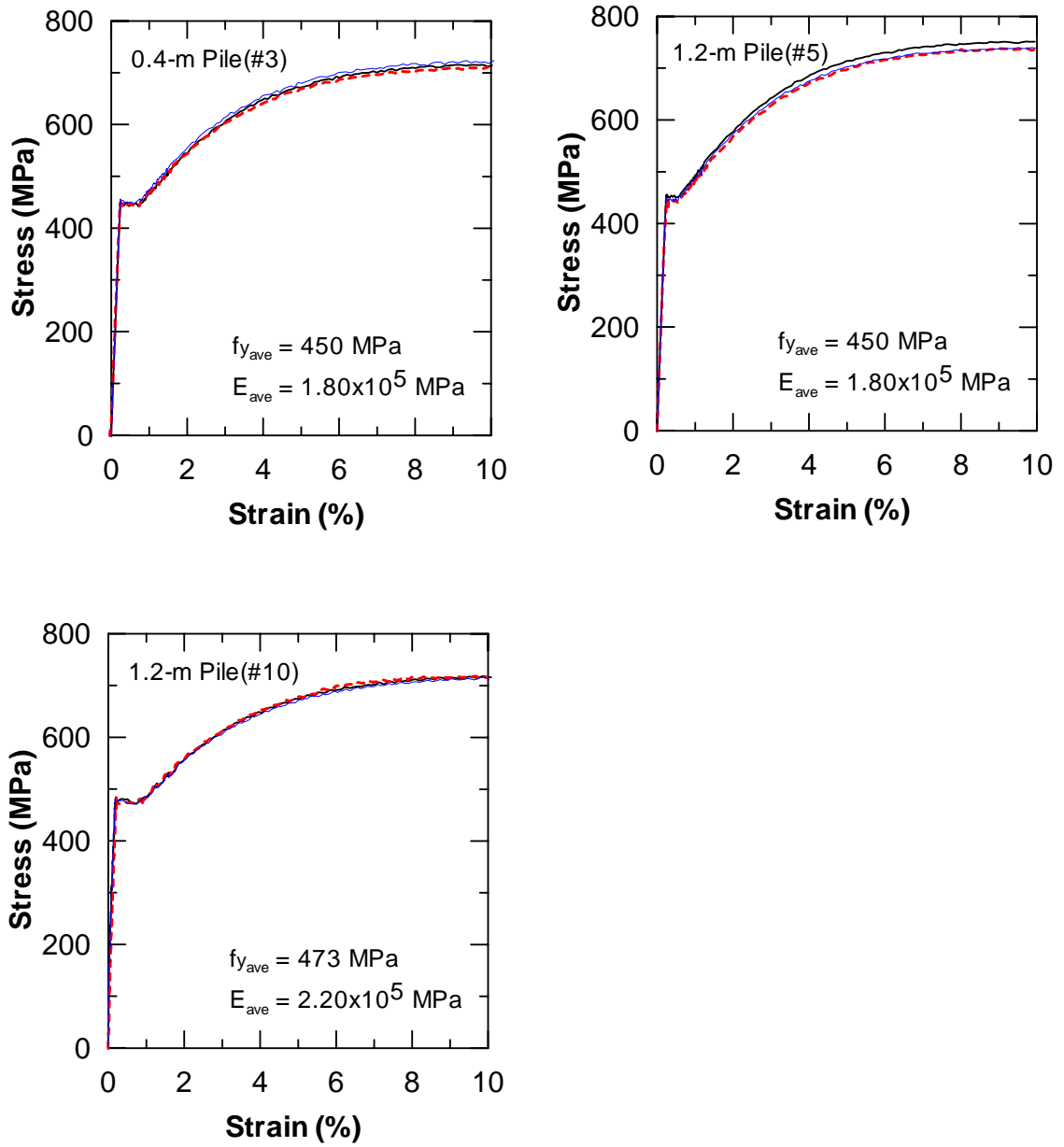


Figure 4.11 Steel Stress- Strain Curves for 0.4-m and 1.2-m Piles



Drilling a Hole for CIDH Pile Installation



Installing Instrumented Steel Cage



Steel Cage in Place



Filling with Concrete

Figure 4.12 Sequence of CIDH Pile Installation



Figure 4.13 Construction of Reinforcement for Load Stub



Figure 4.14 Completion of Form Works for Load Stubs



Figure 4.15 Installation of Tiltmeters into Inclinometer Casing

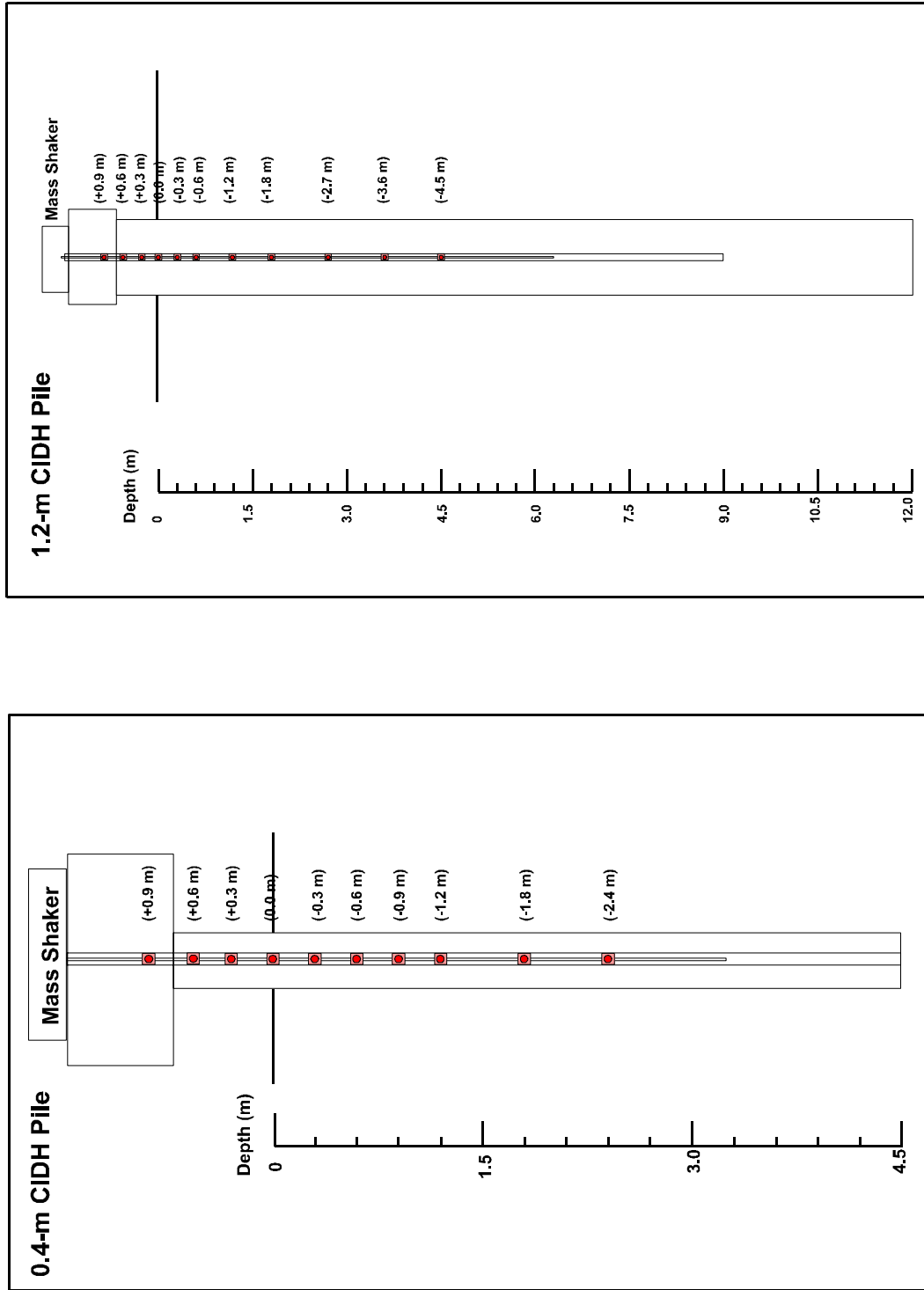
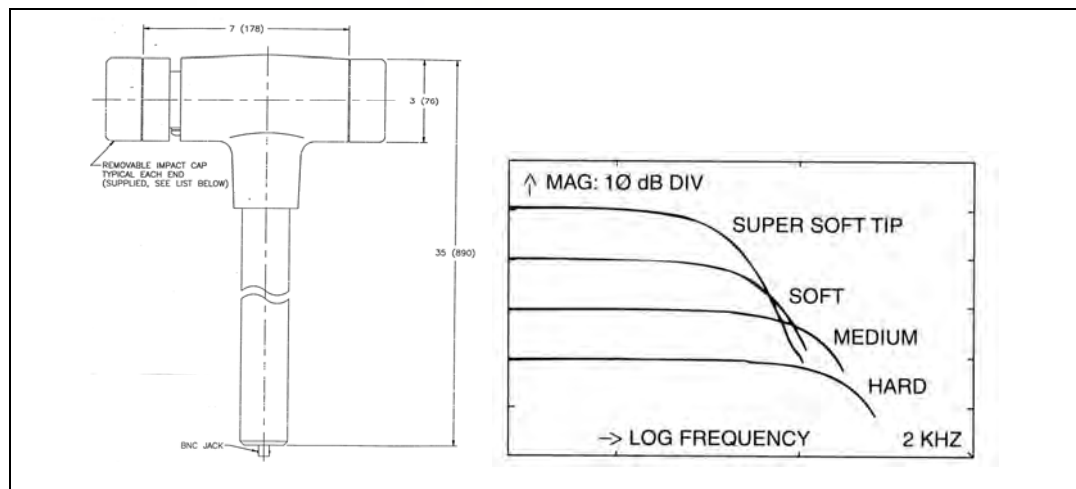
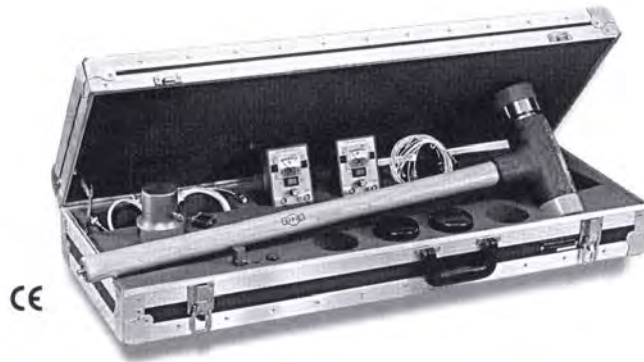


Figure 4.16 Locations of Crossbow Accelerometers for the 0.4-m and 1.2-m CIDH Piles in Forced Vibration Test



### Specifications

Voltage sensitivity	0.22 (1) mV/N (mV/lb)
Frequency range	0.5 kHz
Resonant frequency	2.7 kHz
Linearity error	< 2.0 %
Amplitude range	0-22 kN

### Physical Specifications

Mass	5.44 kg
Head diameter	75 mm
Tip diameter	75 mm
Handle length	889 mm

Figure 4.17 Modal Hammer Used for Impact Vibration Test

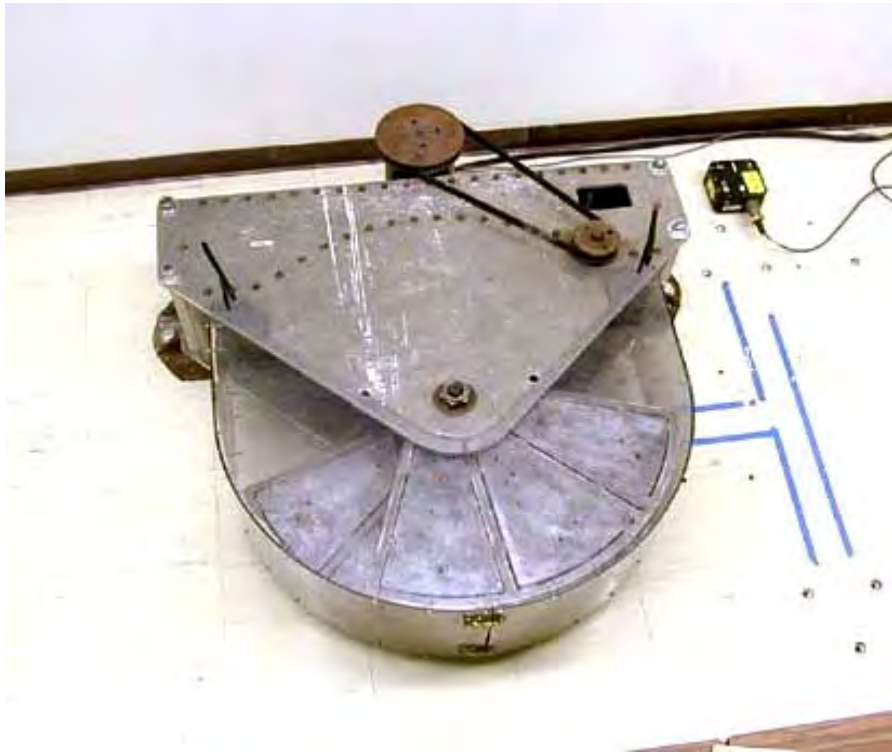


Figure 4.18 Eccentric Mass Shaker



Figure 4.19 Aluminum Buckets with Two Aluminum Plates on Each of Them

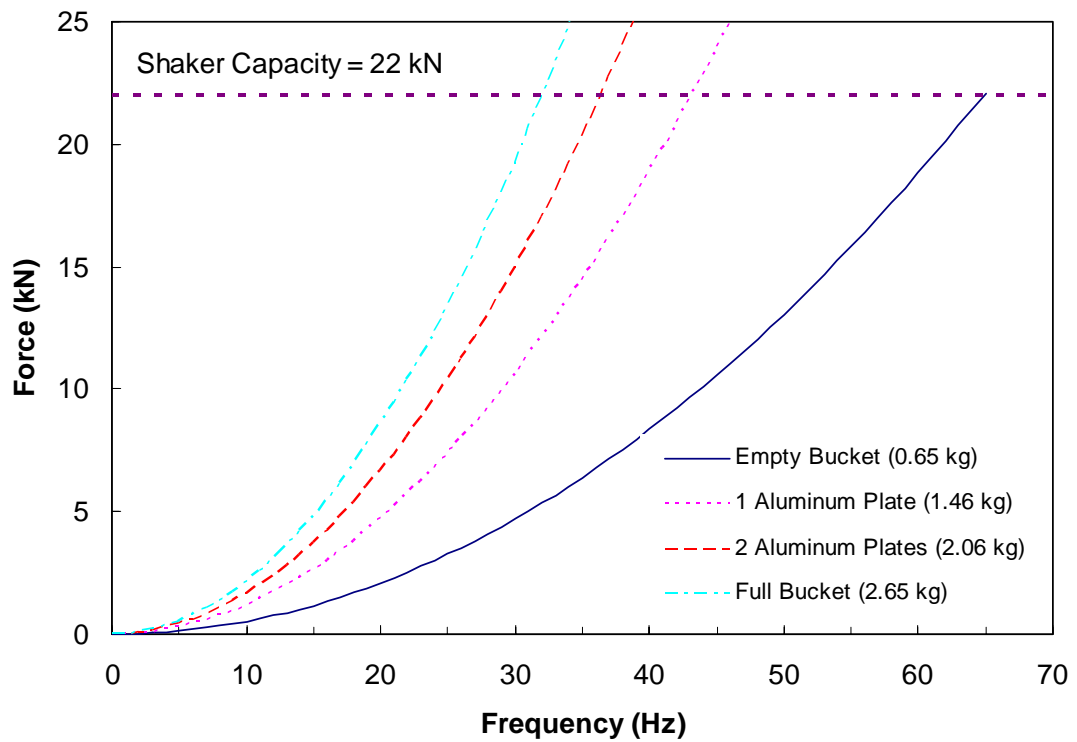


Figure 4.20 Relationship between Dynamic Force and Excitation Frequency for Different Masses of Aluminum Buckets



Figure 4.21 Modal Hammer Striking on Load Stub to Generate Initial Velocity to 0.6-m CIDH Pile for Impact Vibration Test



Figure 4.22 Mass Shaker Mounted on Top of Load Stub of 0.6-m CIDH Pile to Generate Harmonic Force Excitation to the Pile

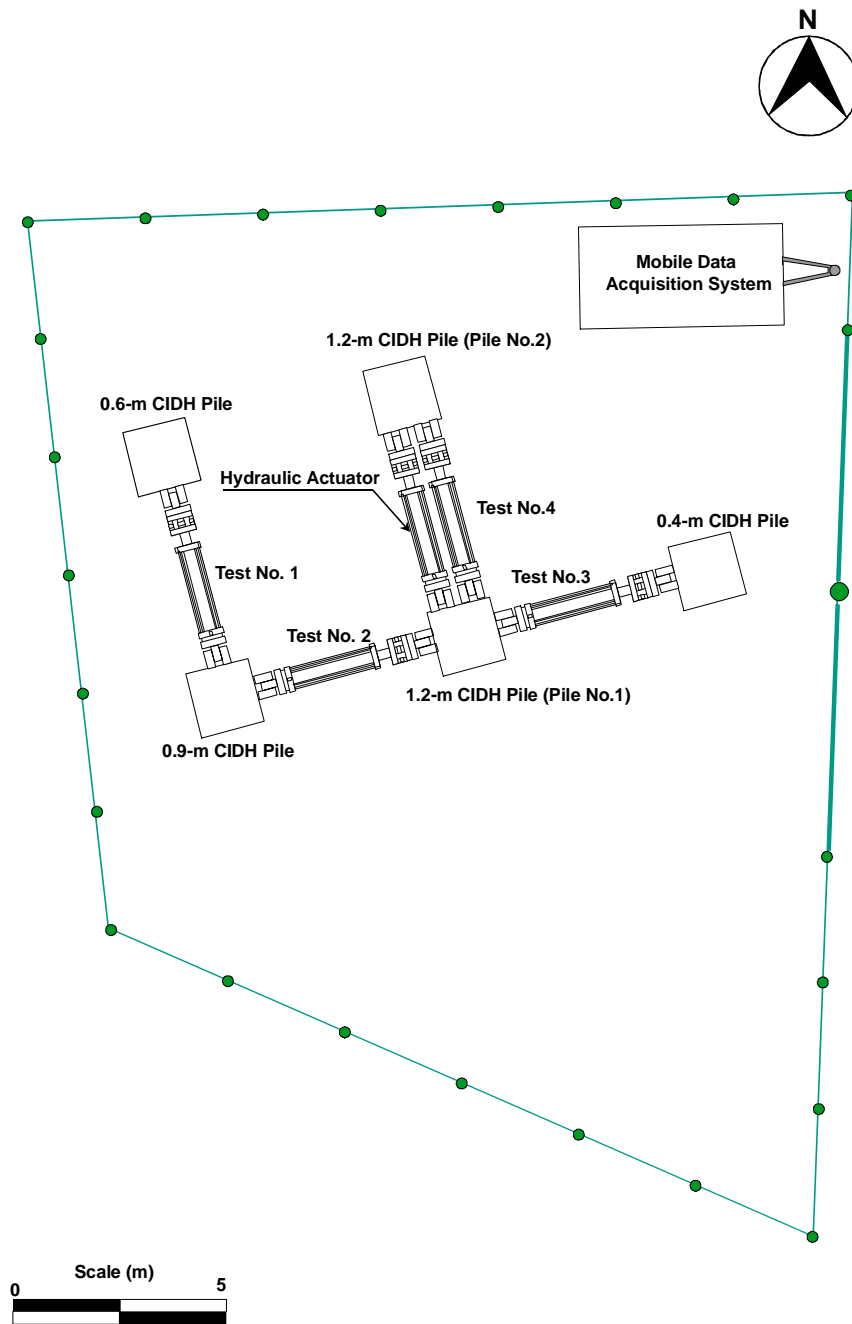


Figure 4.23 Lateral Pile Load Test Sequence

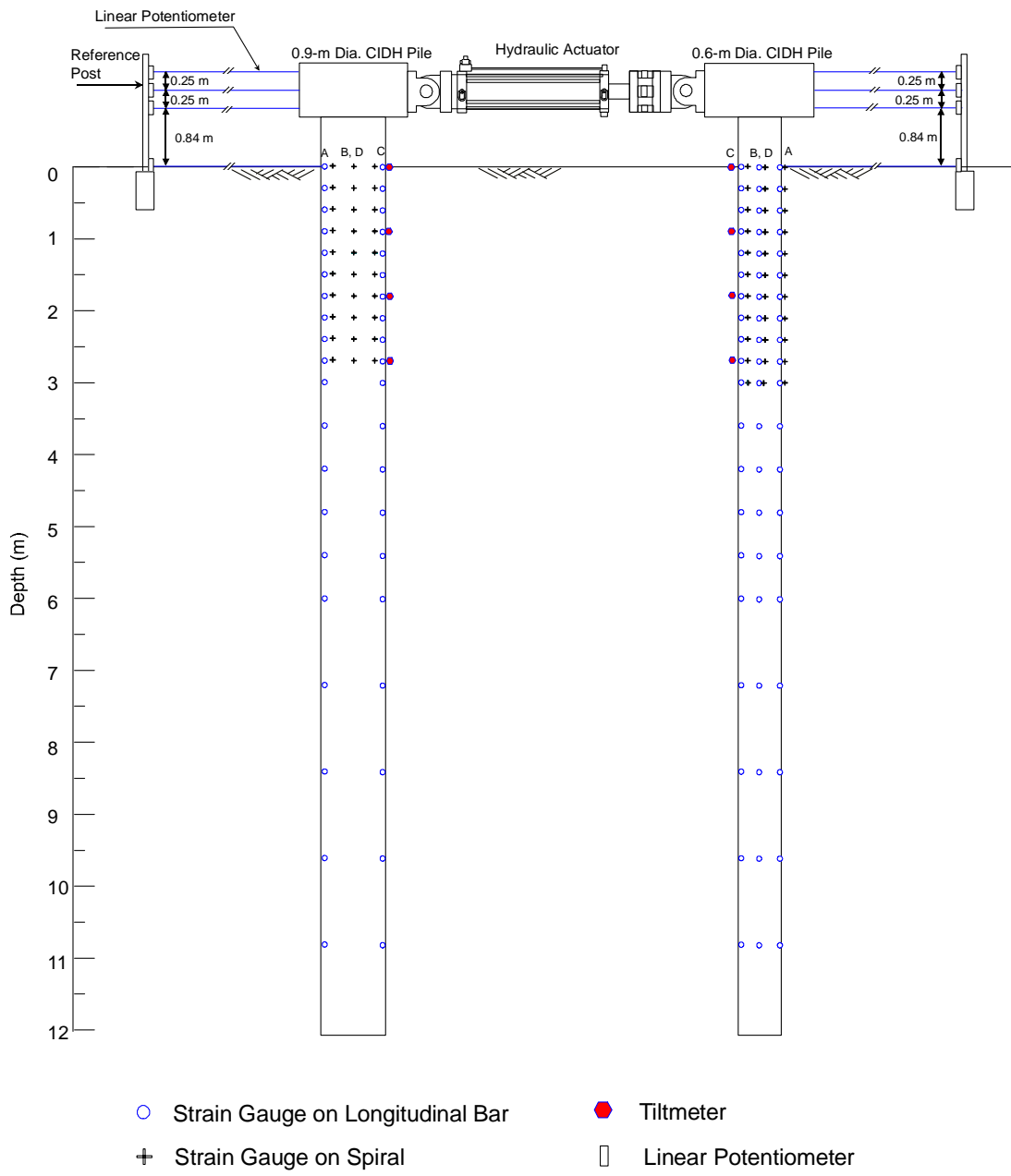


Figure 4.24 Lateral Load Test Set-up and Locations of Instruments (Test No.1)

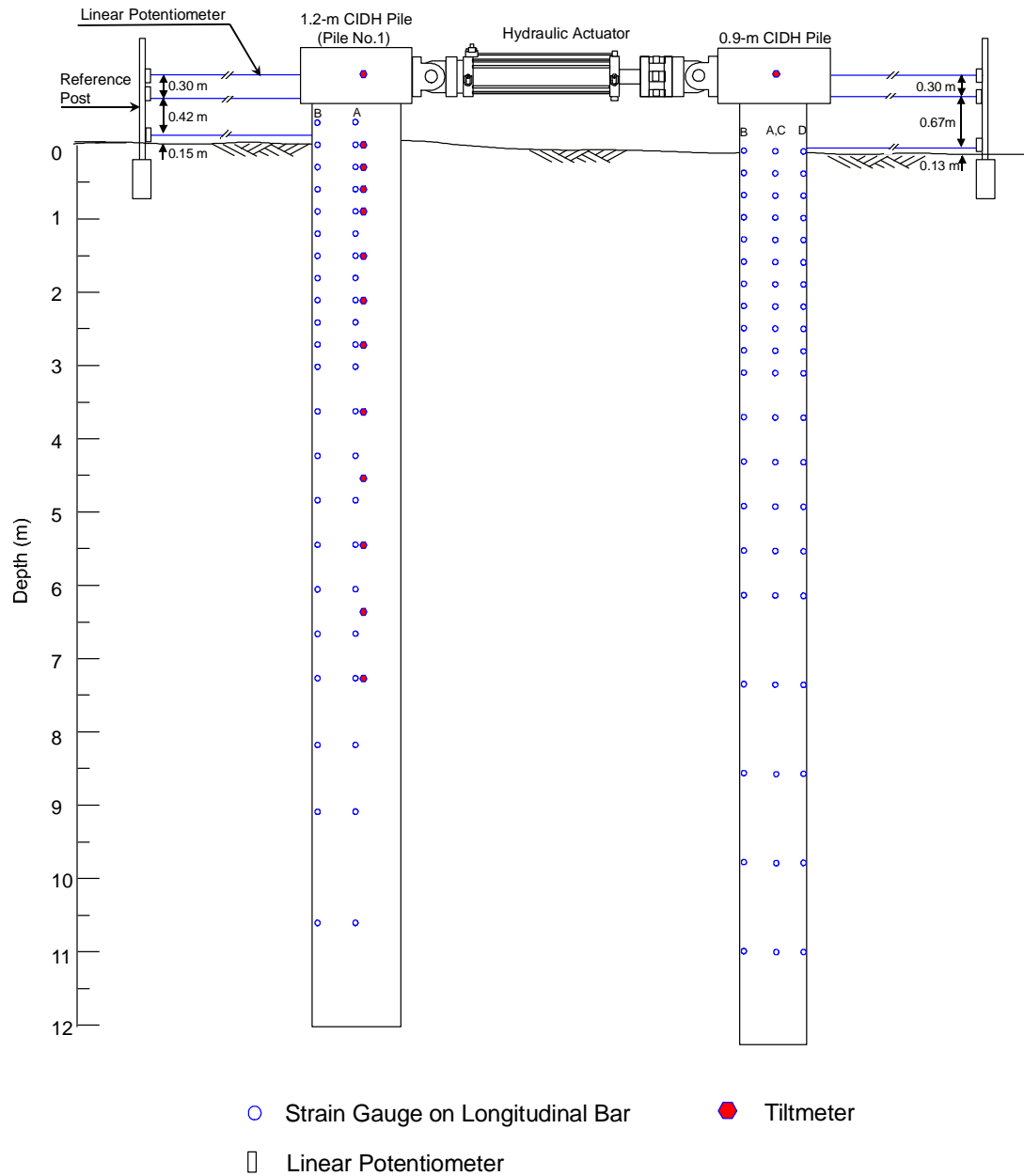


Figure 4.25 Lateral Load Test Set-up and Locations of Instruments (Test No.2)

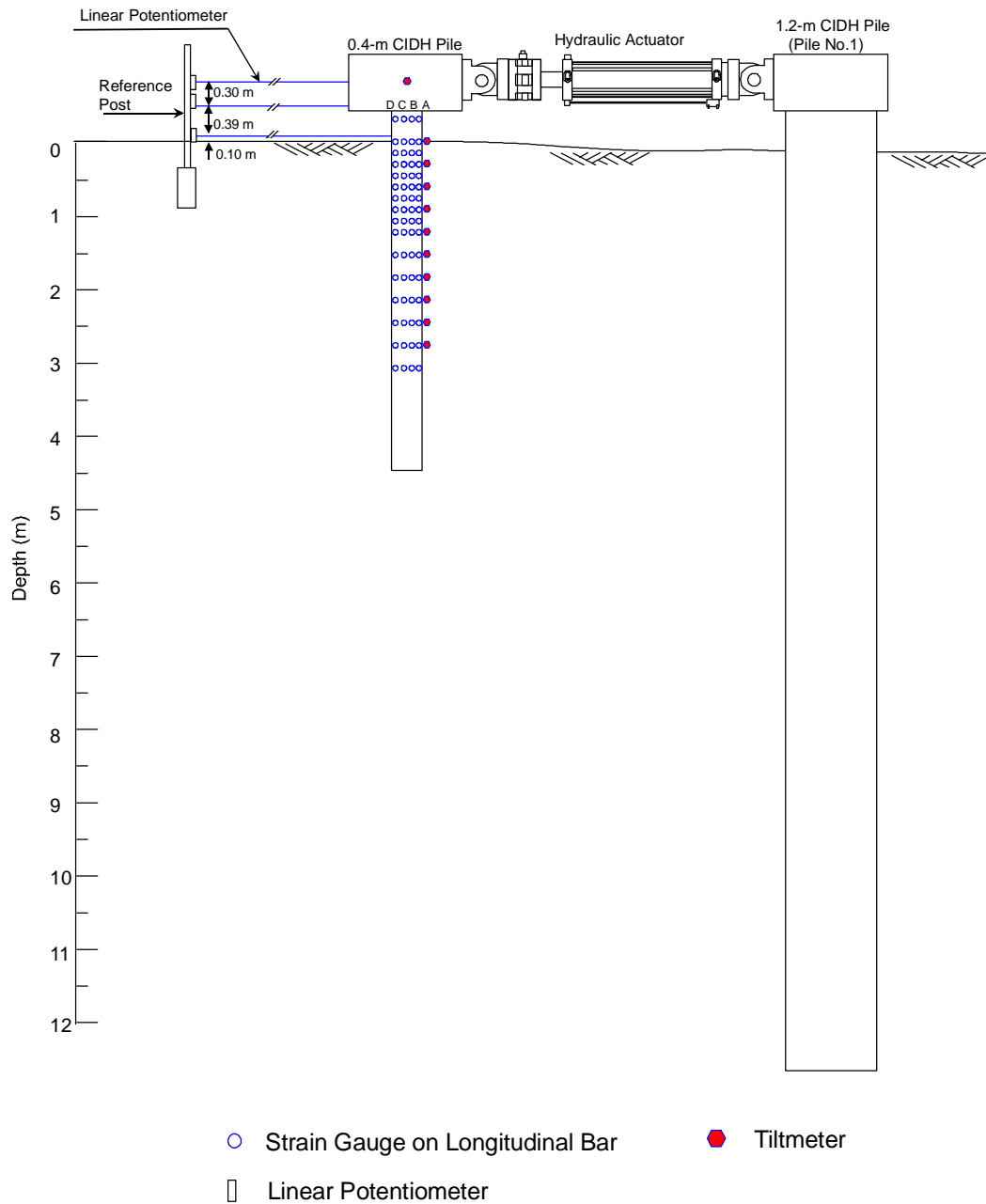


Figure 4.26 Lateral Load Test Set-up and Locations of Instruments (Test No.3)

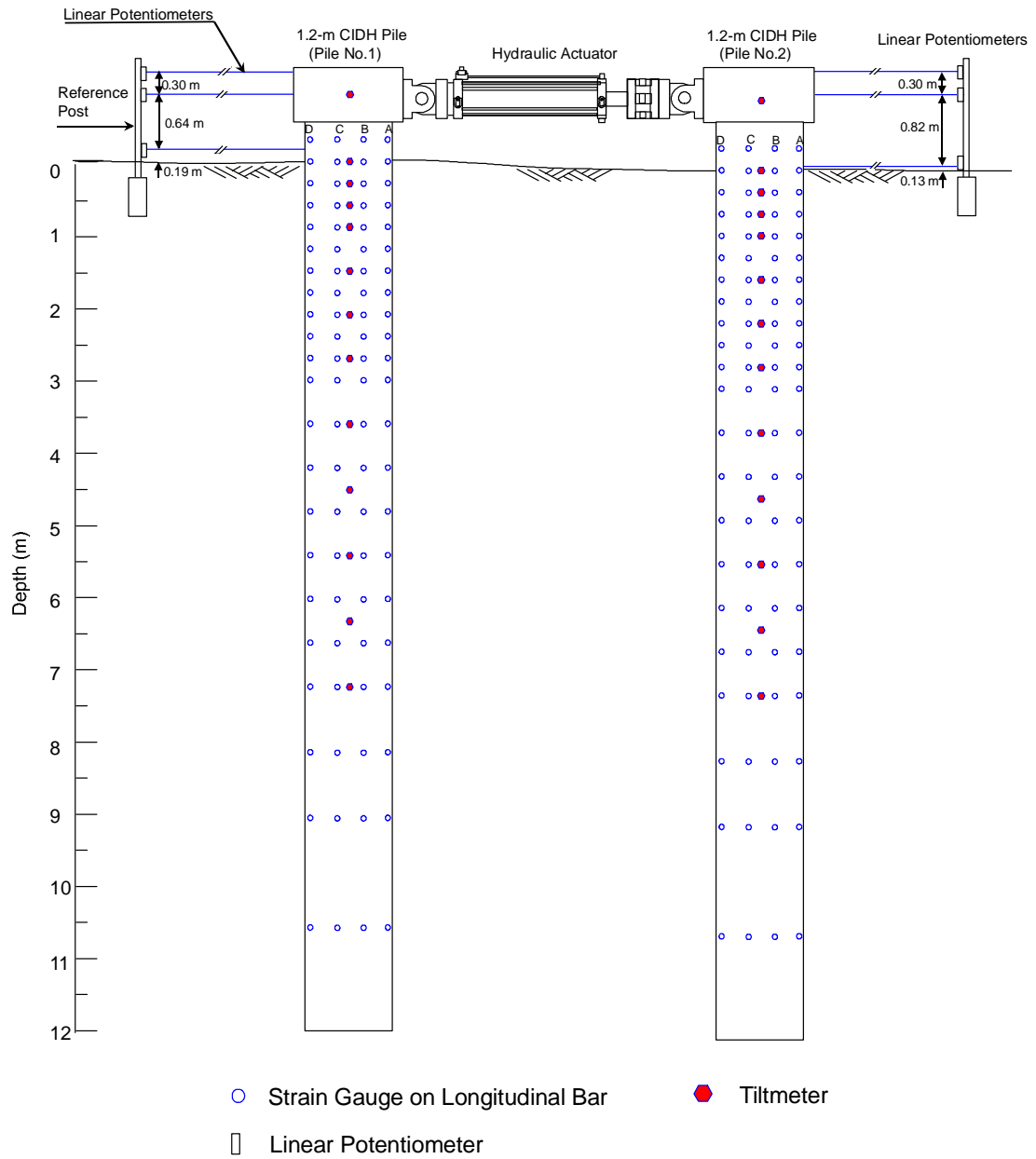


Figure 4.27 Lateral Load Test Set-up and Locations of Instruments (Test No.4)



Figure 4.28 Test Setup for Lateral Load Test No.1



Figure 4.29 UCSD Data Acquisition System

This page is intentionally blank.

## **Chapter 5 TEST RESULTS**

In this chapter, the test results from vibration and lateral load testing are presented. The first section presents the results from vibration testing, which includes the natural frequency, damping ratio, and mode shape of the soil-pile system. The second section provides the results from full-scale lateral load tests. The static and cyclic load-displacement curves of each pile together with strain gauge data are given. A brief description of pile damage and photographs are also provided. At the end of this section, the test results are discussed in specific topics, including the location of maximum moment and inelastic performance of CIDH piles.

### **5.1 Vibration Testing**

The results from three types of vibration tests (i.e., ambient, impact, and forced vibration tests) are presented in this section. The natural frequencies of the soil-pile systems obtained from different types of vibration tests are compared and discussed. This is followed by the results and discussions on the system damping ratio. Finally, the mode shapes of individual soil-pile systems derived from the strain gauge and accelerometer data are presented.

#### **5.1.1 Natural Frequency**

##### **5.1.1.1 Ambient Vibration Test**

The tests results obtained from both N-S and E-W directions are essentially the same; therefore, only the results for E-W direction are presents in the plots. Figure 5.1 through Figure 5.3 present the power spectrum from ambient vibration tests for the 0.4-m, 0.6-m and 0.9-m CIDH piles, respectively. The power spectrums presented in the plots were directly obtained from the signal analyzer, which allows the user to simply process the data in both time and frequency domain during the test. The plots represent the amplitude of acceleration in frequency domain before and after harmonic forced vibration

tests. The highest peak of acceleration represents the fundamental natural frequency of the soil-pile system. The results from the 1.2-m CIDH pile are not presented herein because the peak of the natural frequency of the soil-pile system could not be observed as shown in Figure 5.4. This is due to the fact that the pile had a very large stiffness; therefore, its vibration was so small that the amplitude of vibration was approximately noise level.

In general, the test results show that the natural frequency of the system decreases with increasing the degree of soil disturbance (i.e. the natural frequency of the system after conducting the forced vibration test was less than that of the undisturbed soil condition). Figure 5.2 shows that after lateral load test No.1 (i.e., 0.6-m pile vs. 0.9-m pile), the natural frequency of the 0.6-m pile significantly decreases from about 15 Hz to 3 Hz due to the degradation of pile integrity, with the pile reaching the failure at the end of the test. Figure 5.3 shows that the natural frequency of the 0.9-m pile before and after the lateral load test decreases from 25.4 Hz to 17.5 Hz. This is due to the fact that the force acting on the pile during the lateral load test caused the development of a gap deeper into the ground. As a result, the free standing length of the pile was longer and therefore lowered the system's stiffness. However, approximately 2.5 months after the test, the gapping of the soil surrounding the pile disappeared due to the rain and other environmental factors. The natural frequency of the system was then measured again. The natural frequency of the system was nearly fully recovered as presented in Figure 5.3. Figure 5.4 presents a comparison of the power spectrums of all pile diameters for the undisturbed soil condition. As expected, the natural frequency of the of the system increases with increasing the pile stiffness (i.e., pile diameter). A summary of natural frequencies obtained from ambient vibration tests is given in Table 5.1.

#### 5.1.1.2 Impact Vibration Test

The Frequency Response Function (FRF) of each pile obtained from the impact vibration test is presented in Figure 5.5 through Figure 5.9, which corresponds to the ratio

of the pile acceleration to the force applied using a modal hammer. Figure 5.10 presents the FRF of all piles in the same plots. The results from ambient and impact vibration tests are reasonably in good agreement. However, the natural frequency based on the impact vibration tests is better defined due to a higher amplitude of excitation. The natural frequency of the 1.2-m pile could be determined using the impact vibration test whereas this was not possible by means of the ambient vibration test. Similar findings as the ambient vibration tests were obtained. A summary of natural frequencies obtained from impact vibration tests is provided in Table 5.1.

#### 5.1.1.3 Forced Vibration Test

Figure 5.11 through Figure 5.19 present the frequency response curves for each pile obtained from forced vibration tests at different levels of amplitude of shaking. The excitation force ( $F = m\omega^2r$ ) is not constant. It is a function of the mass of the bucket,  $m$ , the angular frequency,  $\omega$ , and the radius to center of gravity of mass,  $r$ . For a given bucket (i.e.,  $m$  and  $r = \text{constant}$ ), the amplitude of acceleration depends on the square of angular frequency. Therefore, in order to consider the response due to the constant dynamic force throughout the frequency response curve, the measured acceleration,  $a$ , on the y-axis, was normalized by  $\omega^2$ . The peaks in the response curves represent the natural frequency of the system. Figure 5.11 and Figure 5.12 shows that there are two peaks in the response curves. The first peak represents the natural frequency of the translation mode. The second peak represents the natural frequency due to rocking caused by the unexpected loosening of the motor of the shaker during the testing. This explanation was obtained from the filed observation on the motor of the shaker at the end of the last test on the 0.4-m pile, as well as the results from the impact vibration tests. The results from the impact vibration tests show that this rocking mode was not observed either before the shaking where the motor was still completely fixed to the shaker or when the shaker was removed but existed at the end of the forced vibration as presented in Figure 5.5 and Figure 5.6.

It can be observed that the natural frequencies obtained from forced vibration test are somewhat lower than those obtained from ambient and impact vibration tests. The excitation force produced by the shaker was large enough to form a small gapping around the pile resulting in lowering the system stiffness, and consequently reducing the system natural frequency. The natural frequency of the system depends on the level of excitation force and the number of test runs. Figure 5.16 presents frequency response curves for the 1.2-m pile (No.1) at different levels of horizontal excitation force. Considering at the same force level, the natural frequency of the system progressively drops between the initial and the final sweep tests. The natural frequency tends to be constant with increasing number of sweep tests because the gap length was stabilized (i.e., shakedown effect). In addition, as the amplitude of excitation force increases, the natural frequency of system decreases. This might be due to two possible reasons: 1) the pile becomes nonlinear as the amplitude of the excitation increased and/or 2) the gap length increases with excitation force. In order to verify this, at the end of the sweep tests with the pile experiencing the maximum level of excitation force, additional sweep tests were performed at lower amplitudes of excitation force. By doing this, the gap length or the free standing height of the pile remained unchanged. If the decrease in natural frequency was due to the pile nonlinearity, lowering the amplitude of shaking would increase the natural frequency of the system. In fact, the test results for the 1.2-m pile (No.1) in Figure 5.17 indicates that the natural frequency of the system remained the same even though the amplitude of shaking changed, inferring that the decrease in natural frequency was essentially due to the growth of the gap length with amplitude of shaking (i.e., free standing height increased with amplitude of shaking). Similar results were observed for the other pile diameters as presented in Figure 5.13, Figure 5.15, and Figure 5.19. Figure 5.20 presents a comparison of response curves for different pile diameters which shows that the natural frequency of the system increases with an increase of pile diameter. Table 5.2 summarizes the natural frequencies of individual piles obtained from forced vibration tests.

## 5.1.2 Damping Ratio

### 5.1.2.1 Impact Vibration Test

Figure 5.21 presents the typical acceleration response of each pile under free vibration obtained from impact vibration tests. As expected, the motion of the piles decays with time. This decay is more rapid for the larger pile relative to the smaller pile. Based on these decayed curves, the damping ratios were estimated using the logarithmic decrement method. The damping values were also obtained by the method of half-power bandwidth of the Frequency Response Function peaks. The damping ratios based on both methods are in good agreement. The damping ratio varies with pile diameter from approximately 3% for the 0.4-m pile to about 25% for the 1.2-m pile as summarized in Table 5.3. The results indicate that motion in the larger pile decays more rapid than that of the smaller one. The damping of the system is mainly attributed to radiation damping because material or hysteretic damping is negligible in small strain testing (i.e. impact test). The radiation damping, associated with energy carried away from the foundation by stress waves traveling in the soil, is a function of contact area and excitation frequency (Dobry and Gazetas 1985). For that reason, as the pile diameter becomes larger, the excitation frequency and contact area increase, and consequently increasing the damping of the system.

### 5.1.2.2 Forced Vibration Test

Table 5.2 summarizes damping ratios of the system for each pile obtained from forced vibration testing by using the half-power bandwidth method. Considering the same pile diameter, the damping ratios obtained from the forced vibration tests were generally lower than those obtained from impact test as presented in Figure 5.22. It should be noted that for impact vibration test, only damping ratio under undisturbed soil condition were plotted the figure. One possible explanation regarding the lower damping ratio obtained from the forced vibration is that a formation of gapping caused by forced

vibration tests decreased the amount of energy that could be carried away from the foundation, consequently decreasing the overall damping ratio of the system. The damping ratios varied from approximately 1% for the 0.4-m pile to about 24% for the 1.2-m pile.

Figure 5.23 presents the relationship between damping ratio of the system and the mass of the bucket, which directly relates to the amplitude of excitation force. For the 1.2-m pile (No.1), the damping ratio appears to decrease with increasing amplitude of excitation force probably due to the growth of gap length, which reduces the radiation damping. However, this is not consistent for the other diameters for which the damping ratios are much smaller than those of the 1.2-m pile. Two possible reasons can be explained. First, for the smaller pile, the hysteretic damping that increases with force level becomes more predominant and may increase the overall damping of the system even though the radiation damping decreases with the amplitude of shaking. Second, a small error in the measurement of acceleration could significantly cause inaccuracy in the estimation of damping ratio using the half-power bandwidth method.

### **5.1.3 Mode Shape**

The mode shapes of each pile were estimated based on data from a series of strain gauges (S.G.) and/or accelerometers (Acc.) along the piles depending on which types of data were available. It should be noted that for the 0.6-m and 0.9-m piles, accelerometers were not installed along the length of the pile; therefore, only strain gauge data was available. In addition, since the stiffness of the 1.2-m pile was very high, the response of strain gauges due to the dynamic force was insignificant, and therefore the mode shape was obtained using accelerometer data only. To determine mode shape from strain gauge data, pile curvatures were first calculated, and then the 6<sup>th</sup> order polynomial function was fit to the discrete curvature data. Subsequently, the displacement of the pile representing its mode shape was determined by double integration of the curvature function. Figure 5.24 presents mode shapes of each pile based on its resonant frequency at the maximum

level of excitation force plotted in terms of normalized amplitude with a ratio of unity at the pile head. The mode shapes of the 0.4-m pile obtained from both strain gauge and accelerometer data were in good agreement. The results from the mode shape confirm that the pile stiffness increases with pile diameter, as is expected. Furthermore, the depth of zero displacement related to the effective pile length increases with pile diameter.

## **5.2 Lateral Load Testing**

In this section the individual lateral load test results are presented starting from lateral load test No.1 to lateral load test No.4. The load-displacement curves subjected to both static and cyclic loading are presented. The responses of bending strain gauges at different load levels are also given. Furthermore, brief descriptions of the observed failure of the piles, together with photographs are provided.

### **5.2.1 Lateral Load Test No. 1**

#### **5.2.1.1 Load-Displacement Curves**

The 0.6-m CIDH pile was tested under both static and cyclic loading using the 0.9-m CIDH pile as the reaction. Load-displacement curves under static loading for the 0.6-m and 0.9-m CIDH piles are presented in Figure 5.25. For a purpose of comparison, the load-displacement curve of the 0.9-m pile from lateral load test No.2 is also presented in Figure 5.23. The load-displacement curve of the 0.9-m pile obtained from test No.2 is somewhat lower than that obtained from test No.1. Two possible reasons can be explained. First, the soil conditions at different periods of time might be different. The soil condition in Phase I was observed to be relatively dry, whereas that in Phase II might be slightly moist, due to a rain about a week before the test which possibly softened the soil. Second, there might be a human error in the calibration factor of the actuator load by a certain factor. Multiplying the load obtained from the Phase I by a factor of 0.75 yields an excellent agreement with the results from Phase II as presented in Figure 5.26.

It was believed that the second reason is more likely due to the following reasons: 1). The results from the ambient and impact vibration tests on the 0.9-m pile indicated that the system natural frequency during Phase I and before Phase II were almost identical indicated that the system stiffness at two different periods of time were very similar. 2). The back-calculated  $p$ - $y$  curves of the 0.6-m pile using the uncorrected load-displacement curves from Phase I yielded significant too large resistance when compared to back-calculated  $p$ - $y$  curves from the larger pile diameters which appeared to be unreasonable. Based on this information, the load-displacement curves of the 0.6-m pile which was carried out in Phase I was reduced by multiplying with a constant of 0.75 to correct for the human error. The load-displacement curves under static loading for the 0.6-m and 0.9-m CIDH piles after applying the correction factor are presented in Figure 5.27. The load-displacement curve under cyclic loading of the 0.6-m CIDH pile after applying the correction factor is shown in Figure 5.28.

The load-displacement curve under cyclic loading is an inverted S-shape, which indicates the effect of soil gapping. Using the equivalent elasto-plastic load-displacement relationship, yield displacement can be estimated by extrapolating the elastic response (i.e., first yield of the steel) to the maximum load and therefore the displacement ductility for each displacement level can be obtained (Priestley *et al.* 1996). The estimated yield displacement was 40 mm. The test pile has displacement ductility of 7.4 and it failed at the first cycle of displacement ductility of 8.1.

#### 5.2.1.2 Longitudinal Strain Gauge Data

The responses of strain gauges at different levels of loading are presented in Figure 5.29. Strain gauge data indicates that the location of maximum moment occurs at depth about 0.9 m corresponding to 1.5D. No significant strains were measured in the longitudinal bars below a depth of 3.6 m (6D). It is noted that all of the strain gauges were damaged during cyclic loading due to the breaking of strain gauge leads at the vicinity of plastic hinge.

### 5.2.1.3 Transverse Strain Gauge Data

The transverse strain profiles in various directions as presented in Figure 5.30 indicate that the both confining steel strains (A and C) as well as shear steel strains (B and D) are insignificant compared to the longitudinal strain. The confining steel strain in the compression side has a similar shape as that observed in the compression rebar. The shear strain on the other hand shows that they are insignificant at all depths. This is because the shear capacity of the reinforcement pile is much larger than that the shear demand and hence the shear force in the pile is taken by the concrete.

### 5.2.1.4 Observed Pile Performance

At a ground displacement of 25.4 mm (48 mm at load point), the occurrence of hair line cracks on the column was observed. During the cyclic loading at 152 mm ground displacement (295 mm at load point equivalent to displacement ductility of 7.4), the concrete started spalling. Rupture of the steel spiral was observed at a depth of 0.3 m below the ground surface during the first cycle with a displacement at a load point of 325 mm (displacement ductility of 8.1). This was followed with three longitudinal rebars at a depth of about 0.3 m in the A direction (Figure 5.31) and then two longitudinal rebars at the same depth in the C direction (Figure 5.32). There were a total of 5 broken longitudinal rebars in the direction of the loading application. After the completion of the test, the soil around the test pile was excavated to investigate the plastic hinge location and the pattern of cracks along the pile. Figure 5.33 and Figure 5.34 present the crack pattern along the pile. There was severe damage on the pile between the depths of 0 m and 0.6 m. The crack pattern apparently occurred at 89 mm intervals corresponding to the spacing of the spiral. The crack width appeared to be smaller at the deeper depth. The cracks become insignificant at a depth greater than 1.8 m below the ground surface.

## 5.2.2 Lateral Load Test No. 2

### 5.2.2.1 Load-Displacement Curves

For lateral load test No.2, the load-displacement curves under static loading for the 0.9-m and 1.2-m CIDH piles are presented in Figure 5.35. The load-displacement curve under cyclic loading of the 0.9-m CIDH pile is shown in Figure 5.36. Similar to the previous test, the shape of the load-displacement curve is an inverted S-shape indicating the effect of soil gapping. The displacement at yield was estimated as 57 mm. It is noted that the displacement in the pull direction could not reach the target due to the pulling limit capacity of the actuator at 980 kN. The pile was laterally loaded until it reached the capacity of the linear potentiometer; the test was then stopped without failing the pile. The maximum displacement at the end of the test corresponded to a displacement ductility of 8.7.

### 5.2.2.2 Longitudinal Strain Gauge Data

The responses of strain gauges at different levels of loading are presented in Figure 5.37. The location of maximum strain corresponding to the maximum moment occurred at a depth of 2.1 m (2.33D). No significant strains were measured in the longitudinal bars below a depth of 4.8 m corresponding to 5.33D.

### 5.2.2.3 Observed Pile Performance

Cracks were noticed along the 0.9-m CIDH pile starting from the depth of 0 to about 2.4 m, which was corresponding to the maximum depth that we could excavate using a backhoe. Severe cracks were observed between depths of 0.9 m and 2.4 m related to the vicinity of the location of maximum moment. Figure 5.38 shows the crack patterns along the 0.9-m CIDH pile.

### 5.2.3 Lateral Load Test No. 3

#### 5.2.3.1 Load-Displacement Curves

For lateral load test No.3, the load-displacement curves under static loading of the 0.4-m CIDH pile is presented in Figure 5.39. The load-displacement curve for the 0.4-m CIDH piles under cyclic loading showing the effect of gapping is presented in Figure 5.40. The yield displacement was estimated as 35 mm for computing the displacement ductility of the pile. The pile performed well under cyclic loading up to a displacement ductility of 5.8 and it failed at a displacement ductility of 6.9.

#### 5.2.3.2 Longitudinal Strain Gauge Data

The strain gauge data (Figure 5.41) shows that the location of maximum moment occurred at a depth of about 0.60 m corresponding to 1.50D. No significant strains were measured in the longitudinal bars below a depth of 2.4 m (6.0D).

#### 5.2.3.3 Observed Pile Performance

At a load of 165 kN, hair line cracks along the column were observed. The cracks of the pile just below the ground surface were observed during the cyclic loading at a displacement at the load point of 61 mm (displacement ductility of 1.74). Spalling of concrete occurred when the pile was loaded at a displacement of 203 mm (displacement ductility of 5.8). Three of longitudinal reinforcing bars were broken at a depth of 0.3 m during the first cycle at a displacement of 244 mm (displacement ductility of 6.9). Figure 5.42 showed the rupture of the reinforcing steels at a depth of 0.3 m below the ground. Figure 5.43 shows the patterns of crack along the 0.4-m CIDH pile. No crack was observed below a depth of 1.2 m.

## 5.2.4 Lateral Load Test No. 4

### 5.2.4.1 Load-Displacement Curves

Load-displacement curves of the 1.2-m CIDH piles under static and cyclic loading are presented in Figure 5.44 and Figure 5.45, respectively. The yield displacement was estimated as 75 mm. As described earlier in the test setup section, Pile No.2 moved more than the displacement target to a displacement of 380 mm due to a problem in controlling the actuator. The pile was then unloaded to zero and the controlled displacement was changed from Pile No.1 to Pile No. 2. The cyclic load test continued to load for 3 cycles at displacement ductilities of 4.1, 5.2 and 6.2. Though the pile did not reach failure, the test was stopped because it reached the capacity of the linear potentiometers. Similar to test No.2, the displacement in the pull direction was limited by the capacity of the actuators at 1960 kN (2 actuators).

### 5.2.4.2 Longitudinal Strain Gauge Data

The strain gauge data presented in Figure 5.46 and Figure 5.47 indicate that the location of maximum moment occurs at a depth of 3.0 m corresponding to 2.5D. No significant strains were measured in the longitudinal bars below a depth of 6.40 m (5.33D).

### 5.2.4.3 Observed Pile Performance

There was no sign of pile damage throughout the test. However, after the excavation, some cracks were observed on Pile No.2 between the depths of 0.75 m and 4.5 m as presented in Figure 5.48. There was no damage on Pile No.1.

### 5.2.5 Comparison of Location of Maximum Moment

The depth of the maximum moment, or the plastic hinge, is one important parameter used in the design of pile under lateral loading. The depth of the plastic hinge depends on the stiffnesses of the soil and pile, as well as the height above ground (Budek, 1997). Typical values assumed in design, based on the design chart developed by Budek (1997), range from  $0.5D$  to  $2.0D$ . The strain profile based on the test data at approximately the yield load of each pile were plotted against the ratio of depth to pile diameter,  $D$ , in the same plot as presented in Figure 5.49. The results show that the depth of the plastic hinge ranges from about  $1.0D$  to  $3.0D$ , which are in reasonable agreement with the Budek design chart (Budek 1997). It appears that this ratio tends to increase with the pile diameter, which is not considered in the current design. Another interesting observation in this plot is that the depth of zero moment occurs at approximately  $6D$  for all pile diameters. Below this depth the moment is insignificant.

### 5.2.6 Observed Inelastic Behavior of CIDH Piles

The amount of transverse reinforcement based on the specification suggested by BDS 1993 appears to be conservative for the design of CIDH piles because this amount of transverse reinforcement was recommended based on the test results of columns. However, in case of the piles, the confinement from the surrounding soil can considerably enhance the inelastic behavior of the pile. Budek (1997) studied the effect of external confinement in improving the inelastic behavior of the CIDH pile by conducting the experiments on CIDH piles with external confinement provided by a series of saddles with the rubber to model confinement from the soil. Budek showed that an adequate seismic performance of CIDH piles can be achieved with only the moderate levels of transverse reinforcement due to the effect of external confinement.

Figure 5.50 show the cyclic load-displacement curves of each pile tested until its failure or until the actuator reached its displacement limit. The test results indicate that

all the test piles have ductile behavior with a displacement ductility of more than 5, even though only low to moderate level of transverse reinforcement of 0.6% was used. This indicates that the equation in the BDS may be conservative in determining the amount of transverse reinforcement in the pile. These test results of CIDH piles in real soil support the finding of a recent research (Budek, 1997). Therefore, the effect of soil confinement, which can reduce the amount of transverse reinforcement, should be considered to incorporate in the future seismic design of CIDH piles, which results in a decrease in the construction cost of deep foundations. The analyses on the effect of soil confinement on the inelastic behavior of the pile are presented in the next chapter.

Based on Figure 5.50, some of interesting behavior of CIDH piles observed from the load-displacement curves can be noted as the followings:

- The strength degradation of the first cycle is significantly greater than the subsequent cycles.
- The displacement ductility of the pile appears to increase as the pile diameter increases.
- The cyclic load-displacement curves are similar to the inverted S-shape, which indicates the effect of gapping. The stiffness of soil-pile system is quite low when the pile displacement is less than the gap width. However, the stiffness becomes stiffer as the pile starts to have a contact with the soil.
- Pile capacity in the pull direction is slightly greater than the push direction, probably due to the effect of interaction between the test pile and reaction pile.
- Hysteretic damping increases as the displacement of the pile increases.

### **5.3 Summary**

The test results from the vibration and lateral load tests for various pile diameters have been presented and some interpretation of the test data has been provided. The results from vibration testing show that the natural frequency of the soil-pile system

increases as the pile diameter increases due to the increase of soil-pile system stiffness. The natural frequencies obtained from both ambient and impact vibration tests are similar, whereas those obtained from the forced vibration tests are somewhat smaller because the development of small gapping occurred due to the dynamic force from the shaker, resulting in increasing the free standing height and decreasing the system stiffness. The damping ratio increases as the pile diameter increases due to the effect of radiation damping which is a function of the contact area and the frequency excitation.

The characteristics of cyclic load-displacement curves as the inverted S-shape indicate the effect of gapping. All of the piles show sufficient inelastic performance with the displacement ductility of more than 5, even though the smaller amount of transverse reinforcement than that suggested by BDS was used. The strain gauge results indicate that the maximum moment occurred at depths approximately 1.0D to 3.0D which generally agree with the typical values used in design (Budek 1997). Furthermore, the depth of zero moment of all pile is approximately 6D.

Table 5.1 Summary of Natural Frequencies of Soil-Pile Systems from Ambient and Impact Vibration Tests

Pile Diameter	Descriptions	Natural Frequency (Hz)			
		Ambient		Impact	
		E-W	N-S	E-W	N-S
0.4 m	Without Mass Shaker	13.6	13.9	13.4	13.7
	With Mass Shaker	12.6	12.9	12.3	12.7
	After Forced Vibration (Test 1)	11.4	11.4	10.6	11.3
	After Forced Vibration (Test 2)	11.1	11.3	10.3	11.1
	After Forced Vibration (Test 3)	11.0	11.3	10.1	10.9
	After Forced Vibration (Test 4)	10.9	11.3	10.0	10.8
	After Forced Vibration (Test 5)	10.6	11.3	9.8	10.8
	Without Mass Shaker	12.1	12.3	11.6	11.8
0.6 m	Without Mass Shaker	18.8	18.8	18.0	18.2
	With Mass Shaker	17.0	17.0	16.5	16.8
	After Forced Vibration	14.9	15.0	13.3	13.6
	Immediately After Lateral Load Test	3.8	2.3	3.1	1.8
0.9 m	With Mass Shaker	25.4	-	25.4	26.3
	After Forced Vibration	24.4	-	23.3	24.7
	Immediately After Lateral Load Test	17.5	16.5	15.8	15.1
	2.5 Months after Lateral Load Test	24.1	24.1	24.0	24.0
1.2 m (Pile No.1)	Without Mass Shaker	-	-	34.5	34.5
	With Mass Shaker	-	-	33.6	33.4
	After Forced Vibration (Rotation Mass = 0.65 kg)	-	-	32.9	31.5
	After Forced Vibration (Rotation Mass = 1.46 kg)	-	-	31.2	29.6
	After Forced Vibration (Rotation Mass = 2.06 kg)	-	-	28.0	26.5
	After Forced Vibration (Rotation Mass = 2.65 kg)	-	-	26.5	25.1
	Without Mass Shaker	-	-	31.5	29.0
1.2 m (Pile No.2)	Without Mass Shaker	-	-	31.8	33.0
	With Mass Shaker	-	-	31.8	32.3
	After Forced Vibration (Rotation Mass = 0.65 kg)	-	-	32.3	32.0
	After Forced Vibration (Rotation Mass = 1.46 kg)	-	-	32.0	32.0
	After Forced Vibration (Rotation Mass = 2.06 kg)	-	-	31.2	32.0
	After Forced Vibration (Rotation Mass = 2.65 kg)	-	-	31.2	31.5

Table 5.2 Summary of Natural Frequencies and Damping Ratios of Soil-Pile Systems from Forced Vibration Tests

Pile Diameter (m)	Mass (kg)	Run Number	Natural Frequency (Hz)	Damping Ratio (%)	Remarks
0.4	0.65	1	10.2	1.2	Raining
	0.65	2	9.3	1.4	
	0.65	3	9.2	1.1	
	0.65	4	9.1	1.9	
	0.65	5	8.7	1.8	
0.6	0.65	1	13.7	2.9	
	0.65	2	13.2	2.5	
	0.65	3	13.0	2.4	
	1.46	1	12.1	2.2	
	1.46	2	11.6	2.2	
	1.46	3	11.4	2.8	
	2.06	1	11.2	2.9	
	2.06	2	11.0	2.9	
	2.06	3	11.0	3.1	
	2.06	4	11.0	3.3	
	1.46	4	10.8	3.1	
	0.65	4	10.8	3.7	
0.9	1.46	1	17.9	5.2	
	1.46	2	18.0	4.6	
	1.46	3	18.0	4.9	
	2.65	1	17.0	3.5	
	2.65	2	16.7	5.8	
	0.65	1	16.9	5.4	
	2.06	1	12.9	6.0	
	2.06	2	12.9	6.0	
1.2 (Pile No.1)	0.65	1	28.3	21.1	
	0.65	2	28.3	23.6	
	0.65	3	28.3	23.6	
	1.46	1	26.3	17.5	
	1.46	2	24.6	20.2	
	1.46	3	24.6	20.2	
	2.06	1	23.8	17.1	
	2.06	2	21.8	15.4	
	2.06	3	21.8	15.8	
	2.65	1	21.5	14.1	
	2.65	2	21.3	16.1	
	2.65	3	21.2	16.1	
	2.06	4	21.0	14.8	
	1.46	4	20.8	10.9	
	0.65	4	20.8	8.2	
1.2 (Pile No.2)	0.65	1	29.3	--	
	0.65	2	29.3	--	
	0.65	3	29.3	--	
	1.46	1	28.0	--	
	1.46	2	27.6	--	
	1.46	3	27.6	--	
	2.06	1	27.3	--	
	2.06	2	27.2	--	
	2.06	3	27.2	--	
	2.65	1	26.7	--	
	2.65	2	26.5	--	
	2.65	3	26.5	--	
	2.06	4	26.5	--	
	1.46	4	26.5	--	
	0.65	4	26.5	--	

Table 5.3 Summary of Damping Ratios of Soil-Pile Systems from Impact Vibration Tests

Pile Diameter	Descriptions	Damping Ratio (%)			
		Logarithmic Decrement		Half-Power Bandwidth	
		E-W	N-S	E-W	N-S
0.4 m	Without Mass Shaker	2.8	2.8	2.6	3.0
	With Mass Shaker	3.2	2.8	3.0	3.3
	After Forced Vibration (Test 1)	-	-	4.5	5.1
	After Forced Vibration (Test 2)	6.2	6.6	4.4	5.1
	After Forced Vibration (Test 3)	5.7	4.1	4.0	2.7
	After Forced Vibration (Test 4)	5.2	4.3	4.3	3.1
	After Forced Vibration (Test 5)	5.1	4.3	4.5	3.0
	Without Mass Shaker	3.8	3.5	3.9	4.6
0.6 m	Without Mass Shaker	4.6	4.5	4.9	5.6
	With Mass Shaker	3.8	3.9	3.8	3.6
	After Forced Vibration	5.6	5.1	5.7	5.7
	Immediately After Lateral Load Test	4.3	4.4	5.3	6.1
0.9 m	With Mass Shaker	8.6	9.9	9.1	10.8
	After Forced Vibration	7.3	7.7	7.0	7.6
	Immediately After Lateral Load Test	5.7	5.9	6.5	6.6
	2.5 Months after Lateral Load Test	-	-	9.1	11.5
1.2 m (Pile No.1)	Without Mass Shaker	21.4	23.2	22.5	29.9
	With Mass Shaker	21.9	24.1	22.3	29.6
	After Forced Vibration (Rotation Mass = 0.65 kg)	21.3	20.9	18.2	24.6
	After Forced Vibration (Rotation Mass = 1.46 kg)	19.2	18.3	18.9	20.7
	After Forced Vibration (Rotation Mass = 2.06 kg)	18.2	15.5	19.2	18.2
	After Forced Vibration (Rotation Mass = 2.65 kg)	17.4	15.8	18.2	15.7
	Without Mass Shaker	20.9	17.8	17.3	18.6
1.2 m (Pile No.2)	Without Mass Shaker	24.7	-	24.7	-
	With Mass Shaker	24.9	-	24.4	-
	After Forced Vibration (Rotation Mass = 0.65 kg)	-	-	22.9	-
	After Forced Vibration (Rotation Mass = 1.46 kg)	-	-	24.1	-
	After Forced Vibration (Rotation Mass = 2.06 kg)	-	-	24.5	-
	After Forced Vibration (Rotation Mass = 2.65 kg)	-	-	24.6	-

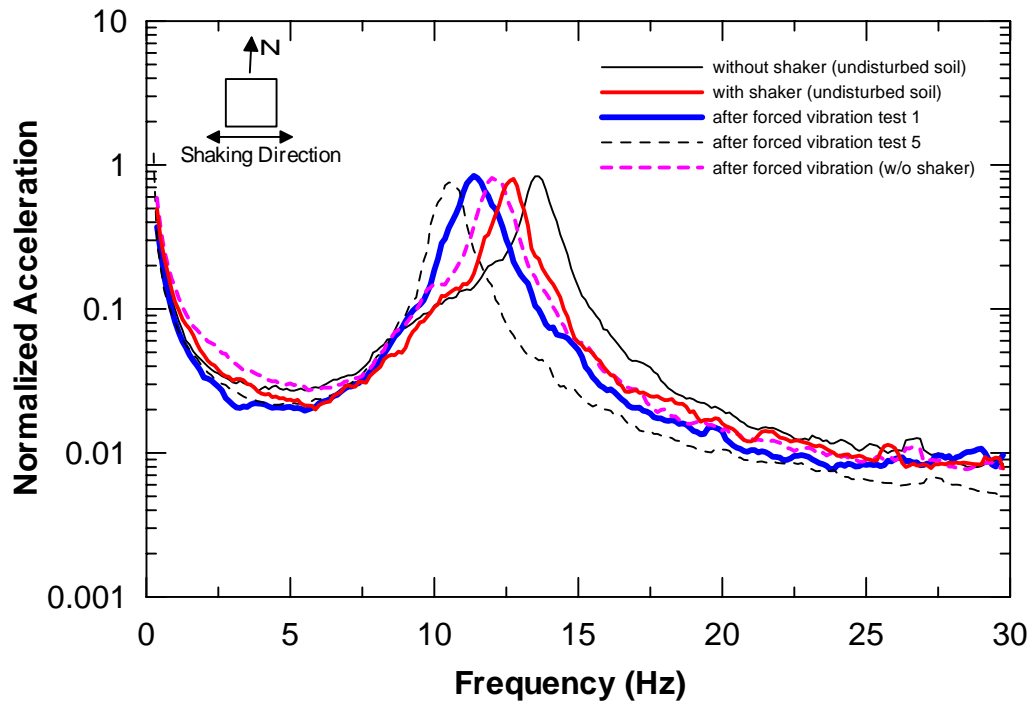


Figure 5.1 Power Spectra for 0.4-m CIDH Pile from Ambient Vibration Tests (E-W Direction)

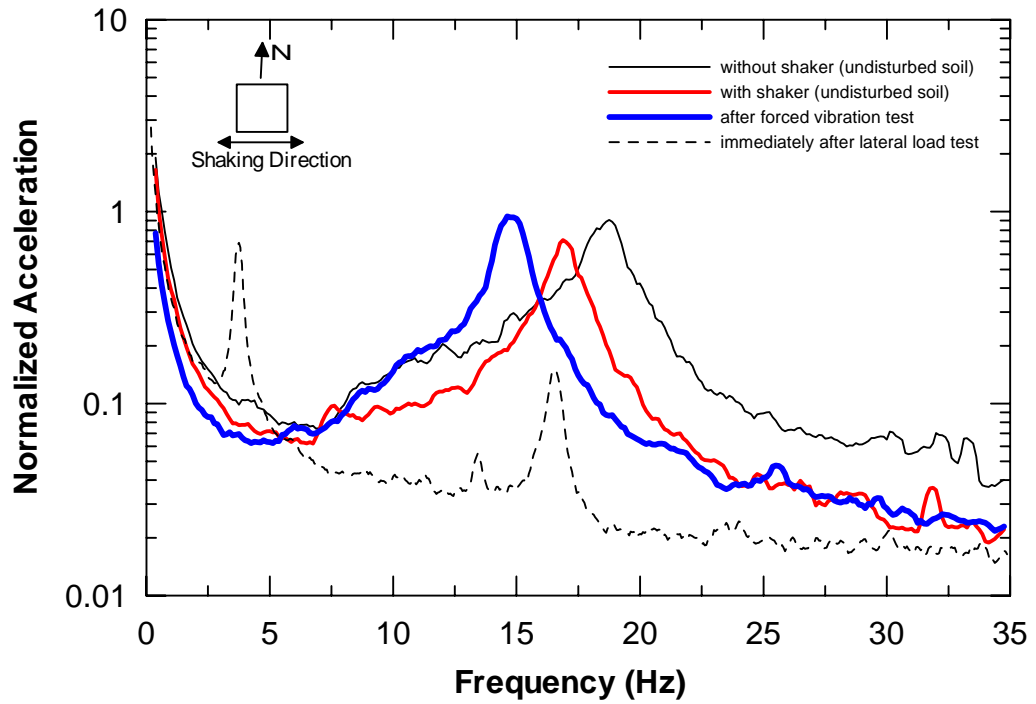


Figure 5.2 Power Spectra for 0.6-m CIDH Pile from Ambient Vibration Tests (E-W Direction)

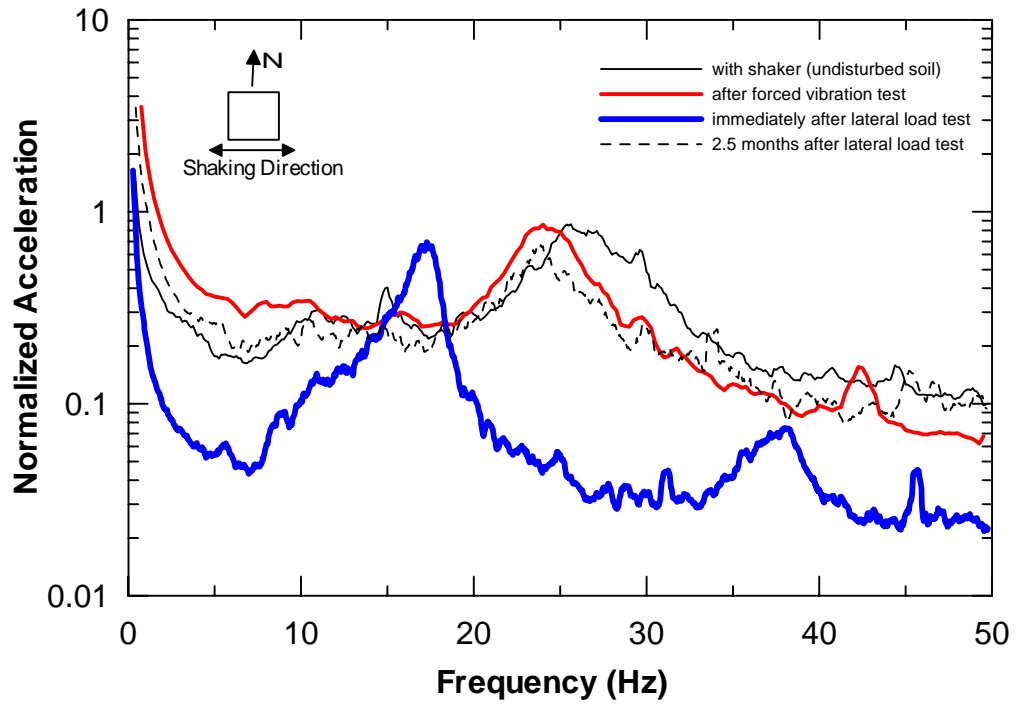


Figure 5.3 Power Spectra for 0.9-m CIDH Pile from Ambient Vibration Tests (E-W Direction)

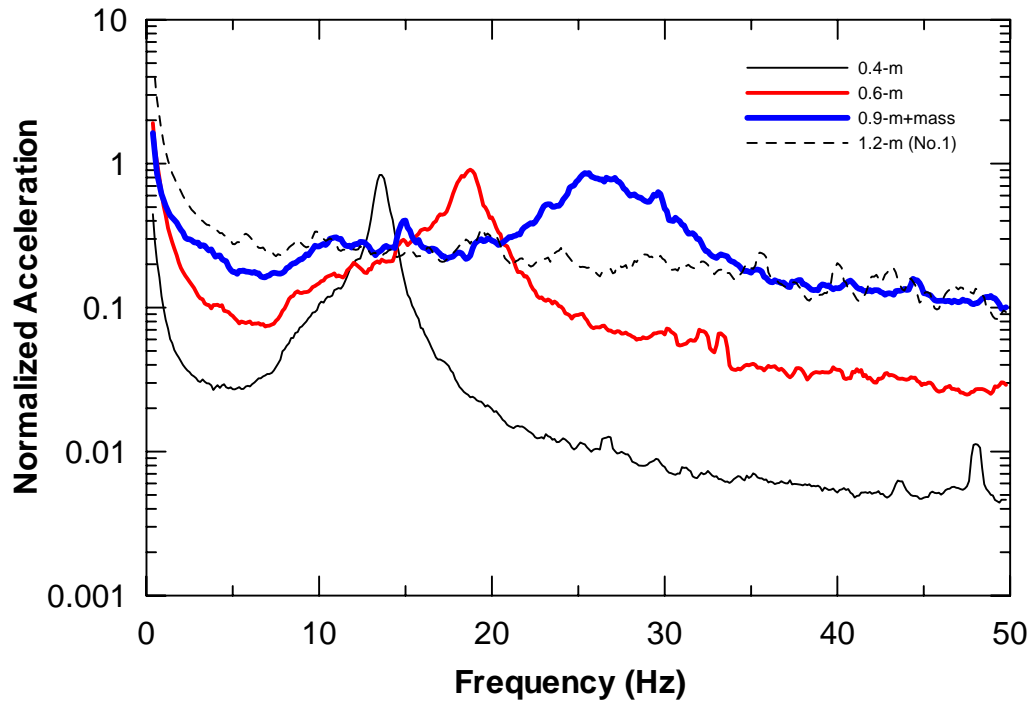


Figure 5.4 Comparison of Power Spectra for Various Pile Diameters from Ambient Vibration Tests (E-W Direction)

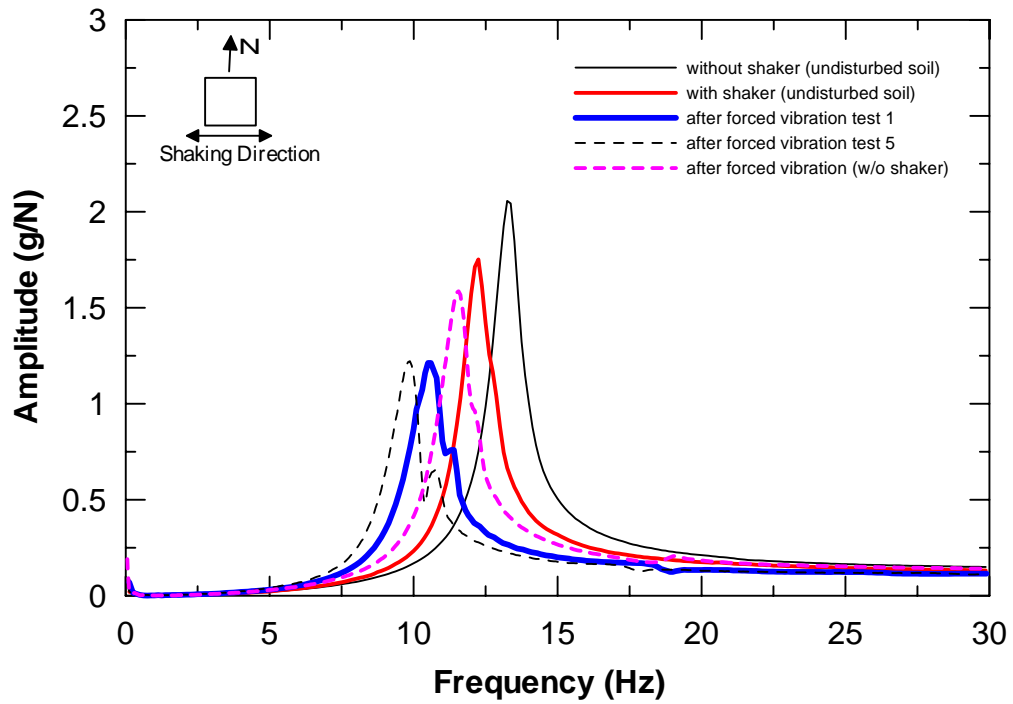


Figure 5.5 Frequency Response Functions for 0.4-m CIDH Pile from Impact Vibration Tests (E-W Direction)

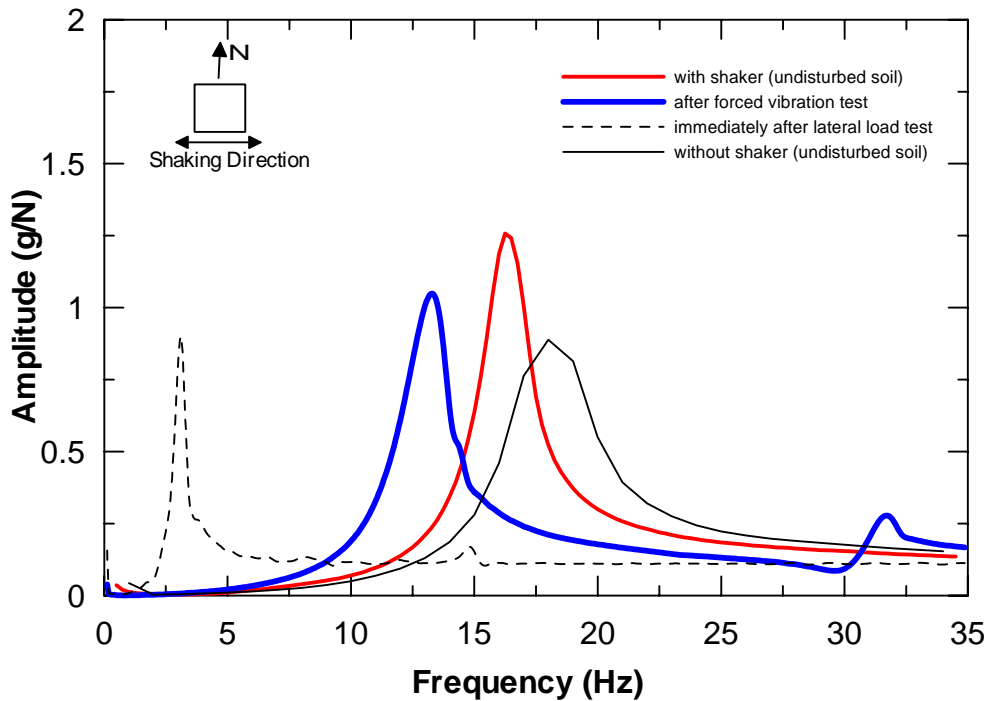


Figure 5.6 Frequency Response Functions for 0.6-m CIDH Pile from Impact Vibration Tests (E-W Direction)

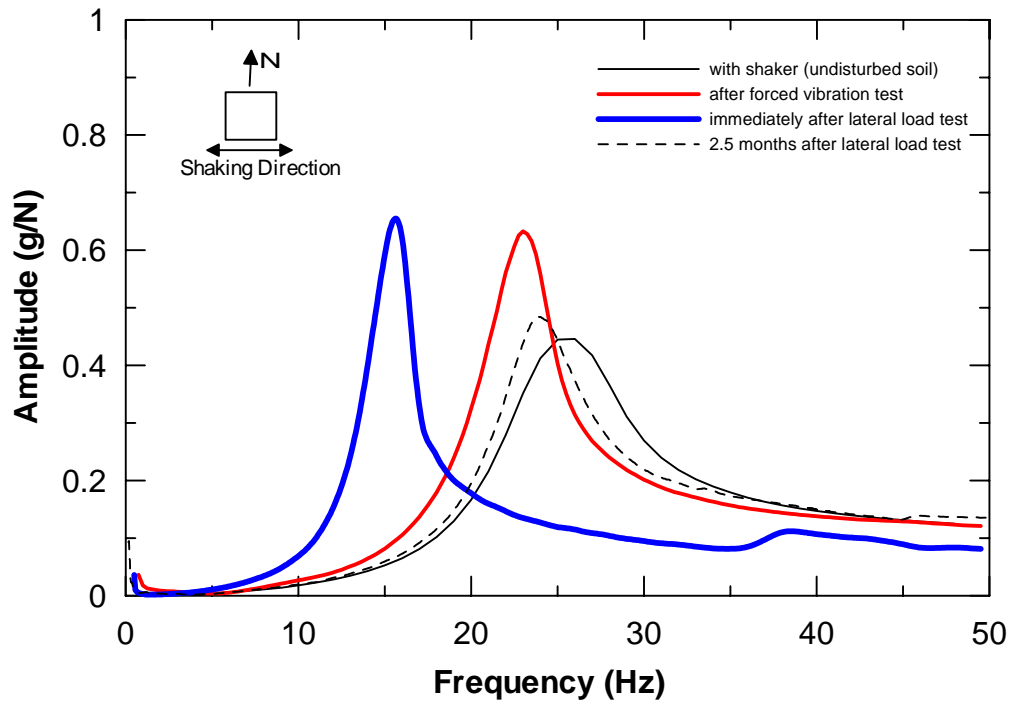


Figure 5.7 Frequency Response Functions for 0.9-m CIDH Pile from Impact Vibration Tests (E-W Direction)

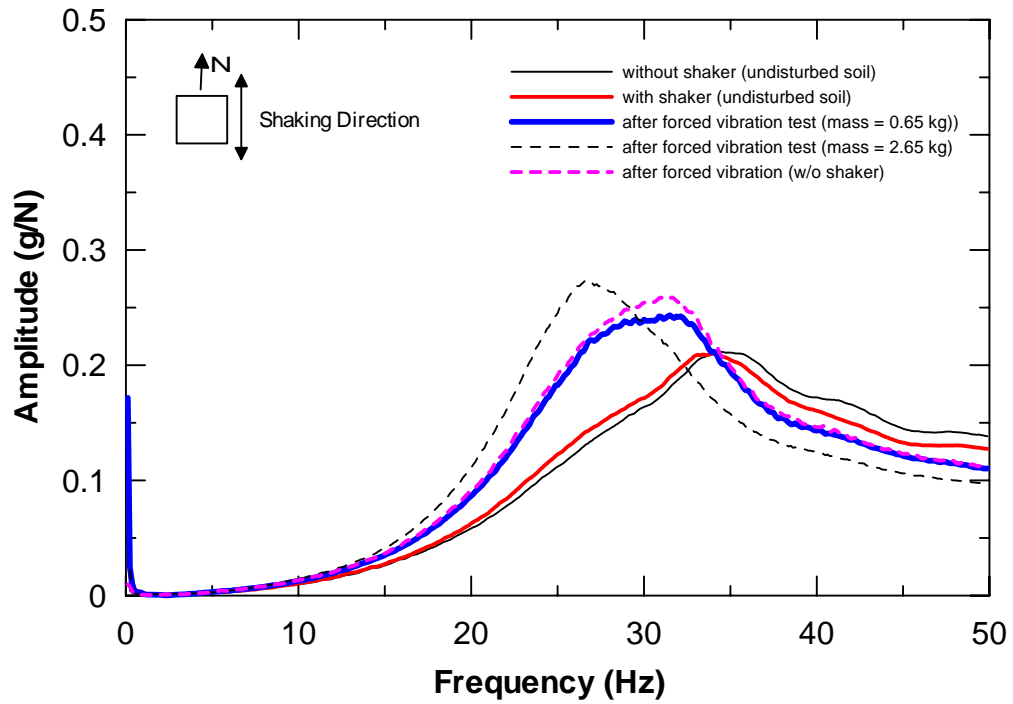


Figure 5.8 Frequency Response Functions for 1.2-m CIDH Pile (No.1) from Impact Vibration Tests (E-W Direction)

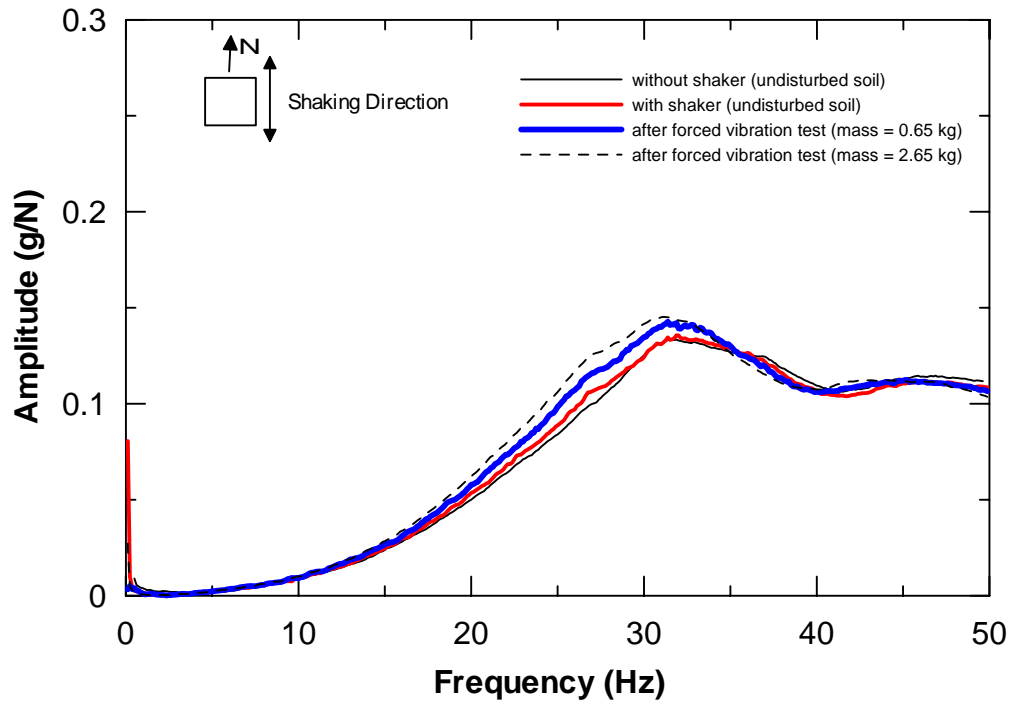


Figure 5.9 Frequency Response Functions for 1.2-m CIDH Pile (No.2) from Impact Vibration Tests (E-W Direction)

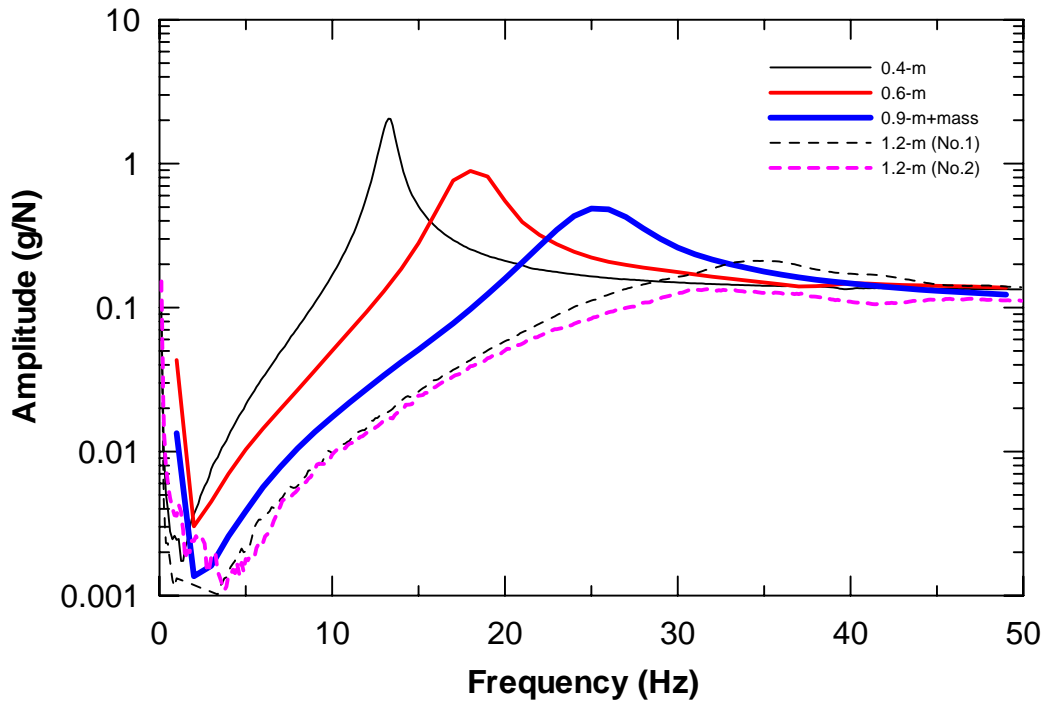


Figure 5.10 Comparison of Frequency Response Functions for Various Pile Diameters from Impact Vibration Tests (E-W Direction)

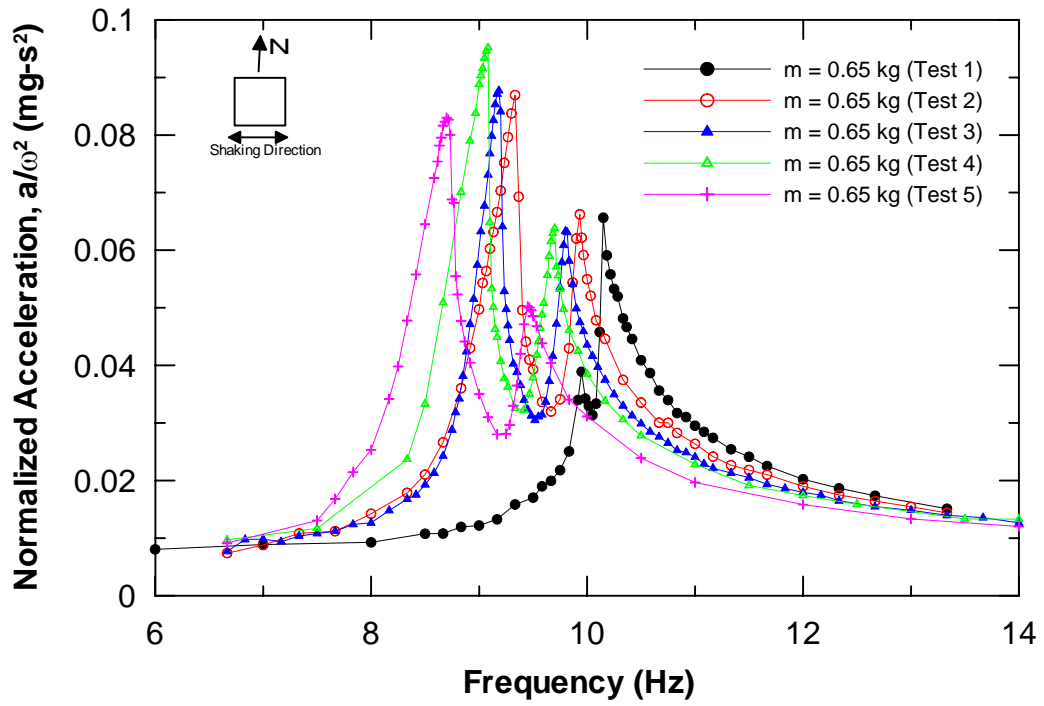


Figure 5.11 Frequency Response Curves for 0.4-m Pile from Forced Vibration Tests

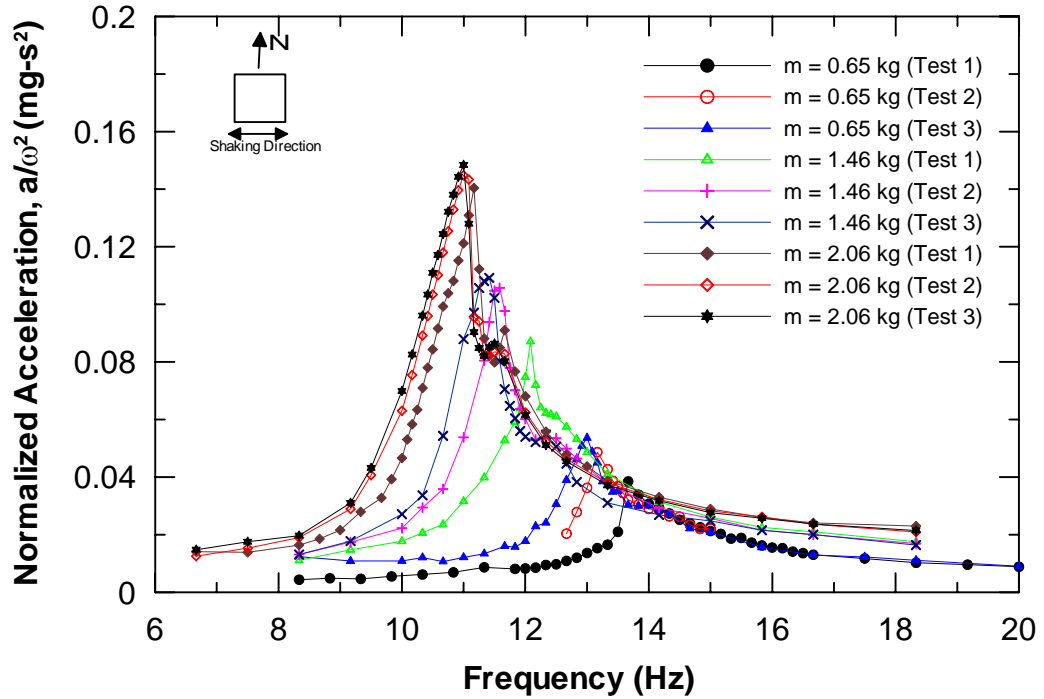


Figure 5.12 Frequency Response Curves for 0.6-m Pile from Forced Vibration Tests

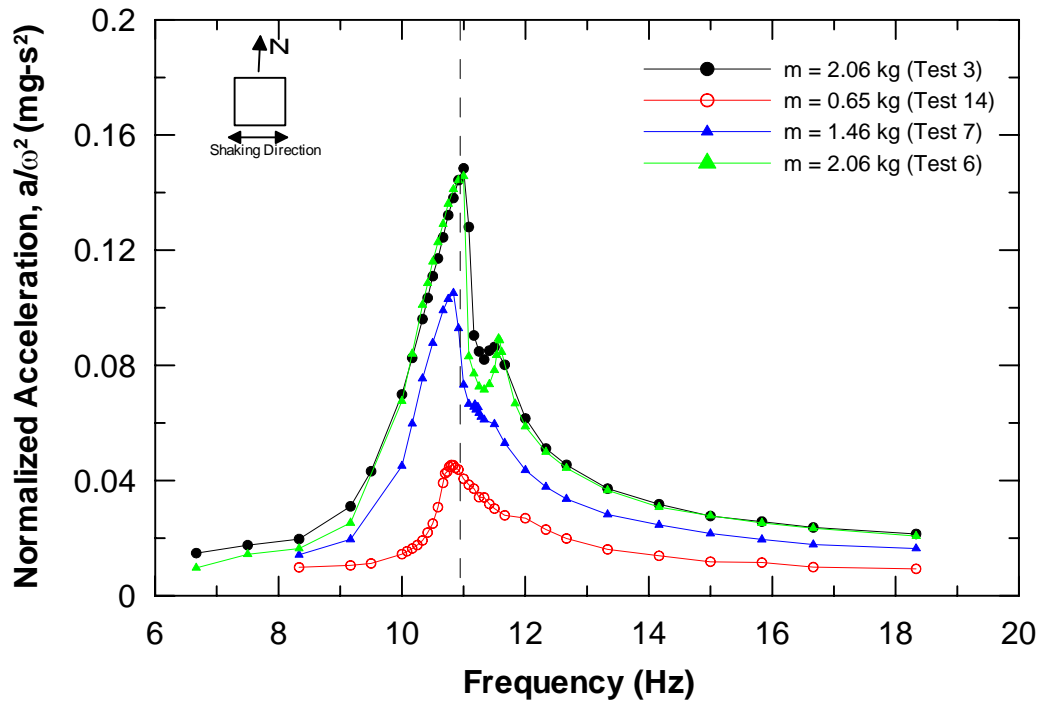


Figure 5.13 Frequency Response Curves for 0.6-m Pile from Forced Vibration Tests (after Pile Experienced Highest Amplitude of Excitation Force)

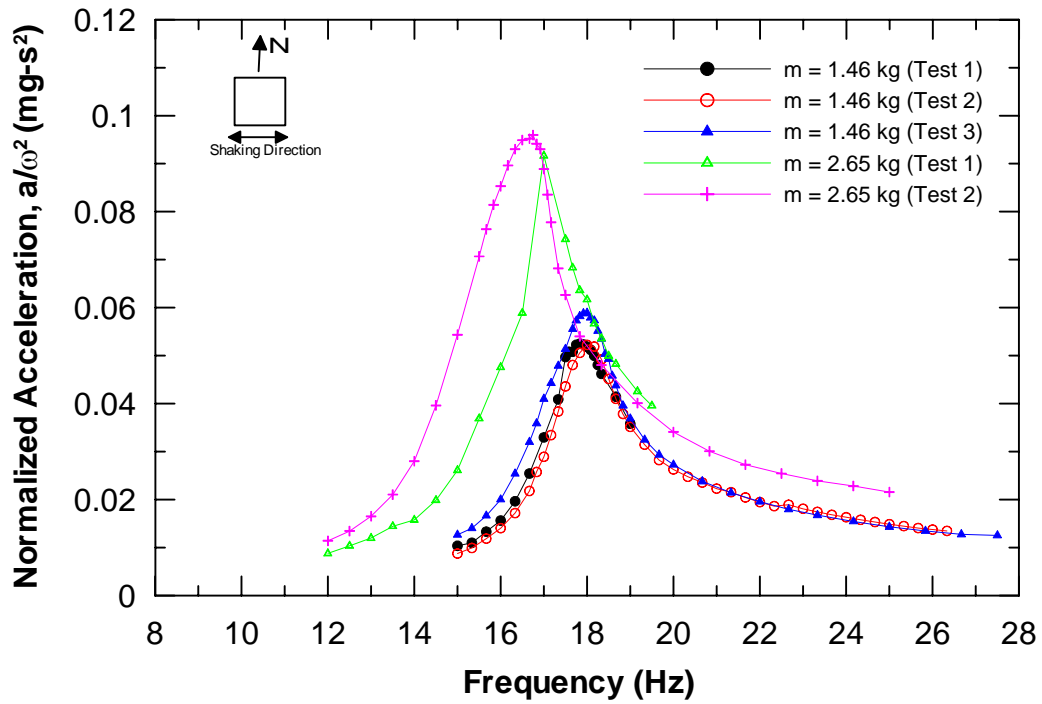


Figure 5.14 Frequency Response Curves for 0.9-m Pile from Forced Vibration Tests

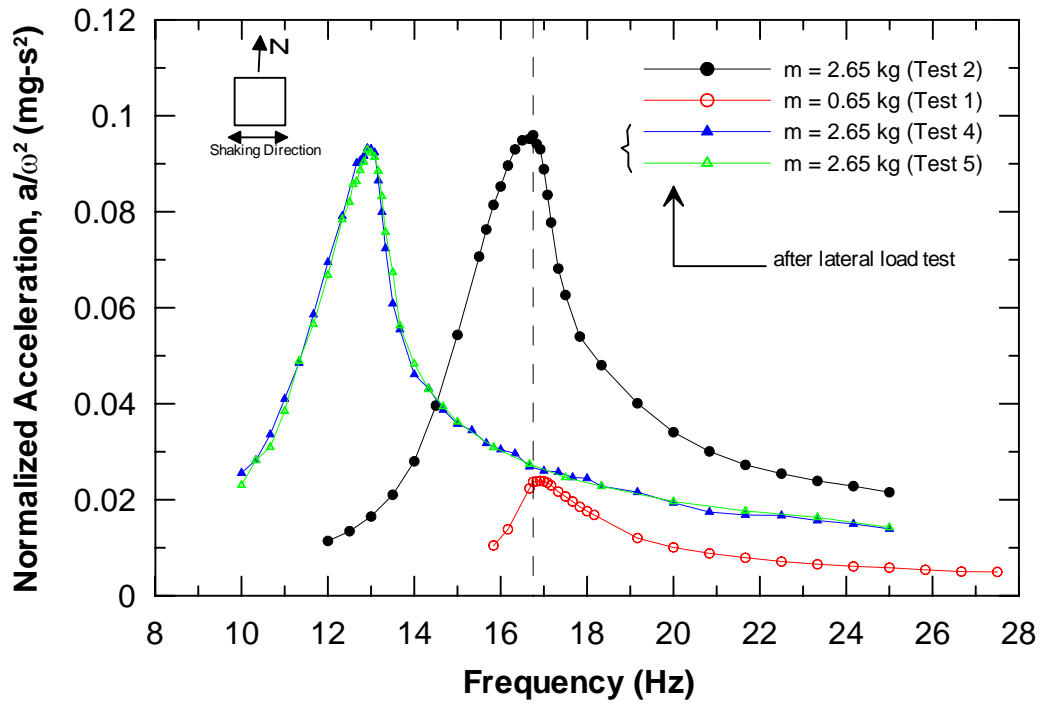


Figure 5.15 Frequency Response Curves for 0.9-m Pile from Forced Vibration Tests (after Pile Experienced Highest Amplitude of Excitation Force)

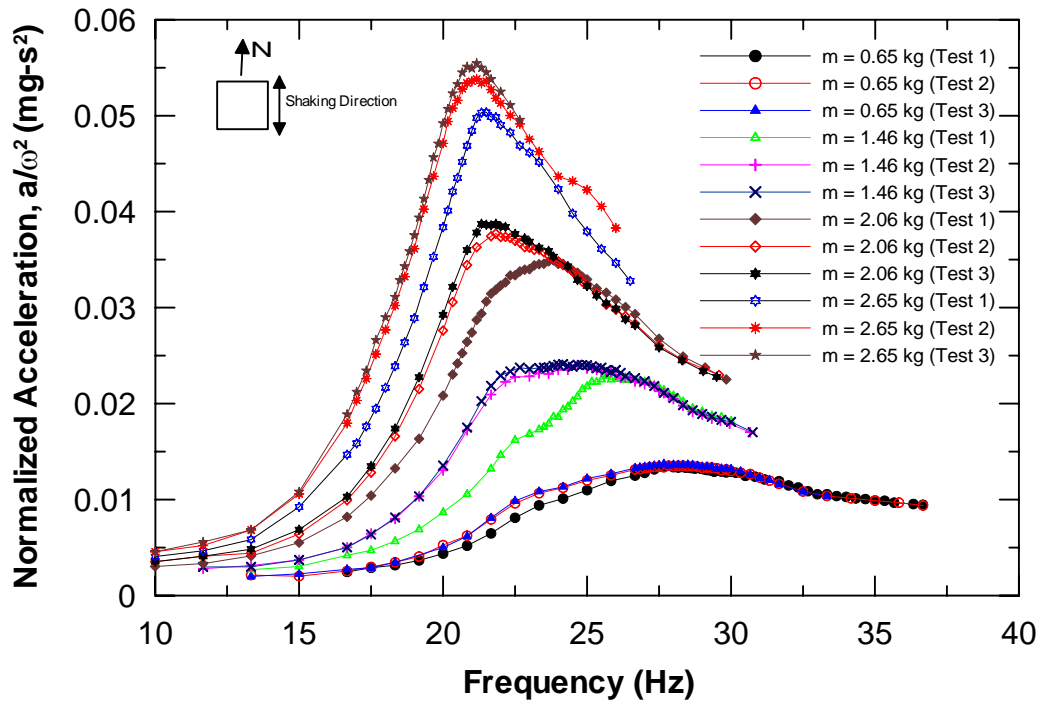


Figure 5.16 Frequency Response Curves for 1.2-m Pile (No.1) from Forced Vibration Tests

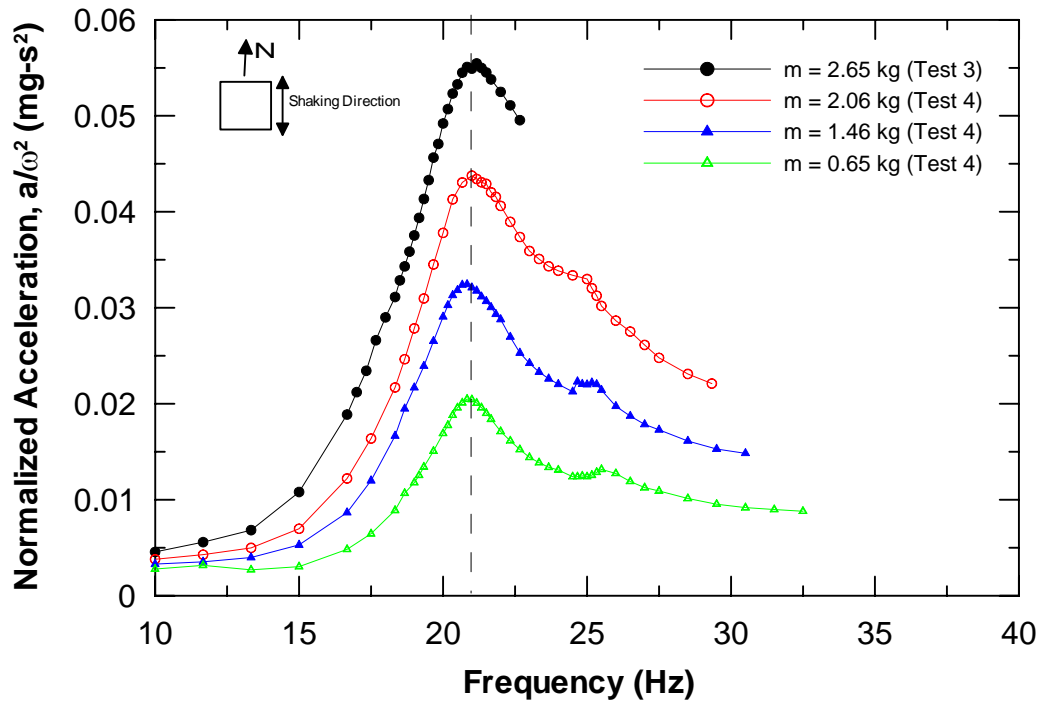


Figure 5.17 Frequency Response Curves for 1.2-m Pile (No.1) from Forced Vibration Tests (after Pile Experienced Highest Amplitude of Excitation Force)

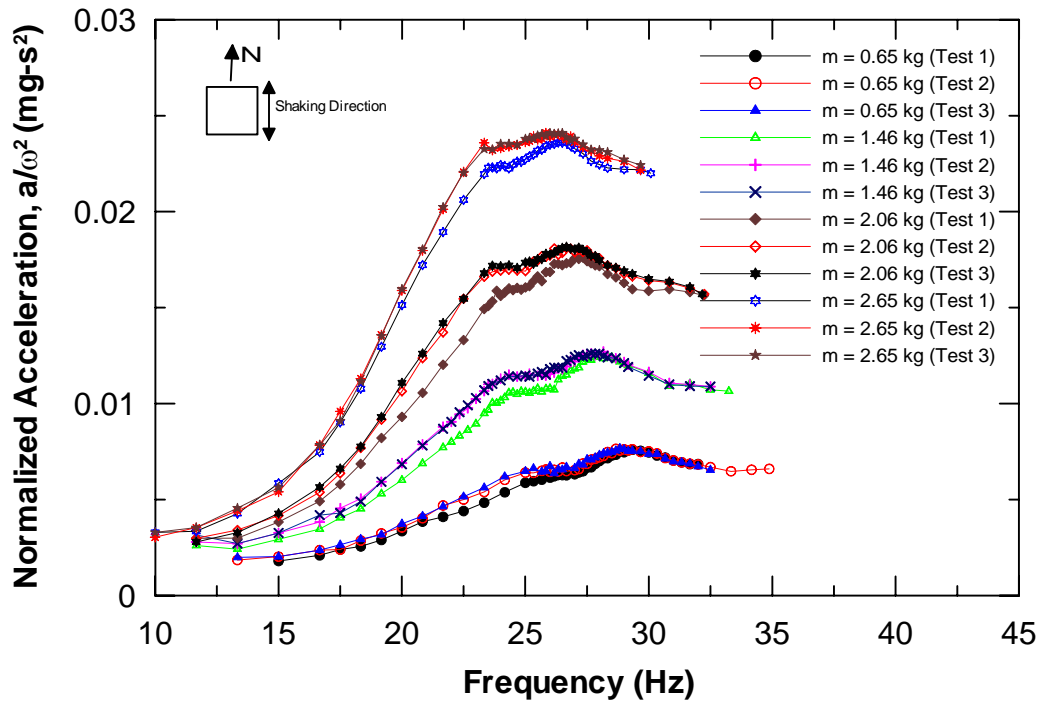


Figure 5.18 Frequency Response Curves for 1.2-m Pile (No.2) from Forced Vibration Tests

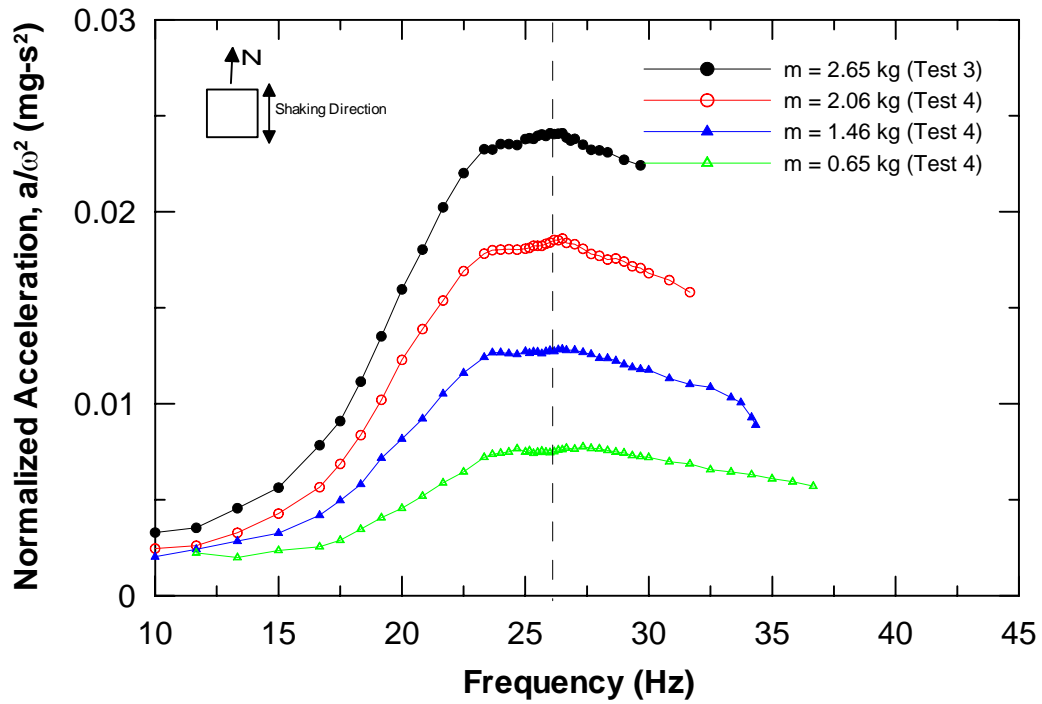


Figure 5.19 Frequency Response Curves for 1.2-m Pile (No.2) from Forced Vibration Tests (after Pile Experienced Highest Amplitude of Excitation Force)

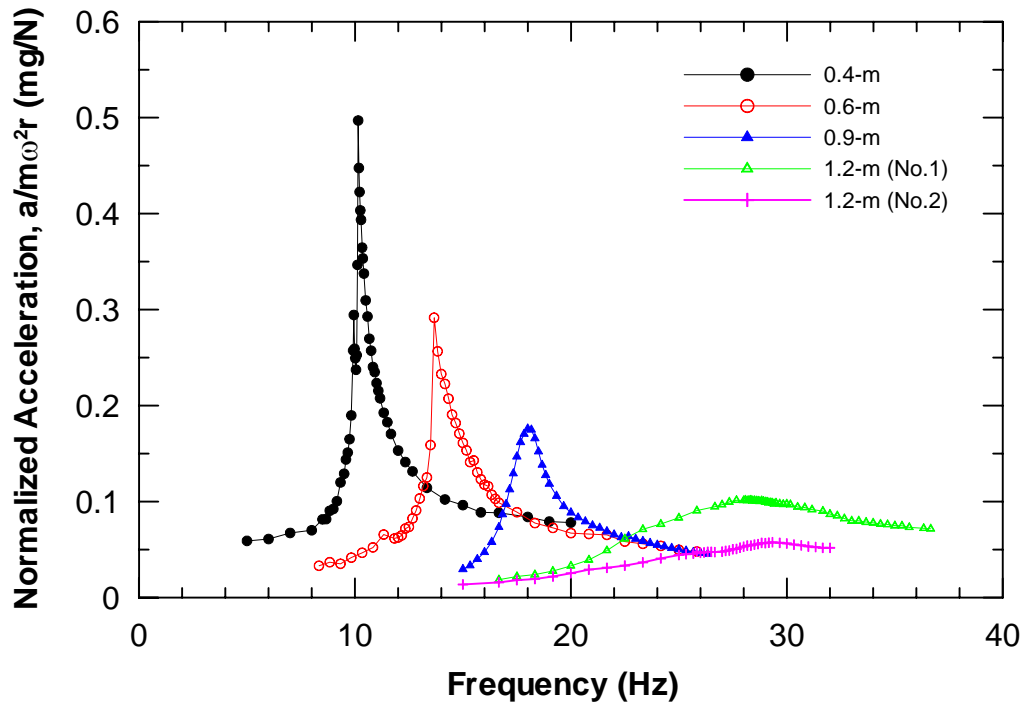


Figure 5.20 Comparison of Frequency Response Curves for Various Pile Diameters from Forced Vibration Tests

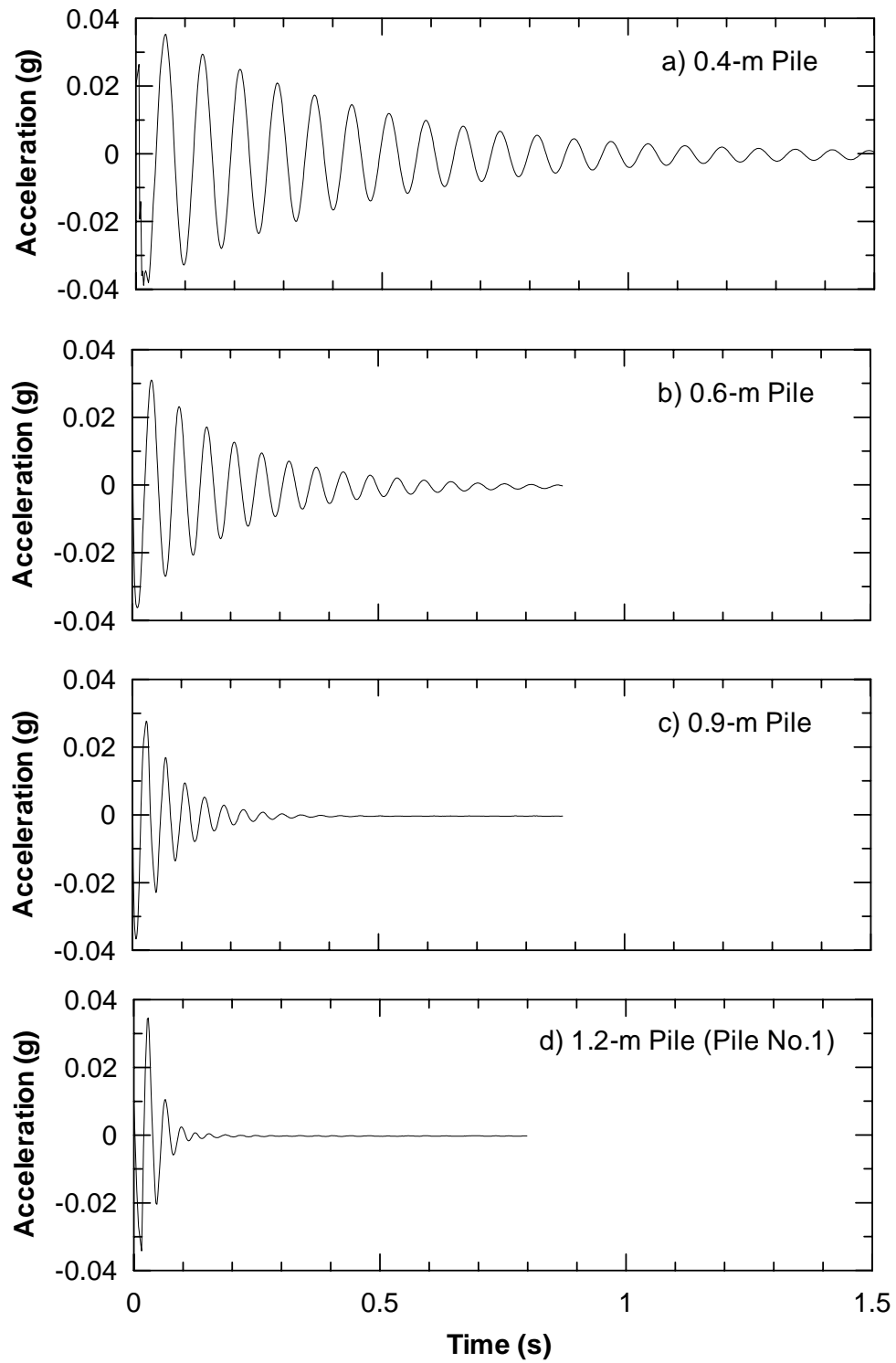


Figure 5.21 Acceleration vs. Time for CIDH Piles from Impact Vibration Tests (E-W Direction)

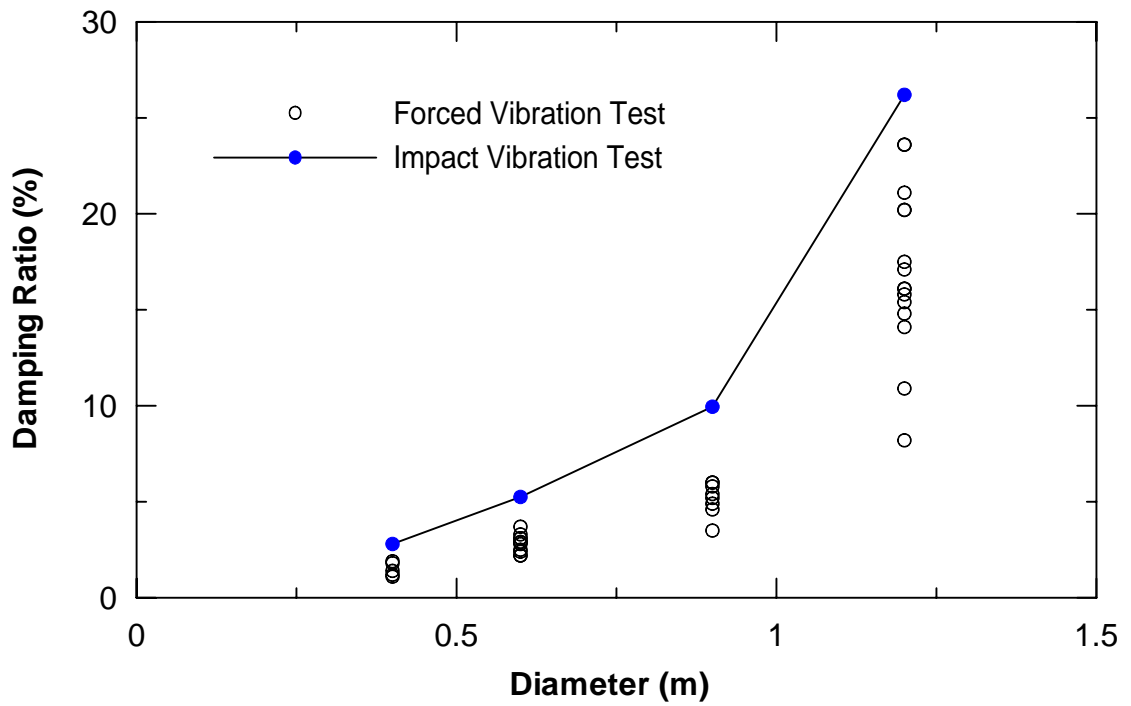


Figure 5.22 Comparison of Damping Ratio Obtained from Impact and Forced Vibration Tests

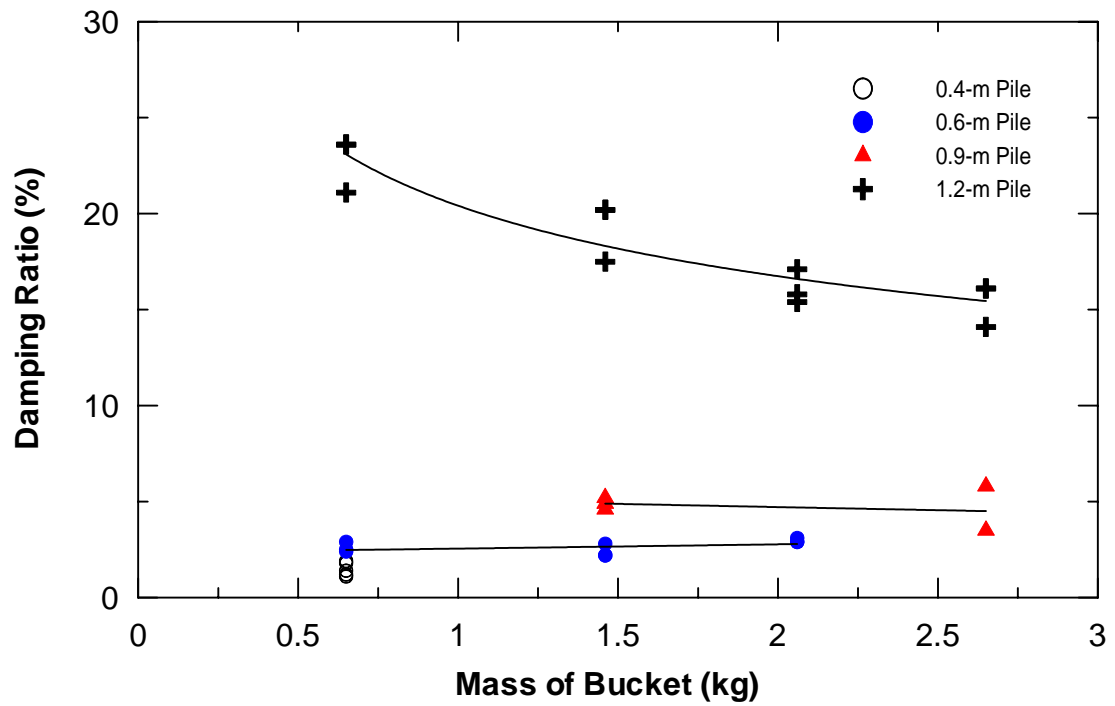
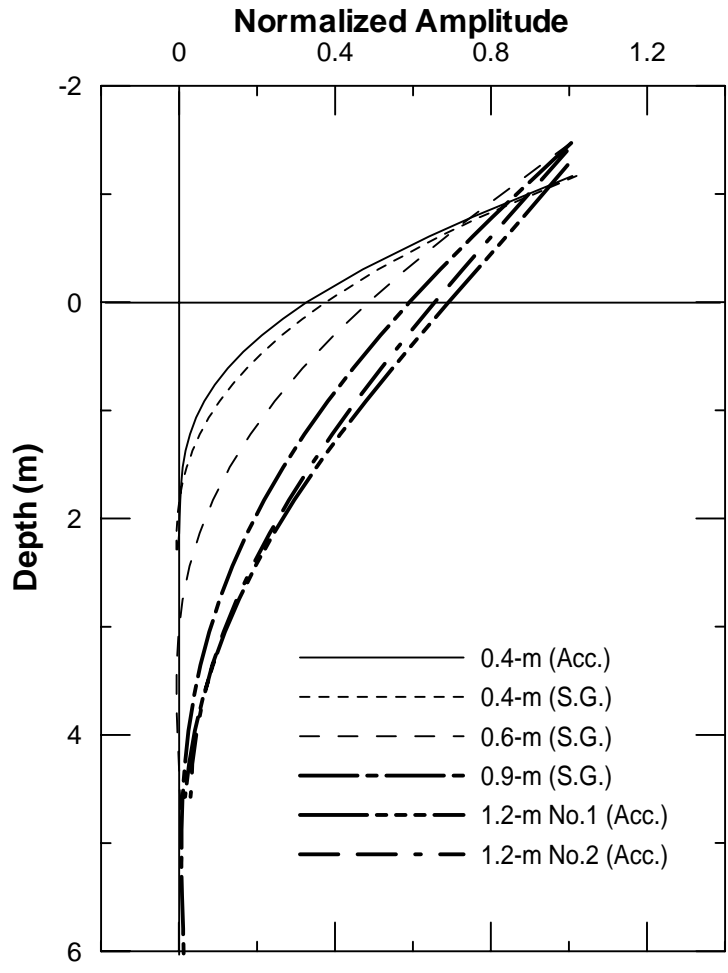


Figure 5.23 Relationship between Mass of Bucket and Damping Ratio for Various Pile Diameters



Acc. = Used Data from Accelerometers  
 S.G. = Used Data from Strain Gauges

Figure 5.24 Mode Shape of Each Pile

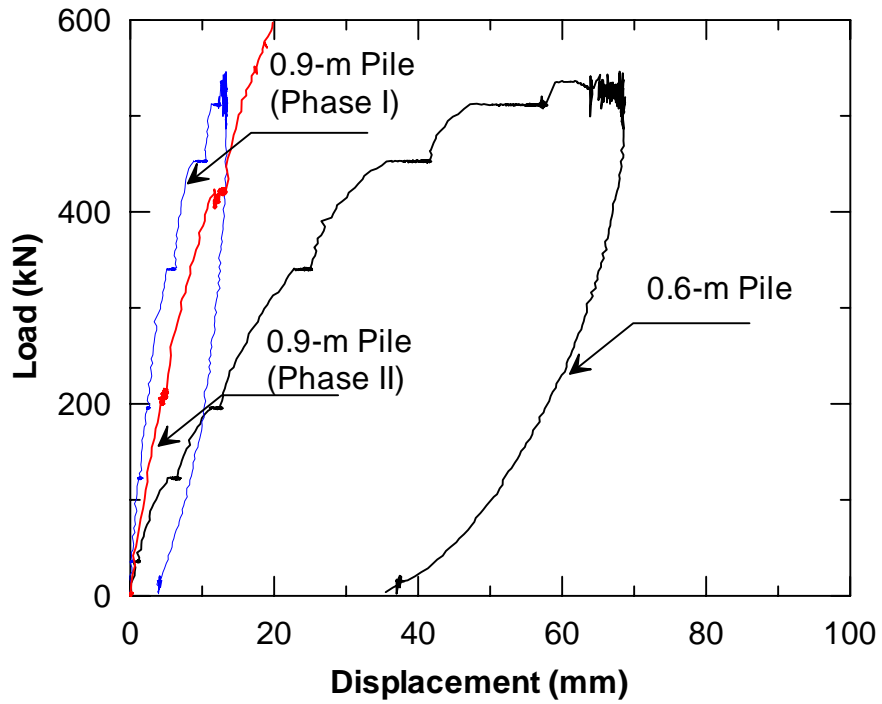


Figure 5.25 Static Load-Displacement Curves for 0.6-m and 0.9-m CIDH Piles before Correction

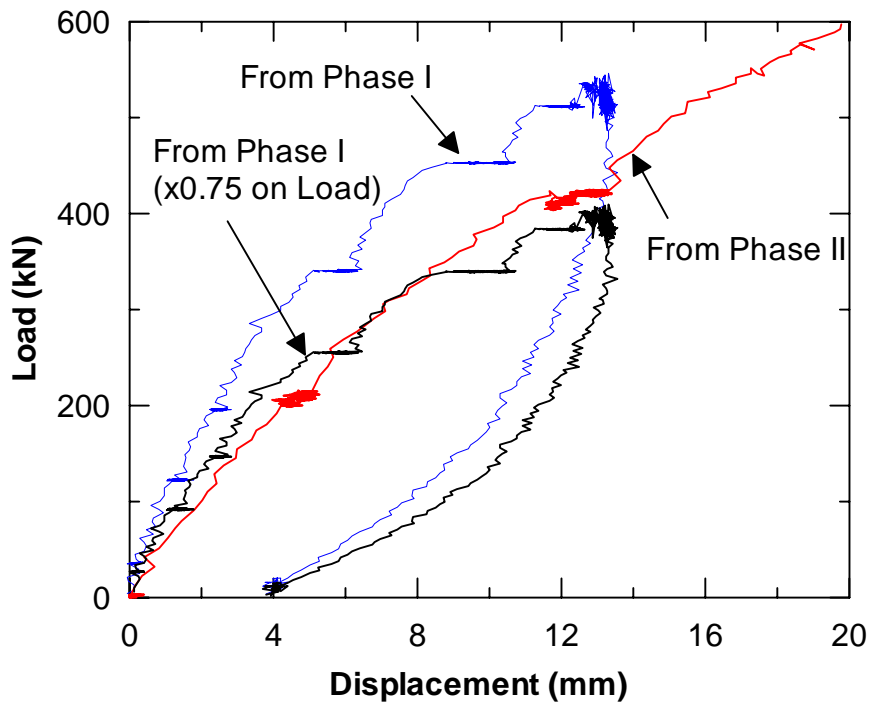


Figure 5.26 Static Load-Displacement Curves of 0.9-m Pile Obtained from Phase I and Phase II

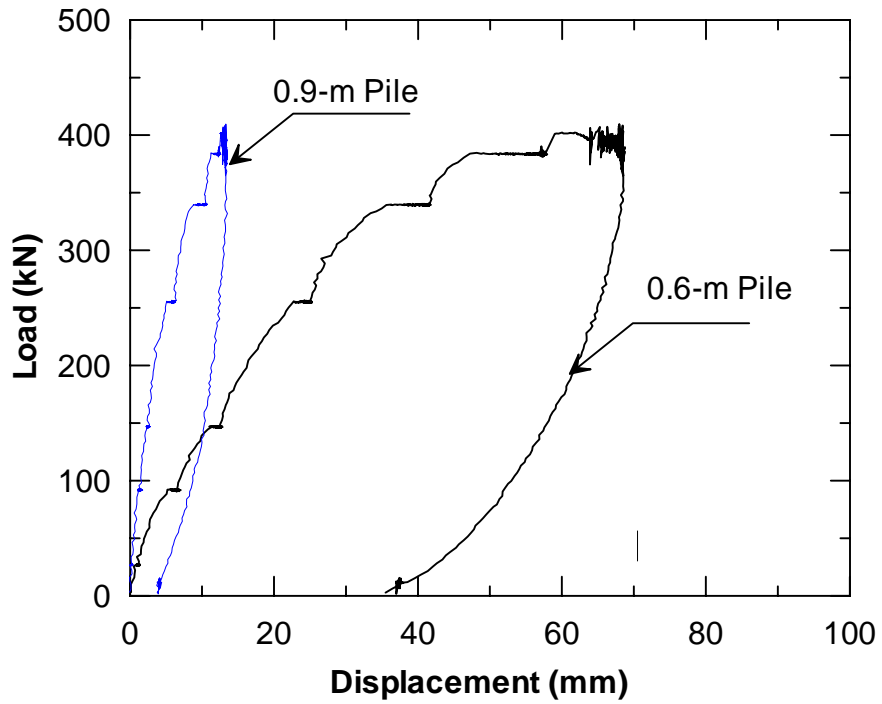


Figure 5.27 Static Load-Displacement Curves for 0.6-m and 0.9-m CIDH Piles after Correction

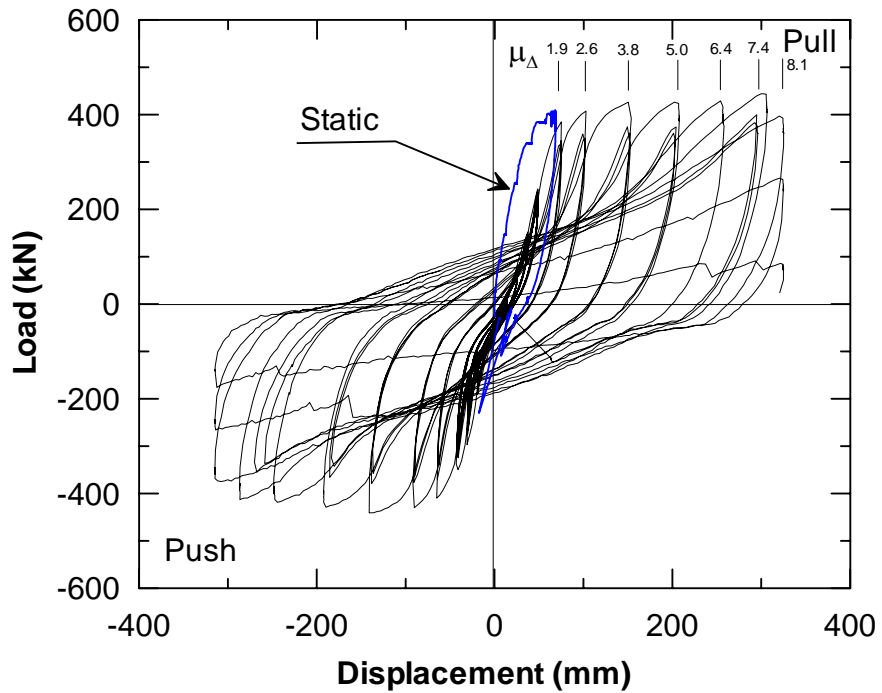


Figure 5.28 Cyclic Load-Displacement Curve for 0.6-m CIDH Pile after Correction

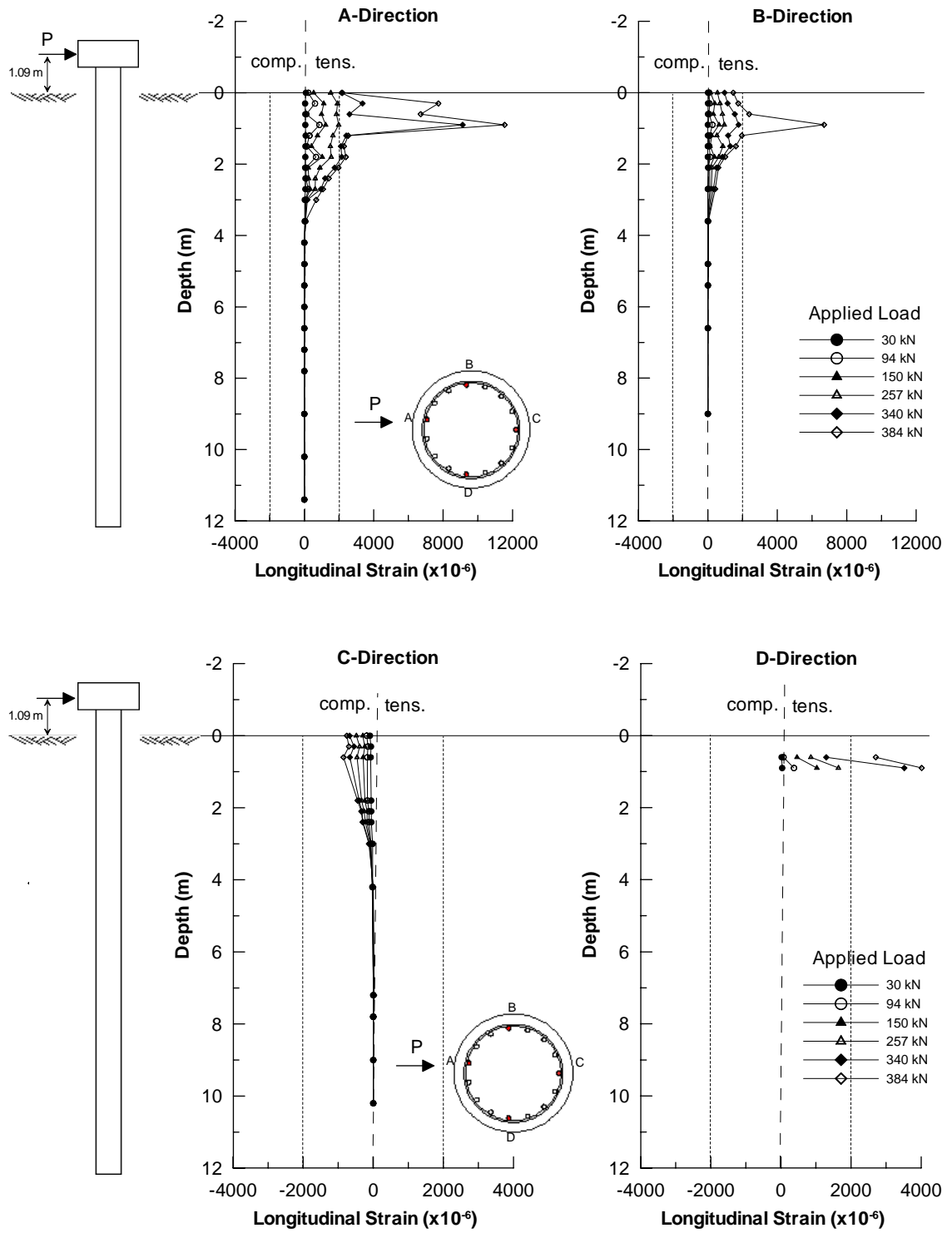


Figure 5.29 Strain Distribution in Longitudinal Reinforcement for 0.6-m CIDH Pile

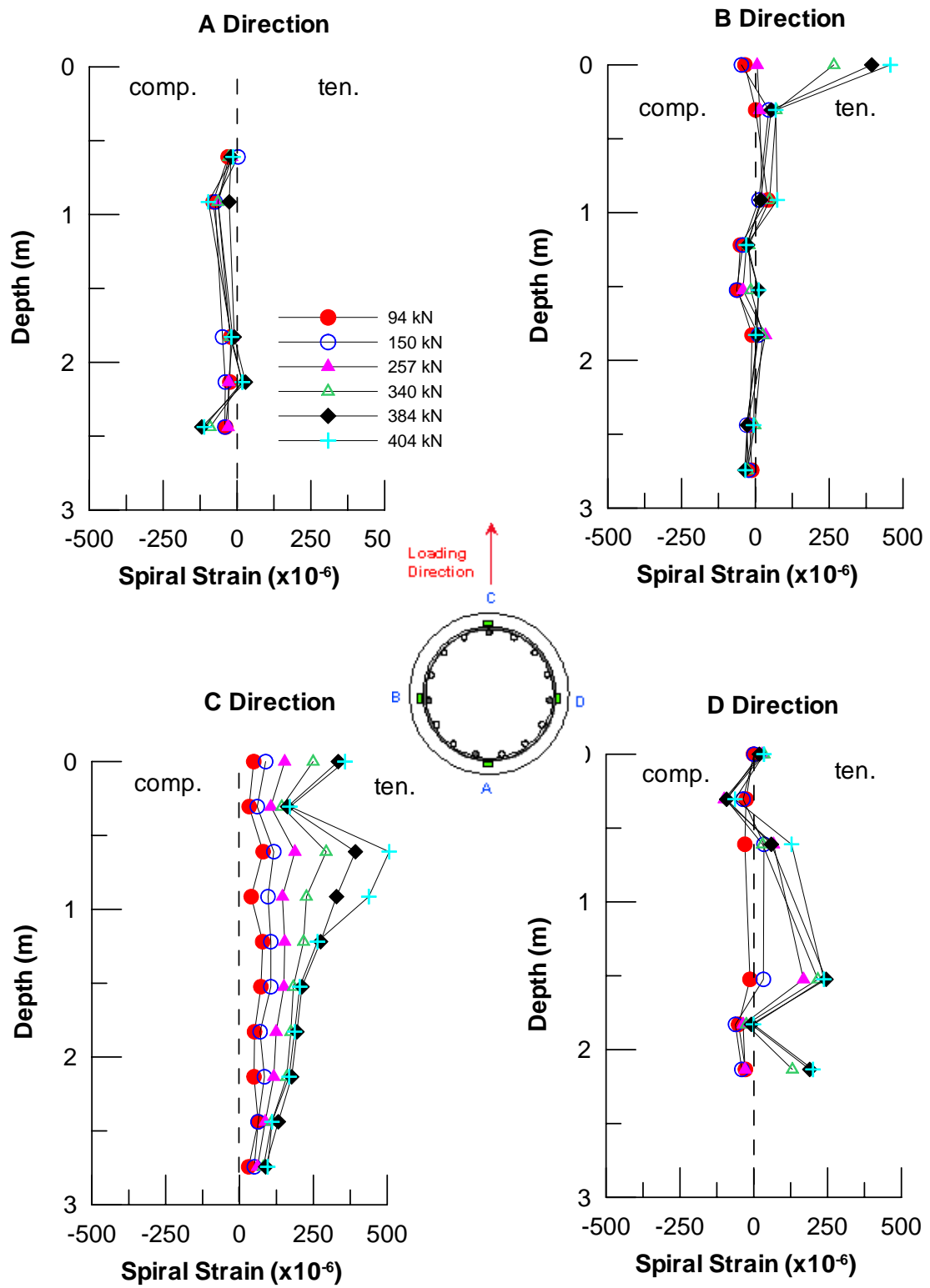


Figure 5.30 Strain Distribution in Transverse Reinforcement for 0.6-m CIDH Pile



Figure 5.31 Rupture of Spiral Reinforcement and 3 Longitudinal Bars in A Direction



Figure 5.32 Rupture of 2 Longitudinal Bars in C Direction



Figure 5.33 Severe Damage of 0.6-m CIDH Pile between Depths 0 m and 0.6 m



Figure 5.34 Crack Patterns along 0.6-m CIDH Pile

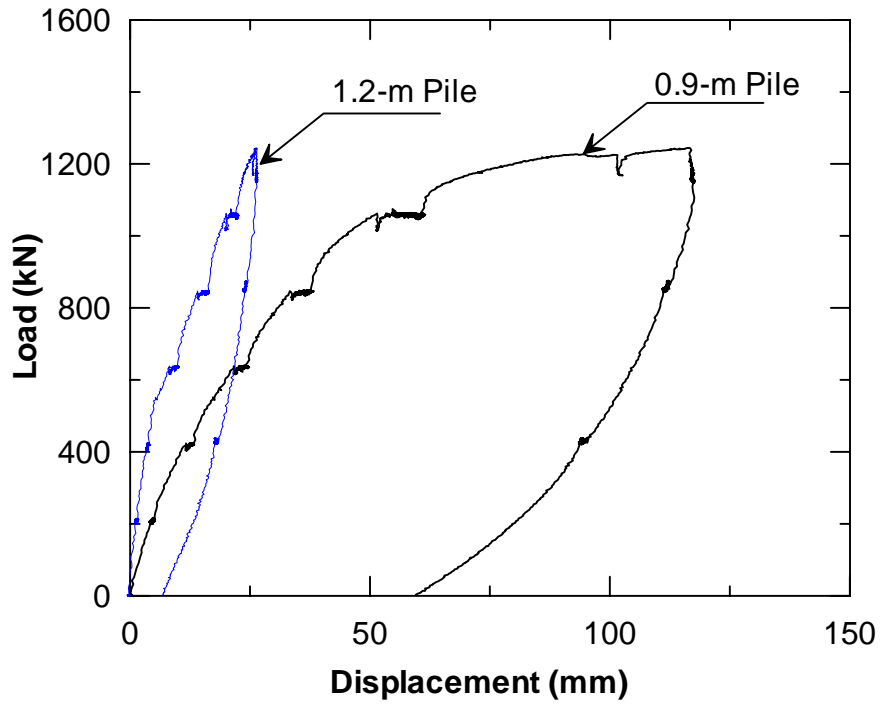


Figure 5.35 Static Load Displacement Curves for 0.9-m and 1.2-m CIDH Piles

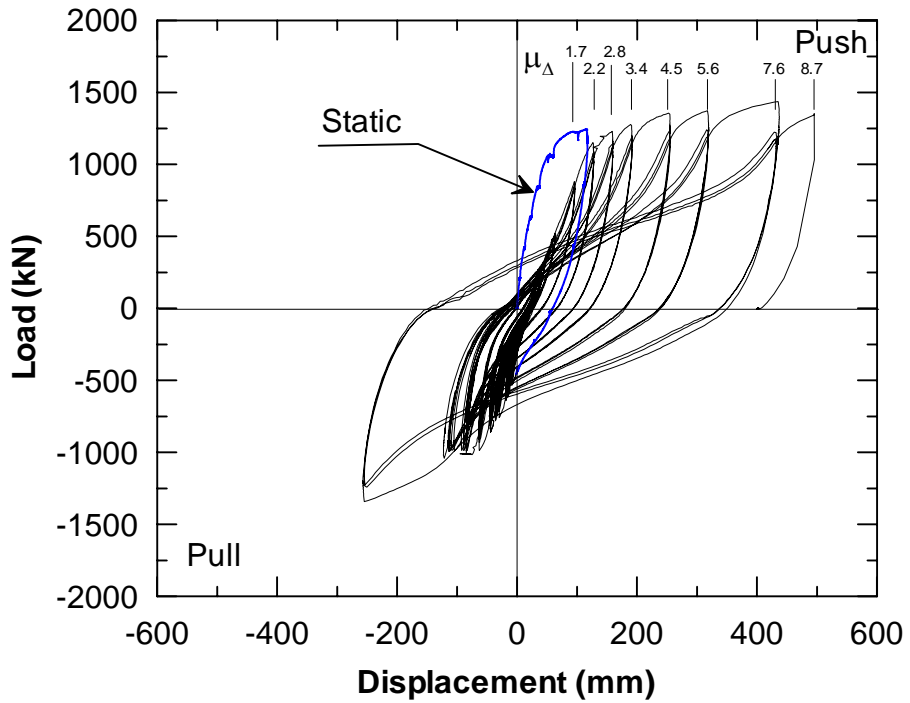


Figure 5.36 Cyclic Load-Displacement Curve for 0.9-m CIDH Pile

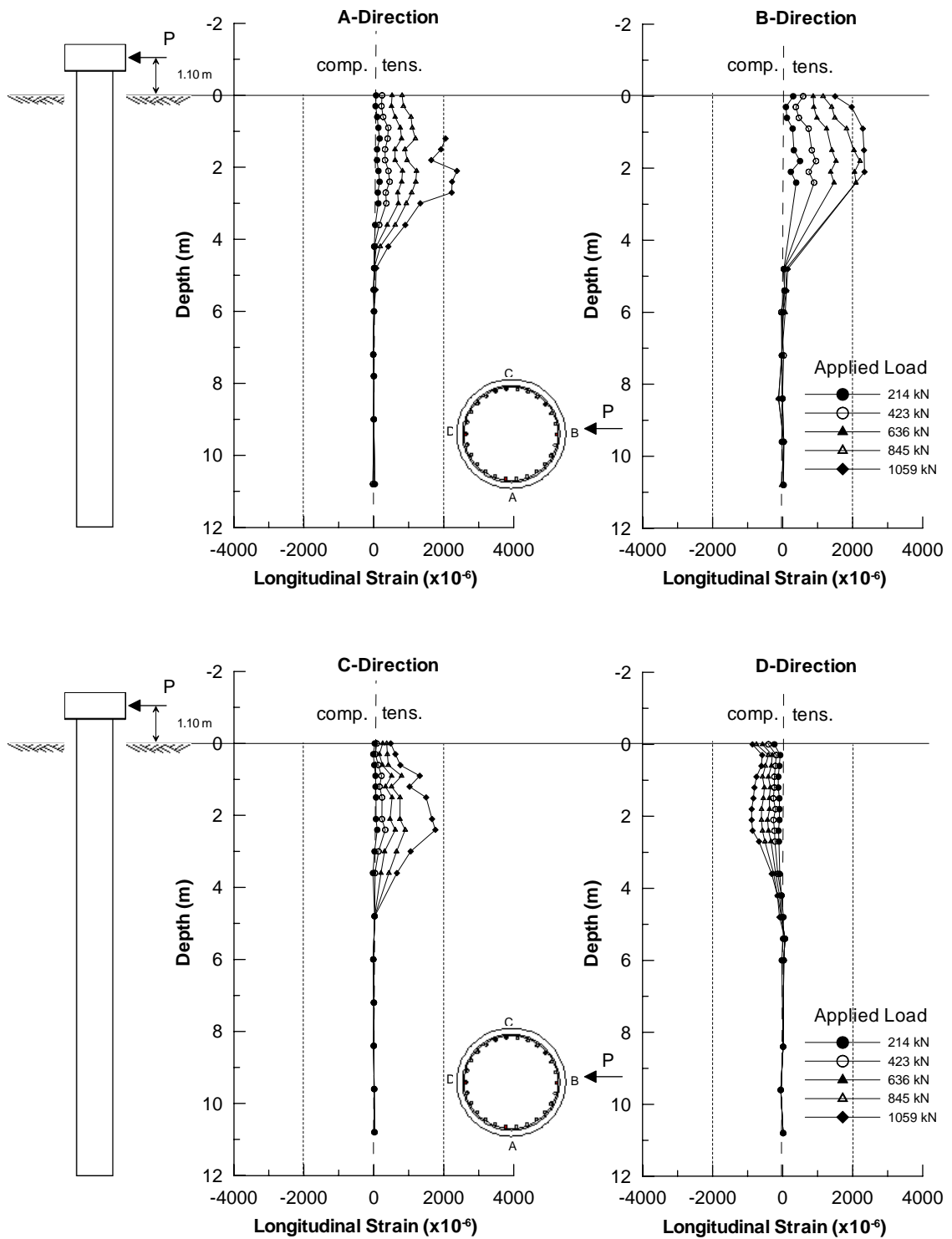


Figure 5.37 Strain Distribution in Longitudinal Reinforcement for 0.9-m CIDH Pile



Figure 5.38 Crack Patterns along 0.9-m CIDH Pile at Depths between (a) 0 m and 1.2 m, and (b) 0.9 m and 2.4 m

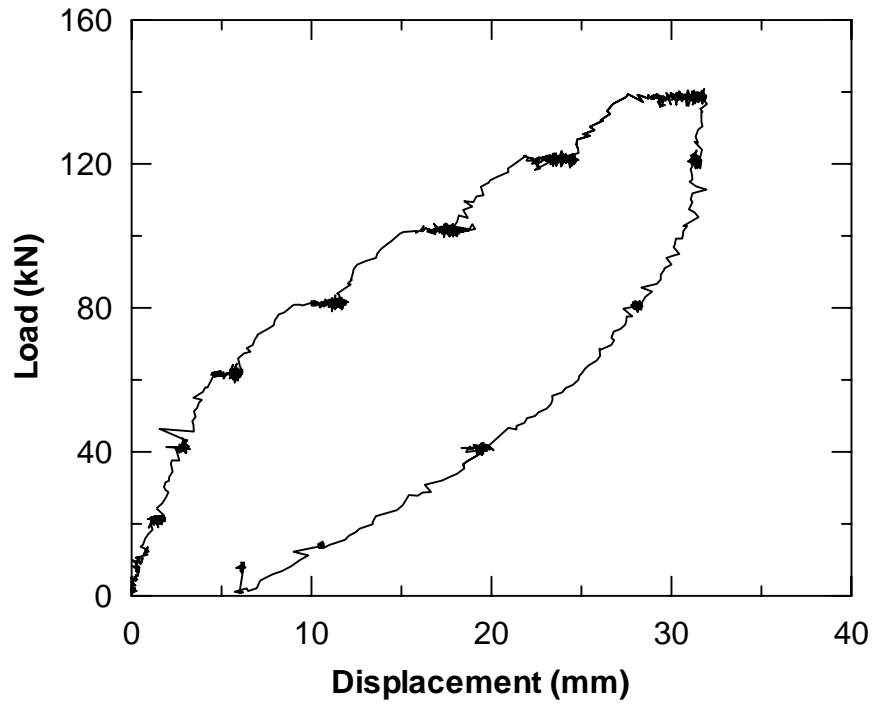


Figure 5.39 Static Load Displacement Curve for 0.4-m CIDH Piles

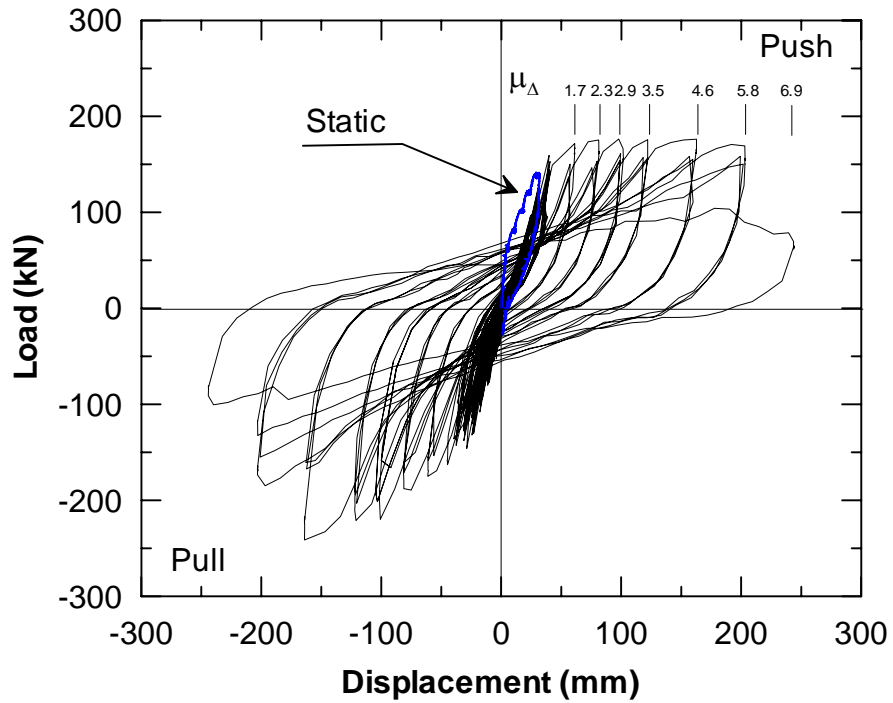


Figure 5.40 Cyclic Load-Displacement Curve for 0.4-m CIDH Pile

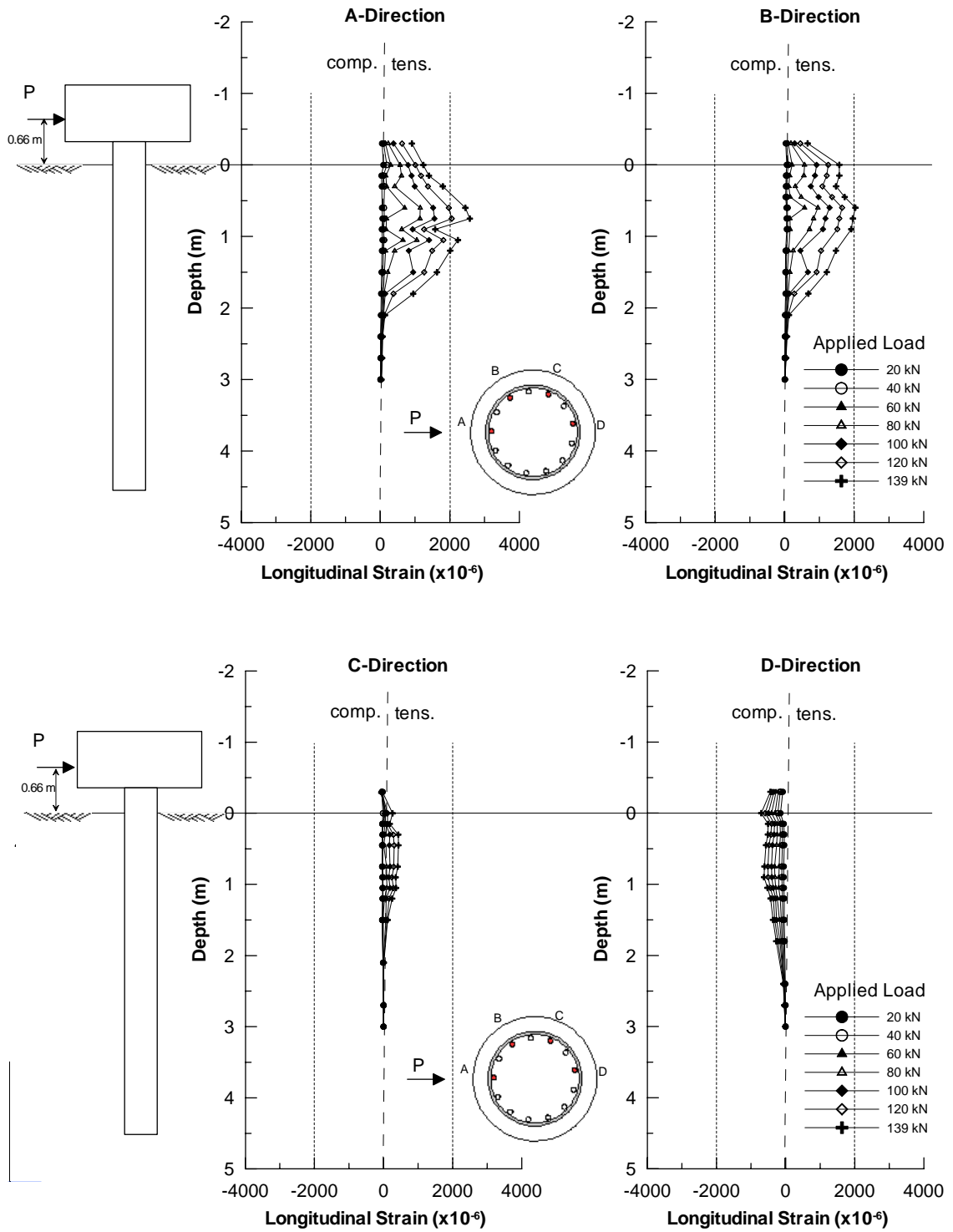


Figure 5.41 Strain Distribution in Longitudinal Reinforcement for 0.4-m CIDH Pile



Figure 5.42 Rupture of Reinforcing Steels of 0.4-m CIDH Pile at Depth of 0.3 m



Figure 5.43 Crack Patterns along 0.4-m CIDH Pile at Depths between 0 m and 1.2 m

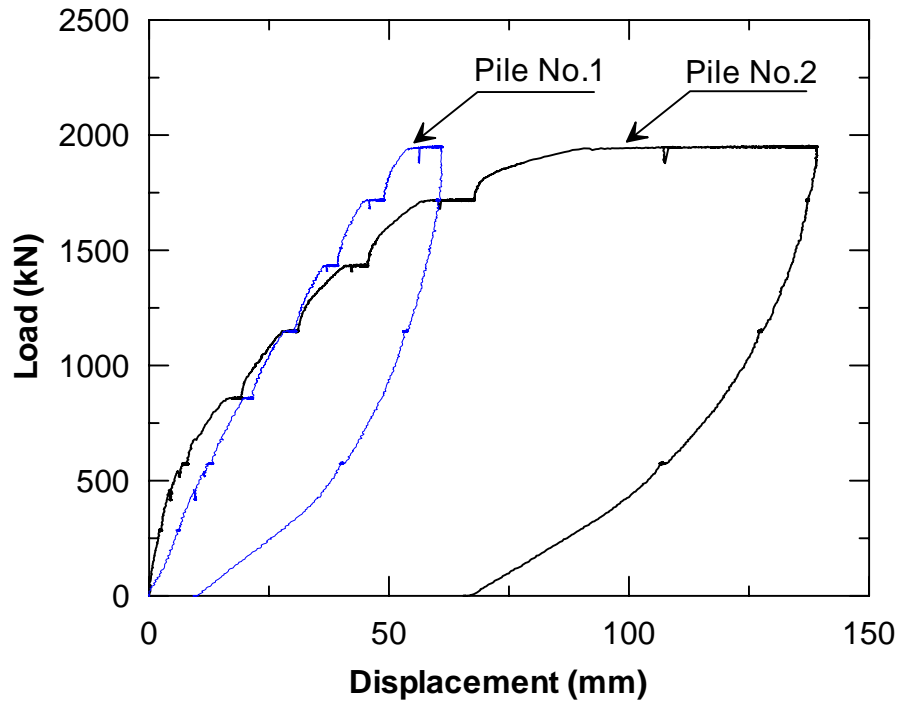


Figure 5.44 Static Load Displacement Curves for 1.2-m CIDH Piles

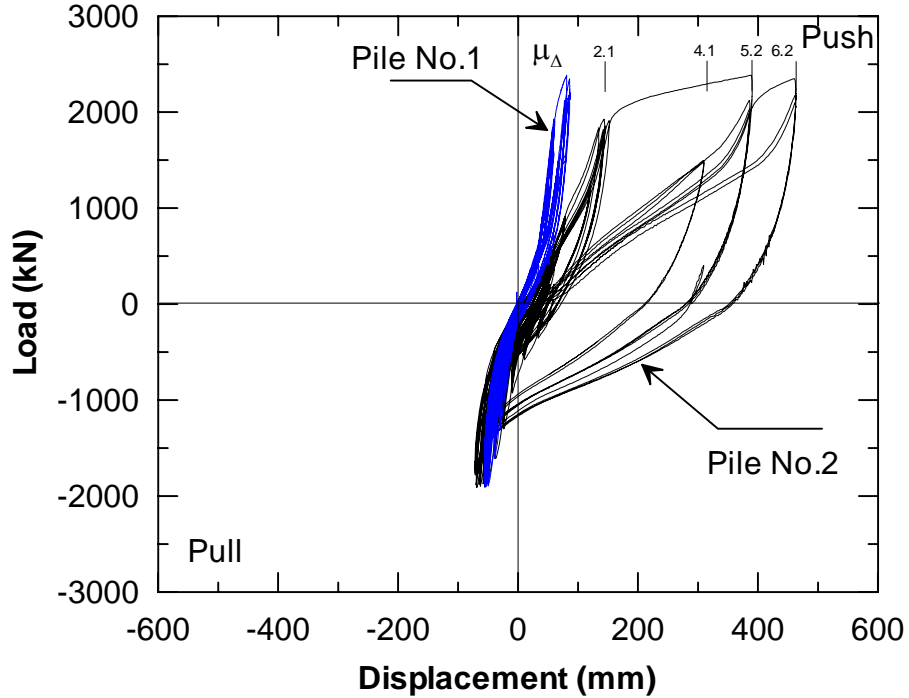


Figure 5.45 Cyclic Load-Displacement Curves for 1.2-m CIDH Piles

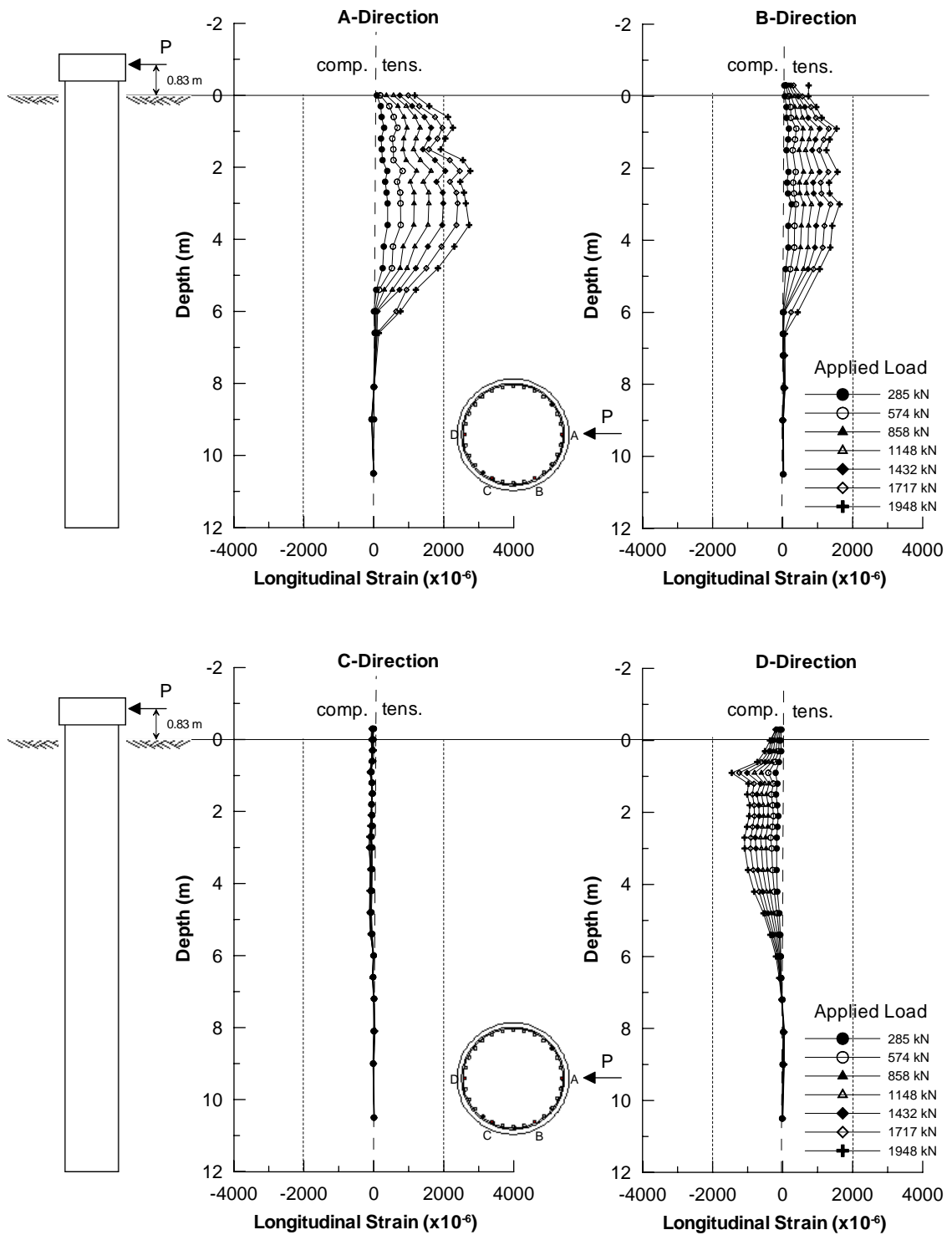


Figure 5.46 Strain Distribution in Longitudinal Reinforcement for 1.2-m CIDH Pile (No.1)

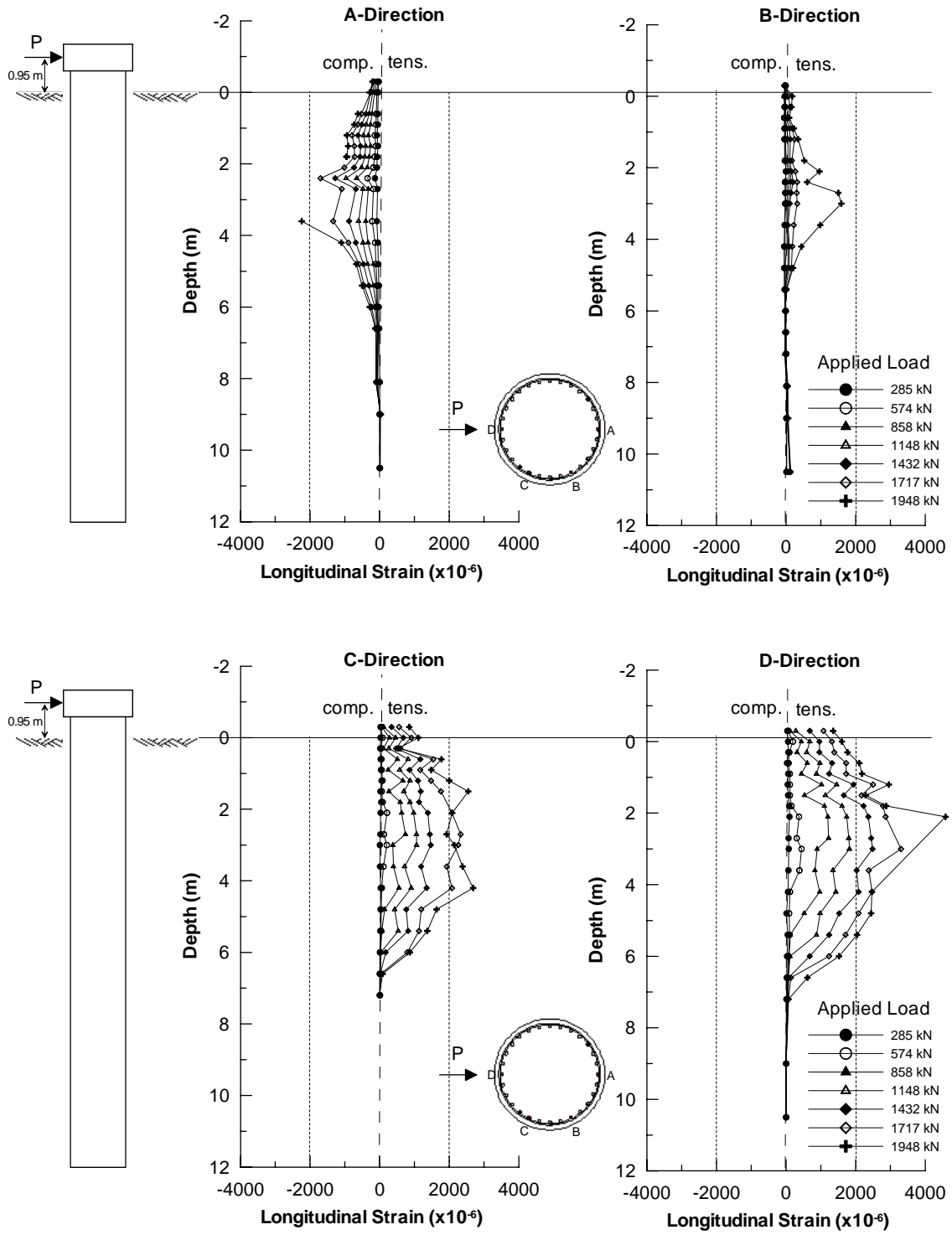


Figure 5.47 Strain Distribution in Longitudinal Reinforcement for 1.2-m CIDH Pile (No.2)



Figure 5.48 Crack Patterns along 1.2-m Pile ( No.2) at Depths between (a) 0.75 m and 1.5 m, and (b) 1.5 m and 4.5 m

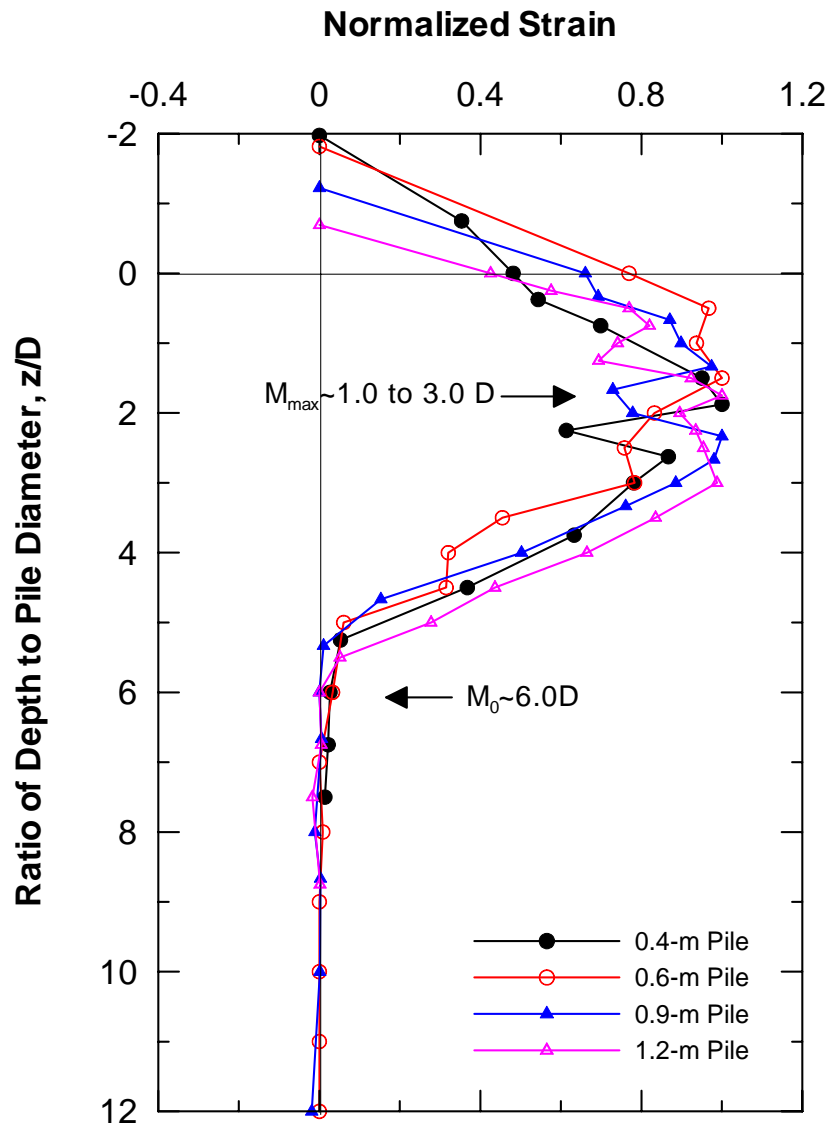


Figure 5.49 Normalized Strain vs. Ratio of Depth to Pile Diameter

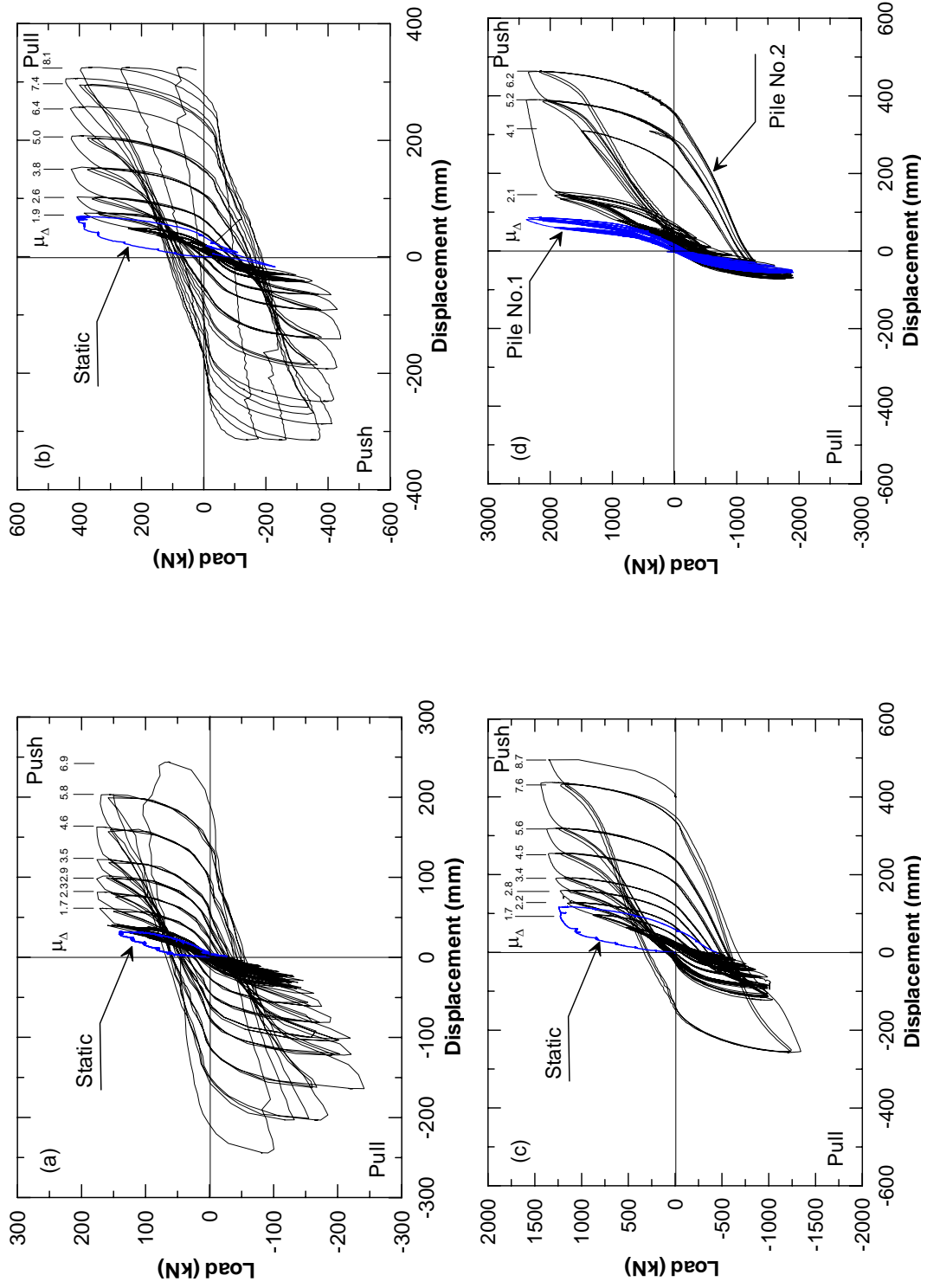


Figure 5.50 Cyclic Load-Displacement Curves for a) 0.4-m Pile, b) 0.6-m Pile, c) 0.9-m Pile, and (d) 1.2-m Piles

This page is intentionally blank.

## Chapter 6 ANALYSIS OF TEST RESULTS

In this chapter, the evaluation of the effect of pile diameter on modulus of subgrade reaction using the results from full-scale experiments is presented. The effect of the pile diameter on the initial modulus of subgrade reaction, the initial slope of  $p$ - $y$  curves, was evaluated using the results from impact vibration tests. This is followed by the evaluation of the effect of pile diameter on  $p$ - $y$  curves at larger strain levels using the back-calculated  $p$ - $y$  curves based on the results from lateral load testing. Furthermore, based on the back-calculated  $p$ - $y$  curves, the methodology to construct the  $p$ - $y$  curves for the weakly cemented soil was proposed and validated with the results from full-scale lateral load testing.

### 6.1 Pile Diameter Effect on Initial Modulus of Subgrade Reaction

In this section, the natural frequencies of soil-pile systems based on the results of the impact vibration tests were used to evaluate the pile diameter effect on the initial modulus of subgrade reaction at a very small strain level. The measured natural frequencies were compared with those estimated from a numerical model. The soil springs in the numerical model were established by implementing three different concepts on initial modulus of subgrade reaction. One is based on Terzaghi's concept (Terzaghi 1955) in which the modulus of subgrade reaction is independent of pile diameter. Another was based on recent research by Carter (1984) and Ling (1988) suggesting that the initial modulus of subgrade reaction may be linearly proportional to pile diameter. The last one was developed based on the findings from finite element analyses in Chapter 3, in which the pile diameter had a little effect on the modulus of subgrade reaction.

### 6.1.1 Method of Analysis

In order to verify the influence of pile diameter on initial modulus of subgrade reaction, a numerical model of the soil-pile system was developed as presented in Figure 6.1. The pile was modeled by using a series of beam elements. The mass distributed throughout the pile element was idealized as a concentrated mass at the nodal points. The flexural rigidity of the pile,  $E_p I_p$ , was computed based upon the uncracked concrete section. Though minor cracking due to shrinkage may be present, these will have an insignificant effect on the stiffness of the pile (Hsu 1993). A summary of flexural rigidity of each pile is presented in Table 6.1. Soil around the pile was modeled by using a series of linear Winkler springs evenly spaced at 0.15 m along the pile length. Since the stepped soil profile is common in weakly cemented sands (e.g. Ashford and Sitar 1994), a simple two-layer soil system seemed to be reasonable to represent the site condition. However, an alternative soil profile with its stiffness increasing with depth was also considered in this analysis. A polynomial function was used to fit the travel time data, and then the shear wave velocity based on this function was computed. The travel-time curve together with associated shear wave velocity for both possible types of soil profiles are presented in Figure 6.2.

Three types of soil springs were considered in this study. One was developed based on Terzaghi's (1955) conclusion in which the modulus of subgrade reaction is independent of pile diameter (i.e.,  $K_{ind}$ ). Another one was developed based on Carter (1984) and Ling's (1988) conclusions in which the modulus of subgrade reaction is linearly dependent on pile diameter (i.e.,  $K_{dep}$ ). The last one was developed based on the finding obtained from the finite element analysis (i.e.,  $K_{fin}$ ) in Chapter 3 in which the pile diameter has a small effect on the initial modulus of subgrade reaction (i.e.

$$\frac{K_1}{K_2} = \left( \frac{D_1}{D_2} \right)^{0.364} \text{ or refer to Eq. (3.3) in Chapter 3).}$$

The Vesic's equation (Eq. 2.3) is usually used to estimate the modulus of subgrade reaction from the soil's Young's modulus for the linear elastic range. The soil spring stiffness can therefore be estimated from the shear wave velocity and the equation modified from the Vesic's Equation, Eq. (2.3) (Ling 1988). The solution obtained from Eq. (2.3) is taken from the beam on the elastic foundation case. Bowles (1988) suggested a modification on Eq. (2.3) in that the modulus of subgrade reaction,  $K$ , for the lateral loaded pile case should be doubled since the pile has soil contact with both sides. However, in reality, soil does not have contact all around the pile when the pile is subjected to lateral loading, but the friction developed at both sides of the pile can increase the overall soil resistance. The average value from lower bound, Eq. (2.3), and upper bound solutions suggested by Bowles seems to be reasonable for the analysis of the laterally loaded pile. This is in agreement with what was proposed by Carter (1984) and Ling (1988) who found that the closest agreement in predicting the pile deflection was obtained by using a factor of 1.0 as

$$K = \frac{1.0E_s}{(1 - \mu_s^2)} \left[ \frac{E_s D^4}{E_p I_p} \right]^{1/12} \quad (6.1)$$

To account for the effect of pile diameter on initial modulus of subgrade reaction, Carter and Ling suggested a linear relationship between the modulus of subgrade reaction and the pile diameter,  $K$ , based on Ling's concept can then be expressed as

$$K = \frac{1.0E_s}{(1 - \mu_s^2)} \left( \frac{D}{D_{ref}} \right) \left[ \frac{E_s D^4}{E_p I_p} \right]^{1/12} \quad (6.2)$$

where  $D_{ref} = 1.0$  m.

Similar to Eq. (6.2), the modulus of subgrade reaction which incorporated the pile diameter effect based on the finding from the finite element analysis in Chapter 3 can be calculated as follows:

$$K = \frac{1.0E_s}{(1-\mu_s^2)} \left( \frac{D}{D_{ref}} \right)^{0.364} \left[ \frac{E_s D^4}{E_p I_p} \right]^{1/12} \quad (6.3)$$

The soil elastic modulus,  $E_s$ , can be determined by

$$E_s = 2\rho V_s^2 (1 + \mu_s) \quad (6.4)$$

where  $\rho$  = soil density, and  $V_s$  = shear wave velocity.

From the above expressions, the initial horizontal modulus of subgrade reaction can be calculated.  $K_{ind}$ ,  $K_{dep}$ , and  $K_{fin}$  can be determined by using Eq. (6.1), (6.2) and (6.3), respectively. The soil spring stiffness can then be computed by multiplying the modulus of subgrade reaction with the soil spring spacing. A summary of soil spring stiffnesses based on different concepts of pile diameter effect on modulus of subgrade reaction for simple two-layer soil system is given in Table 6.1.

Based on the numerical model of soil-pile system, the mass matrix  $[M]$  and stiffness matrix  $[K]$  can be simply formulated. The mode shape and natural frequency of the system can then be calculated by using a modal analysis. Taking the equation of undamped free vibration, where no loads are assumed to act upon the structure, the N degree-of-freedom equation of equilibrium becomes

$$[M] \left\{ \ddot{u} \right\} + [K] \{u\} = \{0\} \quad (6.5)$$

where  $\{u\}$  and  $\left\{ \ddot{u} \right\}$  are the displacement and acceleration vector of an multi-degree-of-freedom system. By assuming simple harmonic motion  $\{u\} = \{\Phi\}_i Y_i \sin \omega_i t$  the equation of free vibration is then simplified to

$$-\omega_i^2 [M]\{\Phi\}_i + [K]\{\Phi\}_i = \{0\} \quad (6.6)$$

where  $\{\Phi\}_i$ ,  $\omega_i$ , and  $Y_i$  are the  $i^{\text{th}}$  mode, frequency, and modal amplitude of free vibration respectively.

The damped natural frequency of the system was then calculated as

$$\omega_D = \omega_n \sqrt{1 - \xi^2} \quad (6.7)$$

where  $\omega_D$  = damped natural frequency,  $\omega_n$  = undamped natural frequency (from Eq. 6.6), and  $\xi$  = damping ratio of the system (obtained from impact vibration test results).

In this study, the Ruaumoko program (Carr 1998), a structural analysis program for inelastic dynamic analysis, was utilized to run a modal analysis to predict the natural frequency of the soil-pile system.

### 6.1.2 Results of Analyses

The computed natural frequencies based on the different concepts on initial modulus of subgrade reaction for a case of simple 2-layer soil profile are given in Table 6.2. It is noted that for the 1.2-m piles, the computed natural frequency of Pile No.1 is higher than that of Pile No.2 because the free standing height of Pile No.1 was lower than that of Pile No.2. The comparison between experimental and computational results was made by plotting the ratio of computed to measured natural frequency against the pile diameter as shown in Figure 6.3 through Figure 6.6. From Figure 6.3, it is clearly seen that for the simple two-layer soil profile the results obtained from Terzaghi's concept (i.e.,  $K_{ind}$ ) give a good agreement on natural frequency prediction over the range of the diameter considered. The computed natural frequency of the system based on  $K_{dep}$  appears to be significantly underestimated at diameters less than 1 m and slightly

overestimated beyond that diameter. Since Terzaghi's approach is consistent with the test results, the comparison between the two concepts can be extrapolated over a wider range of pile diameters by performing a parametric study. The results are shown by the dotted line in Figure 6.3, which confirms the trends above and below the 1-m diameter. Figure 6.4 shows that the soil springs developed from both Terzaghi's concept and the conclusion from the finite element analysis gave reasonable agreement between the computed and the measured natural frequency with similar degree of accuracy. From this, it is inferred that the initial modulus of subgrade reaction for weakly cemented sand appears to have insignificant effect on the pile diameter.

In contrast to Figure 6.4, Figure 6.5 presents the ratio of computed to measured natural frequency against pile diameter using a soil profile where the soil stiffness increases with depth. Though the computed natural frequencies derived from Terzaghi's concept and finite element analysis finding are in better agreement with the measured natural frequency than those obtained from Ling's concept, all of them underestimated the natural frequency with the difference being more significant at a small pile diameter. Additional analyses were conducted to see whether or not the trend of the pile diameter effect will change, if the spring stiffnesses at all depths were increased. Assuming that the equations used to calculate the spring stiffnesses were conservative, the spring stiffnesses were therefore calibrated by multiplying them with a constant until the computed natural frequency of the 1.2-m pile matched well with the measured natural frequency. Analyses were then performed for other diameters using the updated spring stiffnesses. The improvement on the natural frequency prediction was observed as presented in Figure 6.6, but there was no change in the trend. This implies that the simple two-layer soil profile seems to be more appropriate to represent the behavior of cemented soil at a very small strain level. Unlike clean sand whose stiffness increases with depth due to the effect of confining pressure, the behavior of cemented sand at very small strain seems to be independent of depth. This is because at very small strain level the cohesion is the predominant strength component, and therefore the confinement of the

soil does not have much effect on its initial stiffness (Saxena and Lastrico 1978). This finding was also supported by previous research on behavior of artificially cemented sand (Clough *et al.* 1981) presented in Figure 2.25d in Chapter 2, which indicates that the initial modulus of the artificially cemented soil at small strain is independent on the confining pressure.

### 6.1.3 Analysis of Damping

In this section the damping ratio of the systems were estimated using the available equations in the literature to compare with the damping ratio measured from the impact vibration experiments. Gazetas (1991) proposed closed-form expressions to estimate the static stiffnesses and damping coefficients (i.e.,  $K_{HH}$ ,  $K_{MM}$ ,  $K_{HM}$ ,  $\xi_{HH}$ ,  $\xi_{MM}$ , and  $\xi_{HM}$ ) for flexible piles in constant stiffness soil profile as the followings:

$$K_{HH} = DE_s (E_p / E_s)^{0.21} \quad (6.8)$$

$$K_{MM} = 0.15D^3 E_s (E_p / E_s)^{0.75} \quad (6.9)$$

$$K_{HM} = K_{MH} = -0.22D^2 E_s (E_p / E_s)^{0.50} \quad (6.10)$$

$$\xi_{HH} \approx 0.80\beta + 1.10fD(E_p / E_s)^{0.17} / V_s \quad (6.11)$$

$$\xi_{MM} \approx 0.35\beta + 0.35fD(E_p / E_s)^{0.20} / V_s \quad (6.12)$$

$$\xi_{HM} \approx 0.85\beta + 0.85fD(E_p / E_s)^{0.18} / V_s \quad (6.13)$$

where  $K_{HH}$ ,  $K_{MM}$ , and  $K_{HM}$  are static lateral, static rocking, and static swaying-rocking cross stiffnesses of the pile,  $\xi_{HH}$ ,  $\xi_{MM}$ , and  $\xi_{HM}$  are lateral, rocking, and swaying-rocking damping coefficients,  $D$  is pile diameter,  $\beta$  is material damping ratio of the soil,  $V_s$  is shear wave velocity,  $f$  is frequency excitation,  $E_p$  is the Young's Modulus of pile, and  $E_s$  is the Young's modulus of the soil.

The horizontal static stiffness,  $K_h$ , and rotational static stiffness,  $K_\theta$ , of the pile can be estimated by using the following equations:

$$K_h = \frac{K_{HH} K_{MM} - K_{HM}^2}{K_{MM} - K_{HM} M/H} \quad (6.14)$$

$$K_\theta = \frac{K_{HH} K_{MM} - K_{HM}^2}{K_{HH} - K_{HM} H/M} \quad (6.15)$$

where  $H$  is the horizontal force at the pile head, and  $M$  is the moment at the pile head.

The various components of the pile head impedances,  $\sigma_{\alpha\beta}$ , can be determined as

$$\sigma_{\alpha\beta} = K_{\alpha\beta} (k_{\alpha\beta} + 2\xi_{\alpha\beta} i) \quad (6.16)$$

where  $\alpha\beta$  refers to various components (i.e.,  $HH$ ,  $MM$ , and  $HM$ ),  $K_{\alpha\beta}$  is the static pile head stiffness (from Eqs. (6.8) through (6.10)),  $k_{\alpha\beta}$  is the dynamic stiffness coefficient, which is approximately equal to one (Gazetas 1991), and  $\xi_{\alpha\beta}$  is the damping coefficients (from Eqs. (6.11) through (6.13)).

The horizontal and rotational pile head impedances (i.e.,  $\sigma_h$  and  $\sigma_\theta$ ) can be determined in the same fashion as Eqs. (6.14) and (6.15) by replacing  $K_{\alpha\beta}$  terms with  $\sigma_{\alpha\beta}$  terms as:

$$\sigma_h = \frac{\sigma_{HH} \sigma_{MM} - \sigma_{HM}^2}{\sigma_{MM} - \sigma_{HM} M/H} \quad (6.17)$$

$$\sigma_\theta = \frac{\sigma_{HH} \sigma_{MM} - \sigma_{HM}^2}{\sigma_{HH} - \sigma_{HM} H/M} \quad (6.18)$$

The  $\sigma_h$  and  $\sigma_\theta$  are in complex form similar to Eq. (6.16). The horizontal and rotational dampings ( $\xi_h$  and  $\xi_\theta$ ) can then be simply calculated as the ratio between the imaginary part and two times of the real part. Wolf (1985) proposed the equation to estimate the equivalent damping of SDOF system with the pile foundation as

$$\xi = \frac{\xi_{st} + \xi_h \frac{k_{st}}{K_h} + \xi_\theta \frac{k_{st} h^2}{K_\theta}}{1 + \frac{k_{st}}{K_h} + \frac{k_{st} h^2}{K_\theta}} \quad (6.19)$$

where:  $\xi_{st}$  is the damping for the structure,  $k_{st}$  is the stiffness of the structure, and  $h$  is the height of the SDOF structure.

The damping ratio of each pile was calculated using the above expressions and then compared with the measured one as presented in Figure 6.7. The results show a good agreement between predicted and measured damping, though they were somewhat higher than those computed, particularly at high frequencies. This might be due to two possible reasons: (1) the analytical solutions used in this analysis were derived based upon single constant soil modulus, while the soil at the test site consisted of two constant soil modulus layers system, and (2) the damping ratio determined based on logarithmic decrement method at high frequency might have some error due to the limited number of acceleration amplitude peaks during the free vibration testing. The computed damping ratios based on analytical solutions were lower than the measured damping ratios indicating that Gazetas's damping expressions are conservative for the soil and piles tested.

## 6.2 Pile Diameter Effect on $p$ - $y$ Curves

In the previous section, it was shown that the pile diameter has an insignificant effect on the initial modulus of subgrade reaction, the initial stiffness of  $p$ - $y$  curve. In this

section, the back-calculated  $p$ - $y$  curves based on the results from static lateral load tests for various pile diameters are presented. The  $p$ - $y$  curves of each pile at different depths were then compared to provide insight into the effect of pile diameter on  $p$ - $y$  curves at larger strain level.

### 6.2.1 Method for Back-Calculating $p$ - $y$ Curves

The lateral soil resistance per unit pile length developed along the CIDH piles,  $p$ , as well as associated soil-pile displacement,  $y$ , were back-calculated using the basic beam theory. The strain gauge data was utilized extensively in the back-computation of the  $p$ - $y$  curves. Only data from the static tests was used in the analyses because the strain gauge data during the cyclic loading was inconsistent due to the yielding of the pile. The methodology used to calculate  $p$ - $y$  curves is described as the following:

To determine the lateral soil resistances as well as associated pile displacements, the curvature of the pile,  $\phi$ , at each depth was first determined using the strain gauge data. For a steel pipe pile, the neutral axis of the pile remains at the center throughout the test and data from two strain gauges per depth seems to be sufficient to calculate the curvature. In contrast, estimation of the curvature in the reinforced concrete pile is more difficult because the strain measured along the pile is not uniform. The strain is high in the vicinity of the crack and lower at a location far away from the crack. Therefore, more strain gauges are required at each depth in order to obtain reliable curvature. In this study three to four strain gauges were available at each depth. Figure 6.8 presents an example of curvature estimation based on good strain gauge data. Assuming a linear distribution of strain along the pile cross section, the curvature of the pile can be determined using the best fit of a linear function to the strain gauge data. The slope of the linear function represents the curvature of the pile.

The 6<sup>th</sup> order polynomial function was chosen to fit the discrete curvature. Then the rotation of the pile,  $\theta$ , was computed by an integration of the curvature polynomial function along the pile length using the following equation:

$$\theta = \int \phi(z) dz \quad (6.20)$$

where:  $\theta$  is pile rotation,  $\phi(z)$  is polynomial curvature function, and  $z$  is depth.

At this step, the computed rotation along the pile was compared to the measured rotation from the tiltmeters to confirm that the fit polynomial function was reasonable. Subsequently, the soil displacements,  $y$ , were determined by integrating the polynomial function of pile rotation along the pile length using the following expression:

$$y = \int \theta(z) dz \quad (6.21)$$

In order to determine the soil resistance along the pile, the moment of the pile was first computed using the following expression:

$$M = EI * \phi \quad (6.22)$$

where  $M$  is the moment,  $EI$  is flexural rigidity or flexural stiffness of the pile, and  $\phi$  is the pile curvature. Since the  $EI$  of CIDH pile is not constant, the UCFyber (Chadwell 1999), a finite element program for section analysis, was used to obtain the moment-curvature relationship for each pile. Figure 6.9 through Figure 6.12 present the moment-curvature relationship for each pile together with the simplified ones using a quadruple-linear model for the analyses. It is noted that beyond the yield moment, the analyses were not conducted due to the inconsistency of strain gauge data. However the simplified moment-curvature relationship for the entire curves is used for a prediction of load–

displacement curves in the inelastic range of the piles, which will be discussed in the subsequent section.

Again, the 6<sup>th</sup> order polynomial function was chosen to fit the discrete moment data along the length of the pile. The shear forces along the length of the pile were calculated by differentiating the moment data with respect to depth using the following relationship:

$$S = \frac{dM(z)}{dz} \quad (6.23)$$

where  $S$  is shear force,  $M$  is moment and  $z$  is depth.

At this step, the calculated shear force at ground surface was compared with the measured shear force from the actuator load. This step was to confirm that the polynomial function chosen to fit the moment data was reasonable. Then, the lateral soil resistance was determined by the following equation:

$$p = \frac{dS(z)}{dz} \quad (6.24)$$

where  $p$  is the soil resistance per unit pile length,  $z$  is depth, and  $S$  is shear force. With the lateral soil resistance and associated pile displacement computed from the above equations, the  $p$ - $y$  curves of the soil at each depth can be obtained.

## 6.2.2 Back-Calculated $p$ - $y$ Curves for CIDH Piles

### 6.2.2.1 0.4-m $p$ - $y$ Curves

Figure 6.13 shows the back-calculated  $p$ - $y$  curves of the 0.4-m CIDH pile at various depths based on the methodology mentioned in previous section. It can be observed that the soil resistance increases with depth. Furthermore, the soil resistance at the ground surface is not zero as usually assumed in the sand  $p$ - $y$  curves (Reese *et al.* 1974). This is likely because the soil at the test site was weakly cemented sand, and that the cementation, in the form of cohesion, contributed to the soil resistance at the ground surface. The characteristic shape of the back-calculated  $p$ - $y$  curves is similar to that proposed by Ismael (1990) rather than that proposed by Reese and Van Impe (2001) in which the softening of the  $p$ - $y$  curves is expected.

Since the double differentiation of the moment along the pile may lead to a significant error in estimating the soil resistance, a verification of the  $p$ - $y$  curves was required at the end of the process. The back-calculated  $p$ - $y$  curves were used as the input in a numerical model (i.e., beam with a series of nonlinear springs) to predict the lateral responses of the piles and then to compare with the experimental results. Good agreement between computed and measured responses was observed as presented in Figure 6.14 and Figure 6.15, indicating that the back-calculated  $p$ - $y$  curves for the 0.4-m pile are reasonable.

### 6.2.2.2 0.6-m $p$ - $y$ Curves

Figure 6.16 shows the back-calculated  $p$ - $y$  curves of the 0.6-m CIDH pile at various depths. Similar characteristics of the  $p$ - $y$  curves as observed in the 0.4-m pile were also seen in the 0.6-m pile. After the  $p$ - $y$  curves were back-calculated, the analysis was performed to verify that the back-calculated  $p$ - $y$  curves provide a reasonable estimate

of the pile response. Figure 6.17 and Figure 6.18 show the pile responses from the analysis compared to measured test results.

#### 6.2.2.3 0.9-m $p$ - $y$ Curves

The back-calculated  $p$ - $y$  curves of the 0.9-m CIDH pile using the strain gauge data from lateral load test No.2 is presented in Figure 6.19. The results indicate that the soil resistance increases with depth and there is a finite soil resistance observed at the ground surface. Figure 6.20 and Figure 6.21 show the results of the analysis using back-calculated  $p$ - $y$  curves compared to the measured test results. Good agreement between measured and computed responses are observed showing that these back-calculated  $p$ - $y$  curves can reproduce the good estimate of the pile response.

#### 6.2.2.4 1.2-m $p$ - $y$ Curves

The back-calculated  $p$ - $y$  curves of the 1.2-m CIDH pile (No.1) are presented in Figure 6.22. The first portions of  $p$ - $y$  curves (i.e., up to the lateral load of 845 kN) were back-calculated based on the results from lateral load test No.2 while the remaining parts (i.e, from 1059 kN to 1948 kN) were obtained from the results of lateral load test No.4. The reason for not using the data of the lateral load test No.4 to back-calculate the entire  $p$ - $y$  curves is that gapping surrounding pile No.1 was observed before test No.4. This gapping developed during lateral load test No.2 when pile No.1 was served as a reaction to test the 0.9-m pile. Using only the results from lateral load test No.4 would drastically underestimate the soil resistance. The characteristic of the  $p$ - $y$  curves for the 1.2-m pile (No.1) were similar as those observed in the previous other piles. After  $p$ - $y$  curves were back-calculated, an analysis was performed to verify the accuracy of the  $p$ - $y$  curves in predicting the pile response. A comparison between the measured and computed responses using the back-calculated  $p$ - $y$  curves are shown in Figure 6.23 and Figure 6.24, verifying that the back-calculated  $p$ - $y$  curves are reasonable.

Figure 6.25 presents the  $p$ - $y$  curves of the 1.2-m pile (No.2) back-calculated from the results of lateral load test No.4. Excellent agreement between measured and computed responses was observed as presented in Figure 6.26 and Figure 6.27 indicating that these back-calculated  $p$ - $y$  curves provided the decent estimate of the pile response.

### 6.2.3 Comparison of $p$ - $y$ Curves for Different Pile Diameters

A comparison of the  $p$ - $y$  curves from the results of full-scale lateral load tests on various pile diameters provides insight into the effect of pile diameter on the  $p$ - $y$  curves. Figure 6.28 presents a comparison of the  $p$ - $y$  curves of all pile diameters at different depths. It is observed that the back-calculated  $p$ - $y$  curves for all piles are generally similar indicating that the pile diameter has insignificant effect on  $p$ - $y$  curves. The  $p$ - $y$  curves of the 1.2-m (No.2) are in good agreement with those of the 1.2-m (No.1) up to the displacement of approximately 10 mm. Beyond that the  $p$ - $y$  curves of Pile No.1 are stiffer than those of Pile No.2. This is likely because Pile No.2 was located close to the natural slope, and therefore the soil confining pressure which affected the soil resistance at large strain level was less than that of Pile No.1 causing the lower soil resistance.

Similarity of back-calculated  $p$ - $y$  curves for different pile diameters indicates that the pile diameter seems to have an insignificant effect on the  $p$ - $y$  curves for the displacement range of testing. This can be explained by considering the  $p$ - $y$  curves at depth below 0.6 m. The characteristics of back-calculated  $p$ - $y$  curves were somewhat close to the linear elastic case. Results from finite element in the earlier chapter shows that the pile diameter effect is insignificant for the case of linear elastic. For this experimental study, the ratio between the largest to the smallest pile diameters was only 3. Associated with this low ratio, an increase in the soil stiffness due to an increase of the pile diameter based on the finding from the finite element analyses is only 25%. This 25% is relatively very small and likely could not be captured by the full-scale testing where some other factors, such as the inhomogeneity of the soil by its nature, uncertainty in estimating the pile stiffness, some error of the determination of moment of CIDH pile

are more significant and can effect the accuracy of back-calculated  $p$ - $y$  curves. As a result, the back-calculated  $p$ - $y$  curves show that the pile diameter has insignificant effect up to the level of displacement tested.

However, it should be noted that the  $p$ - $y$  curves, back-calculated from the test results, did not reach the ultimate resistance of the soil (i.e. soil resistance seems to increase with the displacement), especially for the smallest diameter because the yield displacement of the pile was controlled by the pile capacity. In general, the ultimate soil capacity increases with the pile diameter because the larger pile mobilized more soil to achieve the ultimate soil resistance resulting in higher soil resistance per unit pile length. At a large displacement, the pile diameter is likely to have some effect but could not be quantified by using strain gauge data to back calculate  $p$ - $y$  curves due to its inconsistency at the displacement beyond the yielding of the pile.

In an attempt to back-calculate the ultimate soil resistance, an envelope of load-displacement curves during cyclic loading was utilized. The ultimate soil pressure of each pile was estimated by extrapolating the final slope of the  $p$ - $y$  curves of each pile to the displacement of  $3D/80$  as used in the standard sand  $p$ - $y$  curves (Reese *et al.* 1974). The soil pressure at this displacement level represents the ultimate soil resistance. In order to verify this assumption of the ultimate soil resistance, these  $p$ - $y$  curves were implemented to predict the load-displacement curves in the inelastic range. Figure 6.29 through Figure 6.33 present a comparison between computed and measured load-displacement curves of various pile diameters. It was found that the envelope of measured load-displacement curves could be well predicted using the  $p$ - $y$  curves with the previous assumed ultimate soil resistance. As a result, the assumption made on the method in estimating the ultimate soil pressure was reasonable.

It is noted that the computed load-displacement curves apparently reached failure much earlier than that the results from the full-scale testing (Figure 6.29 through Figure

6.33). This is likely due to the fact that the soil confinement improved the inelastic performance of the CIDH piles. It achieved this by retarding the spalling of unconfined concrete and hence improved the displacement ductility of the piles. More details on inelastic performance of CIDH pile due to the effect of soil confinement are discussed in the next section.

Since the pile diameter appears to have insignificant effect on the  $p$ - $y$  curves for cemented sand before the soil reaches the ultimate soil resistance, the advantages of increasing the pile diameter size to increase the soil resistance is negligible. However, the benefits can be obtained in many ways as the pile diameter increases: 1) the stiffness as well as the ultimate capacity of the pile increases and therefore decreases the displacement response for a given lateral load, 2) for the construction point of view, it is cost effective compared to small diameter piles with pile cap footing, and 3) using a large diameter pile as the integral pile-shaft column can control the location of the plastic hinge to occur at the column and thus easy to access for the rehabilitation.

### **6.3 Proposed Methodology to Construct $p$ - $y$ Curves for Weakly Cemented Sand**

In this section, a methodology to construct the  $p$ - $y$  curves for weakly cemented sand is proposed. The methodology was developed based on the characteristics of the back-calculated  $p$ - $y$  curves from the experimental results. Figure 6.34 presents the methodology for constructing  $p$ - $y$  curves for weakly cemented sand. Since the back calculated  $p$ - $y$  curves at the same depth indicate that pile diameter has insignificant effect on the  $p$ - $y$  curves, the characteristic of proposed  $p$ - $y$  curves for different pile diameter below the ultimate soil resistance can be represented using a single backbone  $p$ - $y$  curve. The characteristic backbone curve can be estimated using the following expressions

$$p = Cy^{0.5} \quad (6.25)$$

where  $C = 102 * z + 50$ , and  $C \leq 415 \text{ kN/m}^{3/2}$

where,  $p$  = soil resistance per unit pile length in kN/m,  $y$  = soil displacement in mm,  $C$  is depth dependent constant, and  $z$  is depth in meter. It is noted that these expressions are valid only when the suggested units are used. The ultimate soil resistance is determined by adopting a suggestion by Reese *et al.* (1974) in which the soil reaches its ultimate resistance at a displacement of  $3D/80$ .

Figure 6.35 and Figure 6.36 present examples of characteristic shape of the  $p$ - $y$  curves developed based on the proposed methodology. Figure 6.35 shows that the soil resistance increases as the depth increases. Figure 6.36 presents the  $p$ - $y$  curves of different pile diameters, which indicates that the pile diameter has no effect on the  $p$ - $y$  curves below the ultimate soil pressure.

The proposed  $p$ - $y$  curves were verified by implementing them to predict the test results for all pile diameters tested. The  $p$ - $y$  curves were first simplified using the quadruple-linear model in order to incorporate these  $p$ - $y$  curves in a computer program for analyzing lateral pile response, LPILE (Reese *et al.* 2000). Figure 6.37 through Figure 6.40 show that  $p$ - $y$  curves developed based on the proposed methodology can well predict the response of piles under lateral loading for all pile diameters, which indicates the accuracy of proposed  $p$ - $y$  curves for predicting lateral pile response in weakly cemented sand.

#### **6.4 Limitation of Proposed $p$ - $y$ Curves for Design**

Though the earlier section shows that the proposed methodology to construct  $p$ - $y$  curves for weakly cemented sand is simple and reasonable to analyze the pile response for a wide range of pile diameters in weakly cemented, some limitations in implementing this method should be noted. The proposed  $p$ - $y$  curves were developed based on the full-scale test results in weakly cemented sand with the SPT N-values of approximately 40.

Using these  $p$ - $y$  curves for cemented sand material with SPT N-values more than 40 would likely underestimate the soil response. Typical SPT N-Values for cemented sand along the coast of Southern California is often greater than 50, and therefore these  $p$ - $y$  curves are generally conservative for most cases.

In addition, for a case of pile diameter larger than the test pile, extrapolation of proposed  $p$ - $y$  curves may be reasonable, if the pile is long enough that it behaves as a flexible pile (i.e., the lateral response is independent of depth). This is because the derivation of  $p$ - $y$  curves was developed based on that assumption. However, in several cases, particularly for a case of very large pile diameter, the pile length is often relatively short compared to the pile diameter. In this regard, the pile behaves like a rigid pile, where the pile response depends on the pile length. Implementing these  $p$ - $y$  curves for this type of problem is not recommended at this stage due to unavailability of test data on short piles. Further full-scale lateral load tests on short piles are recommended to provide better understanding on the behavior of rigid piles.

## **6.5 Effect of External Confinement from Soil on Bending Behavior**

The test results in earlier chapter shows that even the amount of transverse reinforcement was lower than that suggested by BDS, it can provide sufficient inelastic performance of the CIDH piles with the displacement ductility of more than 5 due to the effect of soil confinement. Furthermore, the previous analyses in section 6.2.3 showed that the numerical soil-pile system model based on the common moment-curvature relationship, which did not account for external pressure from the soil, predicted the failure of the pile much earlier than what observed from the test results. This effect from the soil confinement should be therefore incorporated properly in the analyses in order to yield the reasonable prediction of the inelastic pile response.

In this section, the soil confinement effect was incorporated by using the equivalent amount of transverse reinforcement to represent this effect by increasing the

ultimate curvature of the pile until the computed load-displacement curves using modified moment-curvature relationship matched with the experimental results. An increase in the amount of transverse reinforcement compared to the original amount can be used as an indicator to quantify how much the soil confinement contributes in enhancing the ductility of the pile.

In this study, two piles tested to failure were first considered (i.e., 0.4-m and 0.6-m piles). Figure 6.41 presents the moment-curvature relationship for both piles before and after incorporated the soil confinement effect. The ultimate curvatures of the piles needed to be increased by approximately 1.7 times in order to match the measured responses. Figure 6.42 and Figure 6.43 show a good agreement between the measured and computed load-displacement curves using the modified moment-curvature analysis. It was found that in order to achieve the ultimate curvature ductility as presented in Figure 6.41, the amount of transverse reinforcement for both piles needed to be increased by approximately 100 % from the original amount of 0.6% to 1.3%. This indicates that the effect of the soil confinement for this type of soil was equivalent to the additional 0.7% transverse reinforcement (i.e.,  $1.3\% - 0.6\% = 0.7\%$ ), which relatively high compared to the original amount of transverse reinforcement being used. Neglecting this effect is obviously too conservative in predicting the displacement ductility capacity of the pile.

The analyses were further conducted to predict the inelastic behavior of the 0.9-m and 1.2-m piles, which did not reach the failure during the test due to the limitation of the testing, by using the equivalent transverse reinforcement of 0.7% to model the soil confinement. Figure 6.44 shows the modified moment-curvature relationship, which incorporated the effect of soil confinement together with the unmodified moment-curvature relationship. Figure 6.45 through Figure 6.46 shows the predicted response using the modified moment-curvature curves with the experimental test results. It was found that the displacement ductility at the failure of the 0.9-m and 1.2-m (No.1) piles were more than 7.

The analyses show that the soil confinement can enhance the inelastic behavior of the CIDH piles by increasing its curvature ductility due to the effect of soil confinement. The confinement from dense weakly cemented sand considered in this test could be considered as the equivalent transverse reinforcement ratio of 0.7%. For other types of soils, this effect will be different depending on their strength characteristics. The softer the soil is, the lower the amount of equivalent transverse reinforcement from the soil confinement. For extremely soft soil such as liquefied soil or very soft clay, the effect of soil confinement is likely to be insignificant and therefore the relationship between soil strength and equivalent amount of transverse reinforcement can be plotted as shown in Figure 6.47. Further full-scale experiment should be considered for evaluation of this effect on other different soil types to determine the relationship of the amount of equivalent transverse reinforcement with the soil strength. Implementation of this finding into design should be done carefully due to the limitation of data available at this current stage.

## **6.6 Commentary on Effect of External Confinement from Soil on Shear Capacity of CIDH Pile**

In general, traditional analyses of laterally loaded CIDH piles show that a large shear demand develops below the plastic hinge region. This is particularly true in stiff soils, where the maximum moment that forms the plastic hinge rapidly drops to zero. Associated with this rapid drop in moment is a high shear demand below the plastic hinge. Using current Caltrans design methodology, this high shear demand results in increased spiral reinforcement in the CIDH pile to a depth of several pile diameters. This increase in reinforcement not only increases construction cost, but adversely affects the constructability of the pile, with the additional reinforcement preventing uniform flow of wet concrete.

The current methodology neglects any contribution to the shear capacity of the CIDH pile from the surrounding soil. The soil contribution can be significant, especially

in stiff soils where the shear demand is the highest. Figure 6.48 shows the results from a lateral load test of a 0.6-m diameter CIDH pile. Figure 6.48a shows the moment distribution in the pile using back-calculated  $p$ - $y$  curves from the test data. Figure 6.48b shows the strain in the longitudinal reinforcement, showing the yielding of the reinforcement in the plastic hinge region. Figure 6.48c shows the shear demand calculated from the moment distribution, indicating a large shear demand just below the plastic hinge. However, the development of this high shear is not indicated from the strain on the transverse reinforcement because the shear capacity of the pile is much greater than the shear force applied to the pile. It should be noted that the pile was intentionally designed to fail by the bending mode by ensuring that the shear capacity of the pile was larger than the shear demand. Figure 6.49 shows a comparison of shear force that the pile experienced during the testing with the shear capacity of the CIDH pile provided by the contributions of concrete and transverse reinforcing steel. Theoretical shear strength using an approach of Priestley *et al.* (1996) in case of no axial load is given by

$$V_d = V_c + V_s \quad (6.26)$$

$$V_c = k\sqrt{f'_c} (0.8A_{gross}) \quad (6.27)$$

$$V_s = \frac{\pi}{2} \frac{A_h f_{yh} D'}{s} \cot \theta \quad (6.28)$$

where  $V_d$  is ideal shear strength,  $V_c$  is concrete shear-resisting mechanism,  $V_s$  is transverse reinforcement shear resisting mechanism,  $k$  depends on the member displacement ductility,  $\mu$ , reducing from 0.29 MPa for  $\mu \leq 2$  to 0.05 for  $\mu > 8$ ,  $A_{gross}$  is cross section area,  $D'$  is the core dimension,  $\theta = 30^\circ$ ,  $A_h$  is area of transverse bar, and  $f_{yh}$  is yield strength of transverse bar.

It is clearly seen that the shear force that the pile experienced is lower than the shear capacity provided by the concrete. As a result, the contribution of shear capacity

provided from the transverse reinforcement is insignificant since the transverse steel did not started to mobilize as indicated by the small strain in the transverse reinforcement.

However, the test results on the inelastic behavior of CIDH piles in the earlier section show that the soil contribution is significant in enhancing the bending behavior of CIDH piles. This soil confinement effect is expected to improve the shear capacity of the pile, as well by retarding the spalling of the concrete at location where the shear demand is the highest. Therefore, research on this area should be further investigated. In the research, the test pile should be designed to fail under shear by ensuring the bending capacity of the pile is greater than the shear capacity. The test pile should be extensively instrumented with the strain gauges on both vertical and transverse reinforcements to evaluate the effect of soil confinement in enhancing the shear capacity of the piles. The expected benefit is design recommendations for reduced shear reinforcement in CIDH piles resulted in decreased construction costs.

## **6.7 Summary**

A comparison between the measured and computed natural frequencies based on three different concepts of initial modulus of subgrade reaction showed that the pile diameter appears to have insignificant effect on initial modulus of subgrade reaction. Damping ratios of the soil-pile system at small strain estimated using the expression proposed by Gazetas (1991) yielded the conservative values when compared to the measured values obtained from the vibration testing.

The  $p$ - $y$  curves back-calculated from the results of lateral pile load tests in weakly cemented sand revealed that some soil resistance was observed at the ground surface likely due to the cohesion of the soil. This is different from the characteristic of  $p$ - $y$  curves for clean sand as proposed by Reese *et al.* 1974 and API 1987 where there is no soil resistance at the ground surface due to the lack of soil confinement. A comparison of back-calculated  $p$ - $y$  curves for different pile diameters indicated that pile diameter has

insignificant effect on the  $p$ - $y$  curves before the soil reaches its ultimate resistance. Results from additional analyses to predict the pile response in the inelastic range shows that the ultimate soil pressure increases as the pile diameter increases.

Based on the characteristic of back-calculated  $p$ - $y$  curves, the methodology to construct the  $p$ - $y$  curves for weakly cemented soil tested at the test site was proposed. The  $p$ - $y$  curves of various pile diameters can be represented by using a single backbone curve with varying the ultimate soil pressure with the diameter. The ultimate soil resistance was estimated using the soil pressure at the displacement of  $3D/80$  as suggested by Reese *et al.* (1974). Good agreement between measured and computed pile response using the proposed  $p$ - $y$  curves validated the use of proposed  $p$ - $y$  curves to predict the lateral pile responses. The proposed  $p$ - $y$  curves provided in this study were however appropriate for the weakly cemented soil with the SPT N-values of greater than 40.

The effect of external confinement from soil was evaluated by increasing the curvature ductility of the moment-curvature relationship until the predicted lateral pile response matched with the actual pile behavior measured during the testing. Analyses showed that the effect of soil confinement for dense weakly cemented soil was equivalent to an additional amount of transverse reinforcement of 0.7%, which was greater than the amount of transverse reinforcement of 0.6% being used in the tested piles. Neglecting soil confinement effect appears to be too conservative in estimate the inelastic pile performance.

Table 6.1 Summary of Pile and Soil Properties Used in Natural Frequency Computation for Simple Two-Layer Soil System

Pile Diameter (m)	Pile Flexural Rigidity $E_p I_p$ (MN-m <sup>2</sup> )	Soil Spring Stiffness, $K_s$ (MN/m)					
		Based on $K_{ind}$ Concept		Based on $K_{dep}$ Concept		Based on $K_{fin}$ Concept	
		1 <sup>st</sup> layer	2 <sup>nd</sup> layer	1 <sup>st</sup> layer	2 <sup>nd</sup> layer	1 <sup>st</sup> layer	2 <sup>nd</sup> layer
0.4	40	83	288	33	115	24	82
0.6	238	"	"	50	173	28	96
0.9	1,217	"	"	75	259	32	111
1.2	3,530	"	"	100	346	35	123

Table 6.2 Summary of Measured and Computed Natural Frequency for Simple 2-Layer System

Pile Diameter (m)	Additional Mass	Natural Frequency (Hz)				Ratio of Computed to Measured Natural Frequency		
		Computed			Measured	$K_{dep}$	$K_{ind}$	$K_{fin}$
		$K_{dep}$	$K_{ind}$	$K_{fin}$				
0.4	No	11.3	13.6	12.8	13.6	0.84	1.01	0.94
	Yes	10.9	13.0	12.2	12.5	0.87	1.04	0.98
0.6	No	16.3	18.2	17.5	18.1	0.90	1.01	0.97
0.9	Yes	25.5	26.2	25.9	25.9	0.99	1.01	1.00
1.2 (No.1)	No	36.1	34.0	35.7	34.5	1.05	0.99	1.04
	Yes	35.2	33.2	33.9	33.5	1.05	0.99	1.01
1.2 (No.2)	No	33.9	32.0	32.7	32.4	1.05	0.99	1.01
	Yes	33.1	31.3	31.9	32.1	1.03	0.98	1.00

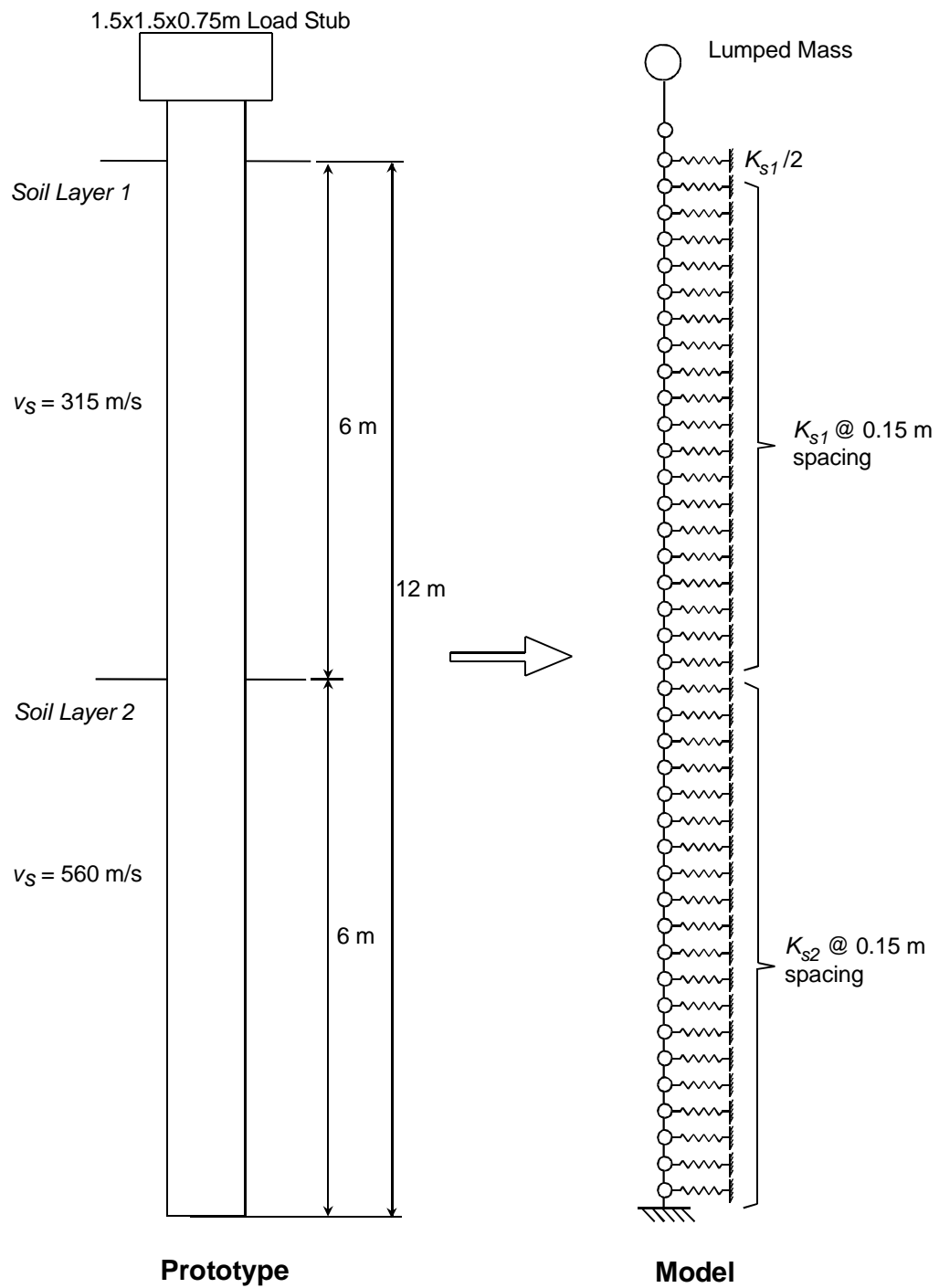


Figure 6.1 Numerical Soil-Pile System Model for Simple Two-Layer System

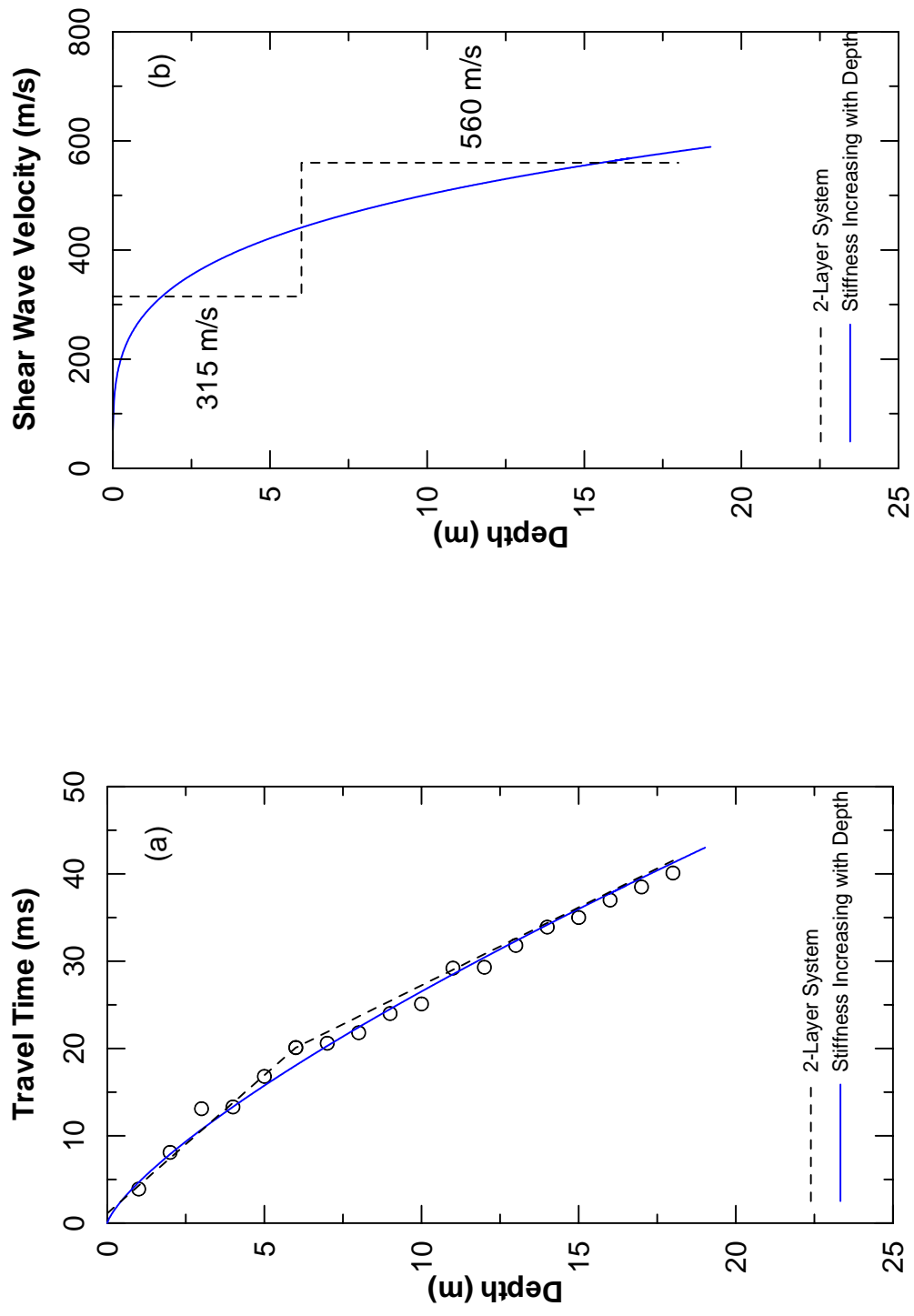


Figure 6.2 Determination of Shear Wave Velocity Profile (a) Travel Time Plot and (b) Shear Wave Velocity

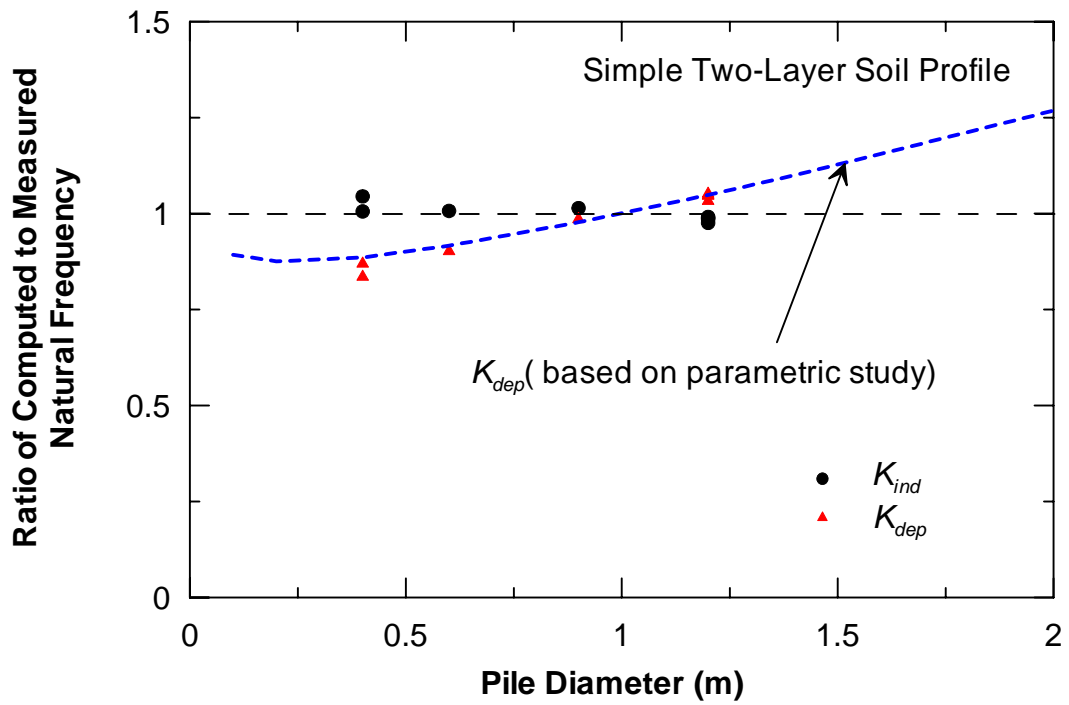


Figure 6.3 Ratio of Computed to Measure Natural Frequency vs. Pile Diameter for Simple Two-Layer Soil Profile ( $K_{ind}$  vs.  $K_{dep}$ )

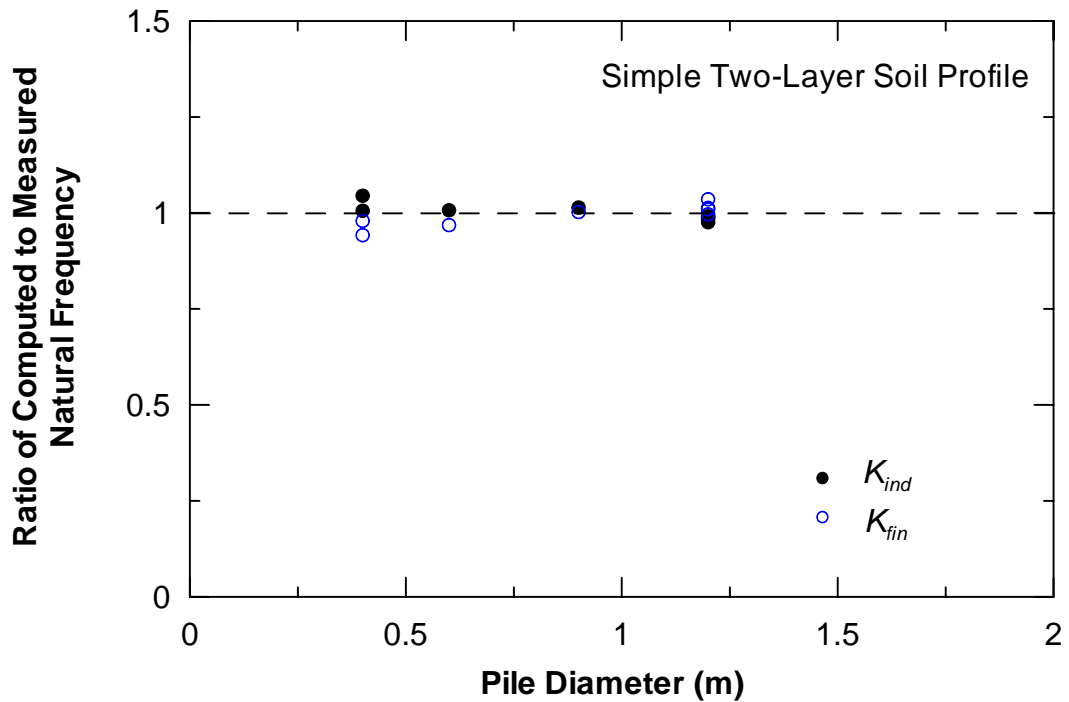


Figure 6.4 Ratio of Computed to Measure Natural Frequency vs. Pile Diameter for Simple Two-Layer Soil Profile ( $K_{ind}$  vs.  $K_{fin}$ )

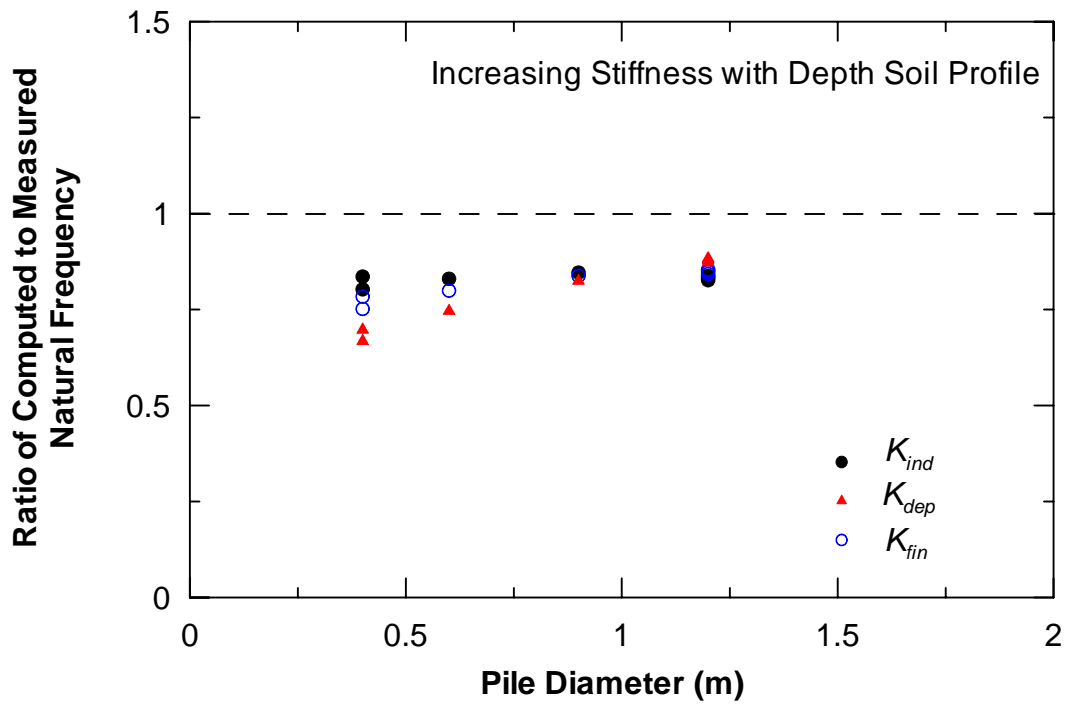


Figure 6.5 Ratio of Computed to Measure Natural Frequency vs. Pile Diameter for Increasing Stiffness with Depth Soil Profile

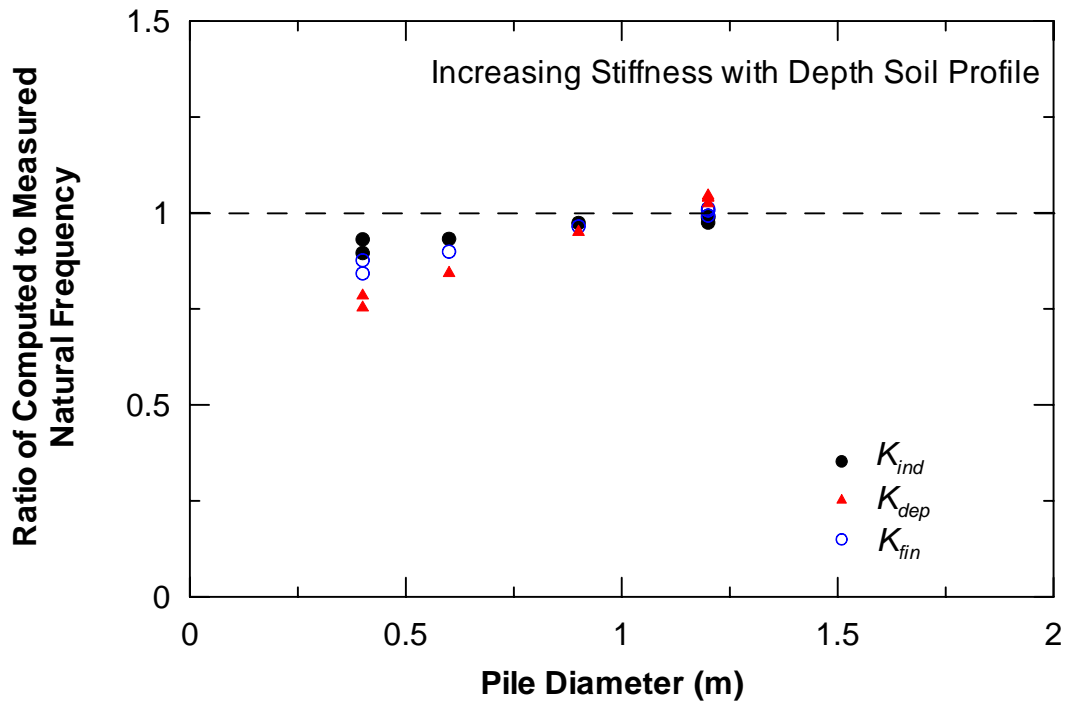


Figure 6.6 Ratio of Computed to Measure Natural Frequency vs. Pile Diameter for Increasing Stiffness with Depth Soil Profile (After increasing soil spring stiffnesses)

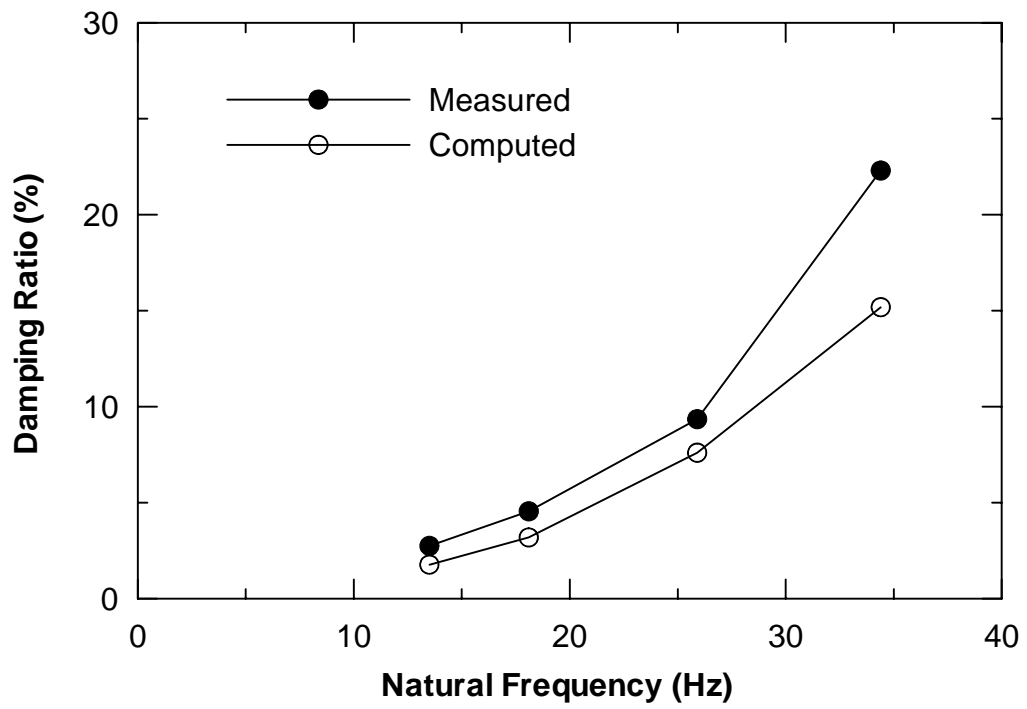


Figure 6.7 Comparison of Measured and Computed Damping Ratios

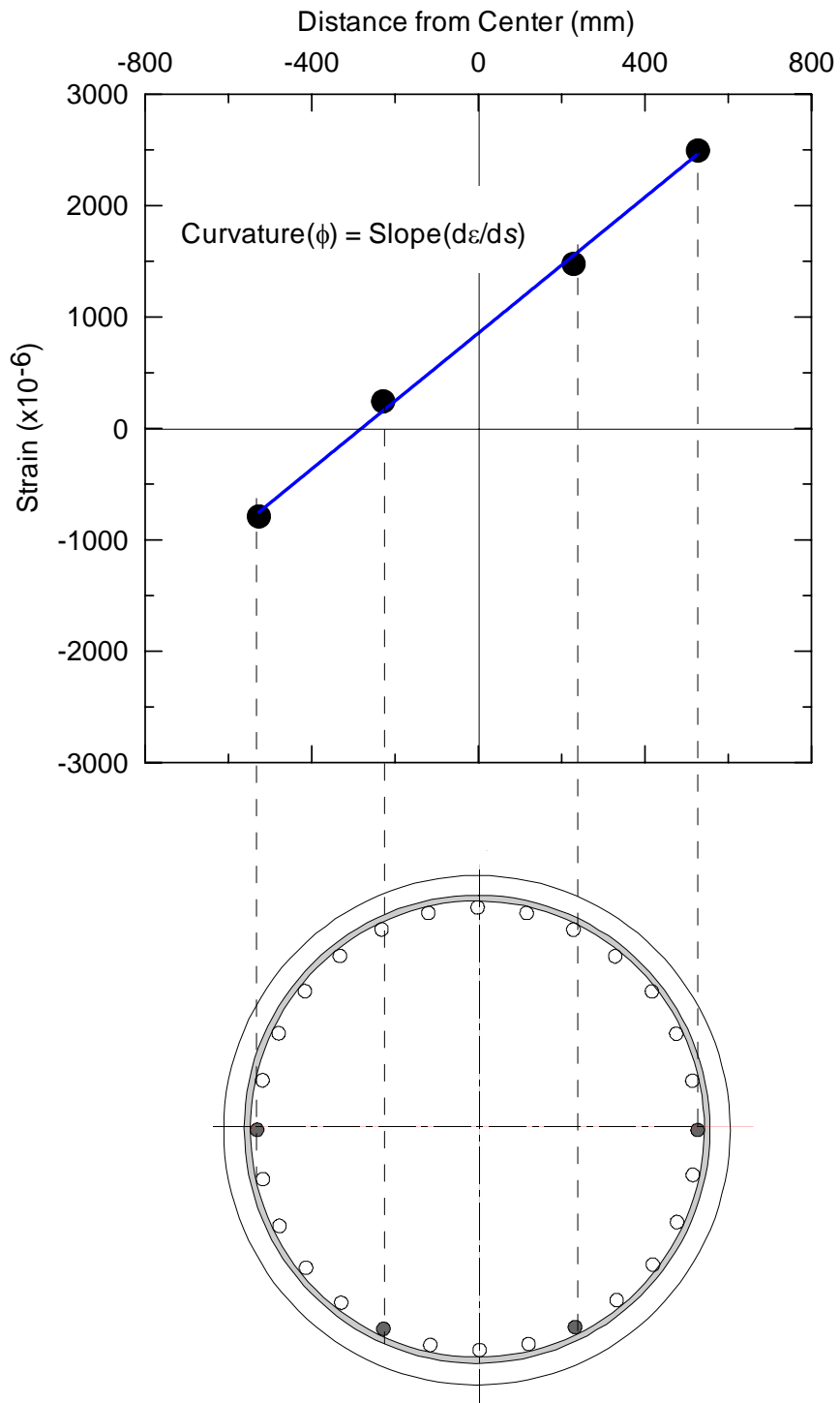


Figure 6.8 Example of Curvature Calculation from Strain Gauge Data (Extracted Data from 1.2-m CIDH Pile (No-1))

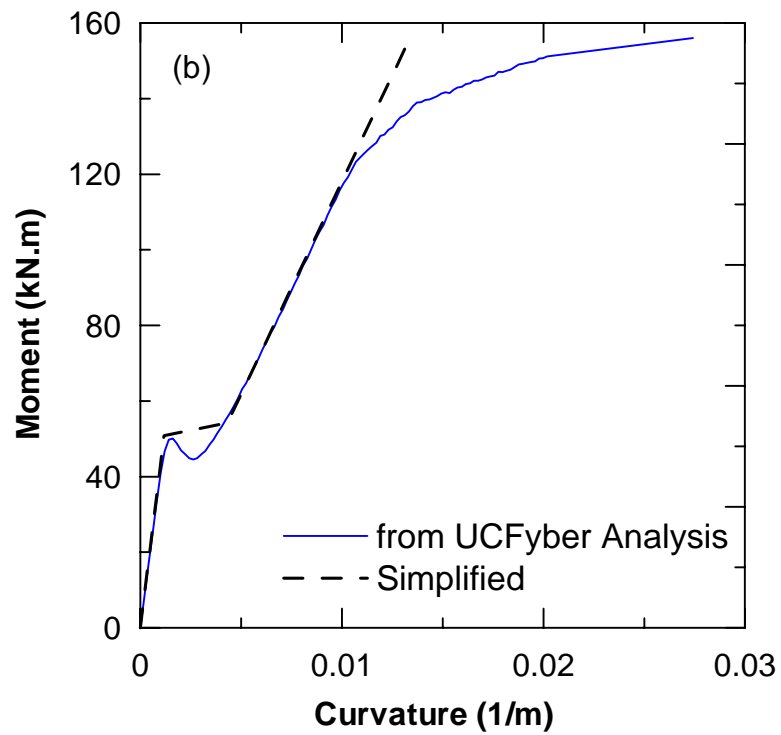
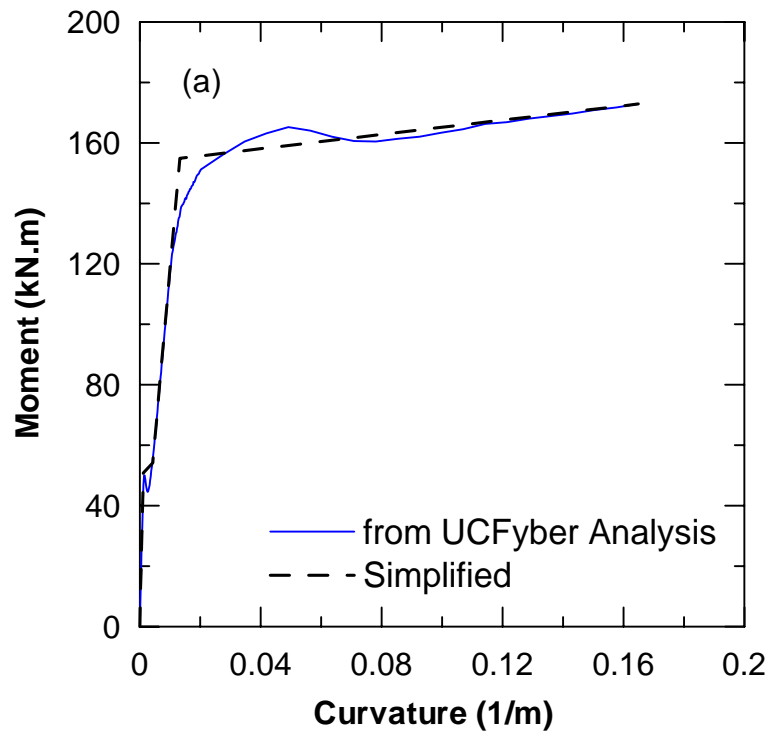


Figure 6.9 Moment-Curvature Relationships for 0.4-m CIDH Pile (a) Entire Curve, and (b) Before Yielding

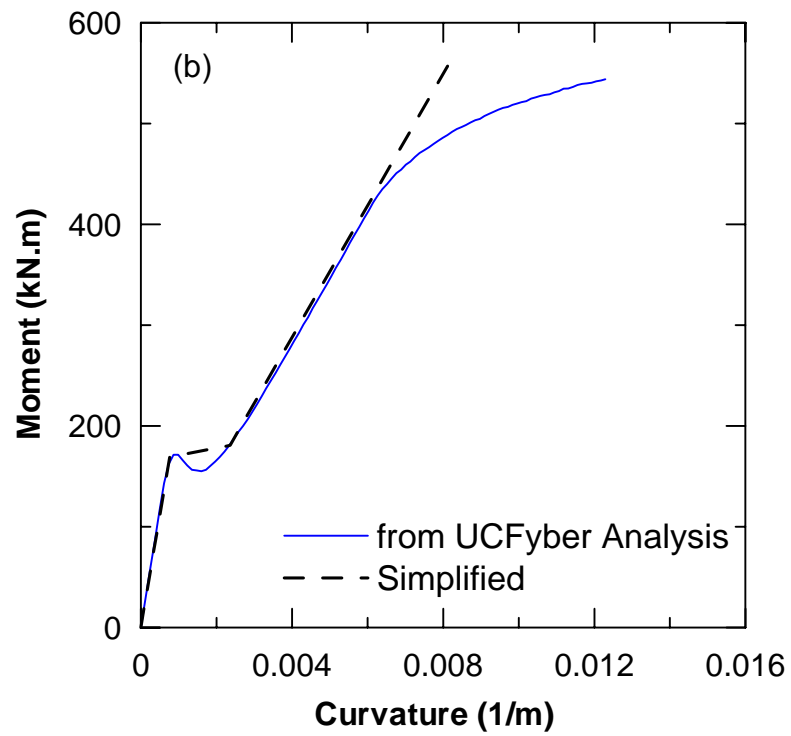
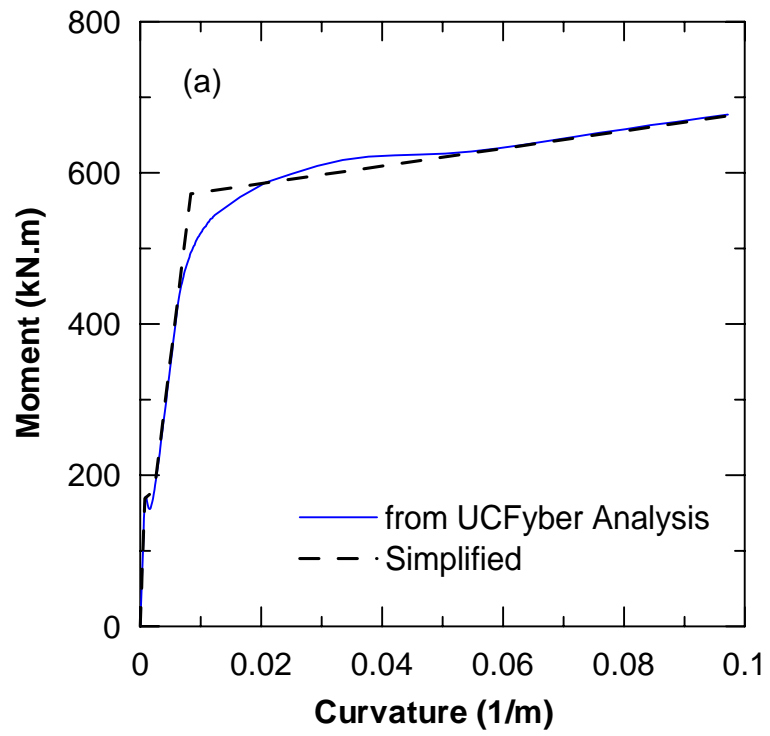


Figure 6.10 Moment-Curvature Relationships for 0.6-m CIDH Pile (a) Entire Curve, and (b) Before Yielding

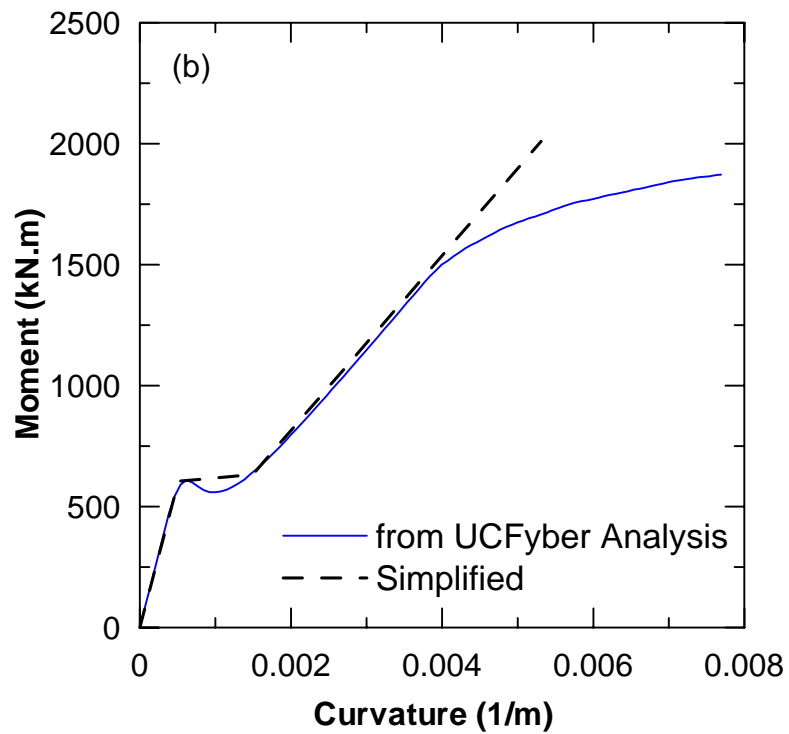
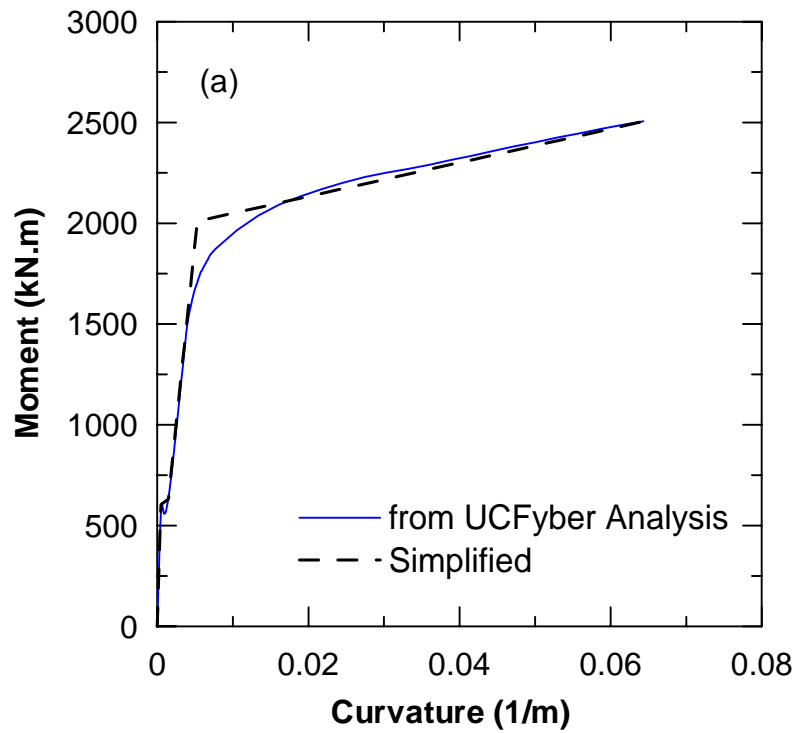


Figure 6.11 Moment-Curvature Relationships for 0.9-m CIDH Pile (a) Entire Curve, and (b) Before Yielding

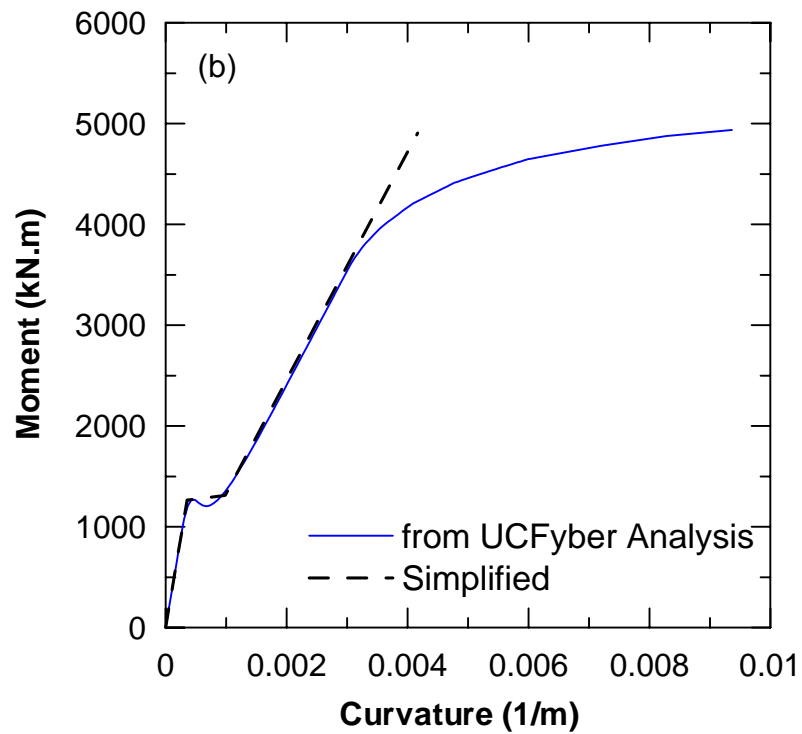
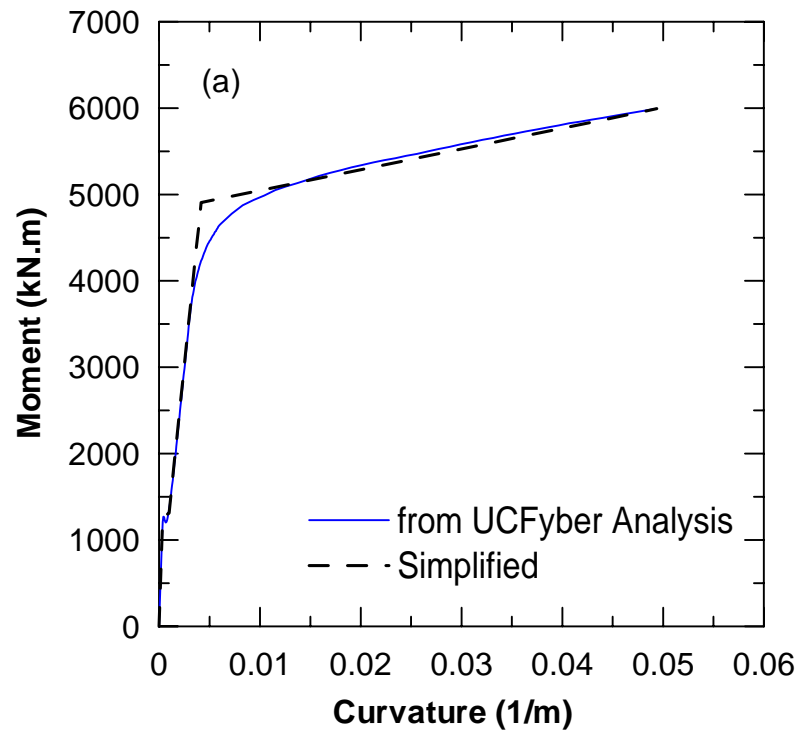


Figure 6.12 Moment-Curvature Relationships for 1.2-m CIDH Pile (a) Entire Curve, and (b) Before Yielding

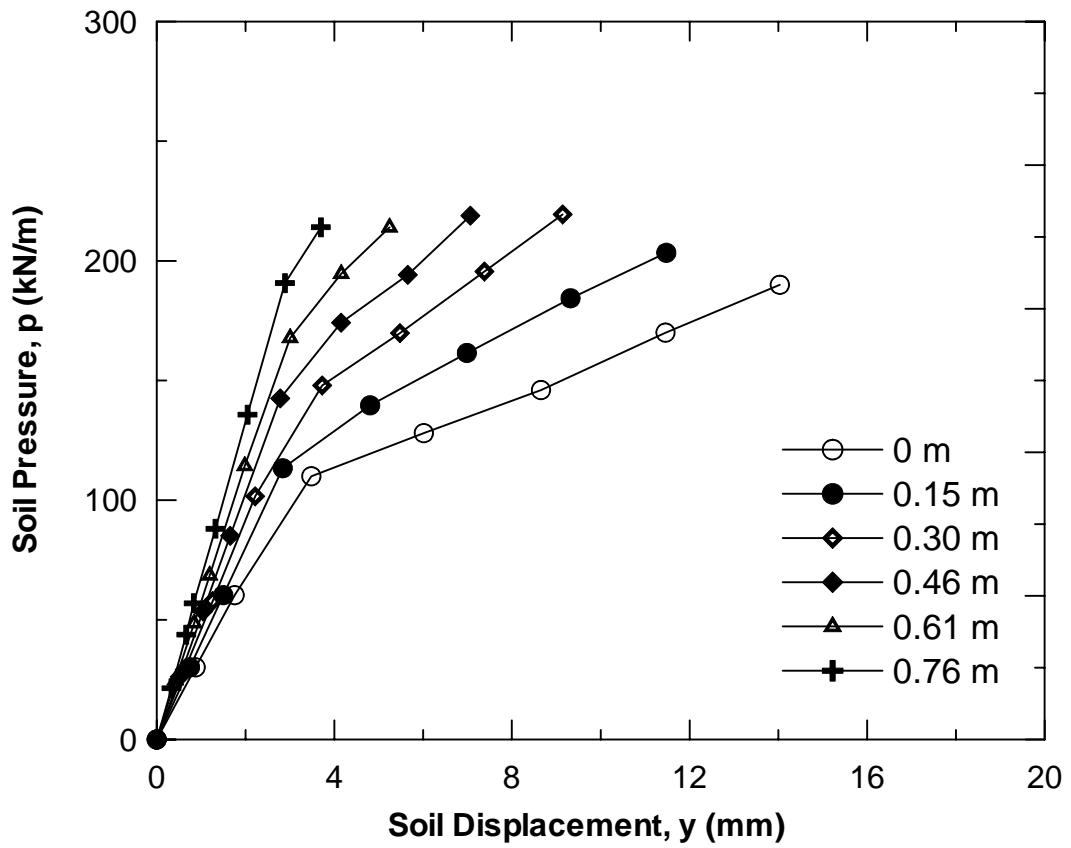


Figure 6.13 Back-Calculated  $p$ - $y$  Curves for 0.4-m CIDH Pile

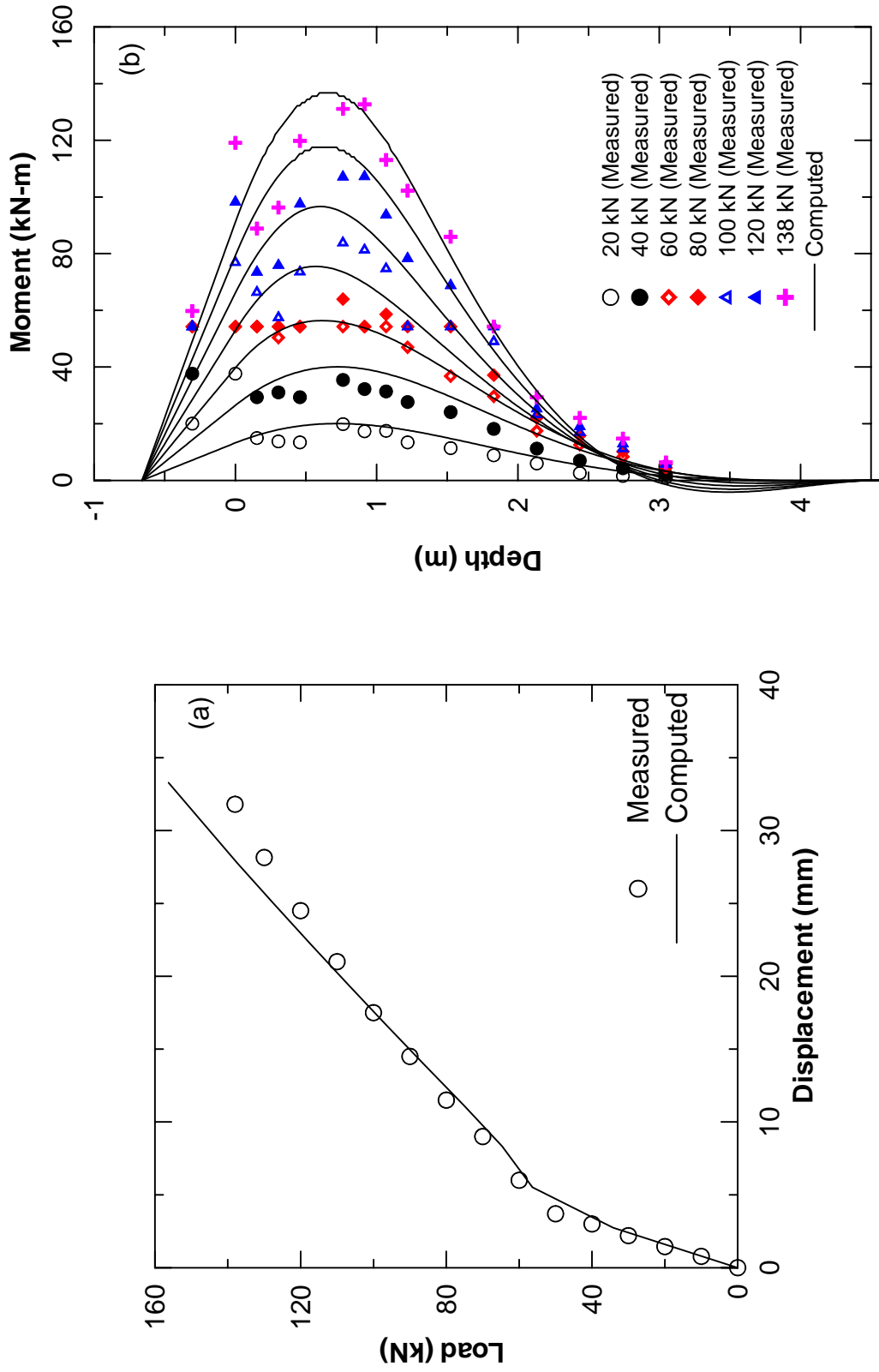


Figure 6.14 Comparison of Test Results and Analysis Using Back-Calculated  $p$ - $y$  Curves for 0.4-m CIDH Pile (a) Load-Displacement Curve, and (b) Moment Profiles

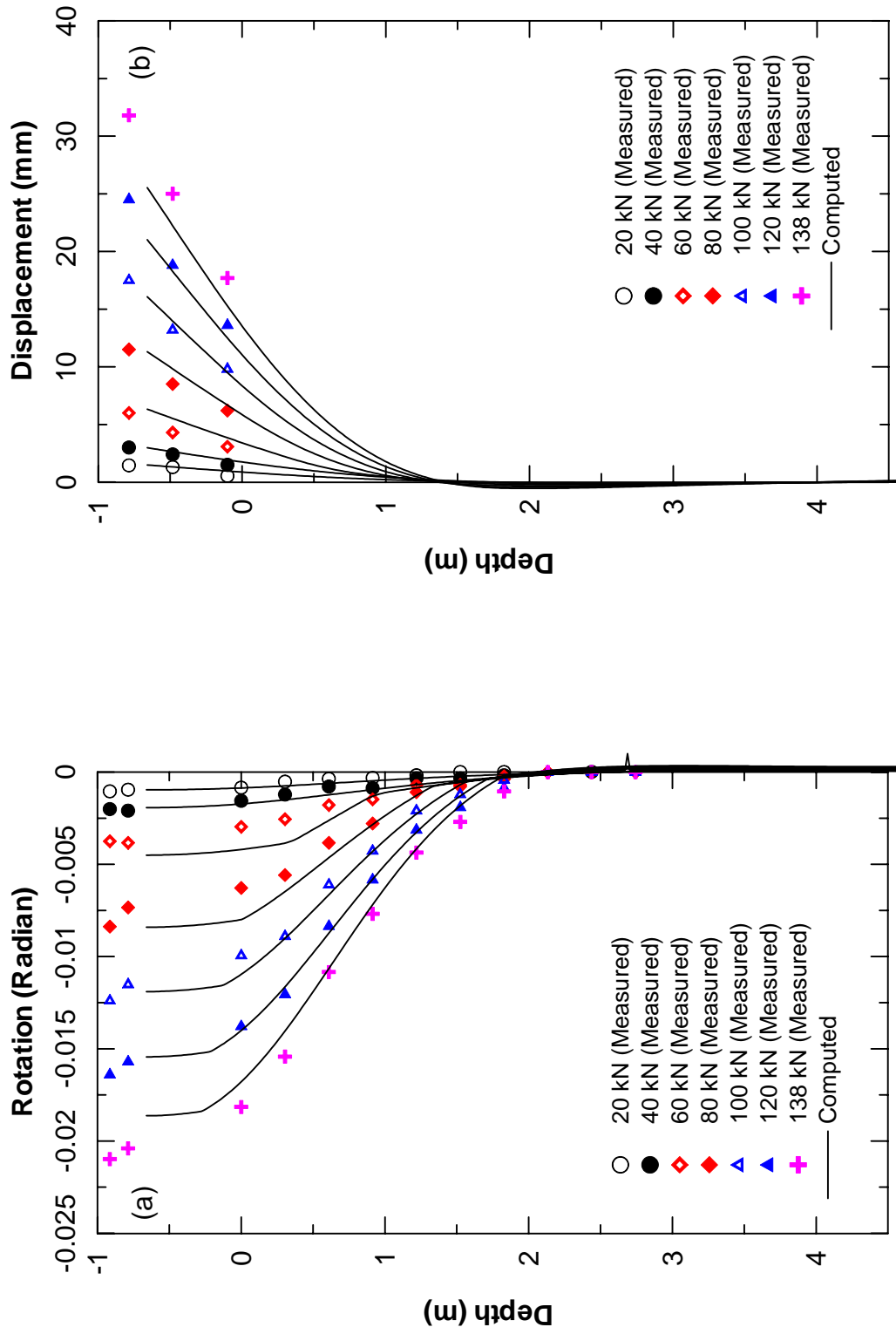


Figure 6.15 Comparison of Test Results and Analysis Using Back-Calculated  $p$ - $y$  Curves for 0.4-m CIDH Pile (a) Rotation Profiles, and (b) Displacement Profiles

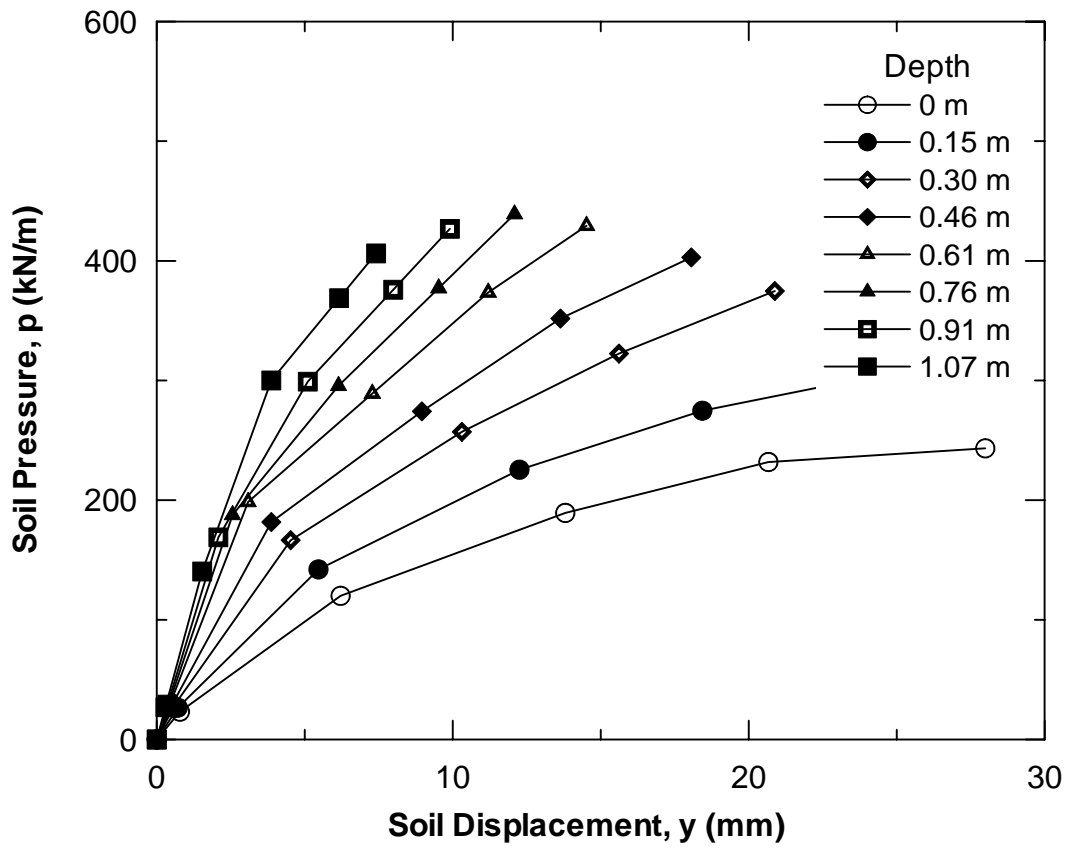


Figure 6.16 Back-Calculated  $p$ - $y$  Curves for 0.6-m CIDH Pile

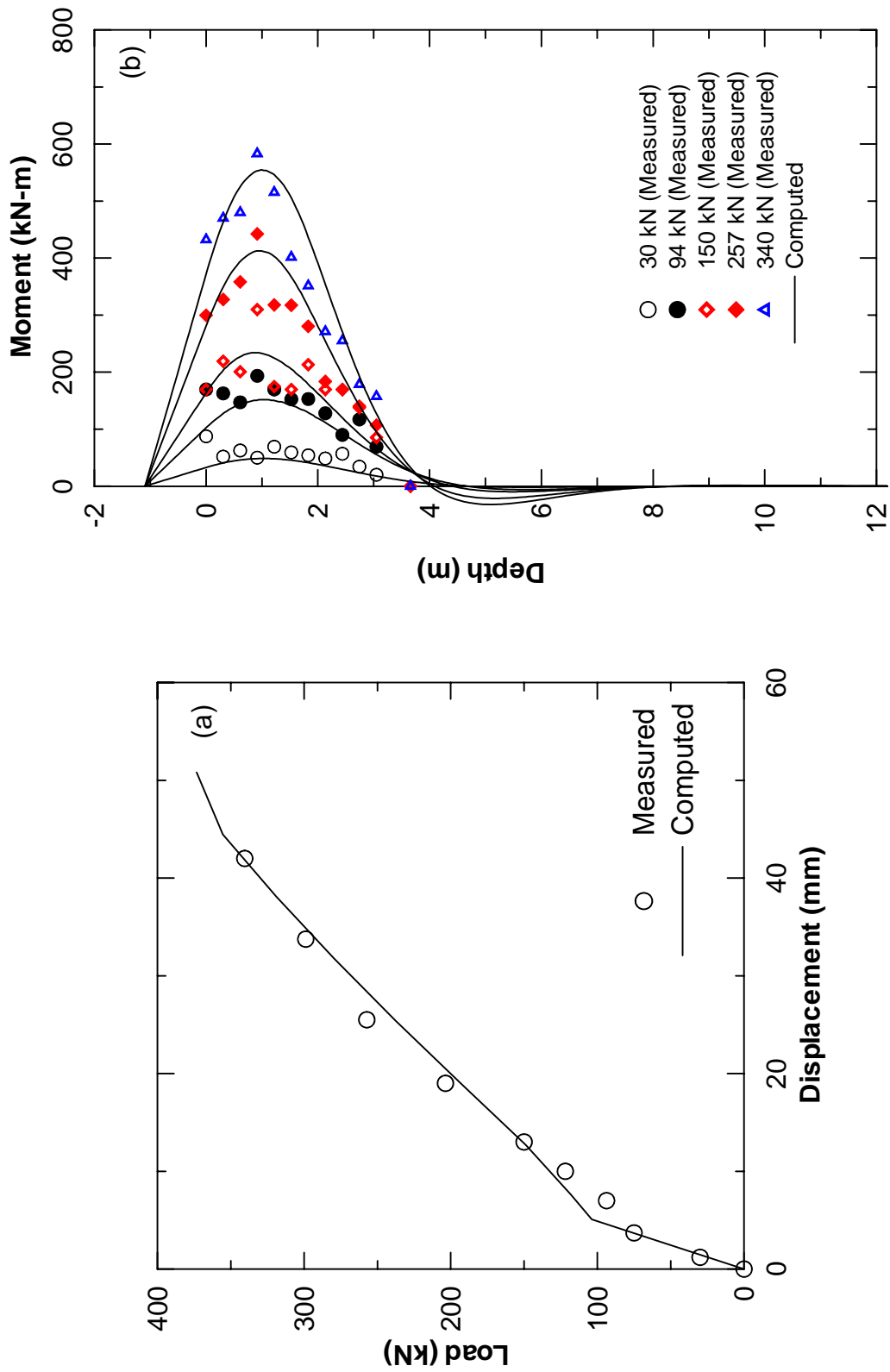


Figure 6.17 Comparison of Test Results and Analysis Using Back-Calculated  $p$ - $y$  Curves for 0.6-m CIDH Pile (a) Load-Displacement Curve, and (b) Moment Profiles

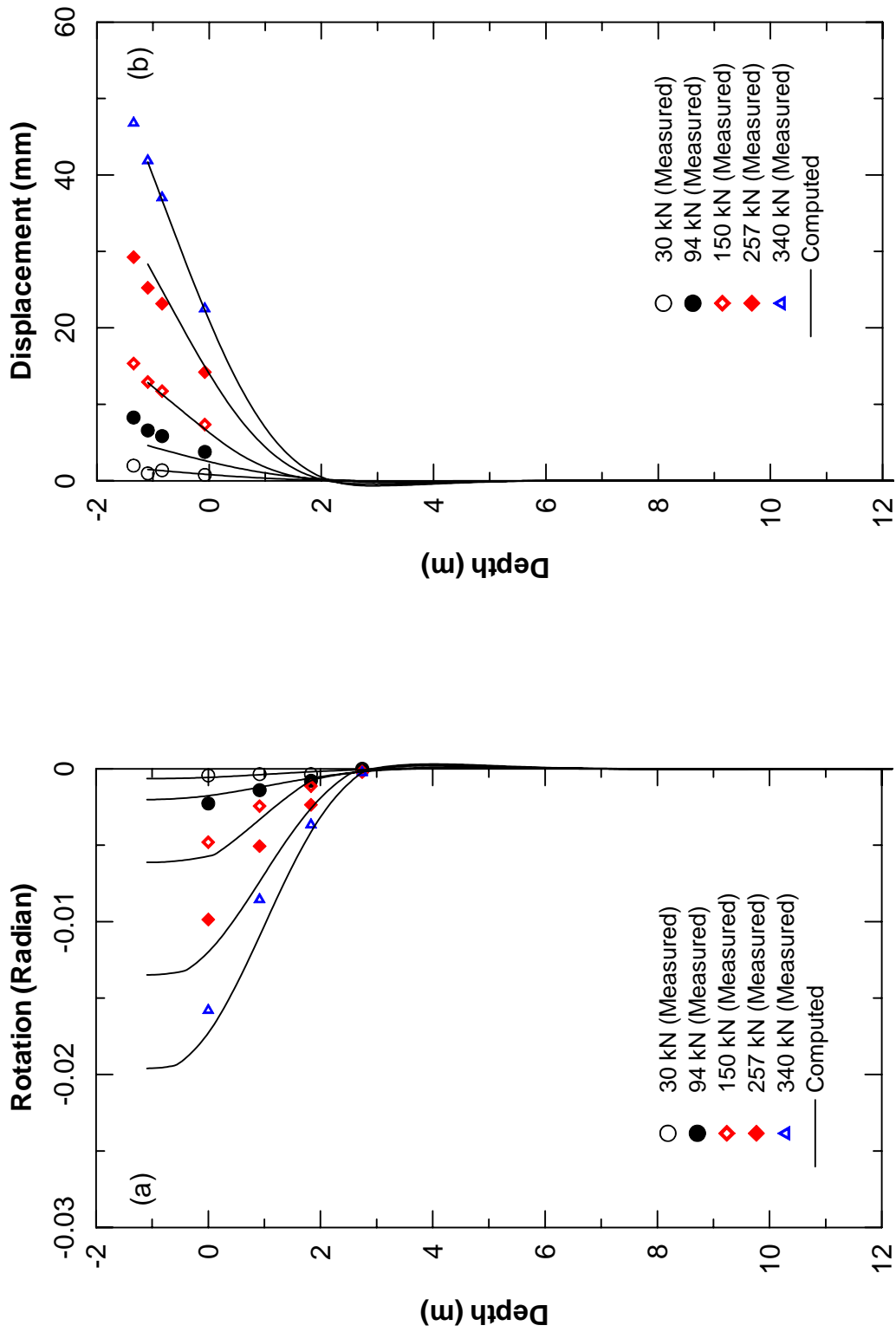


Figure 6.18 Comparison of Test Results and Analysis Using Back-Calculated  $p$ - $y$  Curves for 0.6-m CIDH Pile (a) Rotation Profiles, and (b) Displacement Profiles

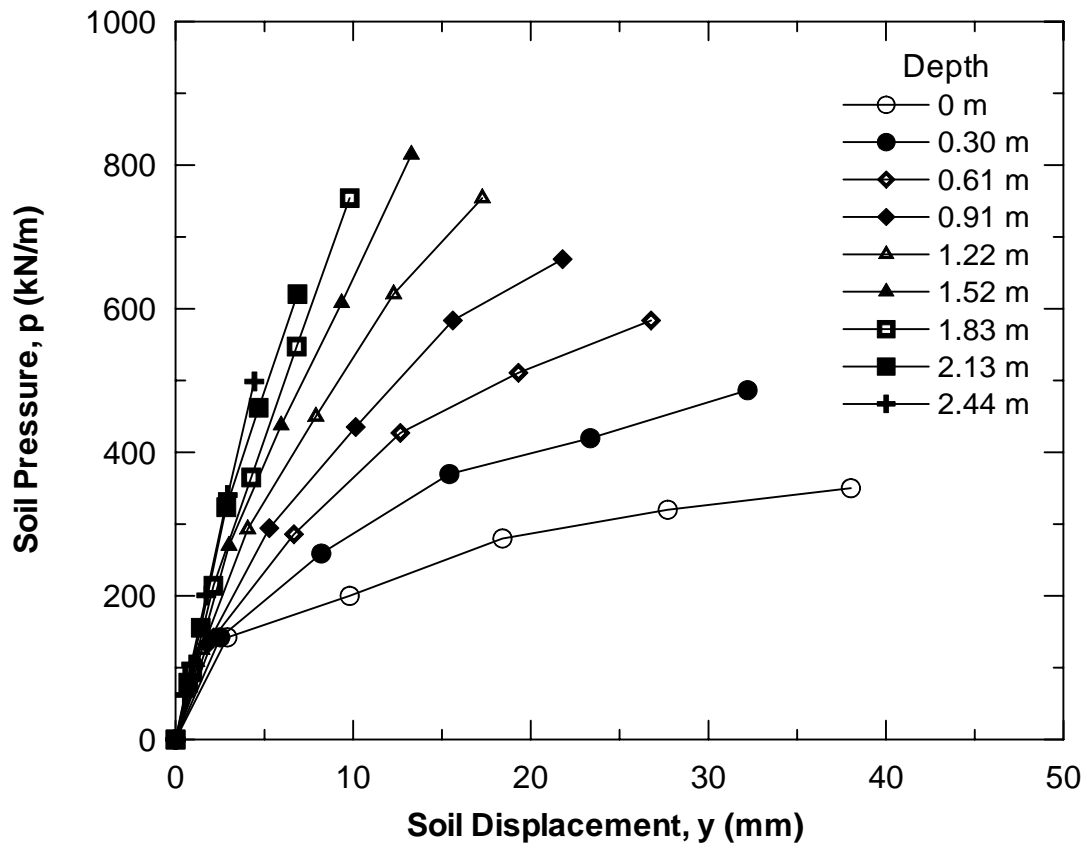


Figure 6.19 Back-Calculated  $p$ - $y$  Curves for 0.9-m CIDH Pile

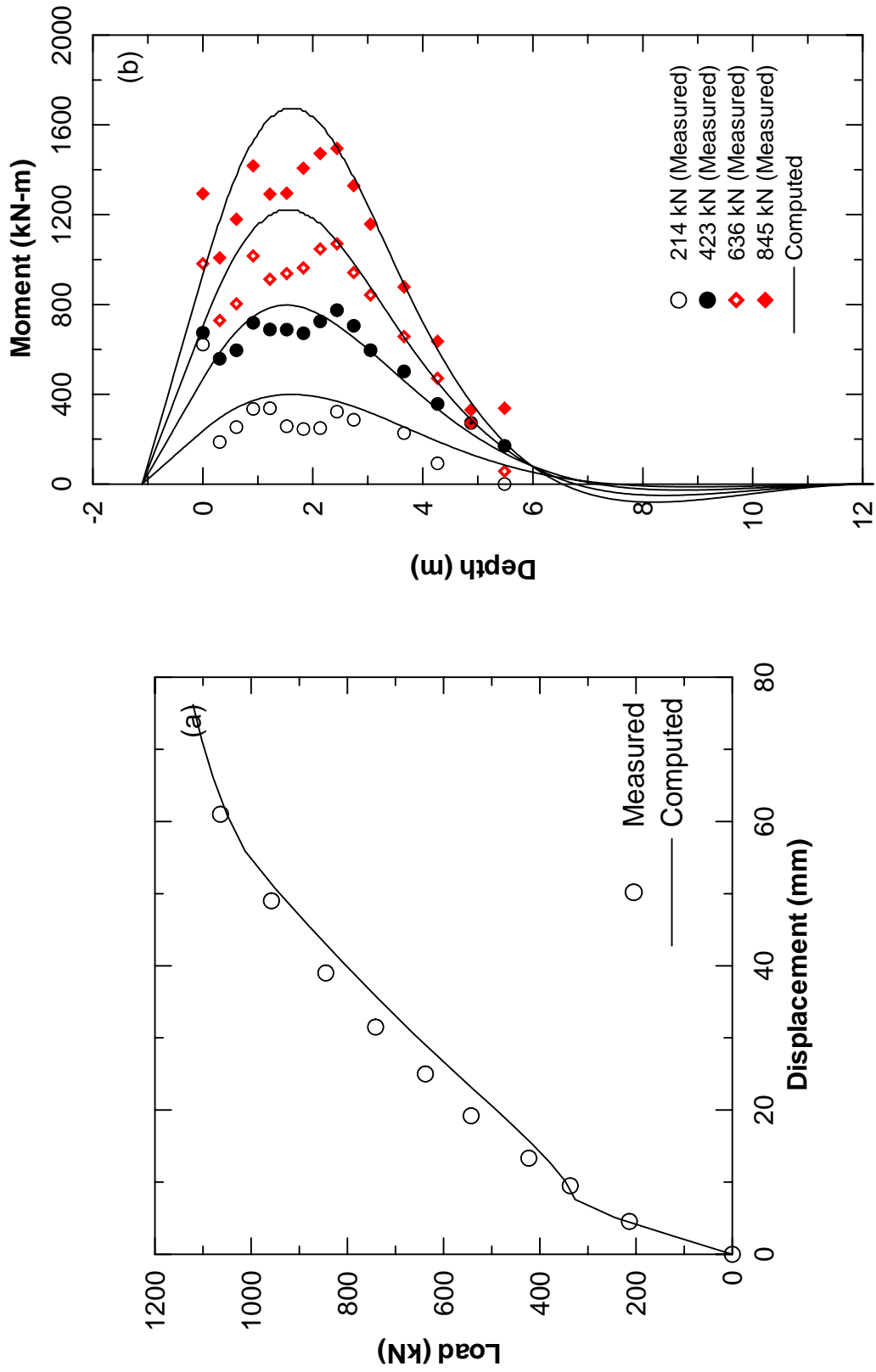


Figure 6.20 Comparison of Test Results and Analysis Using Back-Calculated  $p$ - $y$  Curves for 0.9-m CIDH Pile (a) Load-Displacement Curve, and (b) Moment Profiles

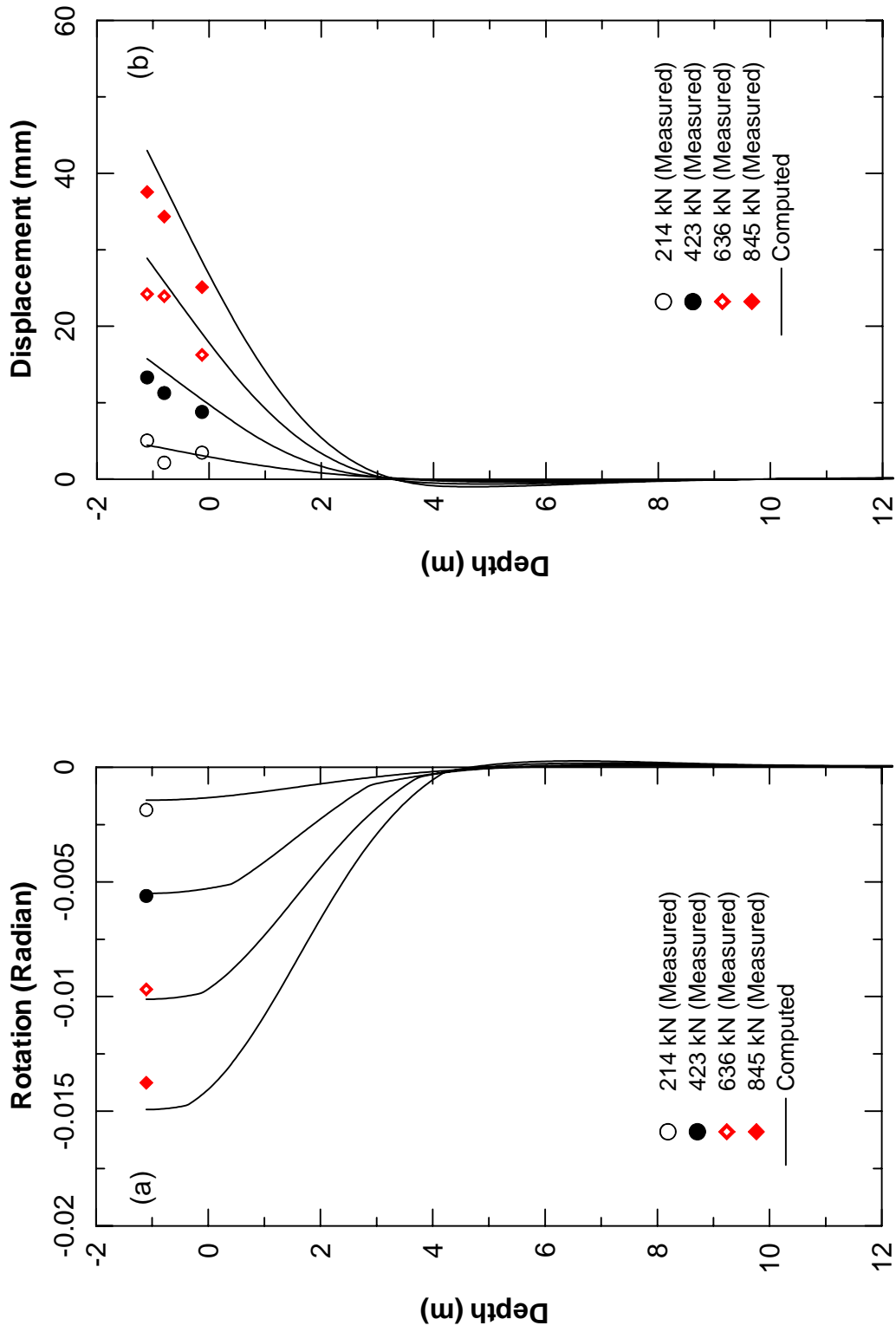


Figure 6.21 Comparison of Test Results and Analysis Using Back-Calculated  $p$ - $y$  Curves for 0.9-m CIDH Pile (a) Rotation Profiles, and (b) Displacement Profiles

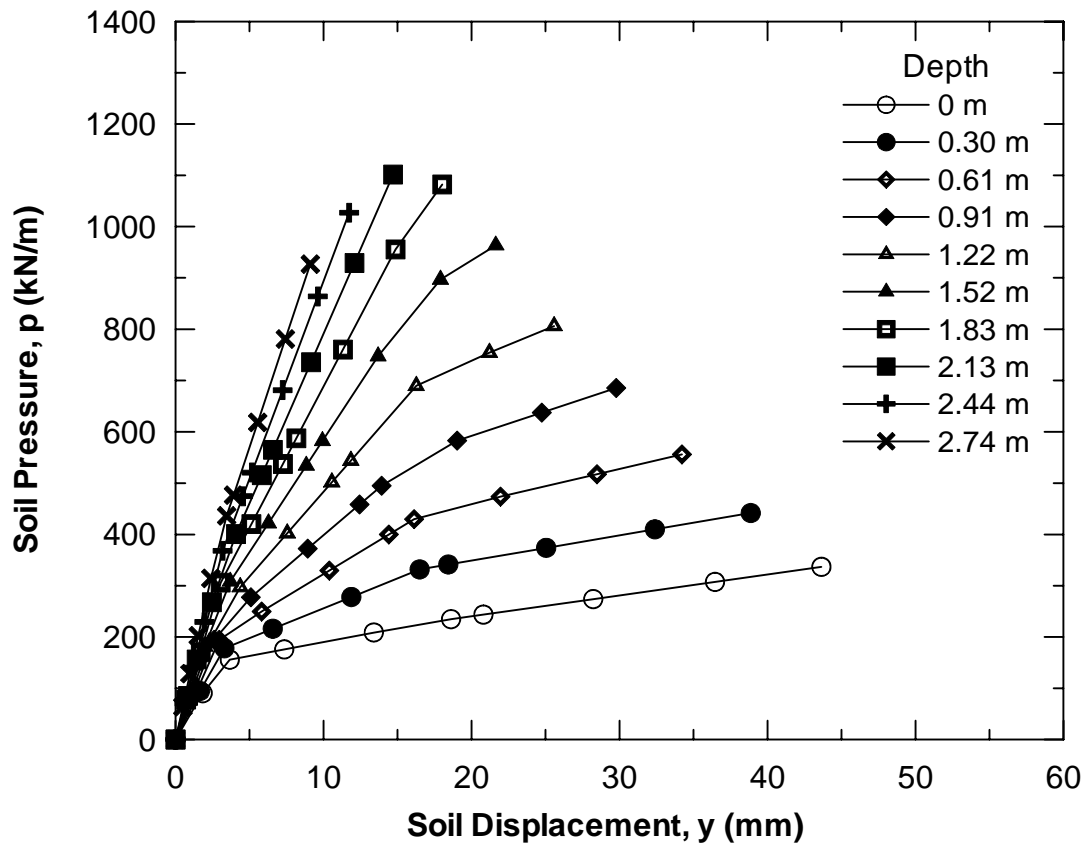


Figure 6.22 Back-Calculated  $p$ - $y$  Curves for 1.2-m CIDH Pile (No.1)

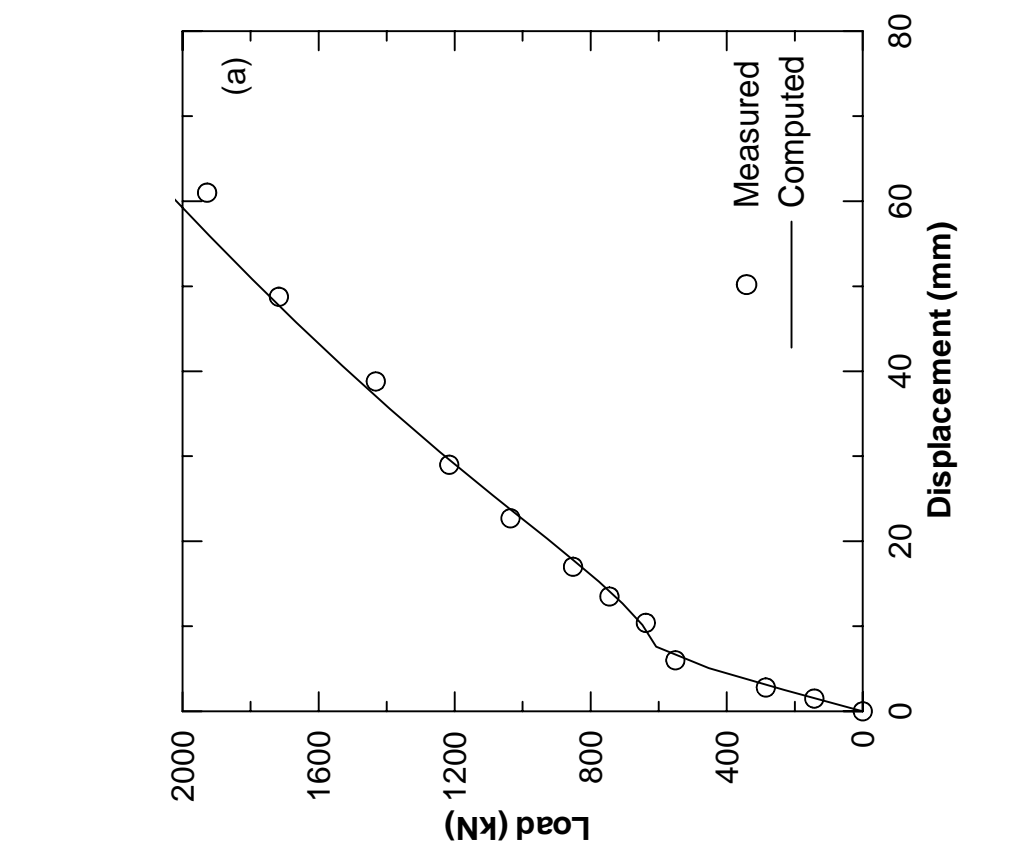
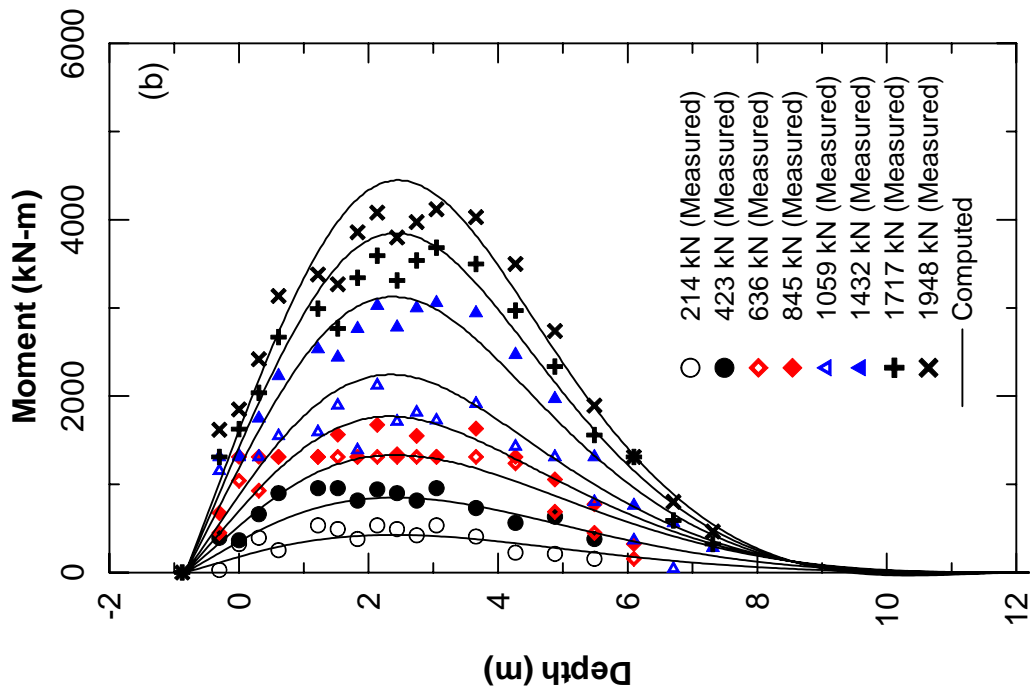


Figure 6.23 Comparison of Test Results and Analysis Using Back-Calculated  $p$ - $y$  Curves for 1.2-m CIDH Pile (No.1) (a) Load-Displacement Curve, and (b) Moment Profiles

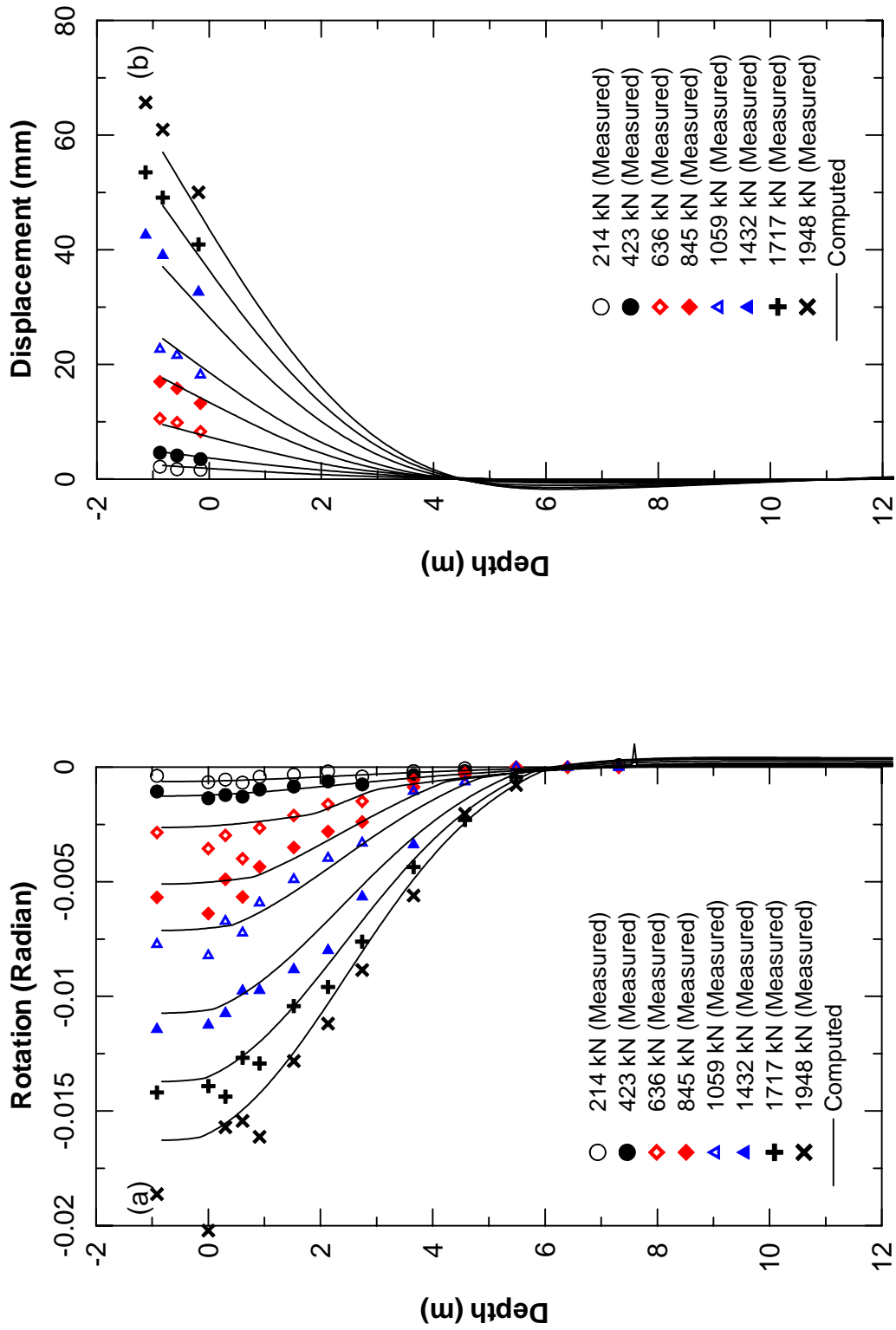


Figure 6.24 Comparison of Test Results and Analysis Using Back-Calculated  $p$ - $y$  Curves for 1.2-m CIDH Pile (No.1) (a) Rotation Profiles, and (b) Displacement Profiles

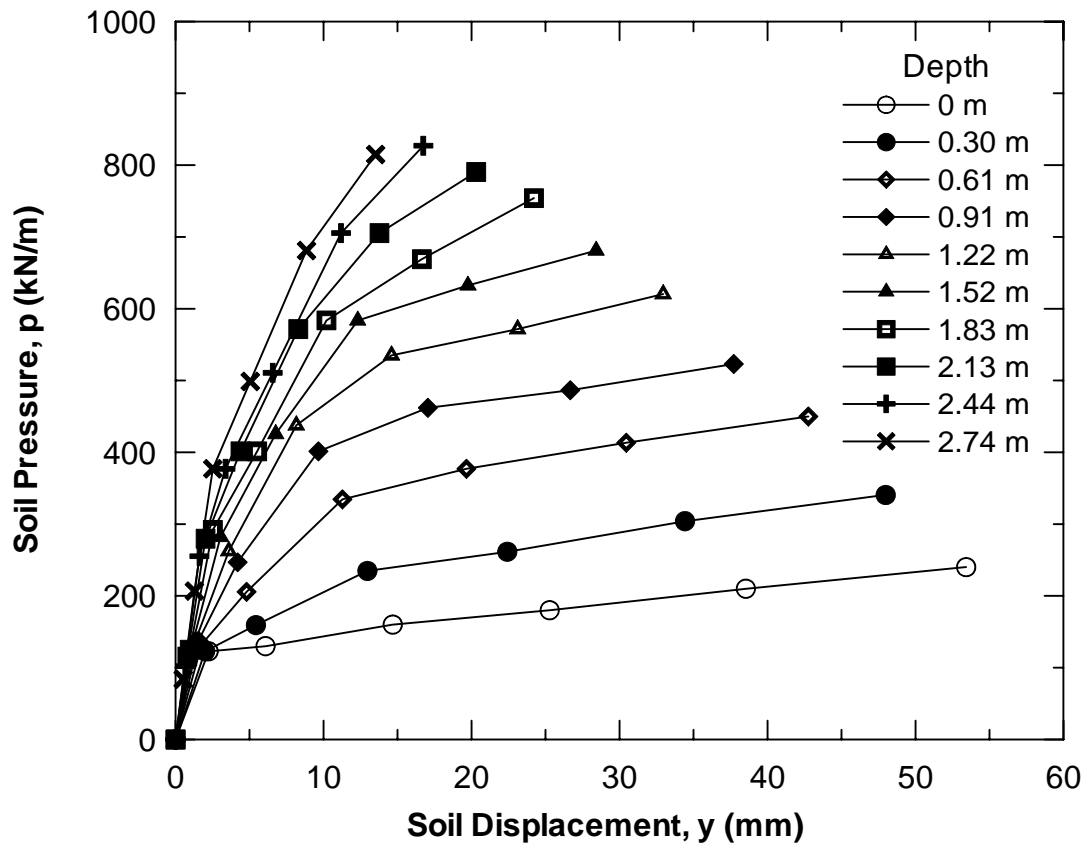


Figure 6.25 Back-Calculated  $p$ - $y$  Curves for 1.2-m CIDH Pile (No.2)

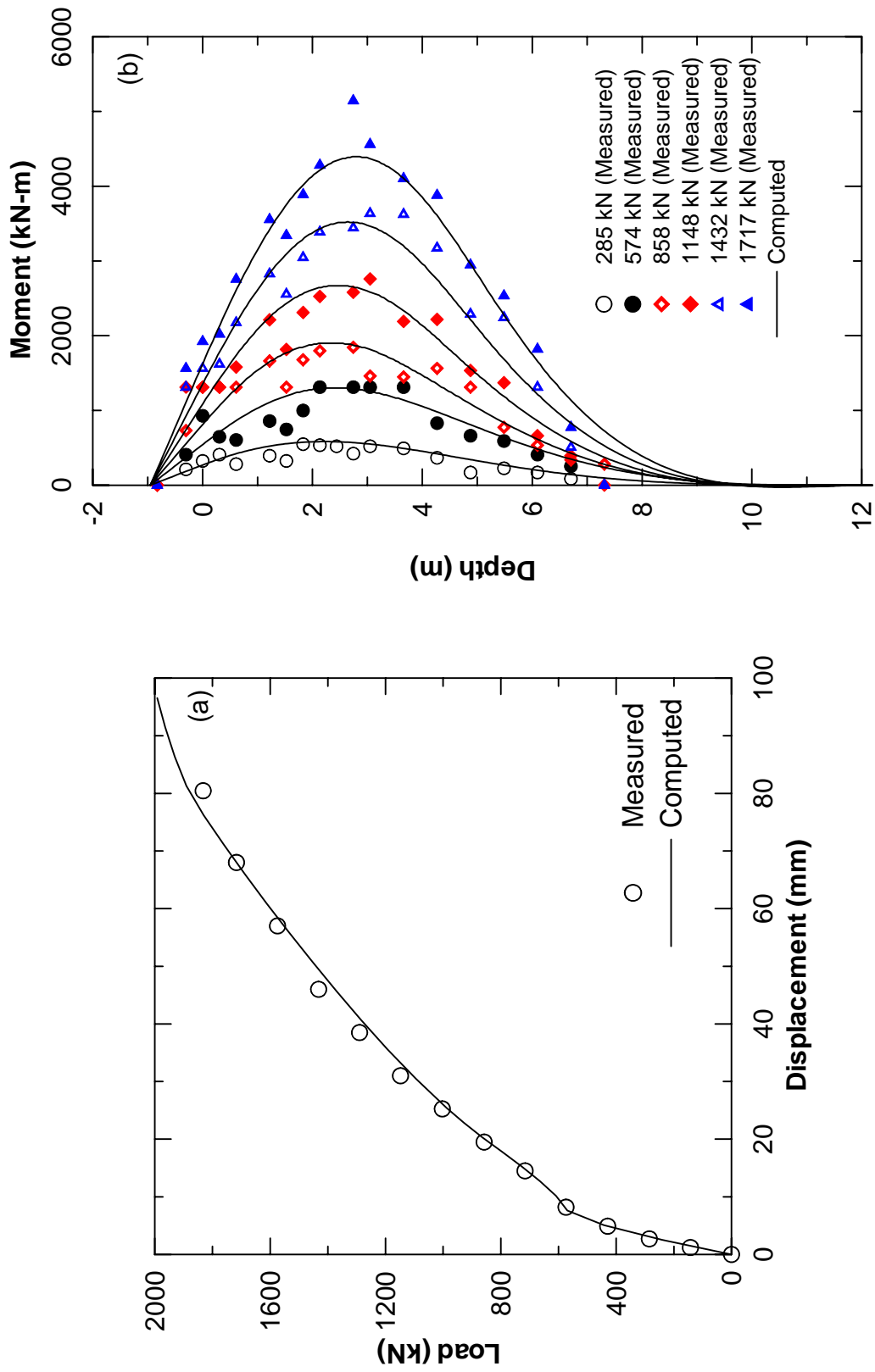


Figure 6.26 Comparison of Test Results and Analysis Using Back-Calculated  $p$ - $y$  Curves for 1.2-m CIDH Pile (No.2) (a) Load-Displacement Curve, and (b) Moment Profiles

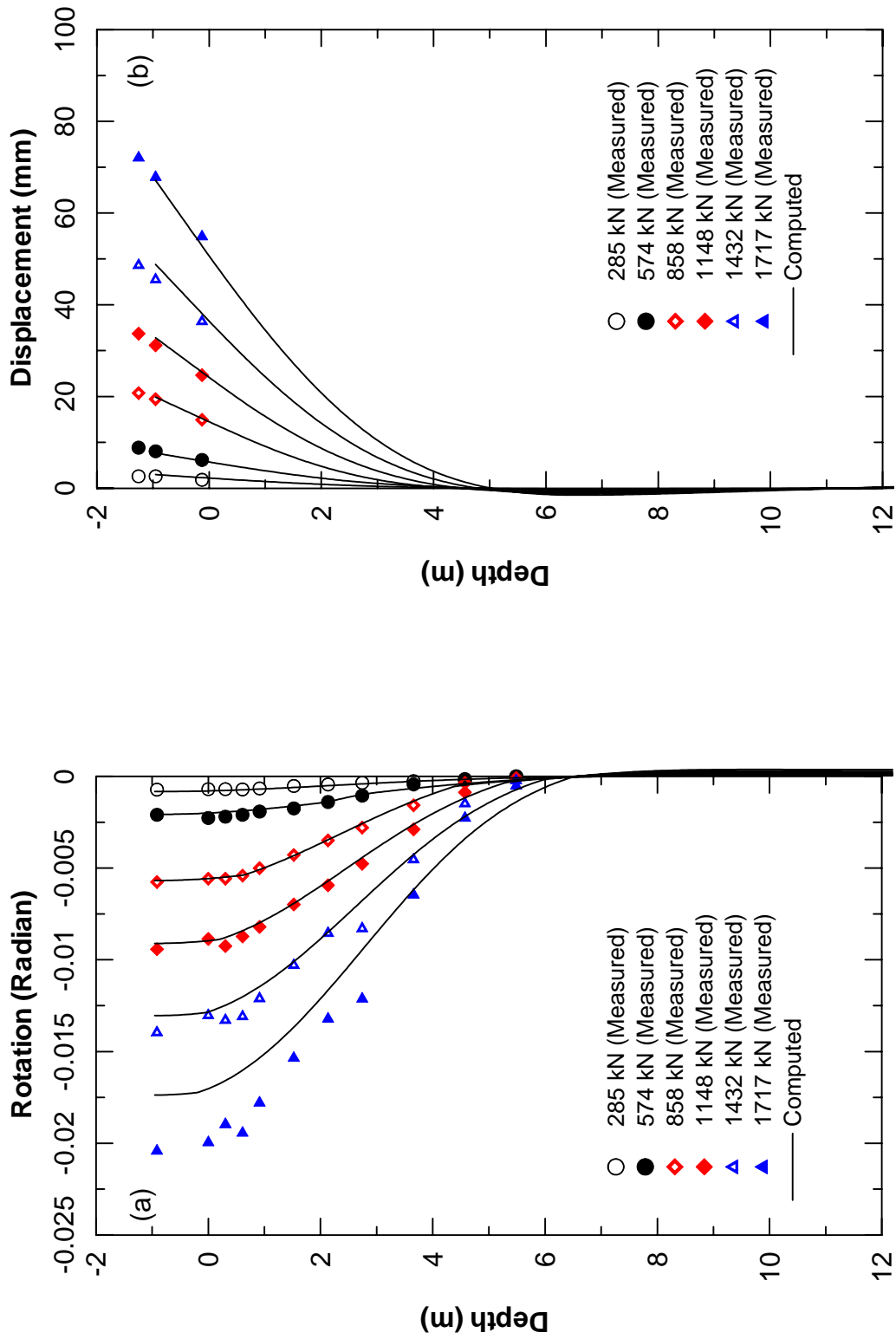


Figure 6.27 Comparison of Test Results and Analysis Using Back-Calculated  $p$ - $y$  Curves for 1.2-m CIDH Pile (No.2) (a) Rotation Profiles, and (b) Displacement Profiles

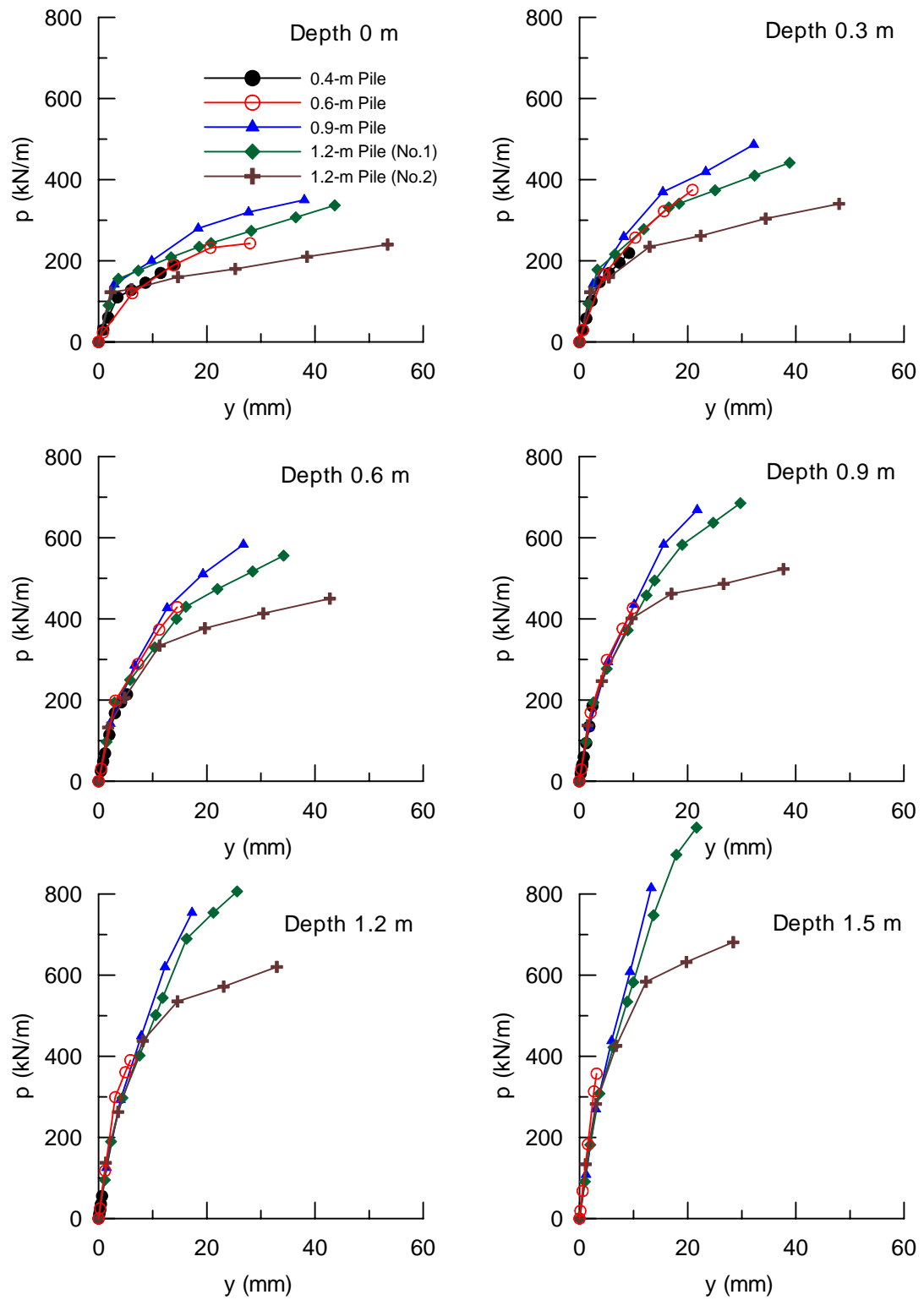


Figure 6.28 Comparison of  $p$ - $y$  Curves for Different Pile Diameters at Various Depths

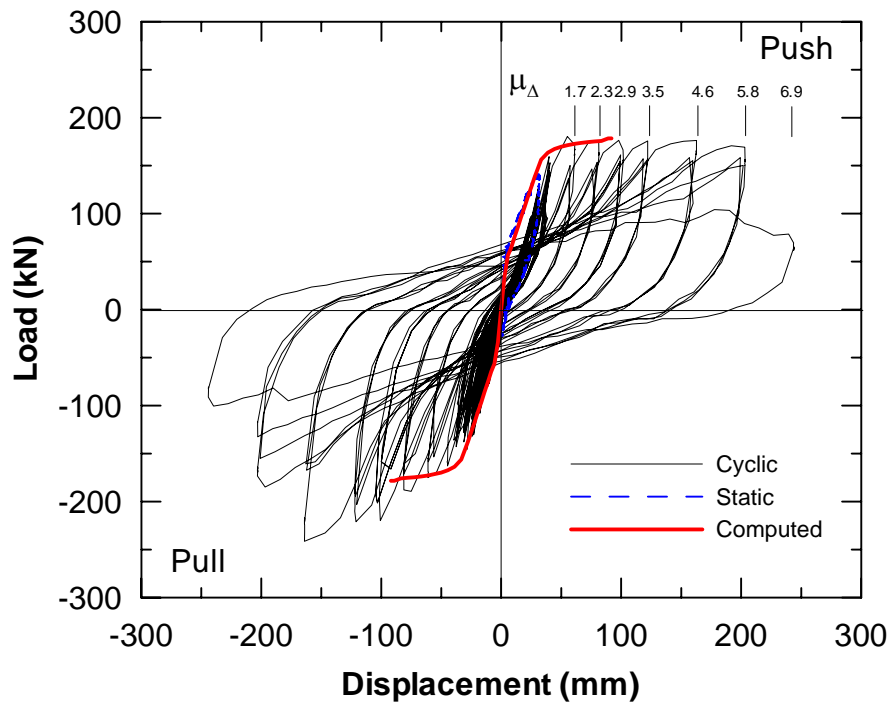


Figure 6.29 Comparison between Measured and Computed Load-Displacement Curves in Inelastic Range for 0.4-m CIDH Pile

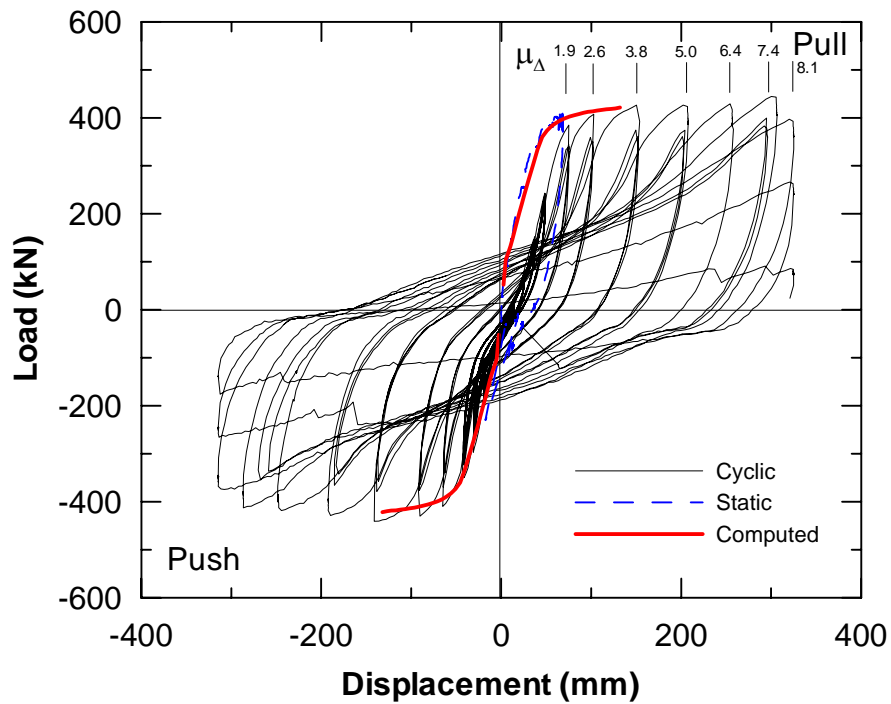


Figure 6.30 Comparison between Measured and Computed Load-Displacement Curves in Inelastic Range for 0.6-m CIDH Pile

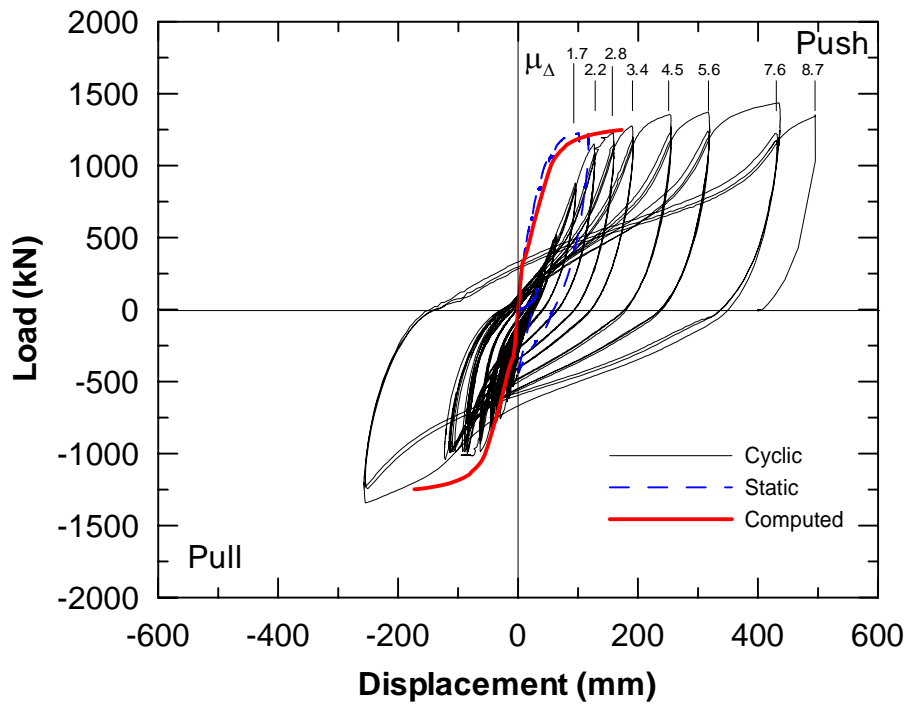


Figure 6.31 Comparison between Measured and Computed Load-Displacement Curves in Inelastic Range for 0.9-m CIDH Pile

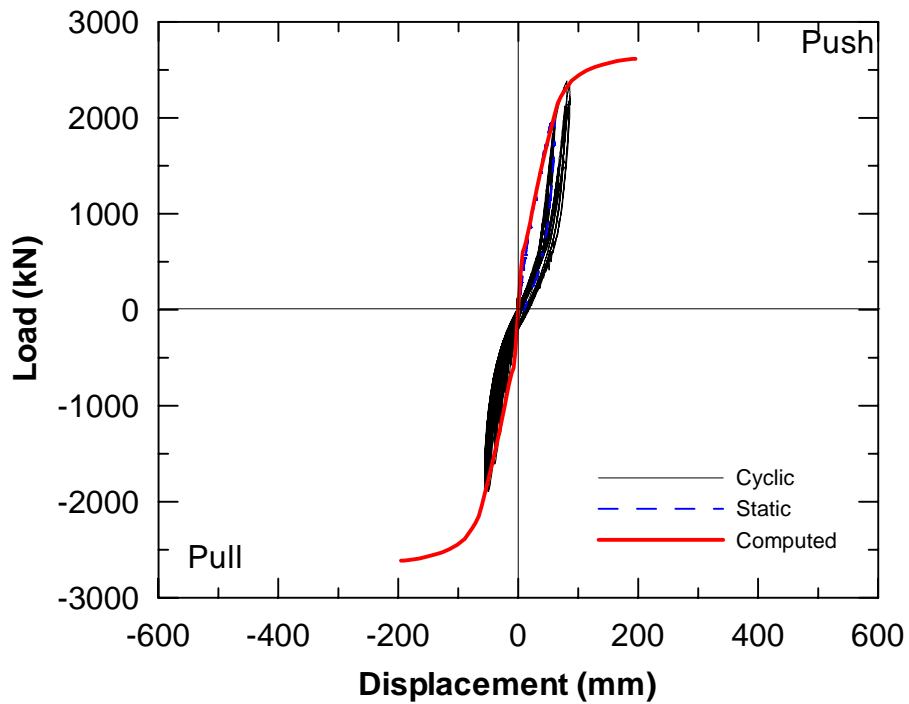


Figure 6.32 Comparison between Measured and Computed Load-Displacement Curves in Inelastic Range for 1.2-m CIDH Pile (No.1)

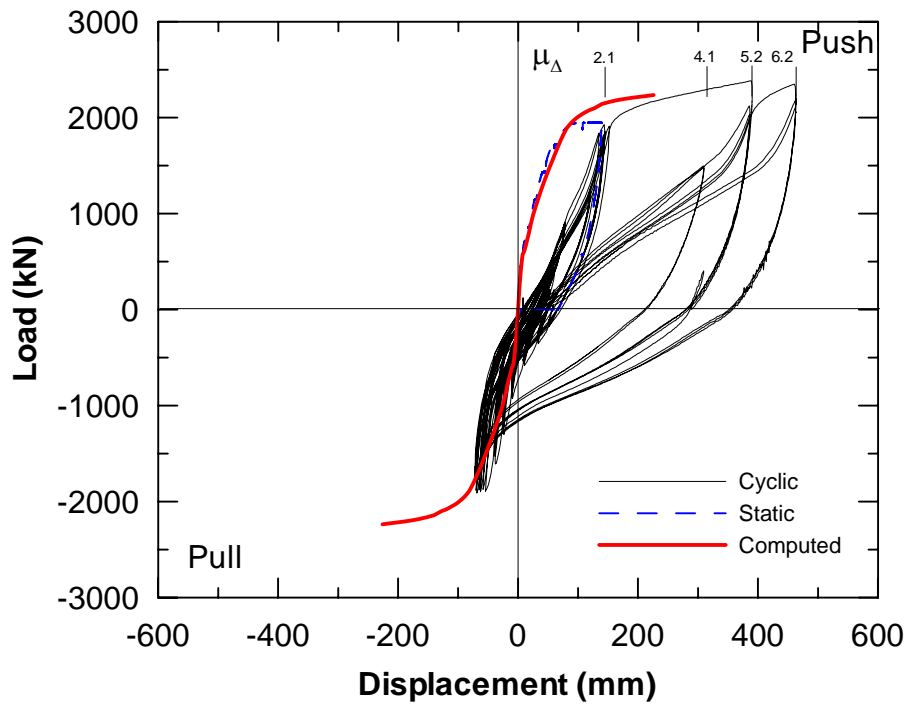


Figure 6.33 Comparison between Measured and Computed Load-Displacement Curves in Inelastic Range for 1.2-m CIDH Pile (No.2)

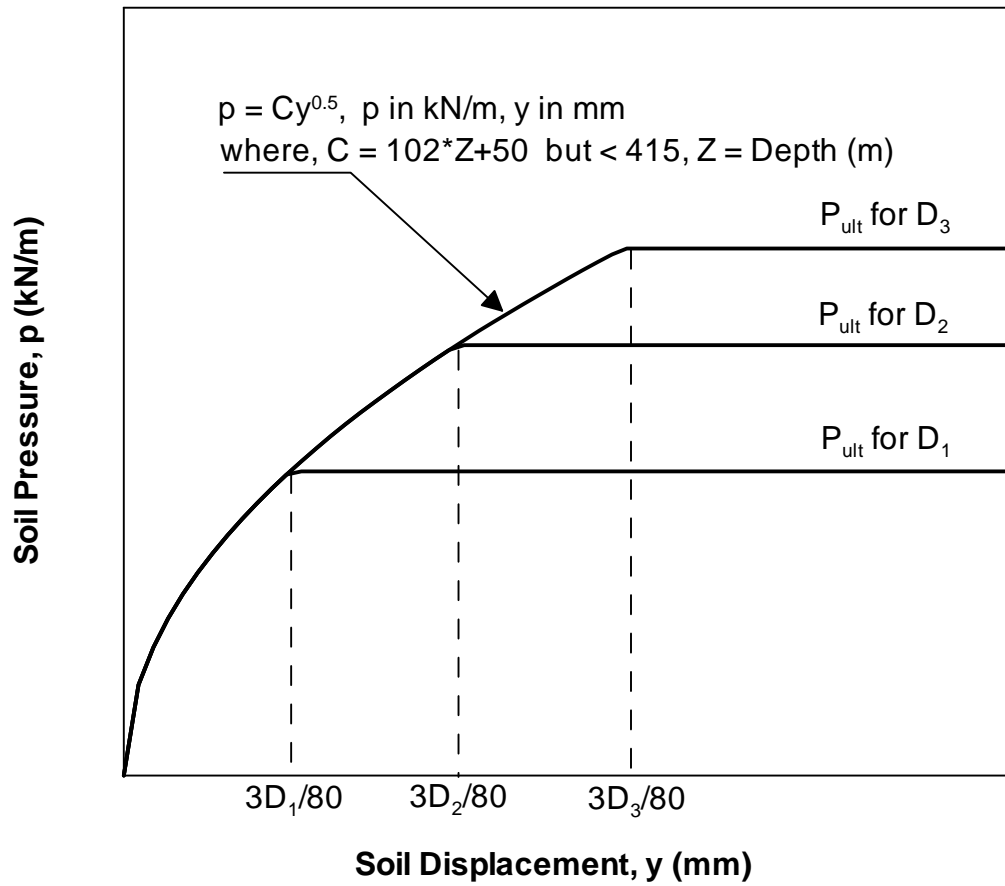


Figure 6.34 Proposed Methodology for Constructing p-y Curves for Weakly Cemented Sand

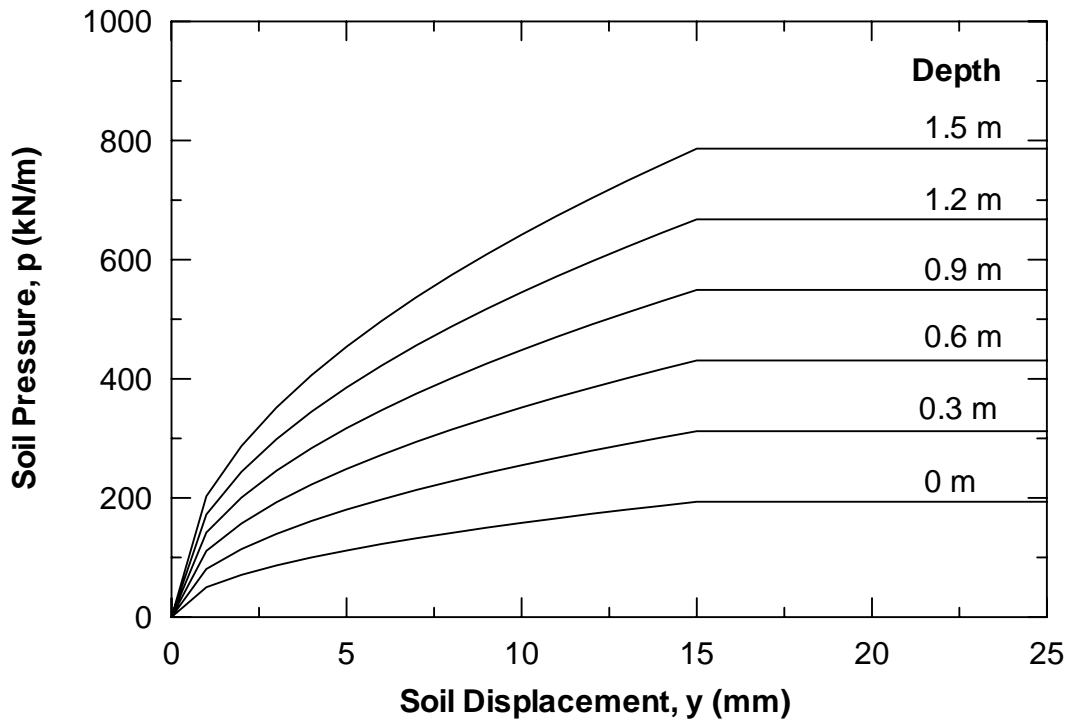


Figure 6.35 Example of Characteristic of Proposed p-y Curves for 0.4-m Pile at Various Depths

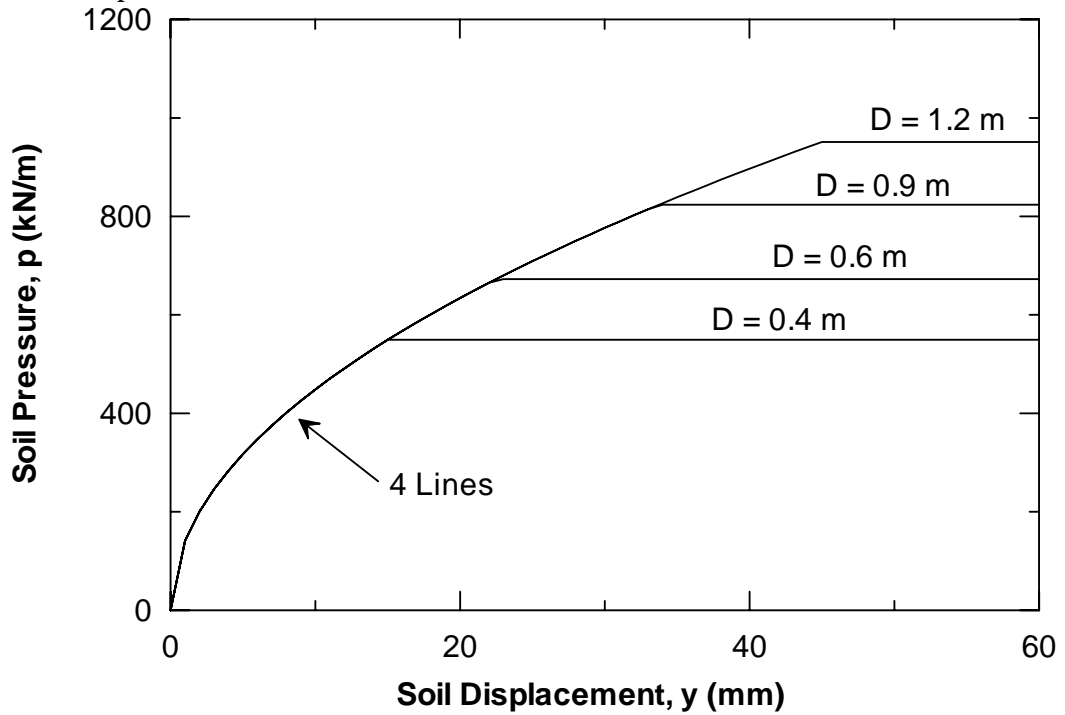


Figure 6.36 Example of Characteristic of Proposed p-y Curves for Various Pile Diameters at Depth of 0.9 m

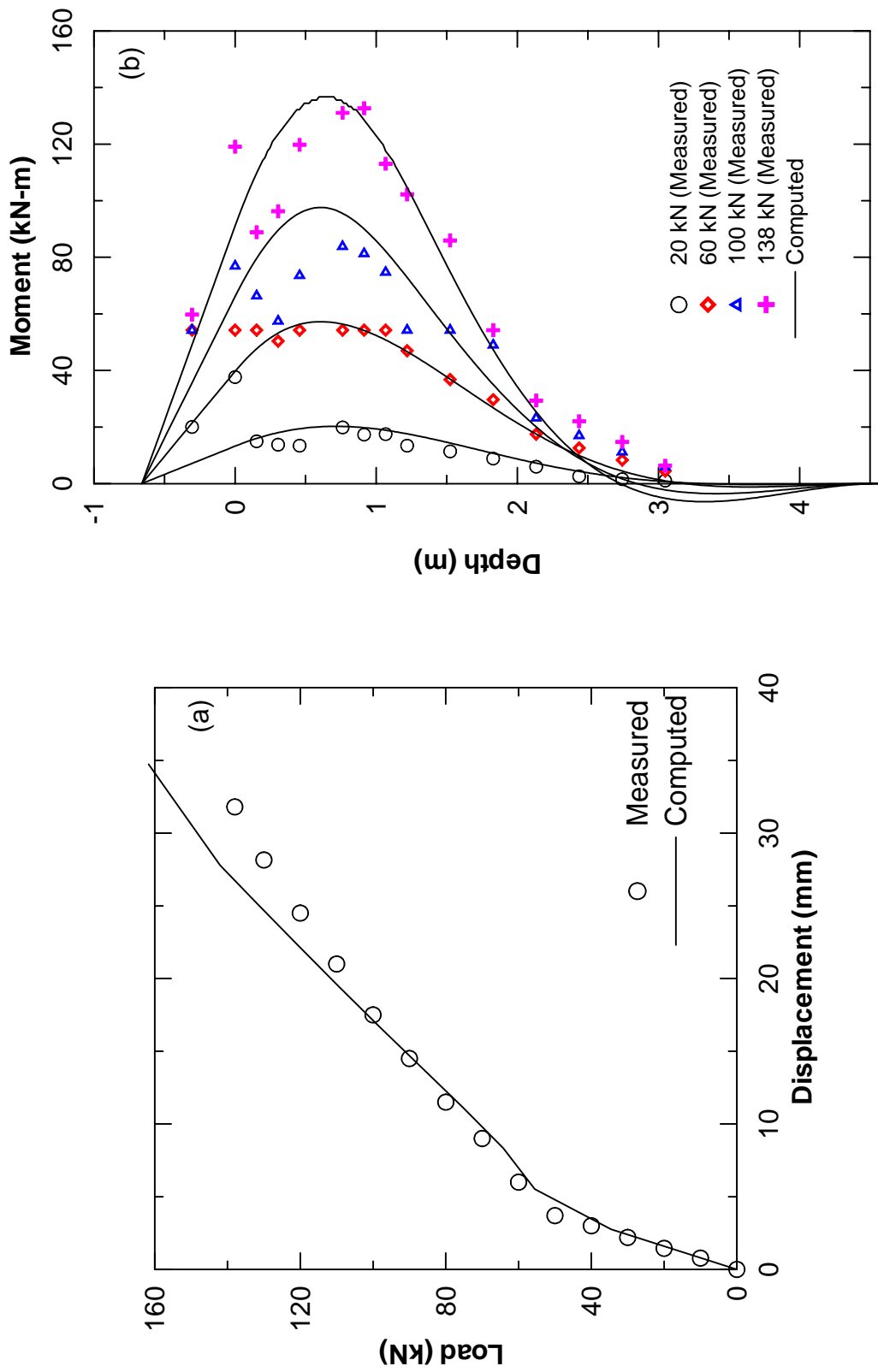


Figure 6.37 Comparison of Test Results and Analysis Using Proposed  $p$ - $y$  Curves for 0.4-m CIDH Pile (a) Load-Displacement Curve, and (b) Moment Profiles

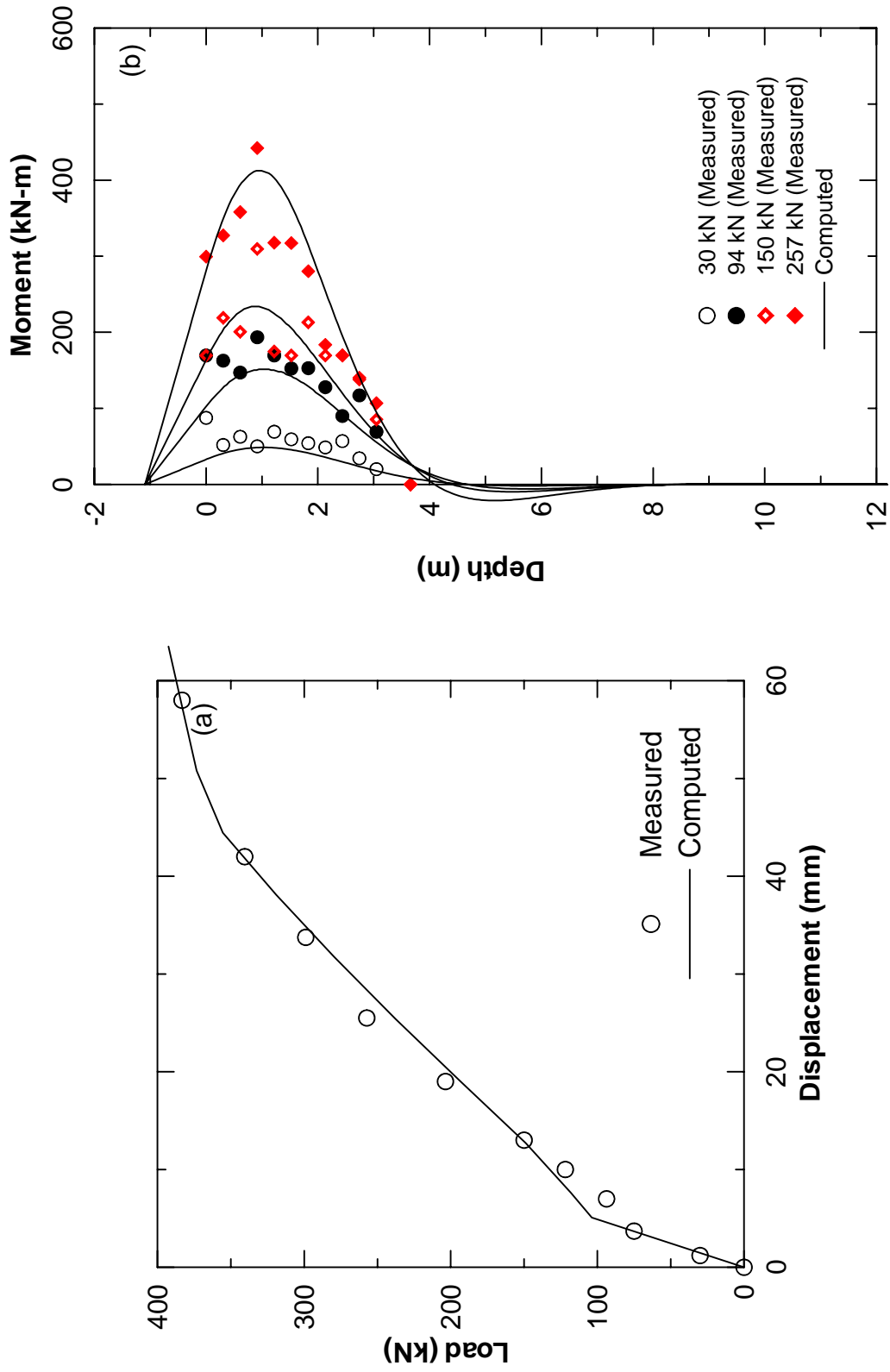


Figure 6.38 Comparison of Test Results and Analysis Using Proposed  $p$ - $y$  Curves for 0.6-m CIDH Pile (a) Load-Displacement Curve, and (b) Moment Profiles

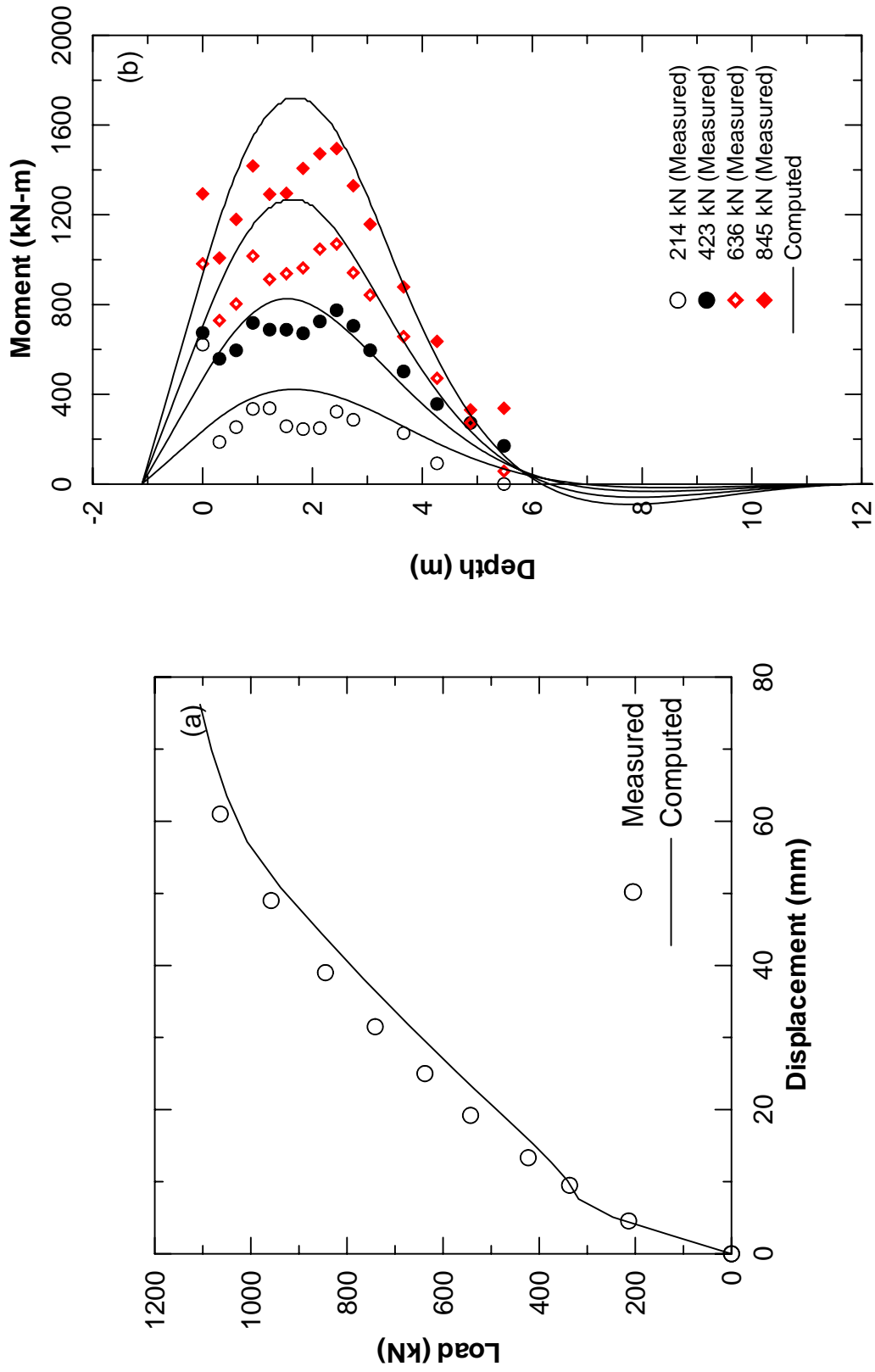


Figure 6.39 Comparison of Test Results and Analysis Using Proposed  $p$ - $y$  Curves for 0.9-m CIDH Pile (a) Load-Displacement Curve, and (b) Moment Profiles

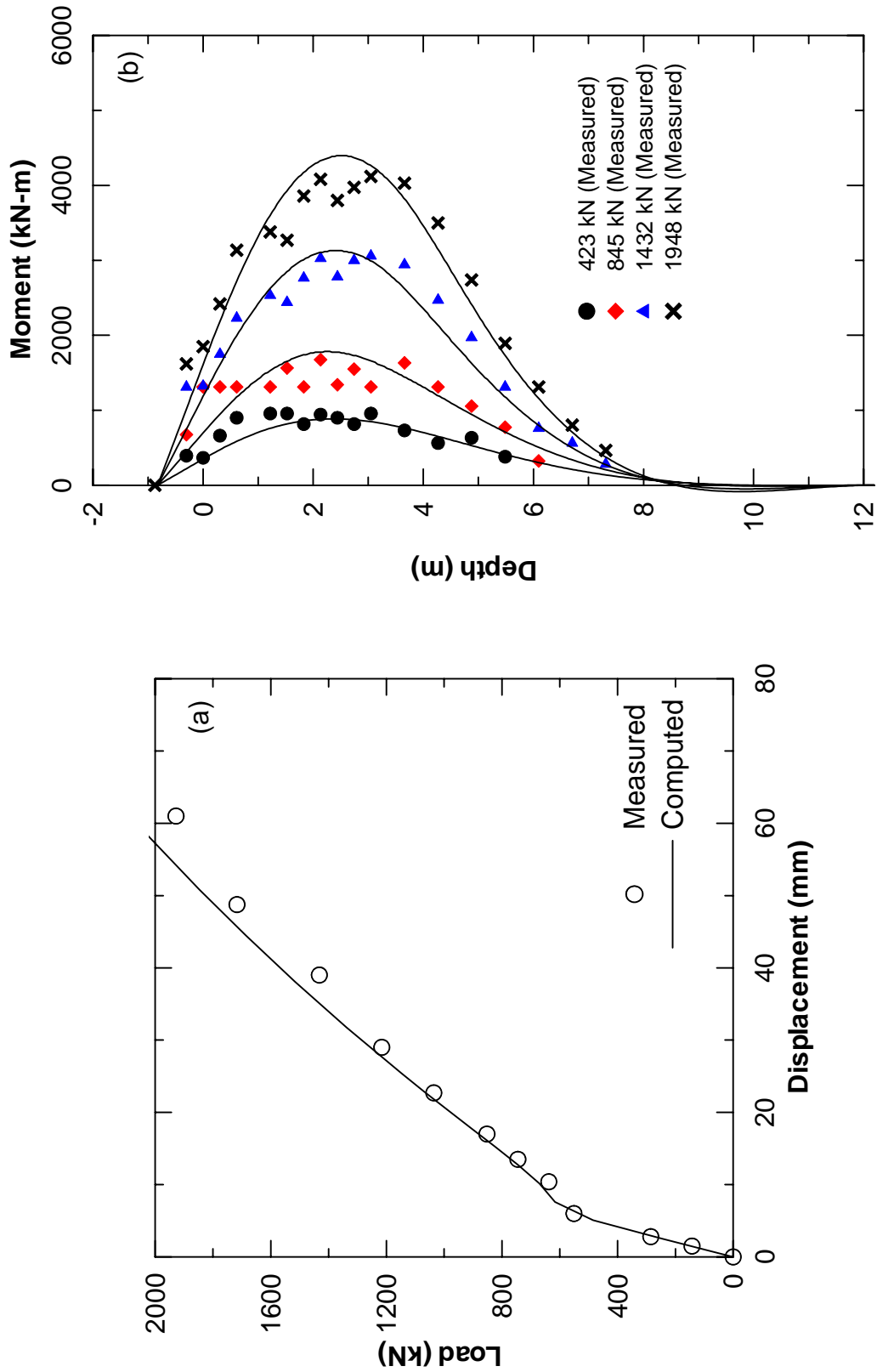


Figure 6.40 Comparison of Test Results and Analysis Using Proposed  $p$ - $y$  Curves for 1.2-m CIDH Pile (No.1) (a) Load-Displacement Curve, and (b) Moment Profiles

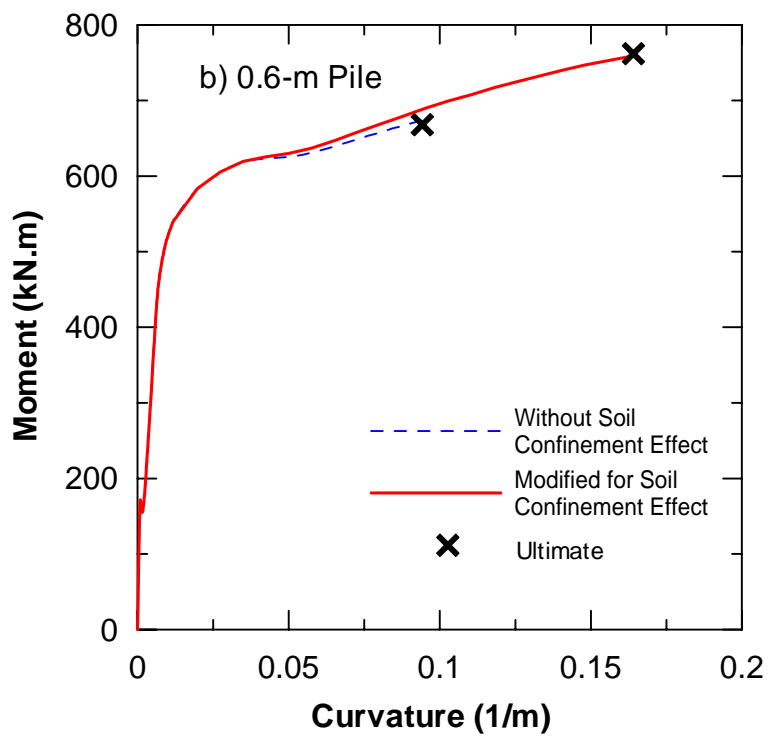
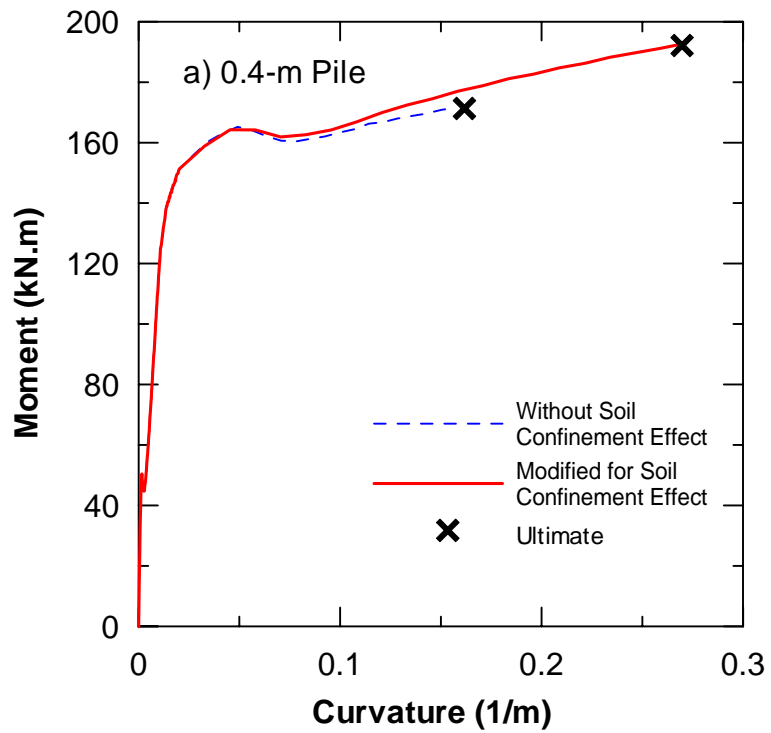


Figure 6.41 Modified Moment-Curvature Relationships for Effect of Soil Confinement (a) 0.4-m Pile, and (b) 0.6-m Pile

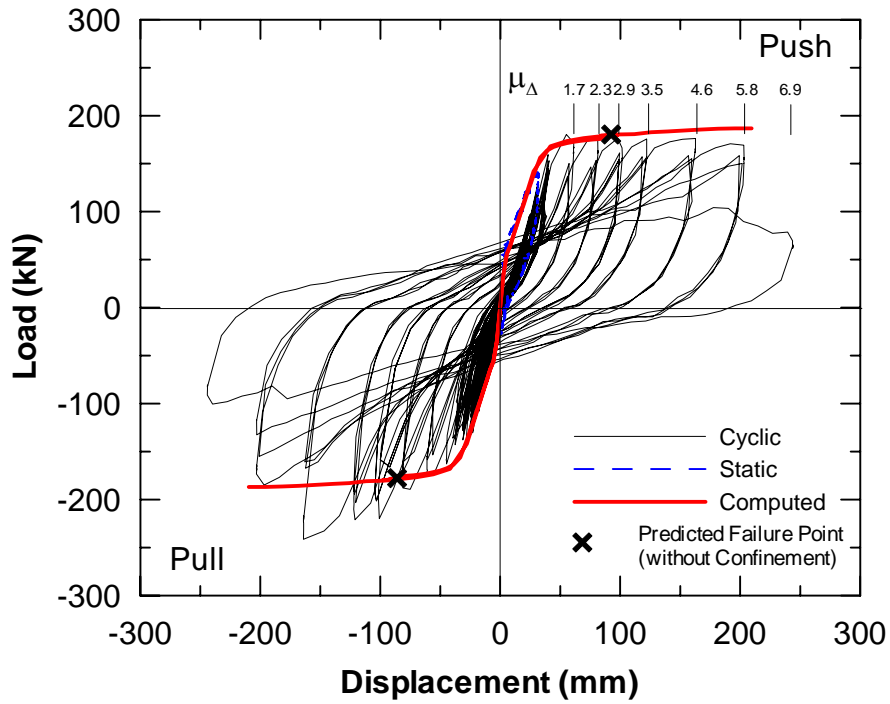


Figure 6.42 Comparison between Measured and Computed Load-Displacement Curves using Modified Moment-Curvature Relationship for 0.4-m CIDH Pile

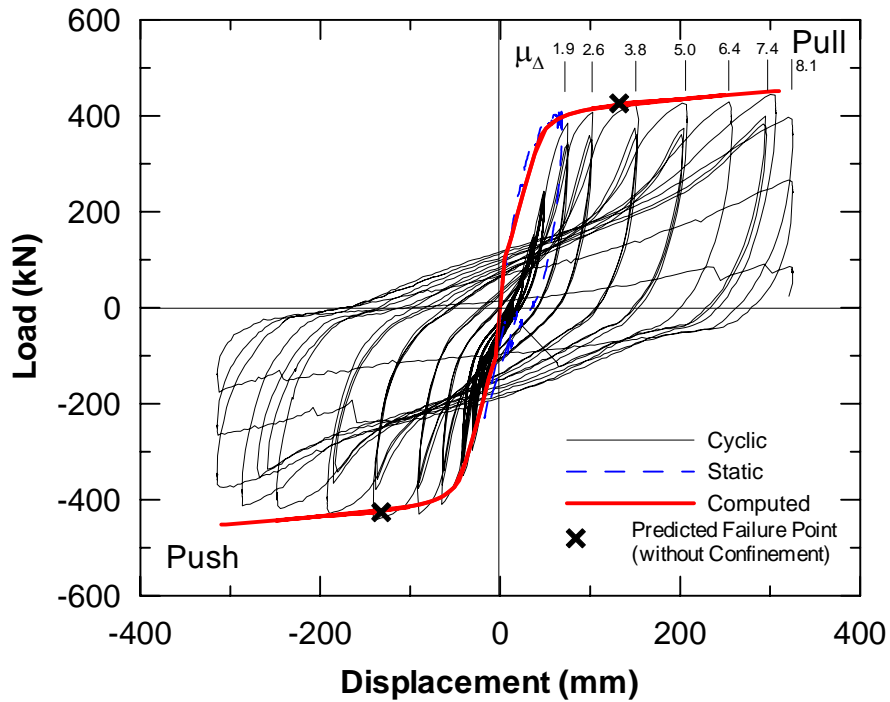


Figure 6.43 Comparison between Measured and Computed Load-Displacement Curves using Modified Moment-Curvature Relationship for 0.6-m CIDH Pile

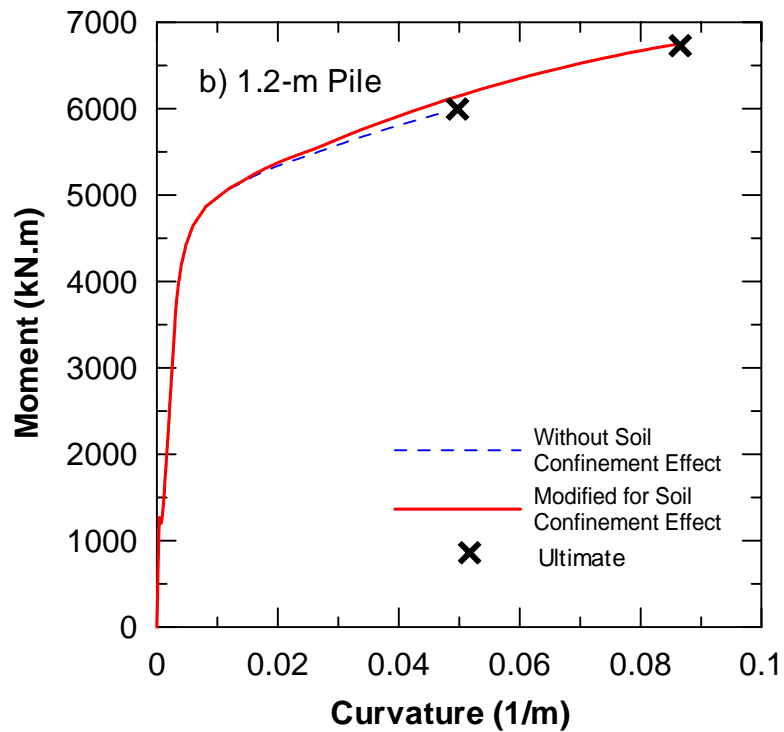
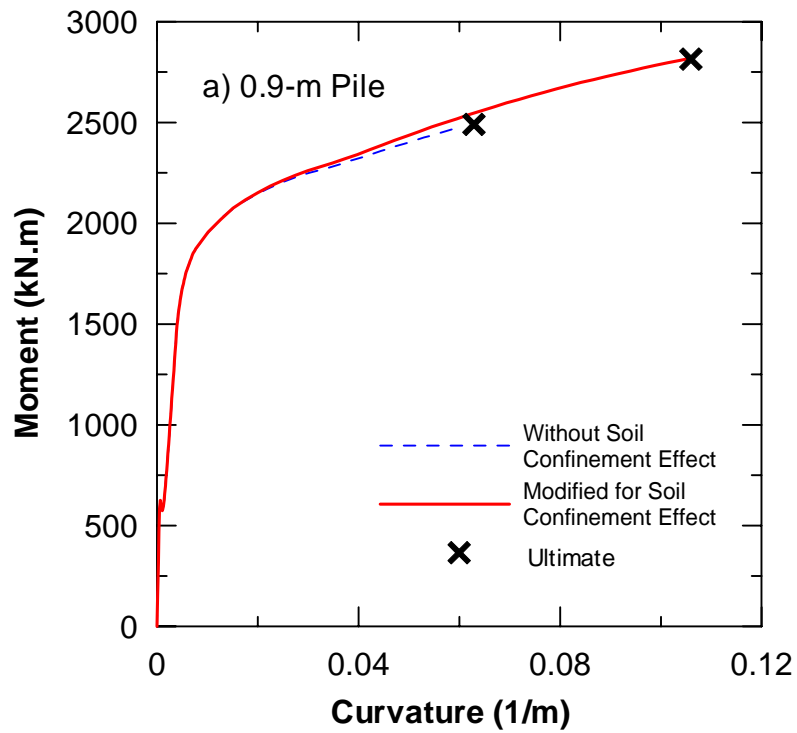


Figure 6.44 Modified Moment-Curvature Relationships for Effect of Soil Confinement (a) 0.9-m Pile, and (b) 1.2-m Pile

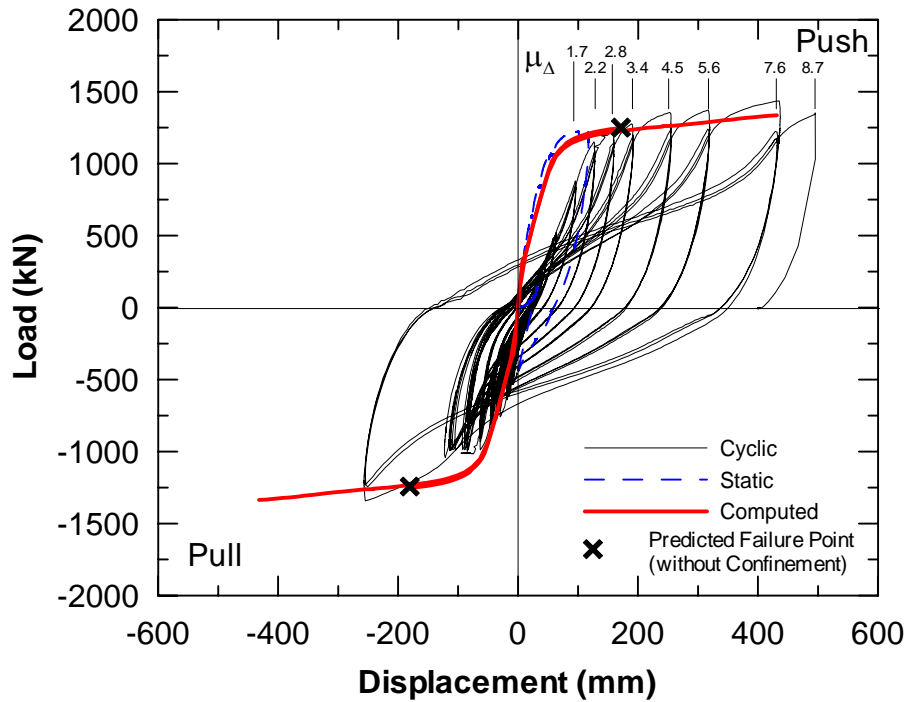


Figure 6.45 Comparison between Measured and Computed Load-Displacement Curves using Modified Moment-Curvature Relationship for 0.9-m CIDH Pile

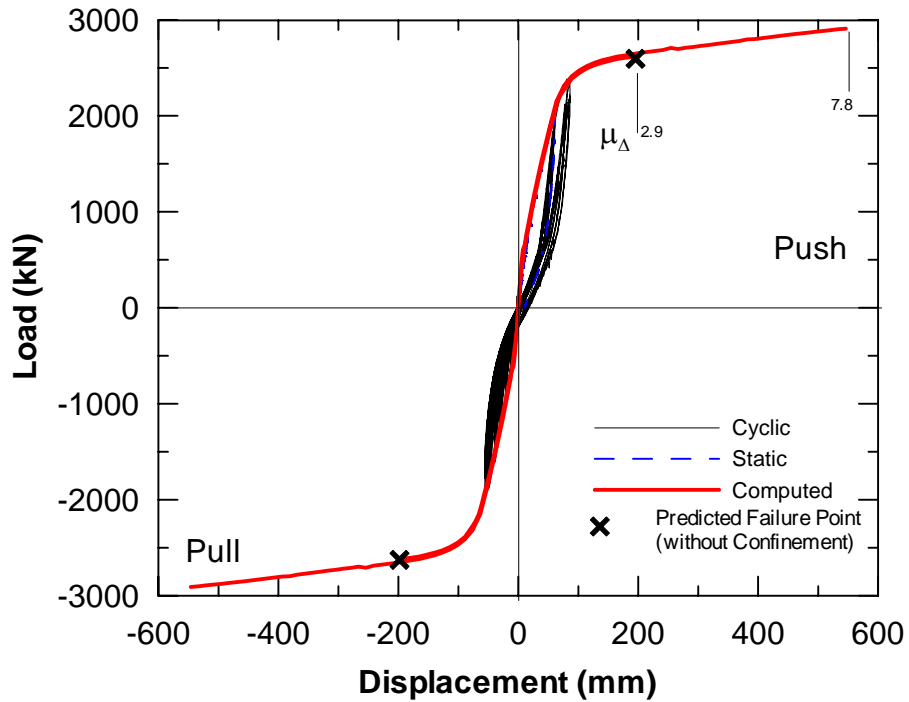


Figure 6.46 Comparison between Measured and Computed Load-Displacement Curves using Modified Moment-Curvature Relationship for 1.2-m CIDH Pile (No.1)

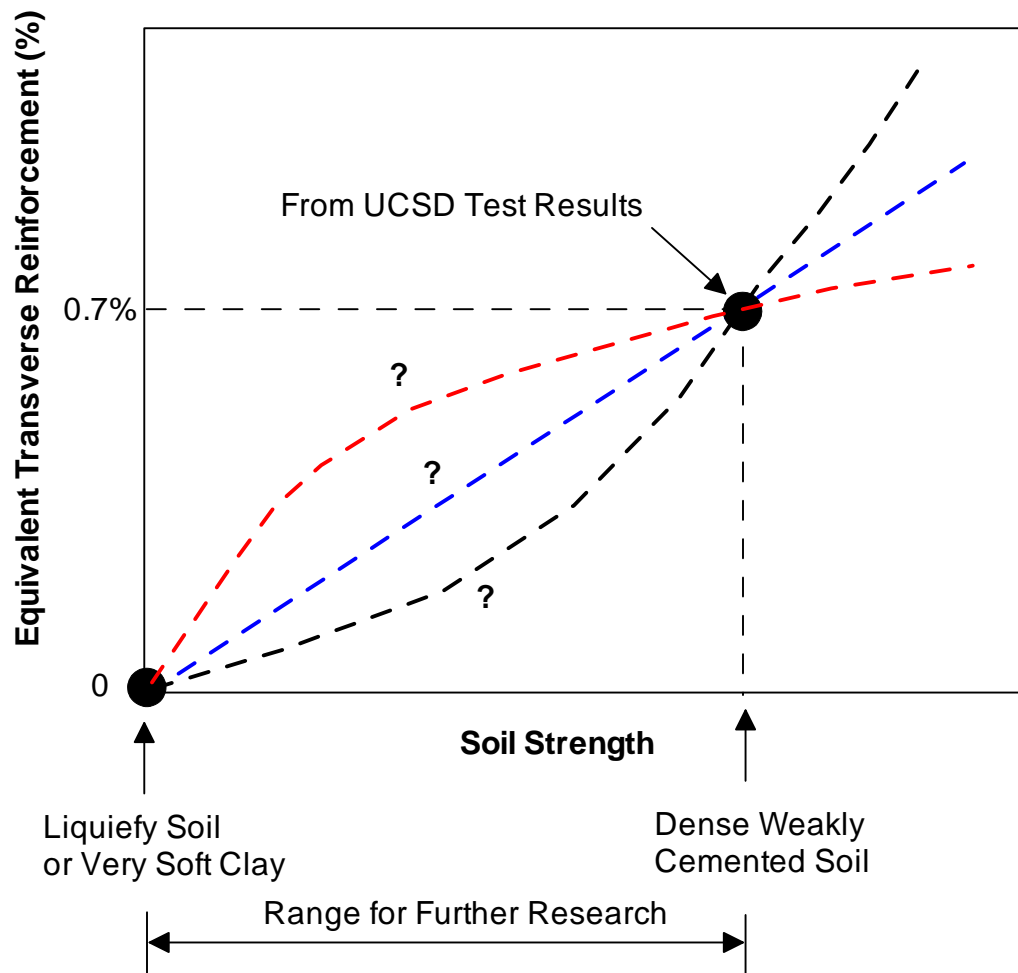


Figure 6.47 Relationship of Equivalent Transverse Reinforcement due to Soil confinement

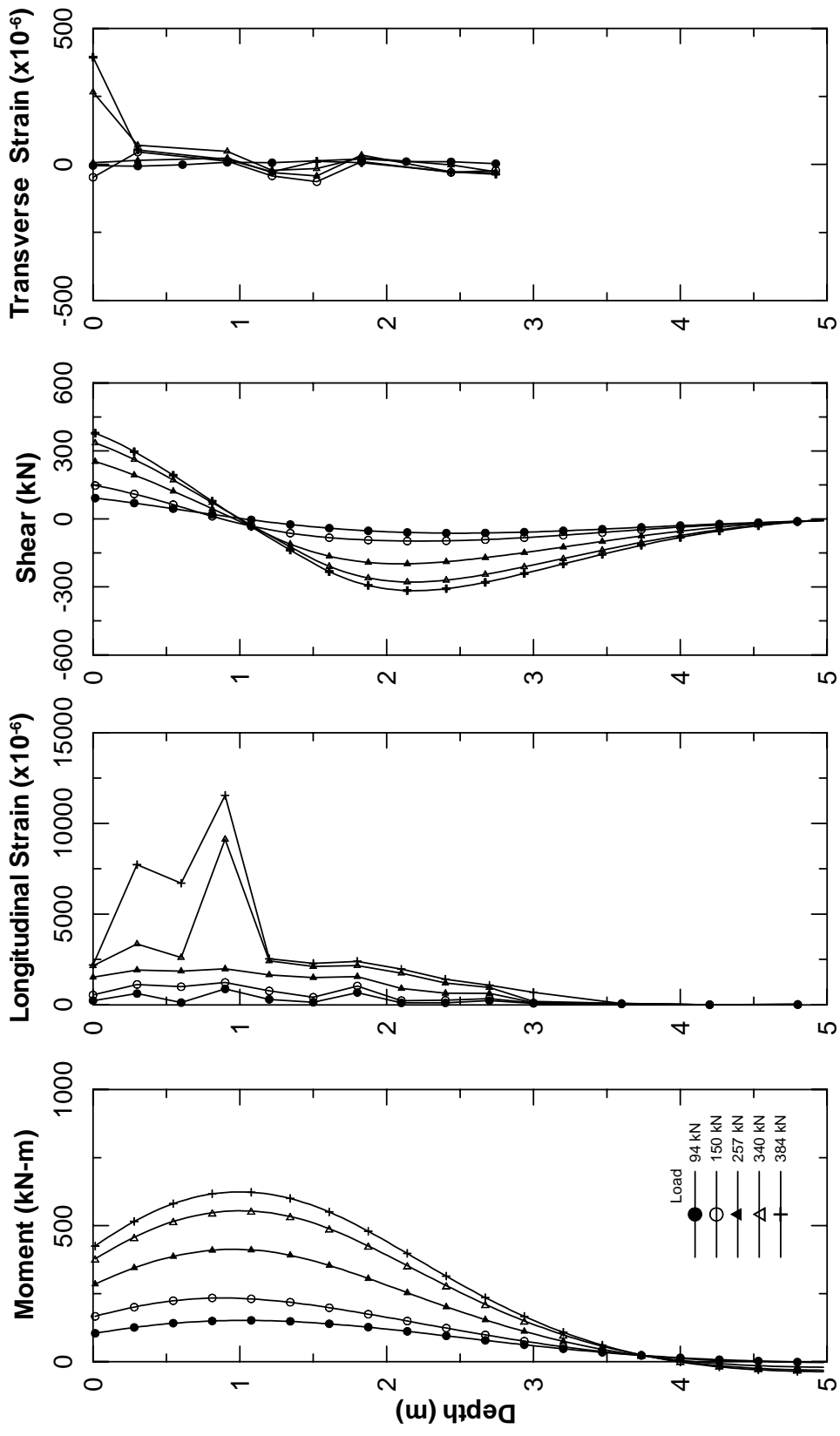


Figure 6.48 Results of Lateral Load Test on 0.6-m Pile

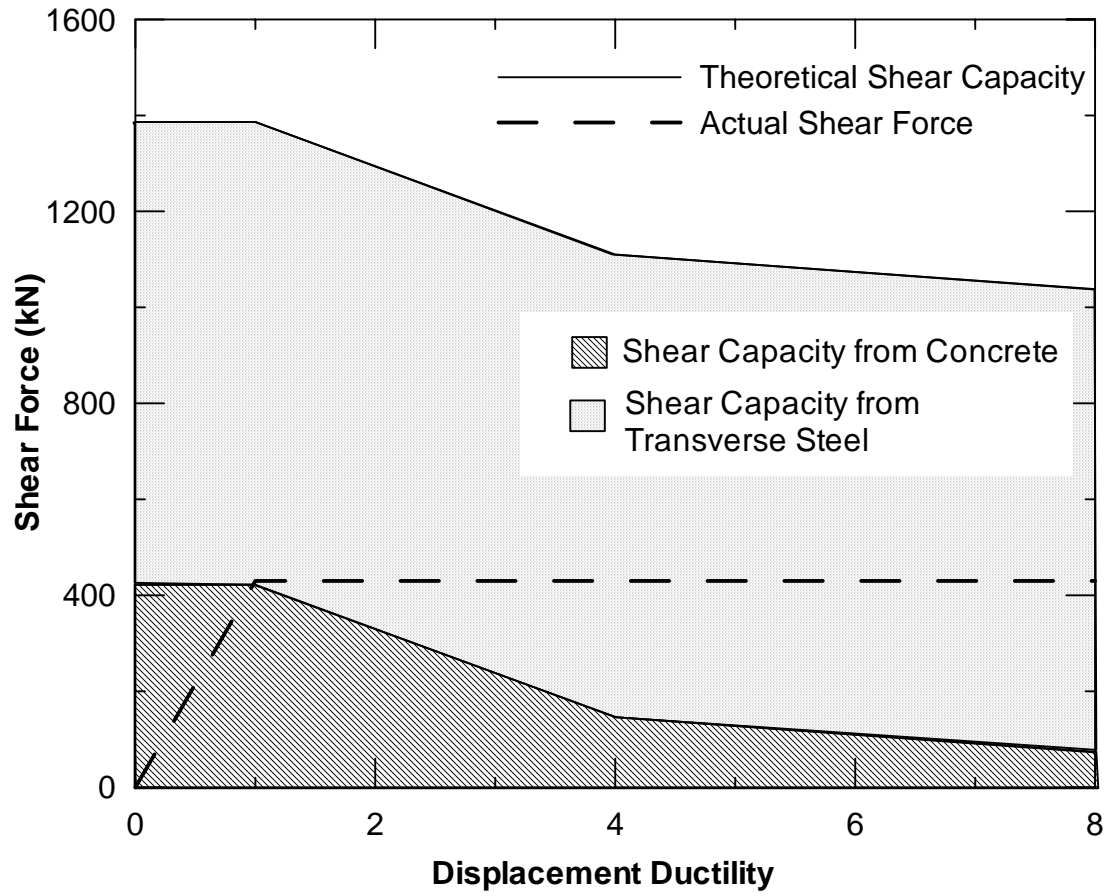


Figure 6.49 Comparison of Theoretical Shear Capacity with Experimentally Observed Shear

This page is intentionally blank.

## Chapter 7 IMPLEMENTATION OF EXISTING $p$ - $y$ CURVES FOR WEAKLY CEMENTED SAND

In this chapter, the capability of various existing  $p$ - $y$  curves in predicting the lateral pile response in weakly cemented sand is evaluated. Results from this portion study can lead to valuable conclusions regarding which of the existing  $p$ - $y$  curves are the most appropriate and how much error would be expected when implementing these  $p$ - $y$  curves to analyze the pile response in weakly cemented sand. Four different types of  $p$ - $y$  curves that are available in engineering practice were considered in this study (i.e., sand  $p$ - $y$  curves, Reese *et al.* 1974 and API 1987; cemented sand  $p$ - $y$  curves, Ismael 1987; silt  $p$ - $y$  curves, Reese and Van Impe 2001).

When analyzing pile response in weakly cemented sand, one of the most acceptable approaches is to neglect the soil resistance from the soil cohesion component. Implementing the sand  $p$ - $y$  curves proposed by either Reese *et al.* (1974) or API (1987) is therefore believed to be a conservative method to analyze the pile response in weakly cemented sand. Therefore, both of them are investigated in this study.

Experimental test results of piles embedded in cemented sand in Kuwait (Ismael 1990) support the previous concept that using sand  $p$ - $y$  curves for predicting the response in cemented sand would be conservative. Ismael proposed the new approach in developing  $p$ - $y$  curves for cemented sand by incorporating the cohesion term into the equations, which is used for determining the ultimate soil pressure. It was found that the proposed  $p$ - $y$  curves could be used to predict the test results with reasonable accuracy. However, the tests were performed on a single pile diameter (0.3 m). Using the existing  $p$ - $y$  curves for cemented sand to predict pile response for a wide range of pile diameters is therefore of interest and are evaluated in the following section.

The last  $p$ - $y$  curves considered in this study were the silt  $p$ - $y$  curves proposed by Reese and Van Impe (2001), which were developed based on the concept by Ismael (1990). The silt  $p$ - $y$  curves incorporate the cohesion term into the sand  $p$ - $y$  curves (Reese *et al* 1974). These  $p$ - $y$  curves were developed based on the theoretical basis alone without any verification from full-scale testing results. A comparison of computed pile response using the silt  $p$ - $y$  curves with the measured pile response is useful in verifying the accuracy of these  $p$ - $y$  curves. Based on these analyses, suggestion for the design of piles in weakly cemented sand is provided.

### 7.1 $p$ - $y$ Curves for Sand

The back-calculated  $p$ - $y$  curves from the full-scale tests were compared to the existing sand  $p$ - $y$  curves to evaluate how well the sand  $p$ - $y$  curves can model the behavior of weakly cemented sand. Two types of sand  $p$ - $y$  curves (i.e., Reese *et al.* 1974 and API 1987) currently available in engineering practice are considered. Sand  $p$ - $y$  curves proposed by Reese *et al.* 1974 were developed based on the results of full-scale lateral pile load tests at Mustang Island, Houston, Texas. The methodology in constructing  $p$ - $y$  curves proposed by Reese *et al.* (1974) is tedious due to several lengthy equations involved in estimating the ultimate soil pressure, as well as the use of more than one function to represent the shape of the  $p$ - $y$  curves.

O'Neill and Murchison (1983) simplified the methodology by using only a single convenient trigonometric equation to represent the Reese's sand  $p$ - $y$  curves. This suggestion was adopted by the American Petroleum Institute (API) and incorporated in its manual on recommended practice (API 1987). One of the differences between the sand  $p$ - $y$  curves and the API  $p$ - $y$  curves is the shape function of the curve; the API  $p$ - $y$  curves are usually stiffer.

Figure 7.1 and Figure 7.2 present a comparison of the back-calculated  $p$ - $y$  curves of weakly cemented sand with the sand  $p$ - $y$  curves proposed by Reese *et al.* (1974) and

API (1987) at several depths. For the purpose of comparison, only the back-calculated  $p$ - $y$  curves for the 0.4-m and 1.2-m piles are presented. The soil properties were estimated based on the corrected SPT-N values measured at the test site. Using correlation proposed by Meyerhof (1956), the friction angle for the first 6-m was estimated as 42 degrees. Below this layer a friction angle of 45 degrees was used. The soil unit weight was assumed as  $20 \text{ kN/m}^3$  for the entire depth. A subgrade reaction constant of  $76 \text{ MN/m}^3$  associated with the property of very dense sand was used for both layers.

As shown in Figure 7.1 and Figure 7.2, the back-calculated  $p$ - $y$  curves for the 0.4-m pile provides significantly higher resistance compared to both existing sand  $p$ - $y$  curves, especially for the first 1 meter depth. Below this depth, the displacement level of the back-calculated  $p$ - $y$  curves is too small and could not be well compared. No soil resistance at the ground surface is observed for both existing sand  $p$ - $y$  curves; whereas, significant soil resistance is noticeable for the back-calculated  $p$ - $y$  curves likely due to the presence of soil cohesion.

Compared with the  $p$ - $y$  curves for the 0.4-m pile, the sand  $p$ - $y$  curves for the 1.2-m pile are in better agreement with the back-calculated  $p$ - $y$  curves, particularly at a displacement of less than 10 mm. Beyond this range, the sand  $p$ - $y$  curves provide less soil resistance although the difference between those two becomes smaller as the depth increases. Below a depth of 1.8 m the initial portions of the sand  $p$ - $y$  curves are stiffer than those of the back-calculated  $p$ - $y$  curves. This is because the initial stiffness of the sand  $p$ - $y$  curves increases linearly with depth, whereas that of back-calculated  $p$ - $y$  curves increases at a slower rate.

In general, API  $p$ - $y$  curves are somewhat stiffer than Reese's sand  $p$ - $y$  curves at all depths and are in better agreement with the back-calculated  $p$ - $y$  curves. It should be noted that the API sand  $p$ - $y$  curves theoretically should give the same ultimate soil pressure as Reese's sand  $p$ - $y$  curves. However, Figure 7.2 shows that at some depths,

there are some differences in ultimate soil pressure based on different assumptions in the respective methods. This is because correction factor  $A$  (discussed in Chapter 2) in the API  $p$ - $y$  curves was more conservative at some depths, resulting in a difference in ultimate soil pressure.

As mentioned earlier, using sand  $p$ - $y$  curves to predict pile response in weakly cemented sand is generally believed to be a conservative method because the cohesion of the soil is neglected. Figure 7.3 shows a comparison of computed load-displacement curves of each pile using the sand  $p$ - $y$  curves to the measured load-displacement curves. Clearly, both sand  $p$ - $y$  curves yield the conservative computed response over the range of the diameter tested. As expected from the comparison of  $p$ - $y$  curves discussed earlier, the API  $p$ - $y$  curves are in better agreement with the experimental test results.

Interestingly, the agreement between the test results and the response predicted using the sand  $p$ - $y$  curves improves as the pile diameter increases. However, this trend indicates that the sand  $p$ - $y$  curves may tend to overestimate the pile response as the diameter increases beyond 1.2 m. This is due to the difference in the characteristics of  $p$ - $y$  curves, as well as the diameter effect incorporated in the sand  $p$ - $y$  curves appearing to be too large for the use in cemented sand. In fact, the back-calculated  $p$ - $y$  curves show that the pile diameter effect on the  $p$ - $y$  curves for cemented sand is insignificant for a range of displacement smaller than the ultimate soil resistance.

Additional analyses were conducted to validate this finding by comparing the load-displacement curves of a pile diameter larger than 1.2 m using the proposed  $p$ - $y$  curves and API sand  $p$ - $y$  curves. This analysis was conducted based on the assumption that the pile response obtained using the proposed  $p$ - $y$  curves results in the measured response in the field. This assumption appears to be reasonable because the earlier study shows that the proposed  $p$ - $y$  curves give an excellent agreement of pile response compared to the experimental test data. Figure 7.4 shows that the predicted pile

response using the API  $p$ - $y$  curves before the pile reaches the yield load are stiffer compared to that computed from the proposed  $p$ - $y$  curves, but the yield load obtained from the API sand  $p$ - $y$  curves are slightly lower than those obtained using the proposed  $p$ - $y$  curves. This finding shows that a non-conservative prediction of pile response in weakly cemented sand may be encountered for large pile diameters, even though the sand  $p$ - $y$  curves, which are believed to be conservative for cemented sand, are implemented.

The ratio of predicted to measured pile responses (pile head displacement, maximum moment, and depth to maximum moment) using the sand  $p$ - $y$  curves proposed by Reese *et al.* and API  $p$ - $y$  curves are presented in Figure 7.5 and Figure 7.6, respectively. In general, increasing pile diameter increases the accuracy in predicting pile response. However, the API sand  $p$ - $y$  curves overestimate the pile capacity as the diameter increases to 1.8 and 2.4 m as indicated in Figure 7.6. In addition, the existing sand  $p$ - $y$  curves underestimate the pile head displacement about 2.5 times for the 0.4-m pile and decrease to about 1.5 times for the 1.2-m pile. The error in estimating the maximum moment for all pile diameters studied is less than 50%, with the error being smaller for the larger piles. The accuracy in predicting the maximum moment is moderate with the error ranging between 10 to 80%. In general, API  $p$ - $y$  curves appear to yield slightly better agreement in predicting the pile response than the Reese's sand  $p$ - $y$  curves, particularly for the pile head displacement.

Based on the analytical study, though conservative for small diameter piles, the sand  $p$ - $y$  curves seem to be inappropriate to analyze the pile response in weakly cemented sand, especially for a large pile diameter. This is mainly due to the pile diameter effect incorporated in the existing sand  $p$ - $y$  curves, which appears to be too much for weakly cemented sand. Therefore, implementing sand  $p$ - $y$  curves to analyze the behavior of laterally loaded piles of large pile diameters should be used with caution.

## 7.2 $p$ - $y$ Curves for $c$ - $\phi$ Soil

Parametric studies in the previous section indicate that the sand  $p$ - $y$  curves are not appropriate for analyzing pile response in weakly cemented sand, particular for large diameter piles. In this section, the existing cemented sand  $p$ - $y$  curves proposed by Ismael (1990) are compared with the back-calculated  $p$ - $y$  curves from the full-scale tests at diameters of 0.4m and 1.2m, as well as implemented to predict the measured pile response for various diameters. Furthermore, the silt  $p$ - $y$  curves proposed by Reese and Van Impe (2001) which accounted for both cohesion and friction angle are considered in this study.

### 7.2.1 Cemented Sand $p$ - $y$ Curves (Ismael 1990)

A review of Figure 7.7 and Figure 7.8 shows that the back-calculated  $p$ - $y$  curves of the 1.2-m pile favorably agree with the cemented sand  $p$ - $y$  curves (Ismael 1990) for most depths; whereas the back-calculated  $p$ - $y$  curves of the 0.4-m pile are somewhat stiffer than the Ismael  $p$ - $y$  curves. The soil properties used in this analysis were similar to those used for the sand  $p$ - $y$  curves, with an addition of a soil cohesion of 20 kPa. This cohesion corresponds to the cohesion of weakly cemented soil and is the lower bound values obtained from the direct shear test results. Figure 7.9 shows the load-displacement curves obtained by using cemented sand  $p$ - $y$  curves compared to the full-scale test results. Good agreement is observed for the 1.2-m pile. However, the predicted pile response decreases in accuracy as the pile diameter decreases, yet in a more conservative way.

The ratio of pile response using cemented sand  $p$ - $y$  curves to the pile response obtained by using the proposed  $p$ - $y$  curves is presented in Figure 7.10. As expected, cemented sand  $p$ - $y$  curves generally yield better prediction of pile response than both sand  $p$ - $y$  curves implemented in the previous section. It is likely due to the fact that the  $p$ - $y$  curves using Ismael methodology can better represent the characteristics of weakly cemented sand, in which these  $p$ - $y$  curves shows some soil resistance at ground surface;

whereas there is no soil resistance observed for the sand  $p$ - $y$  curves. However, the pile diameter effect incorporated in these  $p$ - $y$  curves is still somewhat inappropriate. As observed in Figure 7.10, the agreement of pile response improves as the pile diameter increases for the range of diameter tested. Again, using these  $p$ - $y$  curves for a large pile diameter tends to overestimate the actual pile response. This is confirmed by additional parametric analyses on larger pile diameters (i.e. 1.8 m and 2.4 m).

Among comparisons of the pile response using cemented sand  $p$ - $y$  curves, the error in estimating the maximum moment appears to be the smallest with the error being less than 10% for all pile diameters. The errors in estimating the depth to maximum moment and pile head displacement are moderate and the highest, respectively. If one considers only the magnitude of maximum moment for a design, cemented sand  $p$ - $y$  curves can give a reasonable estimation.

### **7.2.2 $p$ - $y$ Curves for Silt (Reese and Van Impe 2001)**

Silt  $p$ - $y$  curves (Reese and Van Impe 2001) of the 0.4-m and 1.2-m piles were developed using the soil properties used in Ismael  $p$ - $y$  curves. Figure 7.11 and Figure 7.12 present a comparison between the back-calculated  $p$ - $y$  curves and silt  $p$ - $y$  curves at several depths. Though the cohesion term was incorporated into the equations used to compute the ultimate soil pressure, the silt  $p$ - $y$  curves do not show any soil resistance at ground surface. Results in implementing the silt  $p$ - $y$  curves to predict the pile response for various pile diameters are presented in Figure 7.13. Good agreement between the computed response using silt  $p$ - $y$  curves and the test results is observed for the 1.2-m pile. Again, a more conservative response was observed as the pile diameter becomes smaller.

Figure 7.14 presents the ratio of pile response computed using silt  $p$ - $y$  curves to the pile response obtained by using the proposed  $p$ - $y$  curves. Again, as the pile diameter increases, the agreement of computed responses between silt  $p$ - $y$  curves and proposed  $p$ - $y$  curves improves for the range of pile diameters tested. Additional analyses on larger pile

diameters than those tested again indicate that using silt  $p$ - $y$  curves overestimates the pile response.

### 7.2.3 Comparison of Capability of Various $p$ - $y$ Curves

In this section, the ratio of pile head displacement, maximum moment, and depth to maximum moment based on different  $p$ - $y$  curves is compared to evaluate which of the existing  $p$ - $y$  curves are the most appropriate to predict the response in weakly cemented sand. Figures 7.15 to 7.18 show that the cemented sand  $p$ - $y$  curves proposed by Ismael (1990) are the most accurate in predicting the pile response in weakly cemented sand for all diameters tested; whereas, Reese's sand  $p$ - $y$  curves are the most conservative  $p$ - $y$  curves for the range of pile diameters tested. Silt  $p$ - $y$  curves are the second best in predicting pile response. The difference in the pile response is noticeably observed for the 0.4-m pile and it becomes less significant for the 1.2-m pile.

It is noted that none of the existing  $p$ - $y$  curves considered in this study can model the pile response accurately for a wide range of pile diameters. In addition, it appears to be non-conservative if the large diameter piles are implemented as discussed in the earlier section. These  $p$ - $y$  curves should therefore be used with caution when analyzing the lateral response of large diameter piles (more than 1.2 m).

For pile diameter less than 1.2 m, using sand  $p$ - $y$  curves proposed by Reese *et al.* (1974) yields the lower bound for estimating the load-displacement curves, as well as the maximum moment, while the proposed  $p$ - $y$  curves gives the upper bound values. In case of the pile diameter larger than 1.2 m, the API sand  $p$ - $y$  curves provide the upper bound values in estimating the pile response, while the proposed  $p$ - $y$  curves yield the lower bound values.

### 7.3 Summary

The capability in using existing  $p$ - $y$  curves to predict the response of pile in weakly cemented sand for a wide range of pile diameters was evaluated by comparing the computed response to the measured response from the full-scale lateral testing. Four different types of  $p$ - $y$  curves were considered in this study (i.e., sand  $p$ - $y$  curves, Reese *et al.* 1974 and API 1987; cemented sand  $p$ - $y$  curves, Ismael 1987; silt  $p$ - $y$  curves, Reese and Van Impe 2001). Implementation of the sand  $p$ - $y$  curves to predict the response of piles in weakly cemented sand is generally believed to be a conservative method because the resistance from the soil cohesion component is neglected. However, the analysis results showed that using the sand  $p$ - $y$  curves is not conservative when analyzes the response of large diameter piles. The cemented sand  $p$ - $y$  curves proposed by Ismael appear to be the most accurate in predicting the response of pile in weakly cemented sand. However, none of the  $p$ - $y$  curves considered in this study has a capability to accurately predict the pile response in weakly cemented sand for a wide range of pile diameters. This is mainly because the pile diameter effect incorporated in all of these  $p$ - $y$  curves appeared to be too much for the weakly cemented soil tested at the site. In fact, experimental results shows that the pile diameter has insignificant effect on  $p$ - $y$  curves before the soil reached its ultimate soil pressure. Using the existing  $p$ - $y$  curves to predict the pile response in weakly cemented sand should be used with caution, especially for large diameter piles. If the soil condition considered in design is cemented sand with the SPT-N values of more than 40, using the proposed  $p$ - $y$  curves seems to be more appropriate, particularly for large diameter piles because it provides a lower bound estimate of pile response as compared to the use of existing  $p$ - $y$  curves. However, if the cemented sand considered in design has the SPT N-values below 40, the cemented sand  $p$ - $y$  curves proposed by Ismael (1990) may be used by incorporating higher factor of safety when design for large diameter piles.

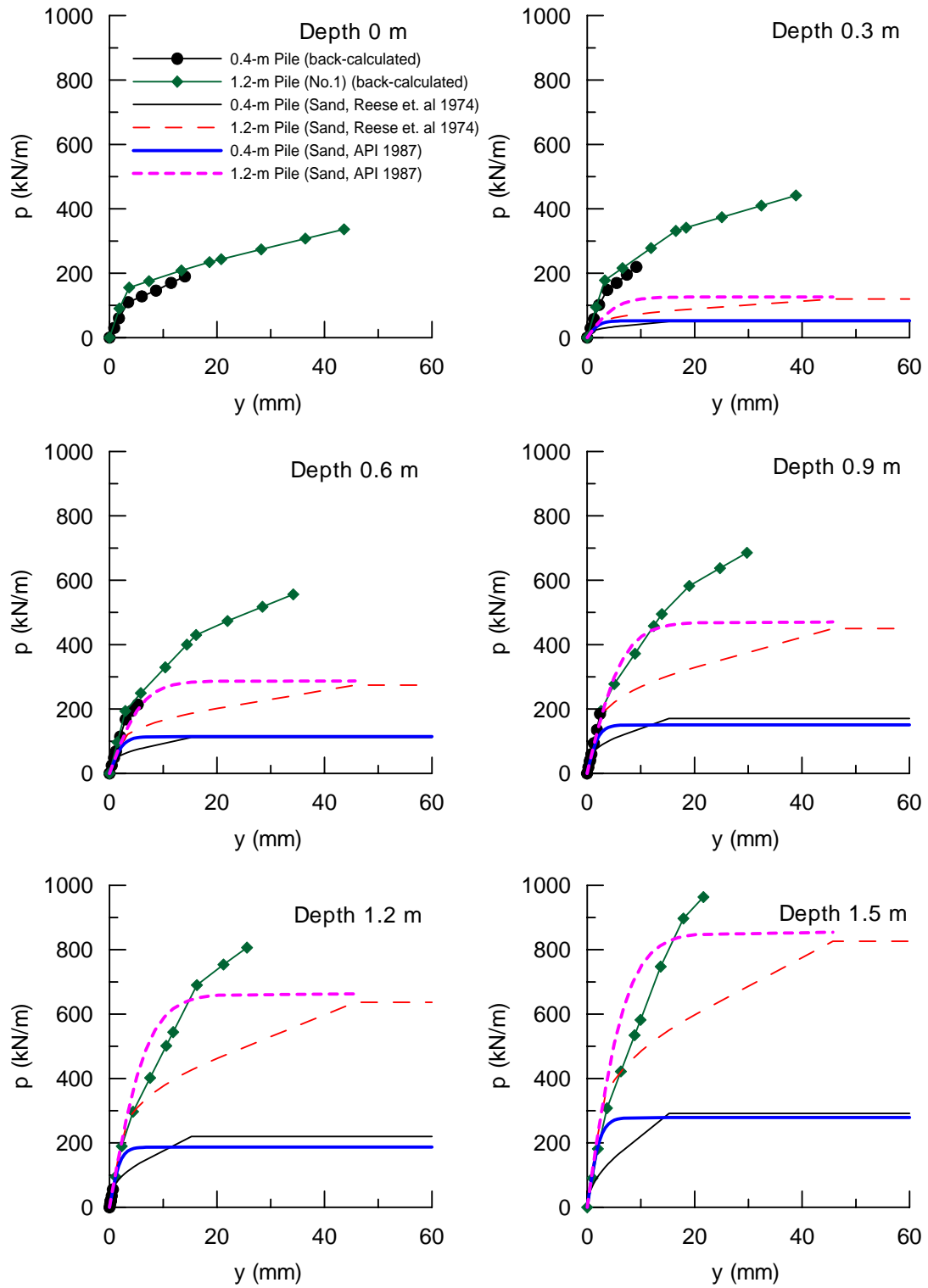


Figure 7.1 Comparison of Back-Calculated  $p$ - $y$  Curves with Sand  $p$ - $y$  Curves (Reese *et al* 1974; API 1987) for Depths 0 to 1.5 m

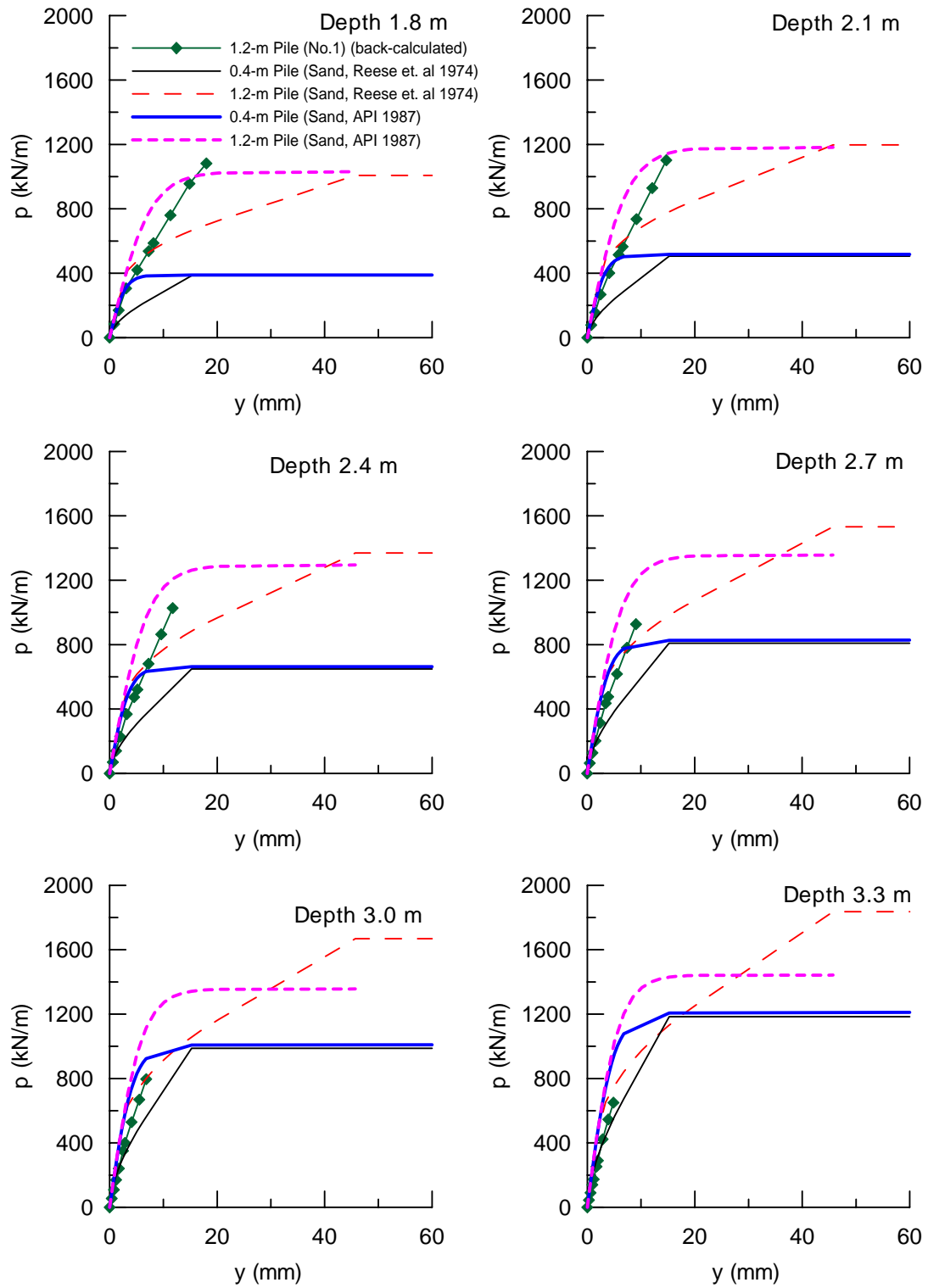


Figure 7.2 Comparison of Back-Calculated  $p$ - $y$  Curves with Sand  $p$ - $y$  Curves (Reese *et al* 1974; API 1987) for Depths 1.8 to 3.3 m

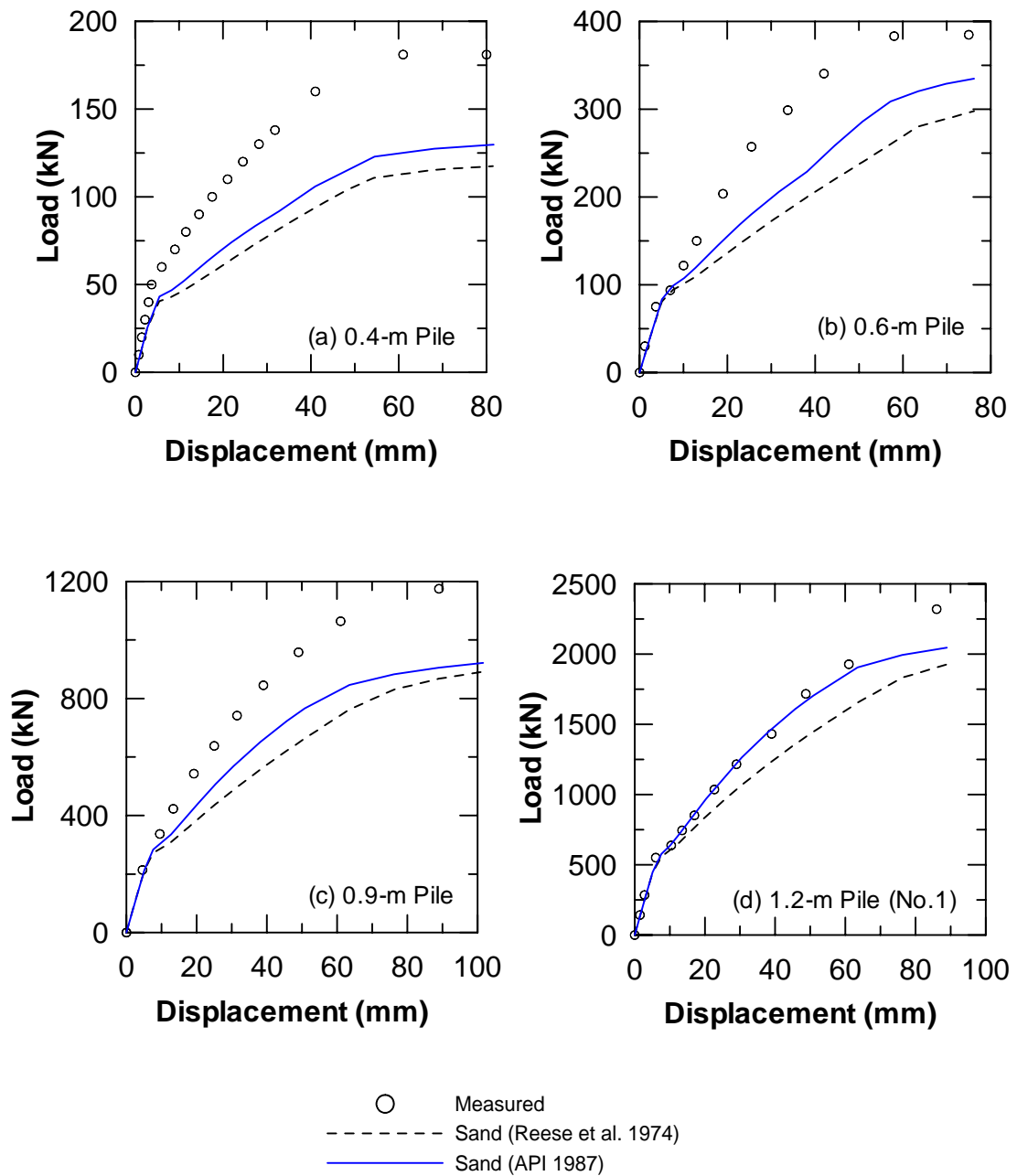


Figure 7.3 Computed Load-Displacement Curves using Sand  $p$ - $y$  Curves (Reese *et al* 1974; API 1987) Compared to Measured Response (a) 0.4-m Pile, (b) 0.6-m Pile, (c) 0.9-m Pile, and (d) 1.2-m Pile (Pile No.1)

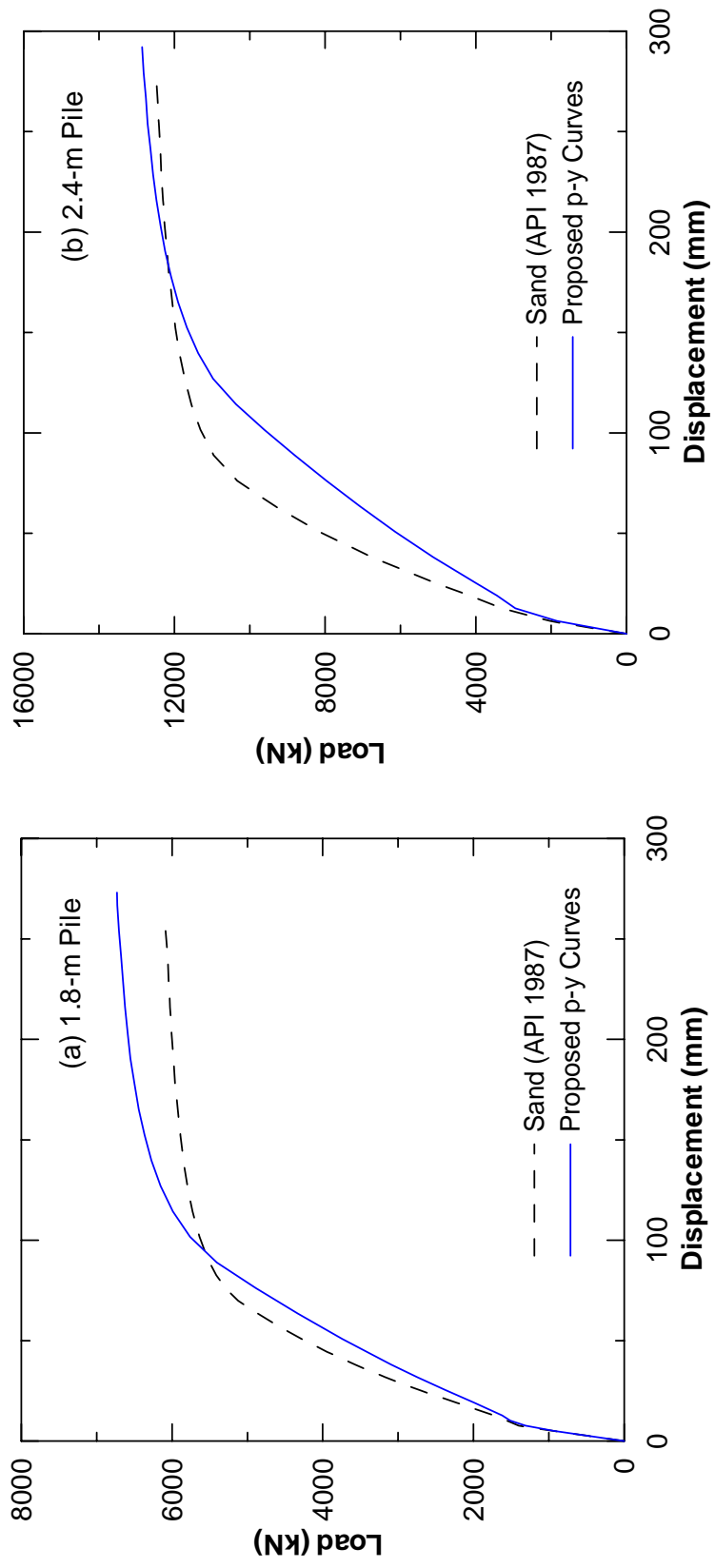


Figure 7.4 Comparison of Load-Displacement Curves using Sand  $p$ - $y$  Curves (API 1987) and Proposed  $p$ - $y$  Curves for (a) 1.8-m Pile, (b) 2.4-m Pile

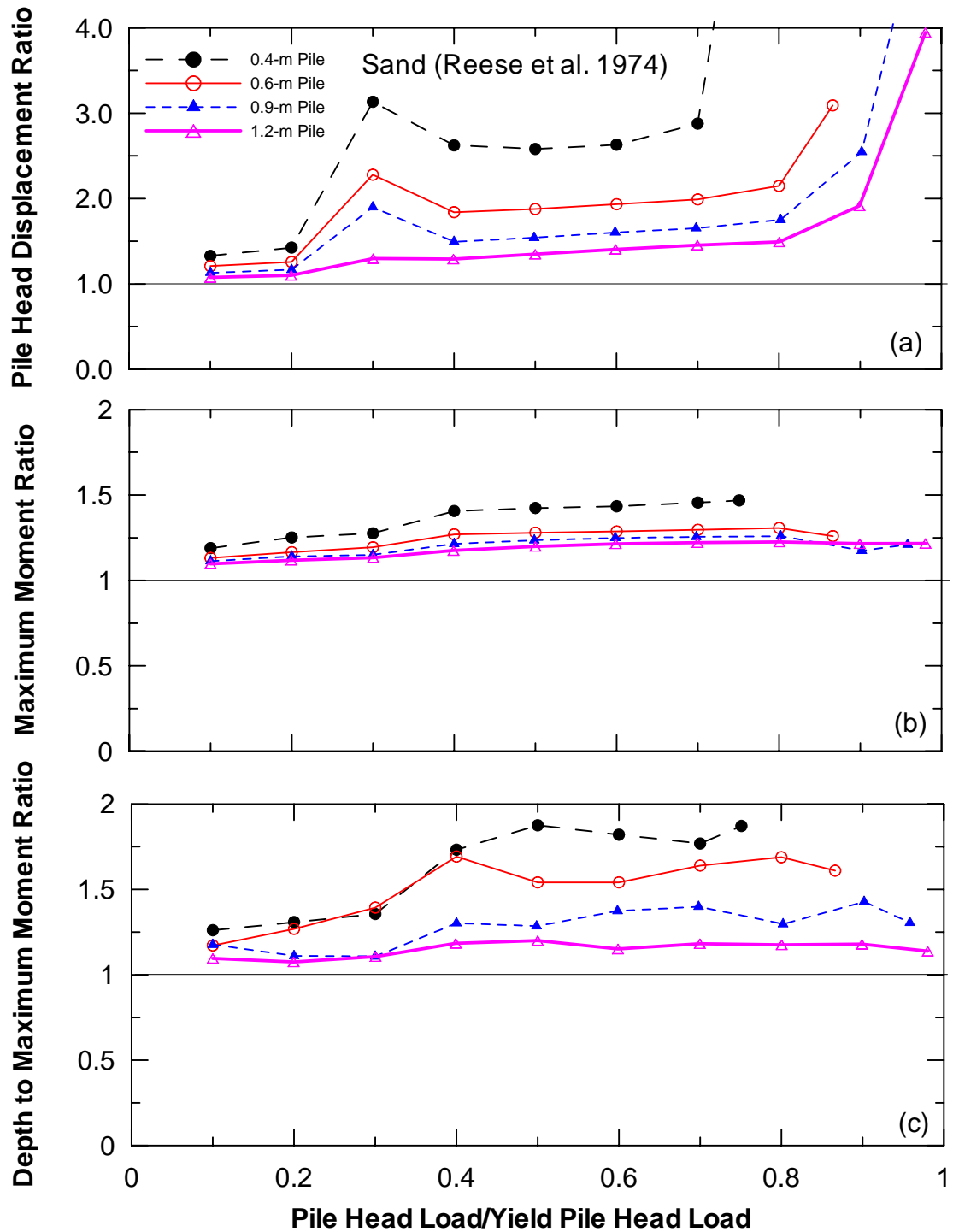


Figure 7.5 Predicted Pile Head Displacement, Maximum Moment, and Depth to Maximum Moment Using Sand  $p$ - $y$  Curves (Reese *et al.* 1974) Compared to Response Obtained Using Back-Calculated  $p$ - $y$  Curves for Different Pile Diameters (a) Pile Head Displacement, (b) Maximum Moment, and (c) Depth to Maximum Moment

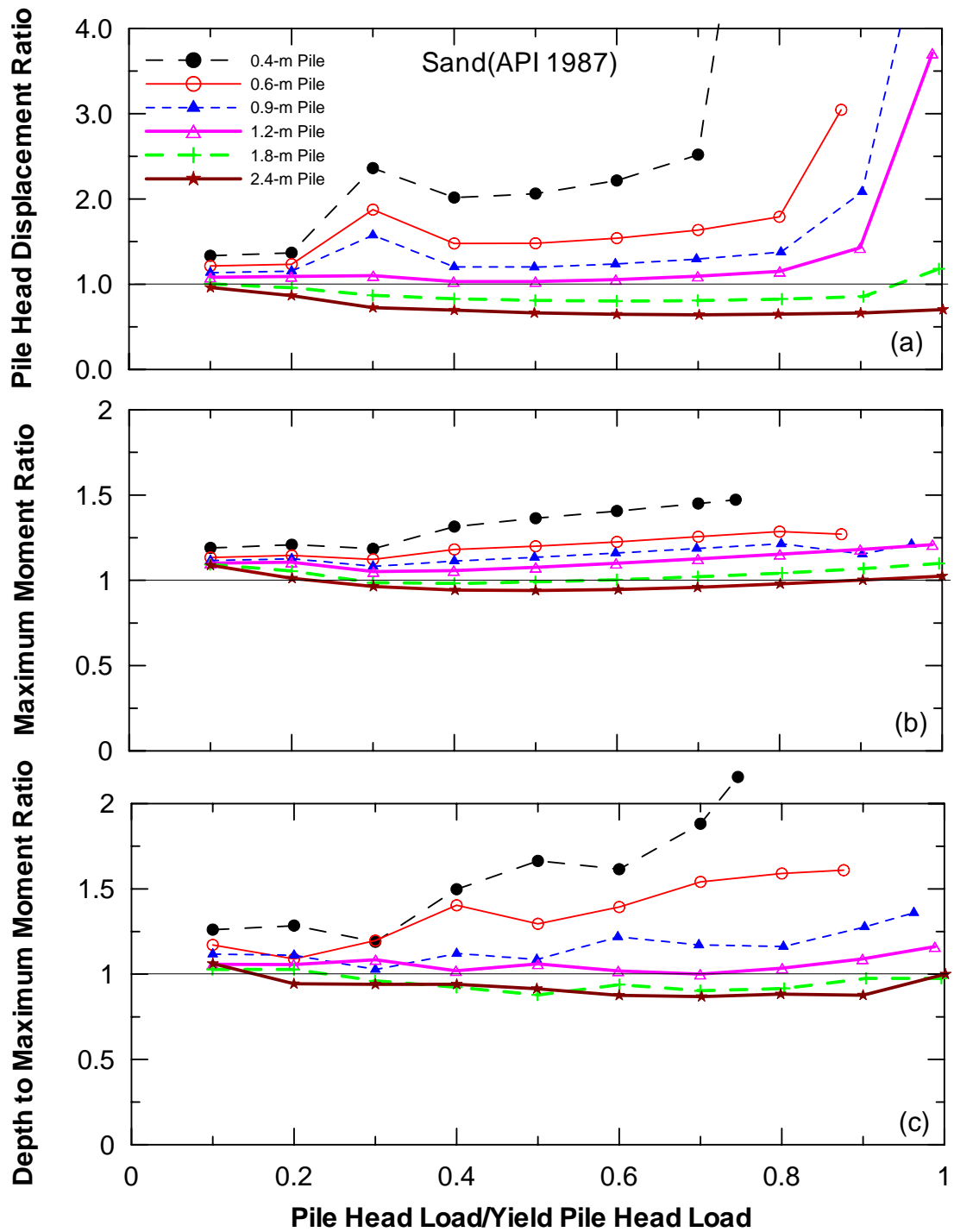


Figure 7.6 Predicted Pile Head Displacement, Maximum Moment, and Depth to Maximum Moment Using Sand  $p$ - $y$  Curves (API 1987) Compared to Response Obtained Using Back-Calculated  $p$ - $y$  Curves for Different Pile Diameters (a) Pile Head Displacement, (b) Maximum Moment, and (c) Depth to Maximum Moment

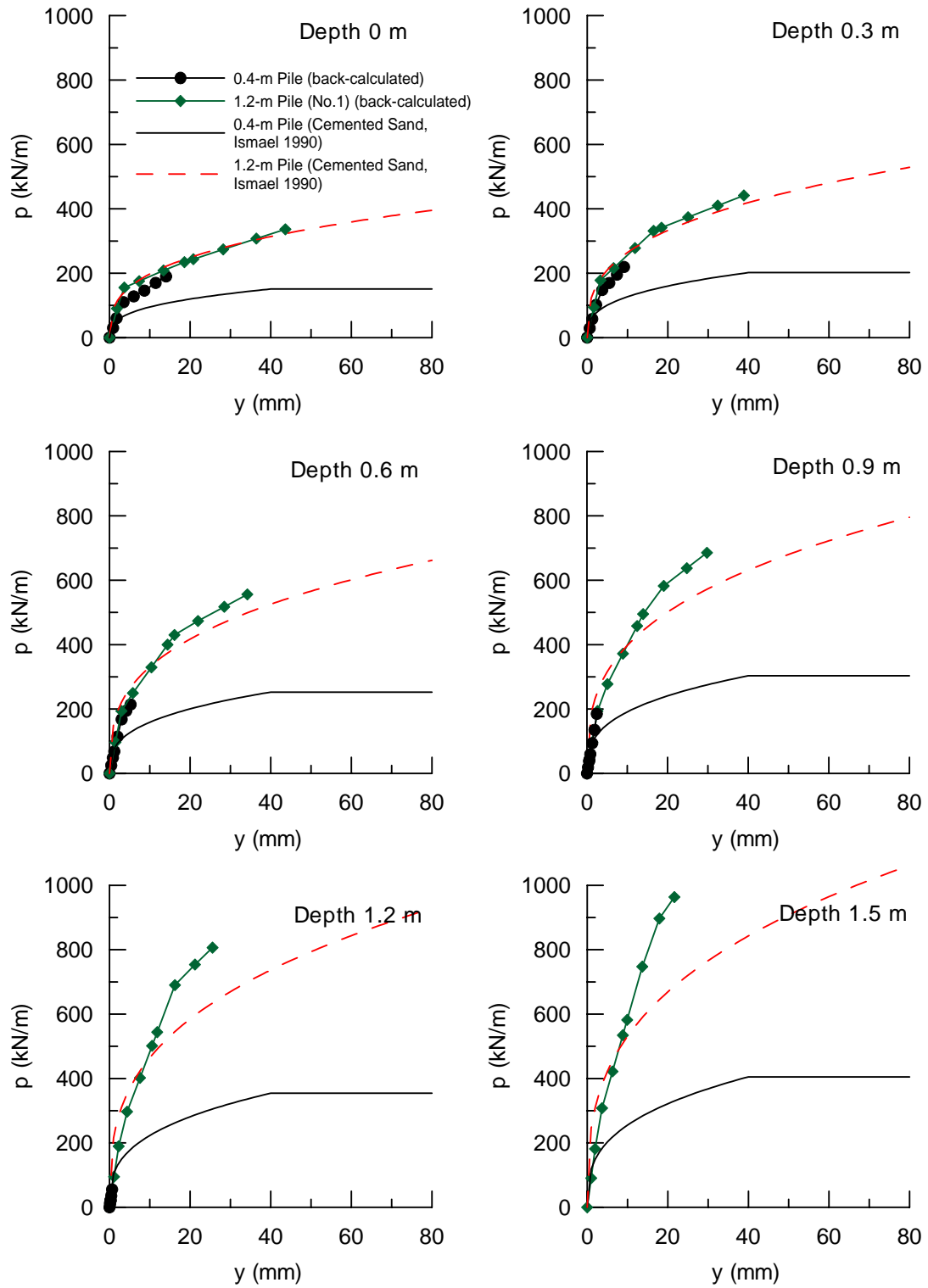


Figure 7.7 Comparison of Back-Calculated  $p$ - $y$  Curves with Cemented Sand  $p$ - $y$  Curves (Ismael 1990) for Depths 0 to 1.5 m

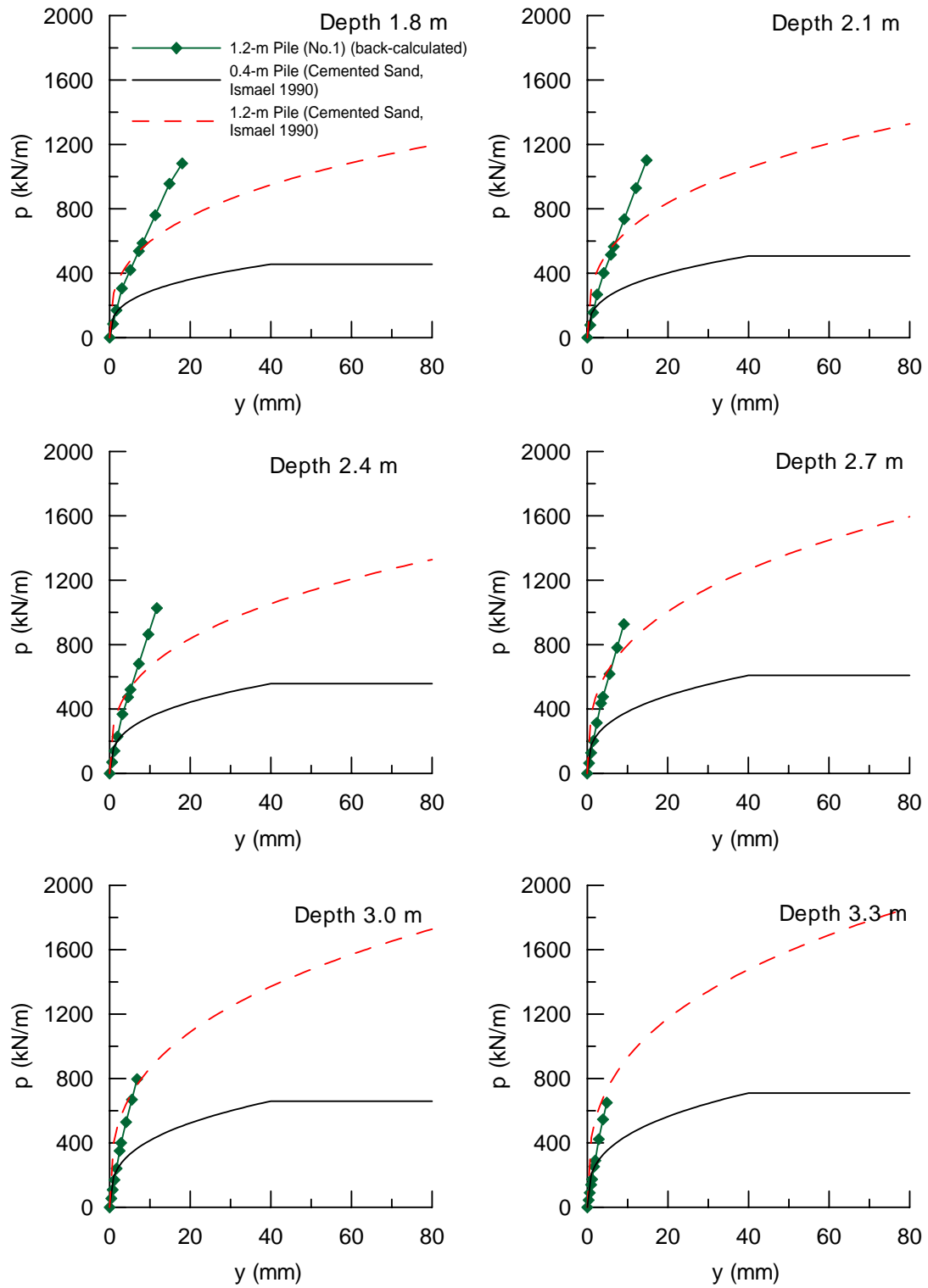


Figure 7.8 Comparison of Back-Calculated  $p$ - $y$  Curves with Cemented Sand  $p$ - $y$  Curves (Ismael 1990) for Depths 1.8 to 3.3 m

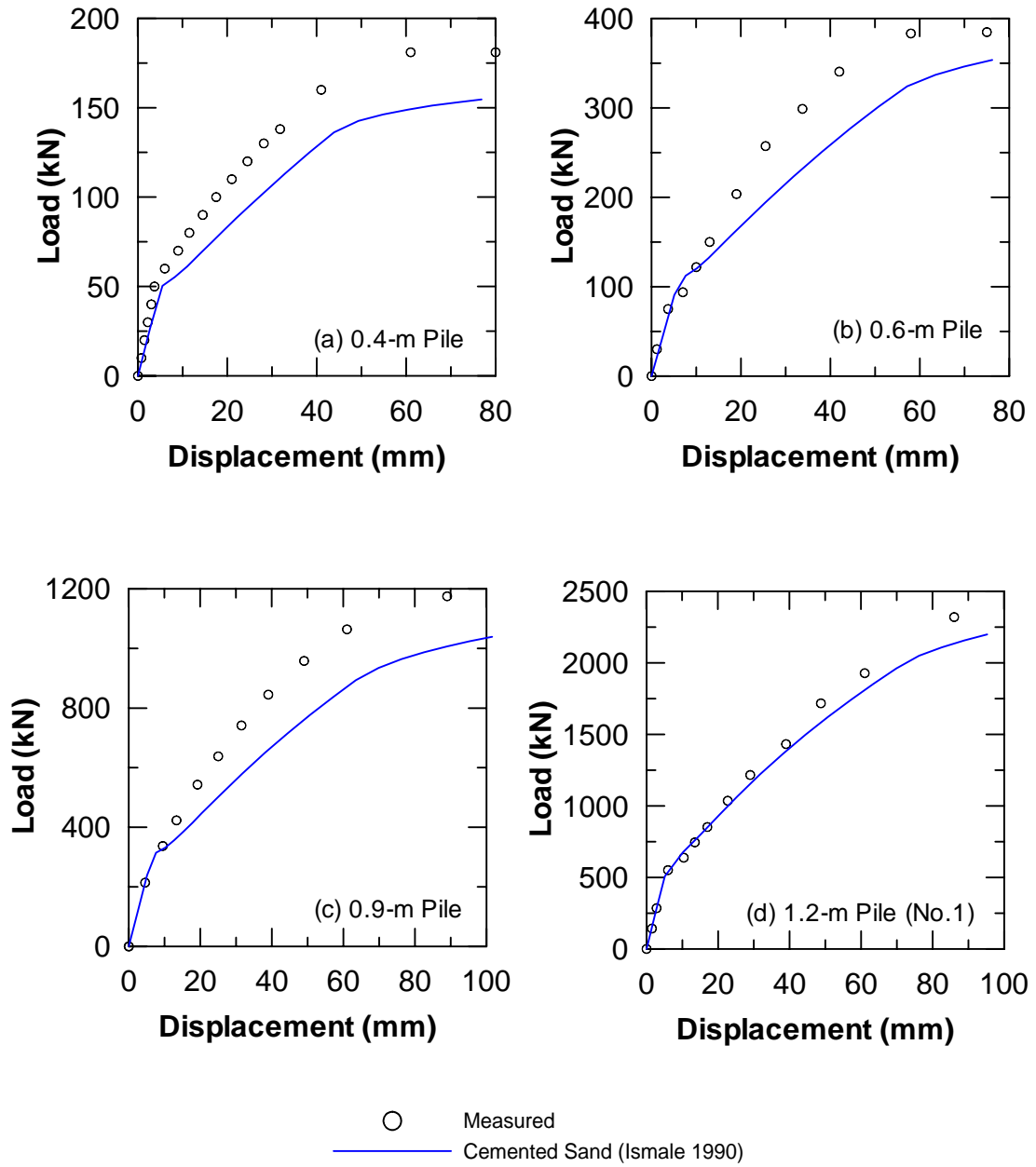


Figure 7.9 Computed Load-Displacement Curves using Cemented Sand  $p$ - $y$  Curves (Ismael 1990) Compared to Measured Response (a) 0.4-m Pile, (b) 0.6-m Pile, (c) 0.9-m Pile, and (d) 1.2-m Pile (Pile No.1)

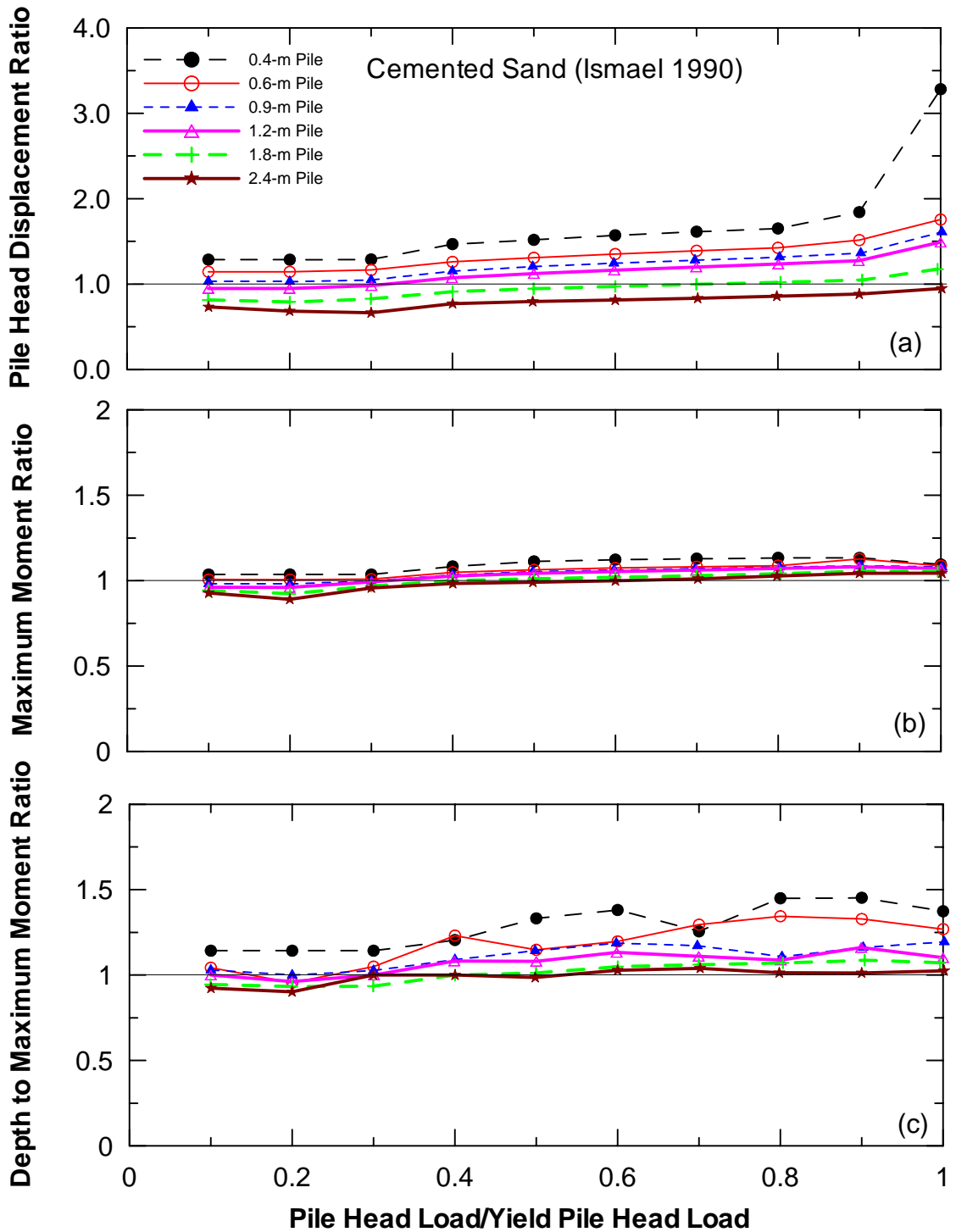


Figure 7.10 Predicted Pile Head Displacement, Maximum Moment, and Depth to Maximum Moment Using Cemented Sand  $p$ - $y$  Curves (Ismael 1990) Compared to Response Obtained Using Back-Calculated  $p$ - $y$  Curves for Different Pile Diameters (a) Pile Head Displacement, (b) Maximum Moment, and (c) Depth to Maximum Moment

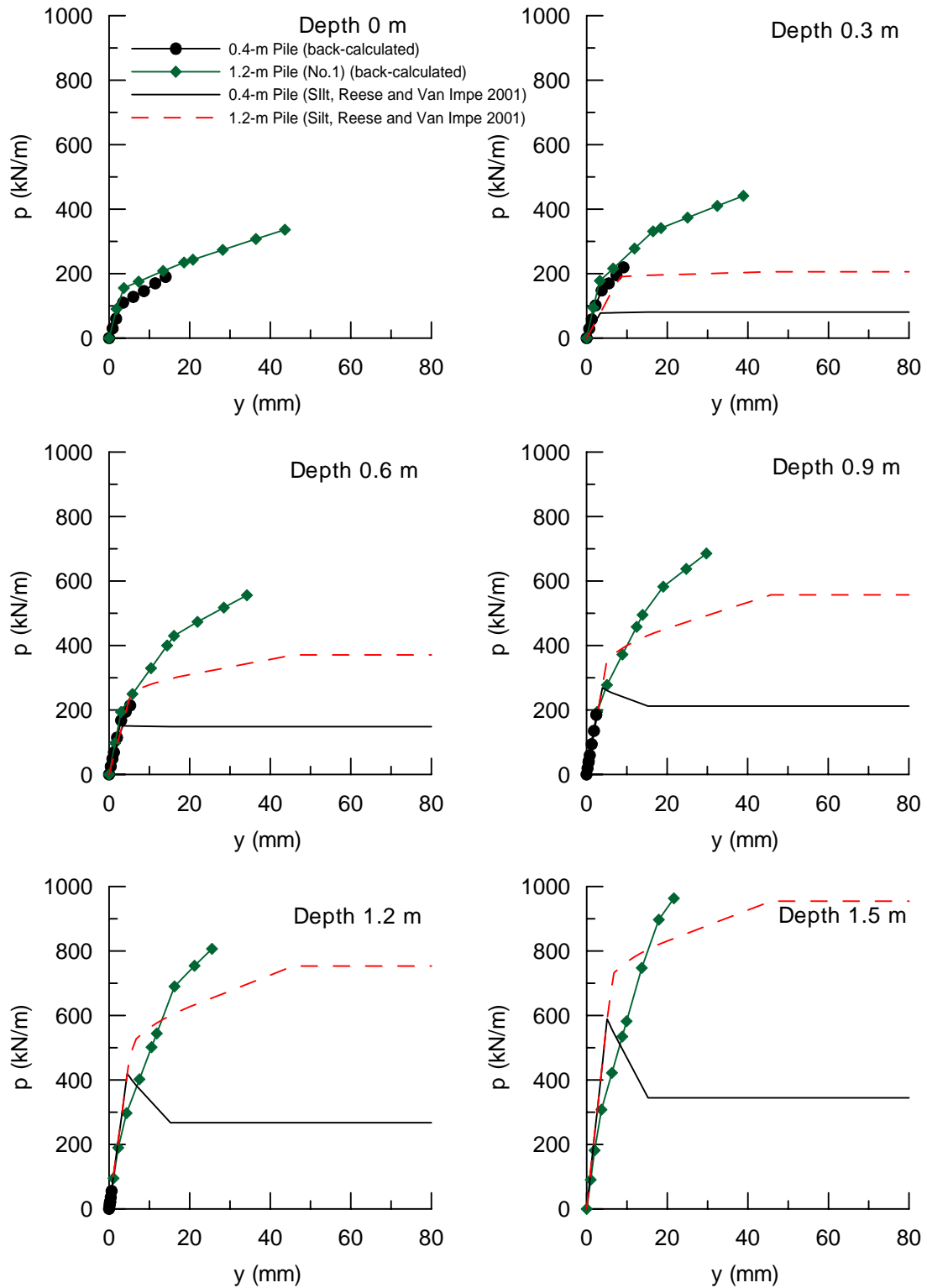


Figure 7.11 Comparison of Back-Calculated  $p$ - $y$  Curves with Silt  $p$ - $y$  Curves (Reese and Van Impe 2001) for Depths 0 to 1.5 m

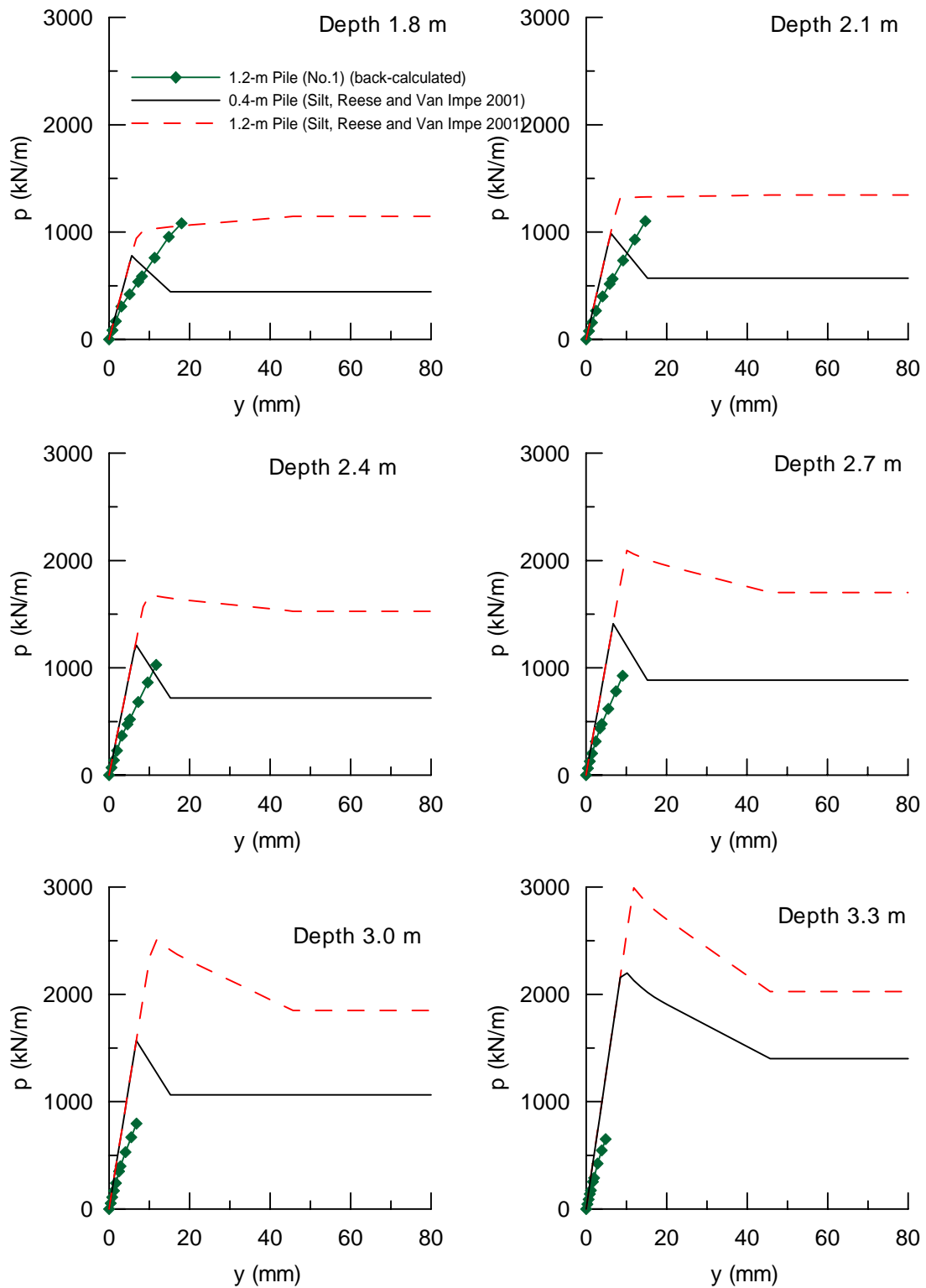


Figure 7.12 Comparison of Back-Calculated  $p$ - $y$  Curves with Silt  $p$ - $y$  Curves (Reese and Van Impe 2001) for Depths 1.8 to 3.3 m

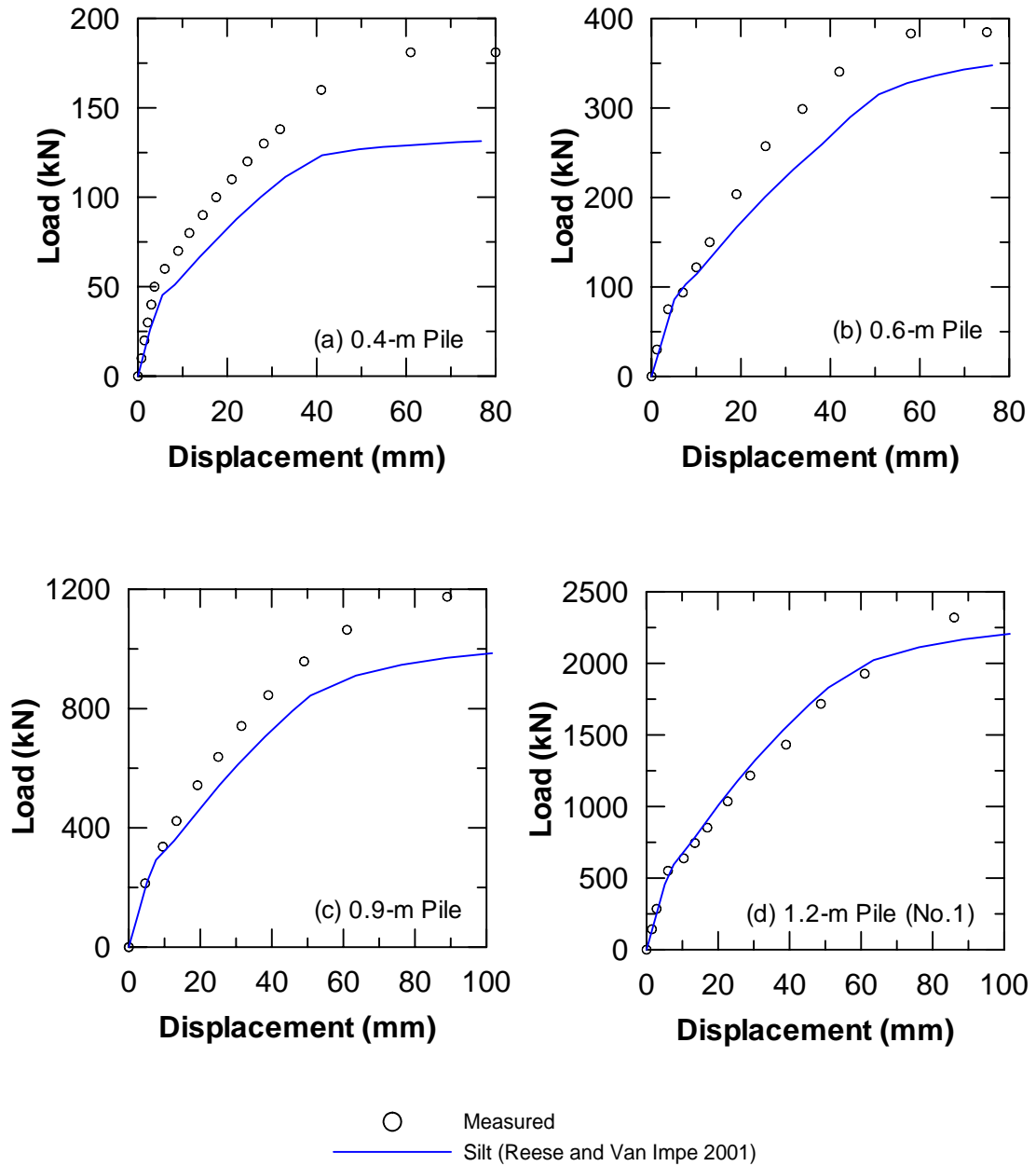


Figure 7.13 Computed Load-Displacement Curves using Silt  $p$ - $y$  Curves (Reese and Van Impe 2001) Compared to Measured Response (a) 0.4-m Pile, (b) 0.6-m Pile, (c) 0.9-m Pile, and (d) 1.2-m Pile (Pile No.1)

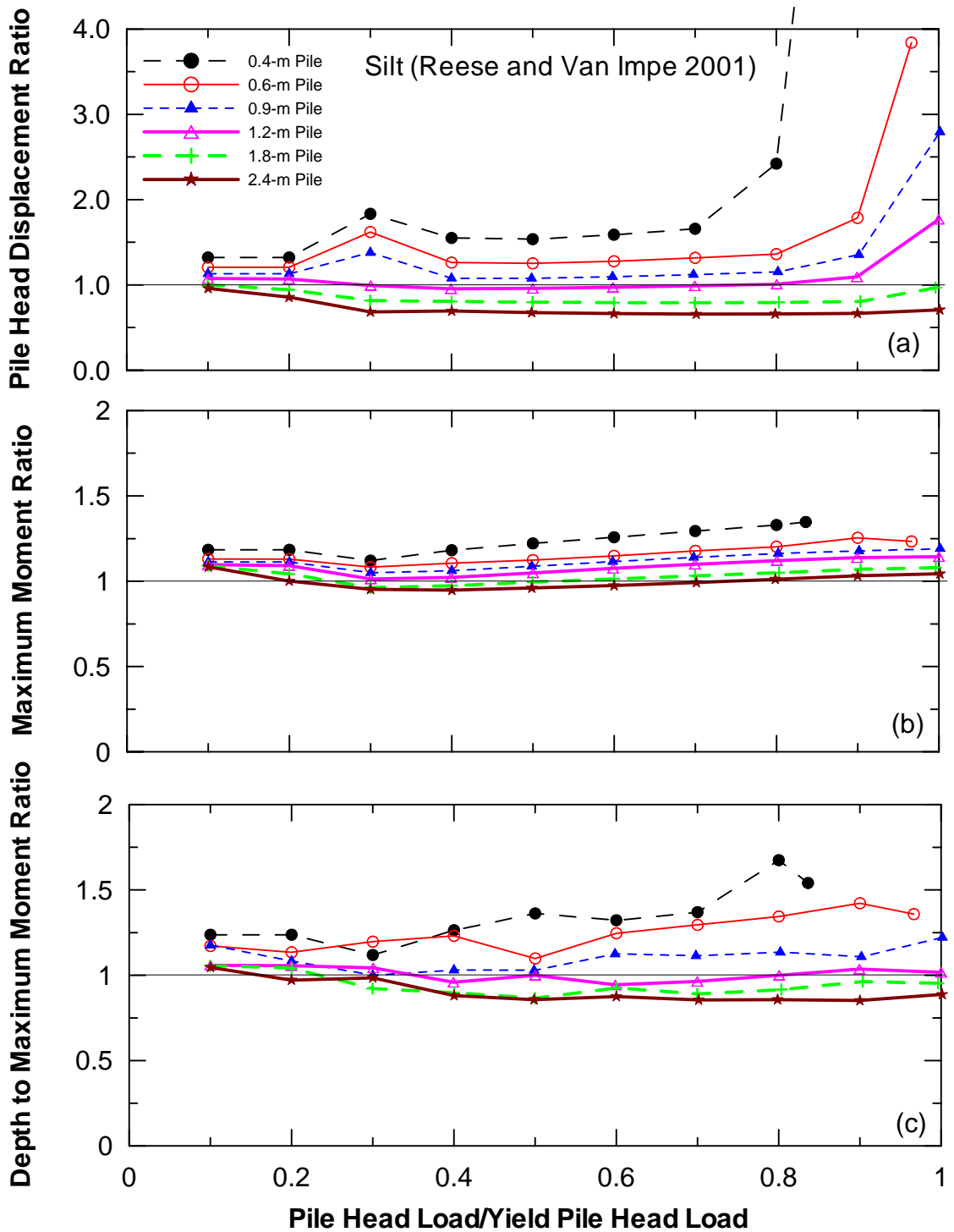


Figure 7.14 Predicted Pile Head Displacement, Maximum Moment, and Depth to Maximum Moment Using Silt  $p$ - $y$  Curves (Reese and Van Impe 2001) Compared to Response Obtained Using Back-Calculated  $p$ - $y$  Curves for Different Pile Diameters (a) Pile Head Displacement, (b) Maximum Moment, and (c) Depth to Maximum Moment

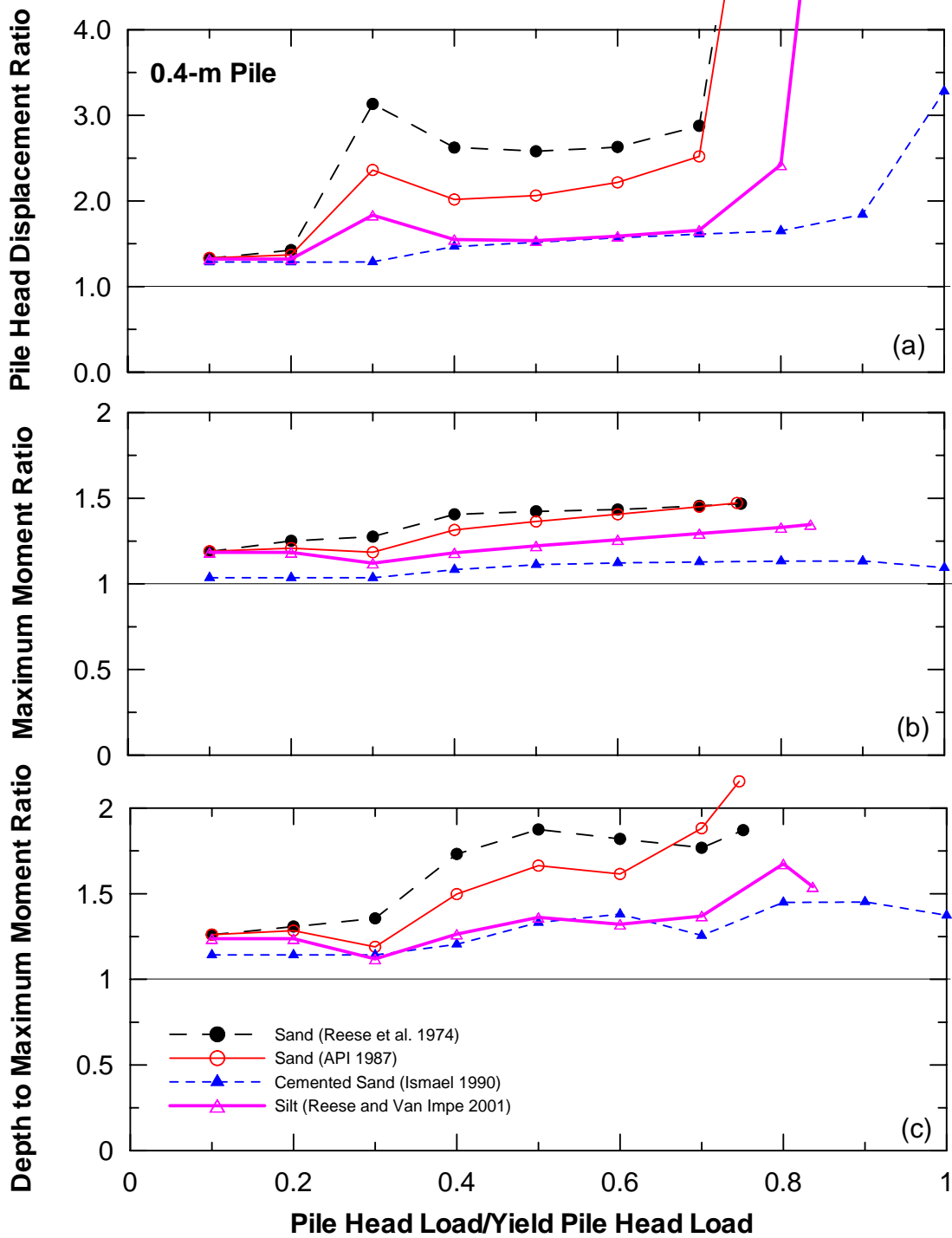


Figure 7.15 Predicted Pile Head Displacement, Maximum Moment, and Depth to Maximum Moment Using Existing  $p$ - $y$  Curves Compared to Response Obtained Using Back-Calculated  $p$ - $y$  Curves for 0.4-m Pile (a) Pile Head Displacement, (b) Maximum Moment, and (c) Depth to Maximum Moment

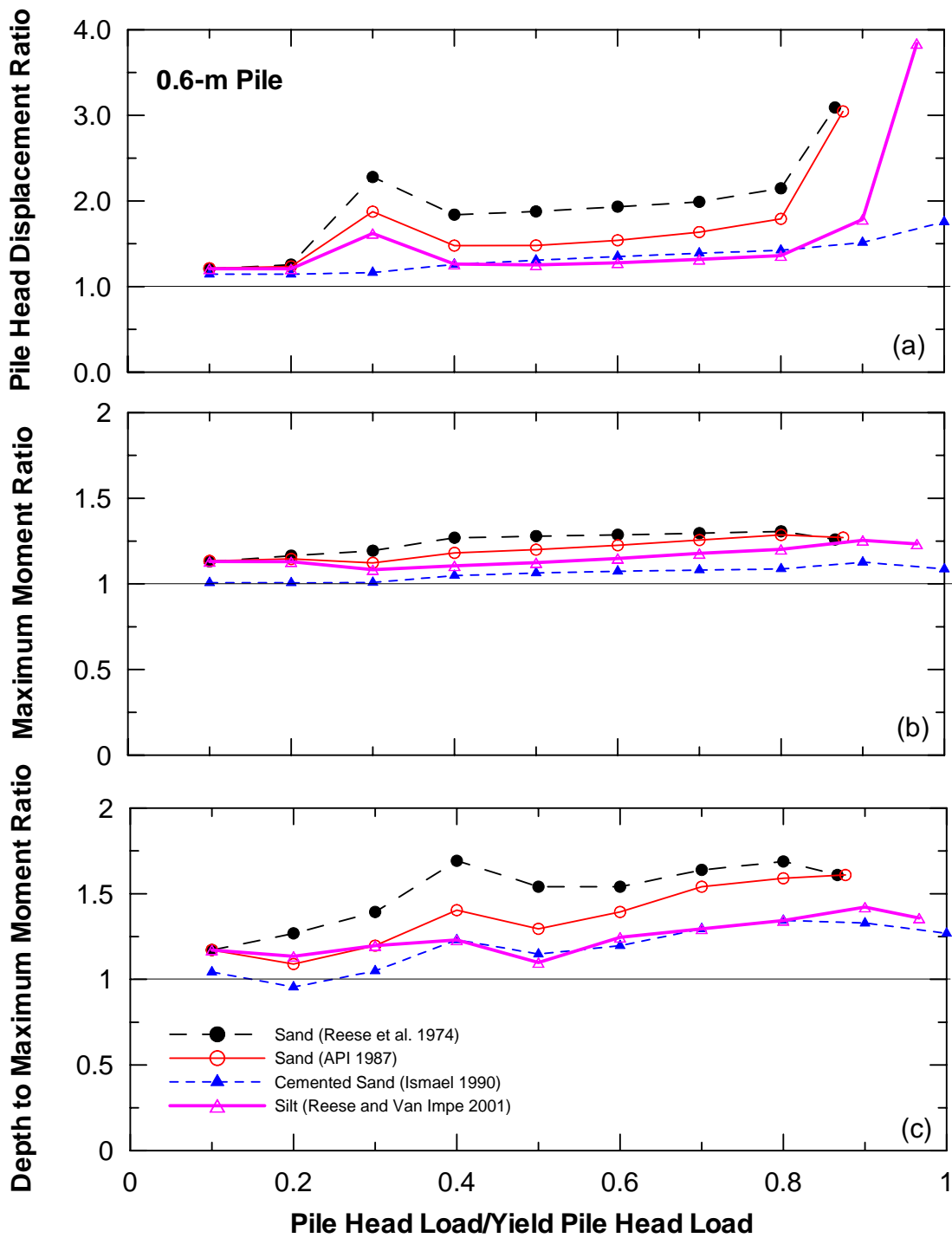


Figure 7.16 Predicted Pile Head Displacement, Maximum Moment, and Depth to Maximum Moment Using Existing  $p$ - $y$  Curves Compared to Response Obtained Using Back-Calculated  $p$ - $y$  Curves for 0.6-m Pile (a) Pile Head Displacement, (b) Maximum Moment, and (c) Depth to Maximum Moment

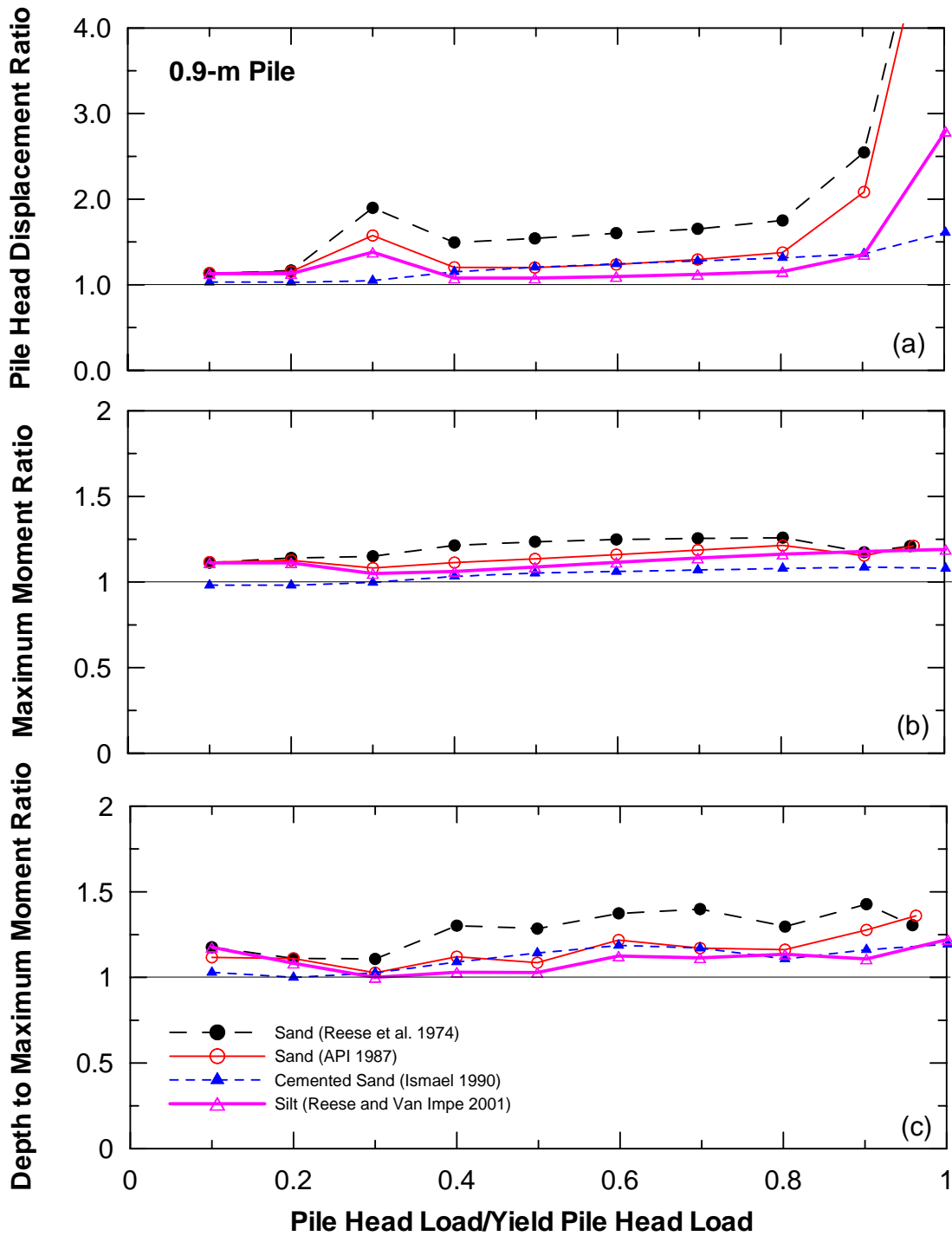


Figure 7.17 Predicted Pile Head Displacement, Maximum Moment, and Depth to Maximum Moment Using Existing  $p$ - $y$  Curves Compared to Response Obtained Using Back-Calculated  $p$ - $y$  Curves for 0.9-m Pile (a) Pile Head Displacement, (b) Maximum Moment, and (c) Depth to Maximum Moment

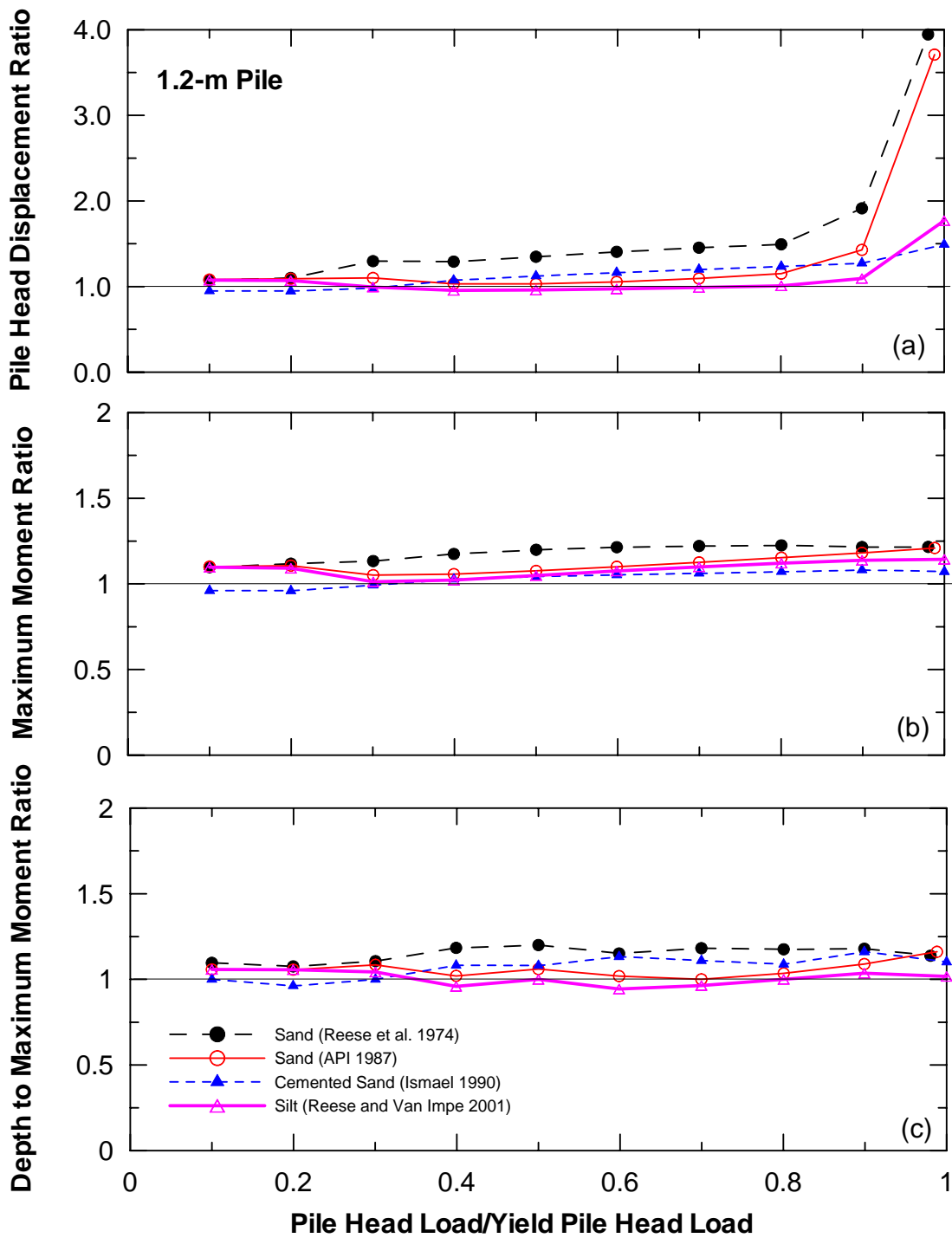


Figure 7.18 Predicted Pile Head Displacement, Maximum Moment, and Depth to Maximum Moment Using Existing  $p$ - $y$  Curves Compared to Response Obtained Using Back-Calculated  $p$ - $y$  Curves for 1.2-m Pile (a) Pile Head Displacement, (b) Maximum Moment, and (c) Depth to Maximum Moment

This page is intentionally blank.

## Chapter 8 SUMMARY AND CONCLUSIONS

### 8.1 Summary

The effect of pile diameter on modulus of subgrade reaction (i.e., the stiffness of the  $p$ - $y$  curves) was investigated in this study. The study included the analytical study on the effect of pile diameter on the pile response in homogeneous soil using 3-D finite element analyses with both linear and nonlinear soil models. This was followed by the evaluation of pile diameter effect using the results from the full-scale lateral pile load tests. Cast-In-Drilled-Holes (CIDH) piles with various diameters ranging from 0.4 m to 1.2 m were installed in dense weakly cemented sand and tested under both vibration and lateral load testing. The results of vibration tests were utilized to evaluate the effect of pile diameter on the initial modulus of subgrade reaction, while the results from static lateral load tests were used to back-calculate the  $p$ - $y$  curves. The back-calculated  $p$ - $y$  curves for each pile diameter were then compared to evaluate the pile diameter effect at larger displacement levels. In addition to the study of pile diameter effect, the enhancement of seismic performance of CIDH piles due to the effect of external confinement from the soil was evaluated using cyclic lateral load tests.

### 8.2 Conclusions

The main findings of this research study on the effect of pile diameter on the  $p$ - $y$  curves based on both experimental and analytical results are provided as the followings:

- The results from 3-D finite element analysis using linear soil model showed that the pile diameter has some effect on the modulus of the subgrade reaction, but this effect appears to be insignificant, particularly when taking into account the effect of increasing of pile stiffness with the pile diameter.

Furthermore, soil nonlinearity tends to increase the pile diameter effect on the pile response.

- The analyses based on vibration test results showed that pile diameter has very small effect on initial modulus of subgrade reaction.
- Based on the back-calculated  $p$ - $y$  curves of various pile diameters, it was found that the pile diameter has insignificant effect on the  $p$ - $y$  curves at the displacement level below the ultimate soil resistance. Beyond this range, the ultimate soil resistance increases as the pile diameter increases.
- Using the standard  $p$ - $y$  curves currently available in the literature underestimates the soil resistance in weakly cemented sand for small diameter piles, but tends to overestimate the soil resistance to large diameter piles. Therefore, the use of these standard  $p$ - $y$  curves for large diameter piles in weakly cemented sand should be used with caution.
- The proposed methodology for developing  $p$ - $y$  curves for weakly cemented sand are simple and appears to be appropriate to use for cemented sand along the coast of Southern California with the SPT  $N$ -values of above 40.
- Results from the cyclic lateral pile load tests showed that only moderate level of transverse reinforcement (0.6%) can provide adequate seismic performance with the displacement ductility of more than 5 because the external confinement from the soil considerably enhances inelastic behavior of CIDH piles. The confinement effect of the soil at the test site was estimated to be equivalent to the additional amount of transverse reinforcement of 0.7%
- The results from lateral load tests show that the depth of plastic hinge ranges from 1.5D for the 0.4-m pile to 2.5D for the 1.2-m pile, which is in the range of typical values assumed in design (Budek 1997). The magnitude of moment becomes negligible at depth below 6D for all pile diameters tested.

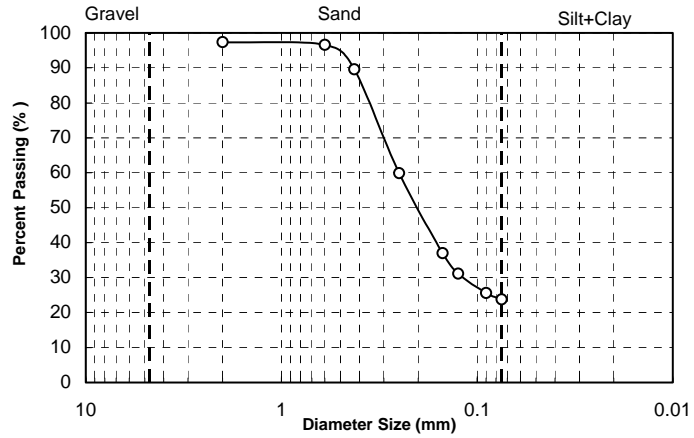
## **APPENDIX A**

THIS PAGE LEFT BLANK

## Grain Size Distribution

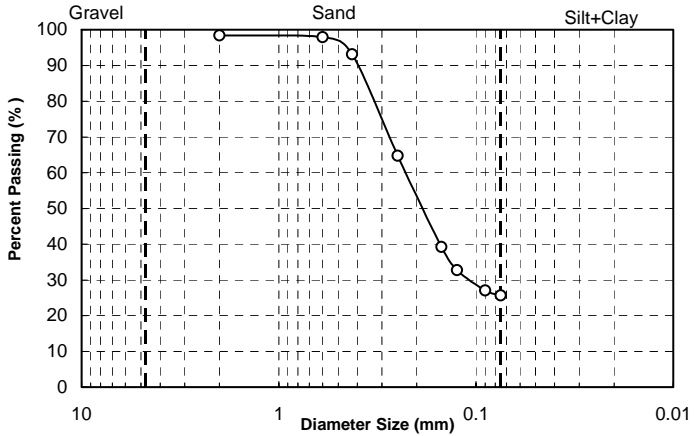
Location : East Campus  
 Borehole : BH-1  
 Sample No : S-1  
 Depth : 1.52-1.98 m

Sieve No.	Sieve Size (mm)	Passing %
# 10	2.000	97.4
# 30	0.600	96.6
# 40	0.425	89.6
# 60	0.250	59.9
# 100	0.150	37.0
# 120	0.125	31.2
# 170	0.090	25.6
# 200	0.075	23.8
USCS	SM	



Location : East Campus  
 Borehole : BH-1  
 Sample No : S-2  
 Depth : 3.05-3.51 m

Sieve No.	Sieve Size (mm)	Passing %
# 10	2.000	98.4
# 30	0.600	97.9
# 40	0.425	93.2
# 60	0.250	64.7
# 100	0.150	39.2
# 120	0.125	32.8
# 170	0.090	27.0
# 200	0.075	25.7
USCS	SM	



Location : East Campus  
 Borehole : BH-1  
 Sample No : S-3  
 Depth : 4.57-5.03 m

Sieve No.	Sieve Size (mm)	Passing %
# 10	2.000	99.5
# 30	0.600	98.8
# 40	0.425	94.9
# 60	0.250	75.0
# 100	0.150	54.4
# 120	0.125	48.0
# 170	0.090	41.7
# 200	0.075	40.0
USCS	SC	

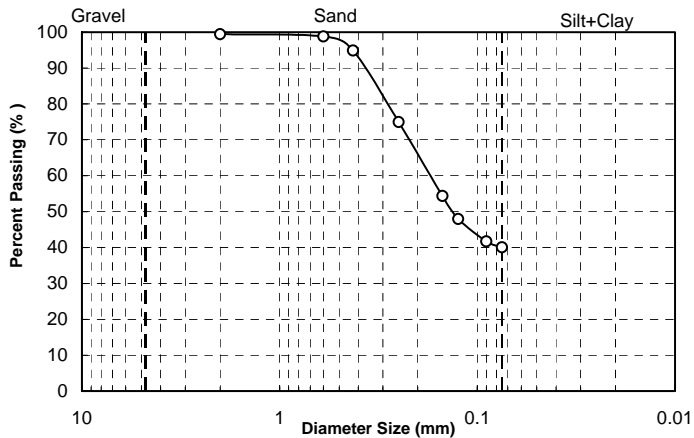
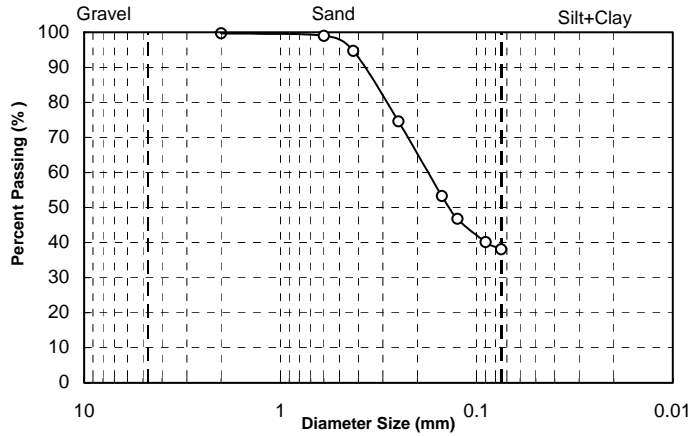


Figure A-1 Results of Gradation Analysis (Borehole BH-1)

## Grain Size Distribution

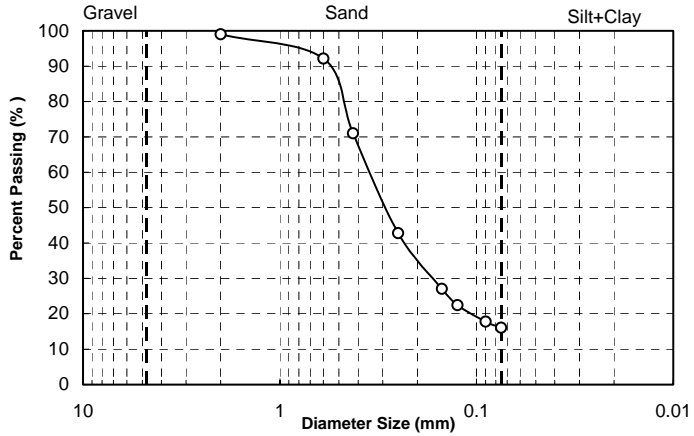
Location : East Campus  
 Borehole : BH-1  
 Sample No : S-4  
 Depth : 6.10-6.55 m

Sieve No.	Sieve Size (mm)	Passing %
# 10	2.000	99.7
# 30	0.600	99.0
# 40	0.425	94.7
# 60	0.250	74.6
# 100	0.150	53.2
# 120	0.125	46.8
# 170	0.090	40.1
# 200	0.075	38.1
USCS	SM	



Location : East Campus  
 Borehole : BH-1  
 Sample No : S-5  
 Depth : 7.62-8.08 m

Sieve No.	Sieve Size (mm)	Passing %
# 10	2.000	99.0
# 30	0.600	92.2
# 40	0.425	71.1
# 60	0.250	42.8
# 100	0.150	27.1
# 120	0.125	22.4
# 170	0.090	17.8
# 200	0.075	16.1
USCS	SM	



Location : East Campus  
 Borehole : BH-1  
 Sample No : S-6  
 Depth : 9.14-9.61 m

Sieve No.	Sieve Size (mm)	Passing %
# 10	2.000	97.9
# 30	0.600	90.0
# 40	0.425	66.0
# 60	0.250	37.4
# 100	0.150	24.9
# 120	0.125	21.2
# 170	0.090	16.9
# 200	0.075	15.4
USCS	SC	

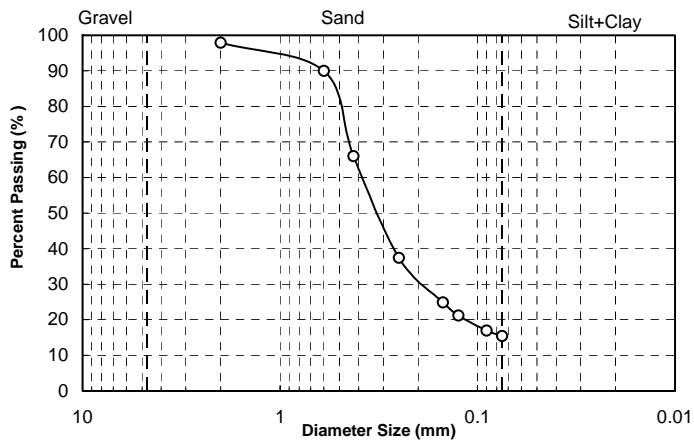
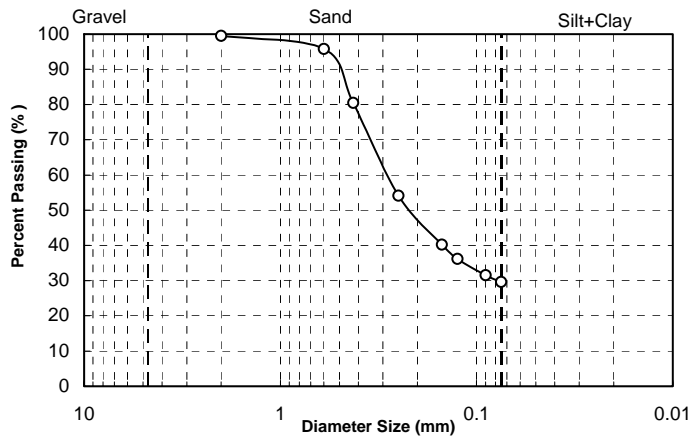


Figure A-2 Results of Gradation Analysis (Borehole BH-1, Continued)

## Grain Size Distribution

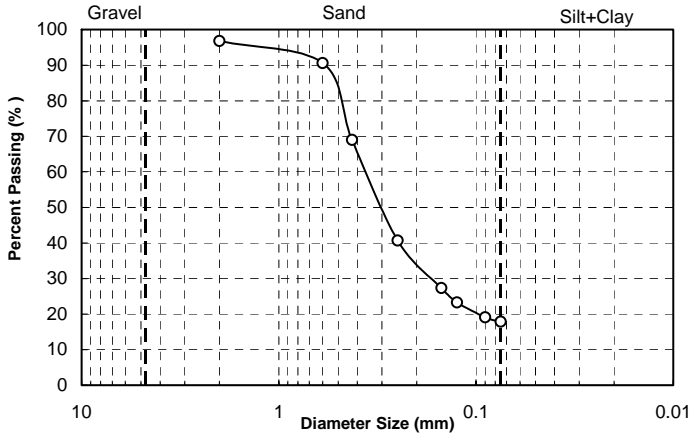
Location : East Campus  
 Borehole : BH-1  
 Sample No : S-7  
 Depth : 10.67-11.13 m

Sieve No.	Sieve Size (mm)	Passing %
# 10	2.000	99.5
# 30	0.600	95.8
# 40	0.425	80.5
# 60	0.250	54.2
# 100	0.150	40.3
# 120	0.125	36.2
# 170	0.090	31.5
# 200	0.075	29.6
USCS	SC	



Location : East Campus  
 Borehole : BH-1  
 Sample No : S-8  
 Depth : 12.19-12.65 m

Sieve No.	Sieve Size (mm)	Passing %
# 10	2.000	96.8
# 30	0.600	90.6
# 40	0.425	69.0
# 60	0.250	40.7
# 100	0.150	27.3
# 120	0.125	23.3
# 170	0.090	19.1
# 200	0.075	17.9
USCS	SC	



Location : East Campus  
 Borehole : BH-1  
 Sample No : S-9  
 Depth : 13.72-14.17 m

Sieve No.	Sieve Size (mm)	Passing %
# 10	2.000	95.9
# 30	0.600	90.6
# 40	0.425	75.9
# 60	0.250	56.1
# 100	0.150	45.1
# 120	0.125	41.5
# 170	0.090	36.9
# 200	0.075	35.3
USCS	SC	

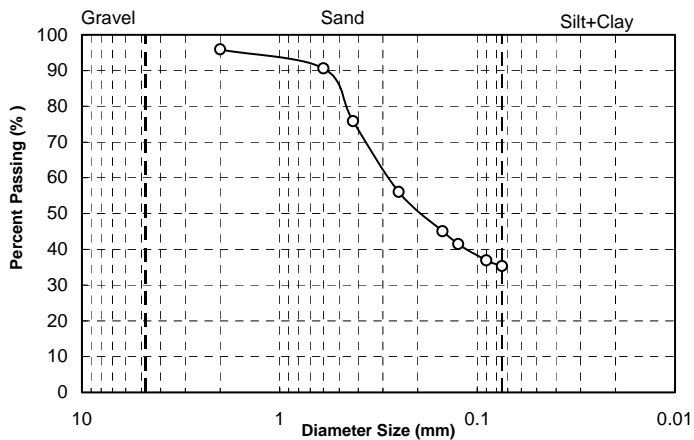
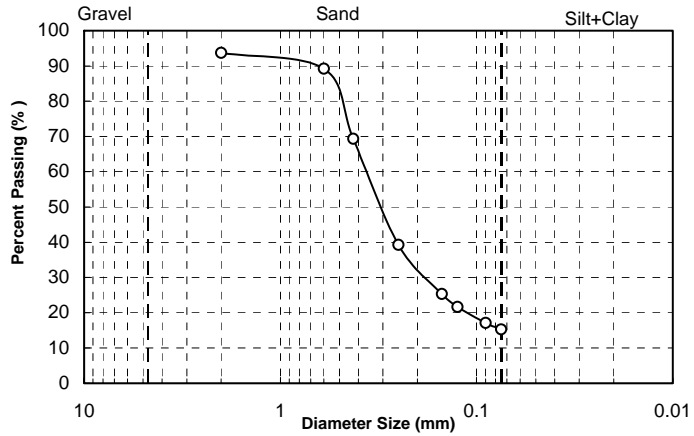


Figure A-3 Results of Gradation Analysis (Borehole BH-1, Continued)

## Grain Size Distribution

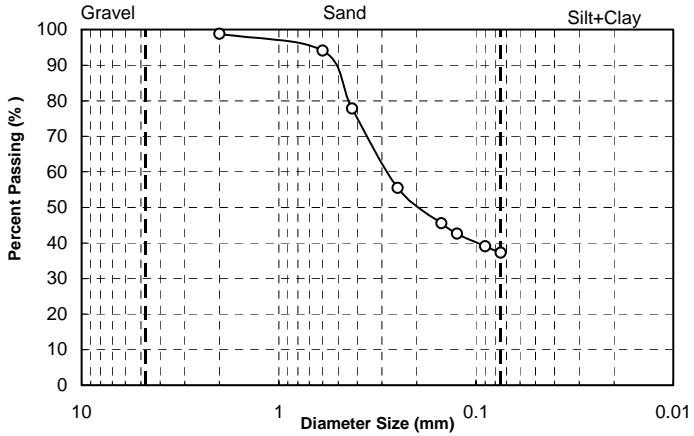
Location : East Campus  
 Borehole : BH-1  
 Sample No : S-11 (Bottom)  
 Depth : 16.76-17.22 m

Sieve No.	Sieve Size (mm)	Passing %
# 10	2.000	93.7
# 30	0.600	89.2
# 40	0.425	69.3
# 60	0.250	39.2
# 100	0.150	25.3
# 120	0.125	21.6
# 170	0.090	17.1
# 200	0.075	15.3
USCS	SM	



Location : East Campus  
 Borehole : BH-1  
 Sample No : S-12 (Top)  
 Depth : 19.81-20.27 m

Sieve No.	Sieve Size (mm)	Passing %
# 10	2.000	98.8
# 30	0.600	94.1
# 40	0.425	77.8
# 60	0.250	55.5
# 100	0.150	45.5
# 120	0.125	42.6
# 170	0.090	39.1
# 200	0.075	37.3
USCS	SM	



Location : East Campus  
 Borehole : BH-1  
 Sample No : S-12 (Bottom)  
 Depth : 19.81-20.27 m

Sieve No.	Sieve Size (mm)	Passing %
# 10	2.000	99.5
# 30	0.600	96.3
# 40	0.425	84.6
# 60	0.250	64.6
# 100	0.150	51.9
# 120	0.125	47.6
# 170	0.090	41.4
# 200	0.075	38.4
USCS	SM	

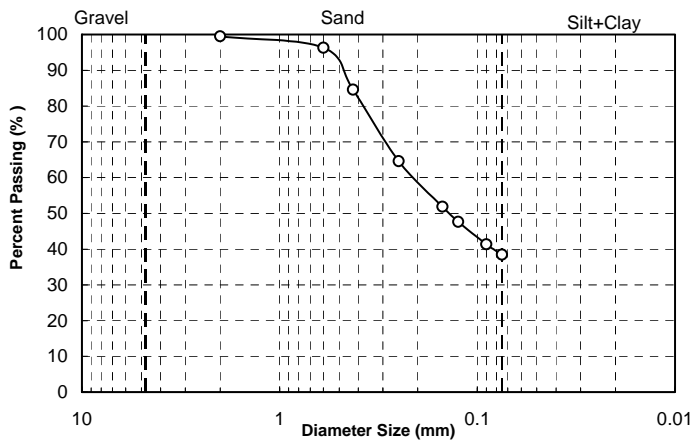
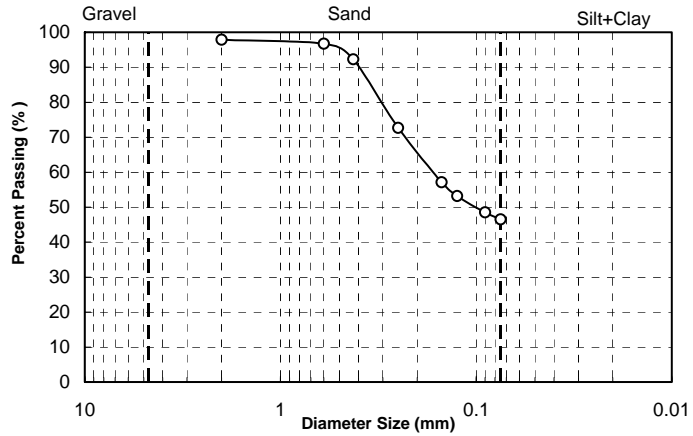


Figure A-4 Results of Gradation Analysis (Borehole BH-1, Continued)

## Grain Size Distribution

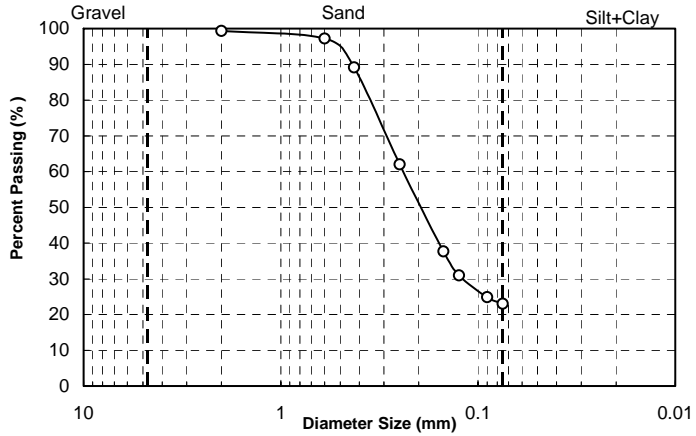
Location : East Campus  
 Borehole : BH-2  
 Sample No : S-1  
 Depth : 1.52-1.98 m

Sieve No.	Sieve Size (mm)	Passing %
# 10	2.000	97.9
# 30	0.600	96.8
# 40	0.425	92.3
# 60	0.250	72.7
# 100	0.150	57.2
# 120	0.125	53.2
# 170	0.090	48.5
# 200	0.075	46.5
USCS	SC	



Location : East Campus  
 Borehole : BH-2  
 Sample No : S-2  
 Depth : 3.05-3.51 m

Sieve No.	Sieve Size (mm)	Passing %
# 10	2.000	99.4
# 30	0.600	97.2
# 40	0.425	89.1
# 60	0.250	62.0
# 100	0.150	37.6
# 120	0.125	30.9
# 170	0.090	24.9
# 200	0.075	23.0
USCS	SM	



Location : East Campus  
 Borehole : BH-2  
 Sample No : S-3  
 Depth : 4.57-5.03 m

Sieve No.	Sieve Size (mm)	Passing %
# 10	2.000	99.0
# 30	0.600	90.0
# 40	0.425	68.4
# 60	0.250	42.4
# 100	0.150	28.3
# 120	0.125	24.0
# 170	0.090	19.6
# 200	0.075	18.3
USCS	SM	

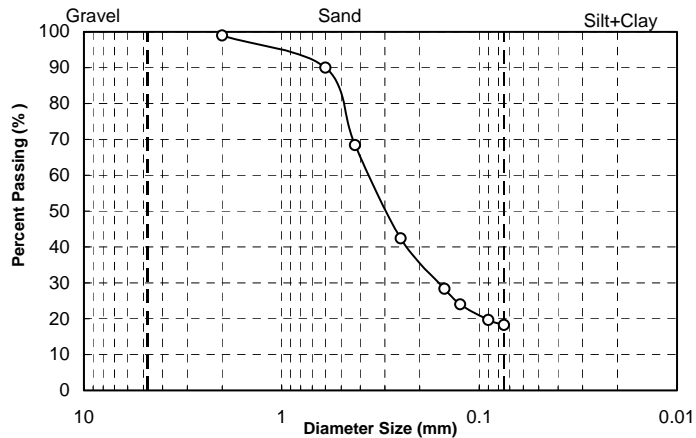
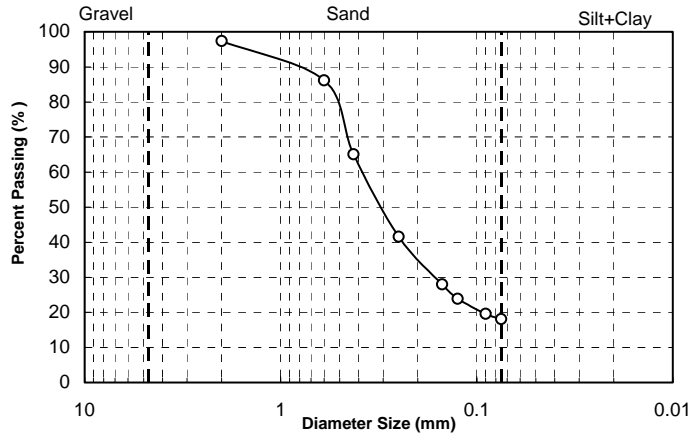


Figure A-5 Results of Gradation Analysis (Borehole BH-2)

## Grain Size Distribution

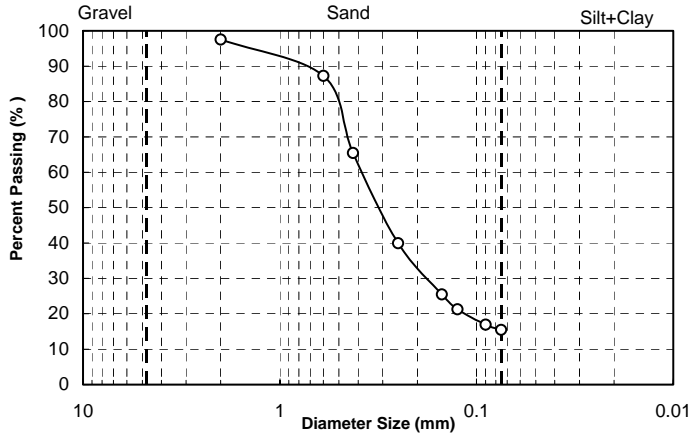
Location : East Campus  
 Borehole : BH-2  
 Sample No : S-4  
 Depth : 6.10-6.55 m

Sieve No.	Sieve Size (mm)	Passing %
# 10	2.000	97.4
# 30	0.600	86.2
# 40	0.425	65.1
# 60	0.250	41.6
# 100	0.150	28.0
# 120	0.125	23.9
# 170	0.090	19.6
# 200	0.075	18.1
USCS	SM	



Location : East Campus  
 Borehole : BH-2  
 Sample No : S-5  
 Depth : 7.62-8.08 m

Sieve No.	Sieve Size (mm)	Passing %
# 10	2.000	97.6
# 30	0.600	87.2
# 40	0.425	65.5
# 60	0.250	39.9
# 100	0.150	25.5
# 120	0.125	21.2
# 170	0.090	16.9
# 200	0.075	15.5
USCS	SM	



Location : East Campus  
 Borehole : BH-2  
 Sample No : S-6  
 Depth : 9.14-9.61 m

Sieve No.	Sieve Size (mm)	Passing %
# 10	2.000	98.1
# 30	0.600	91.3
# 40	0.425	70.7
# 60	0.250	43.5
# 100	0.150	29.2
# 120	0.125	25.1
# 170	0.090	20.6
# 200	0.075	18.8
USCS	SM	

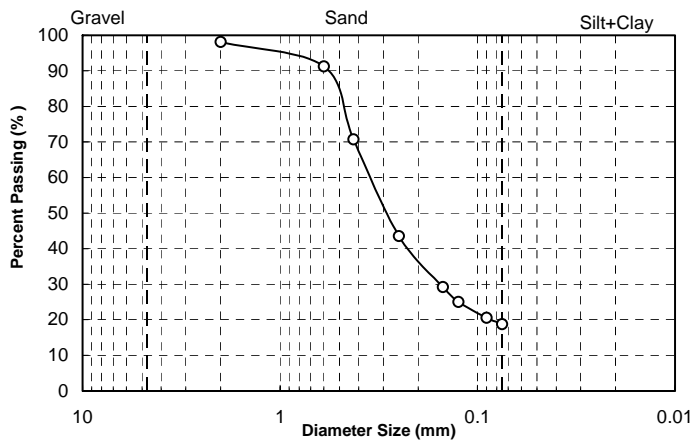
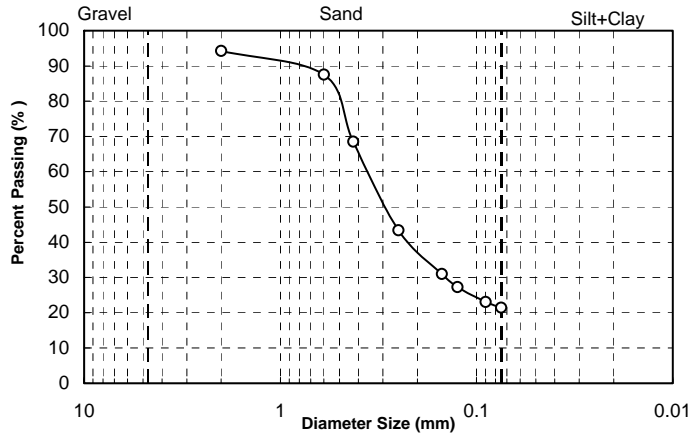


Figure A-6 Results of Gradation Analysis (Borehole BH-2, Continued)

## Grain Size Distribution

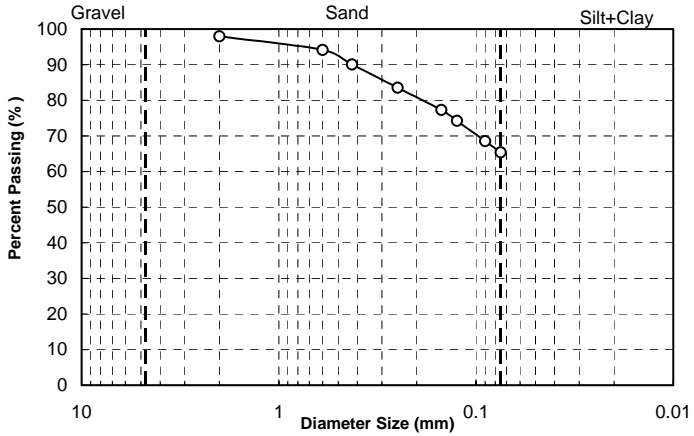
Location : East Campus  
 Borehole : BH-2  
 Sample No : S-7  
 Depth : 10.67-11.13 m

Sieve No.	Sieve Size (mm)	Passing %
# 10	2.000	94.3
# 30	0.600	87.5
# 40	0.425	68.5
# 60	0.250	43.4
# 100	0.150	31.0
# 120	0.125	27.3
# 170	0.090	23.1
# 200	0.075	21.5
USCS	SM	



Location : East Campus  
 Borehole : BH-2  
 Sample No : S-8  
 Depth : 12.19-12.65 m

Sieve No.	Sieve Size (mm)	Passing %
# 10	2.000	98.0
# 30	0.600	94.2
# 40	0.425	90.1
# 60	0.250	83.6
# 100	0.150	77.3
# 120	0.125	74.2
# 170	0.090	68.5
# 200	0.075	65.4
USCS	ML	



Location : East Campus  
 Borehole : BH-2  
 Sample No : S-9  
 Depth : 13.72-14.17 m

Sieve No.	Sieve Size (mm)	Passing %
# 10	2.000	84.8
# 30	0.600	83.6
# 40	0.425	81.7
# 60	0.250	77.5
# 100	0.150	74.0
# 120	0.125	72.7
# 170	0.090	70.1
# 200	0.075	68.2
USCS	ML	

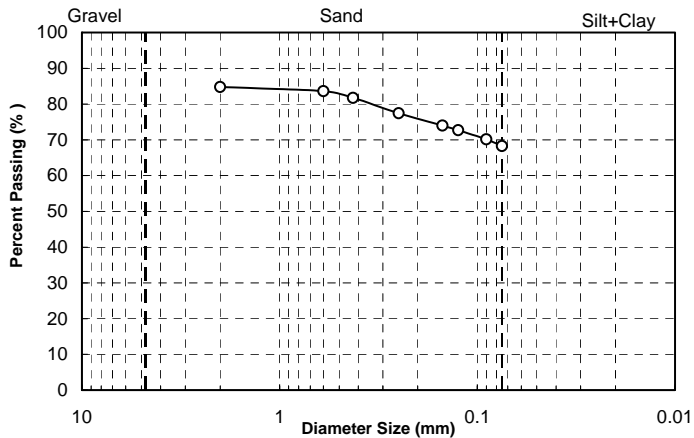
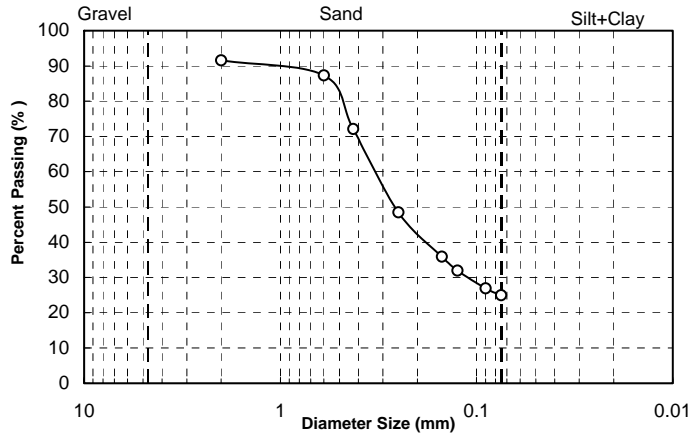


Figure A-7 Results of Gradation Analysis (Borehole BH-2, Continued)

## Grain Size Distribution

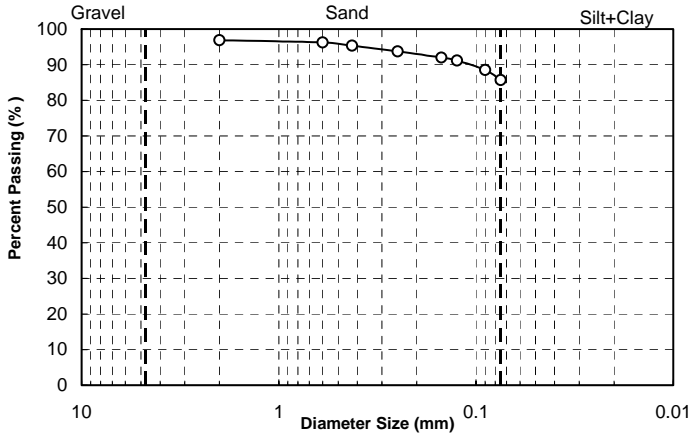
Location : East Campus  
 Borehole : BH-2  
 Sample No : S-10 (Middle)  
 Depth : 15.24-15.70 m

Sieve No.	Sieve Size (mm)	Passing %
# 10	2.000	91.6
# 30	0.600	87.3
# 40	0.425	72.1
# 60	0.250	48.4
# 100	0.150	35.9
# 120	0.125	32.0
# 170	0.090	26.9
# 200	0.075	25.0
USCS	SM	



Location : East Campus  
 Borehole : BH-2  
 Sample No : S-10 (Bottom)  
 Depth : 15.24-15.70 m

Sieve No.	Sieve Size (mm)	Passing %
# 10	2.000	96.9
# 30	0.600	96.3
# 40	0.425	95.4
# 60	0.250	93.7
# 100	0.150	92.0
# 120	0.125	91.2
# 170	0.090	88.5
# 200	0.075	85.7
USCS	ML	



Location : East Campus  
 Borehole : BH-2  
 Sample No : S-11 (Bottom)  
 Depth : 16.76-17.22 m

Sieve No.	Sieve Size (mm)	Passing %
# 10	2.000	90.8
# 30	0.600	89.5
# 40	0.425	88.2
# 60	0.250	86.5
# 100	0.150	84.9
# 120	0.125	84.3
# 170	0.090	82.9
# 200	0.075	81.5
USCS	ML	

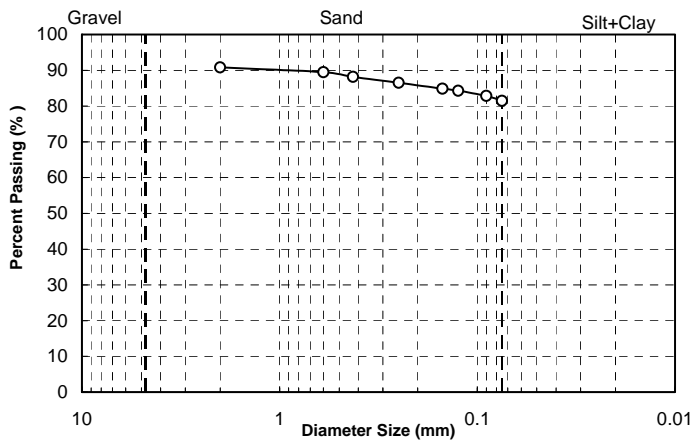
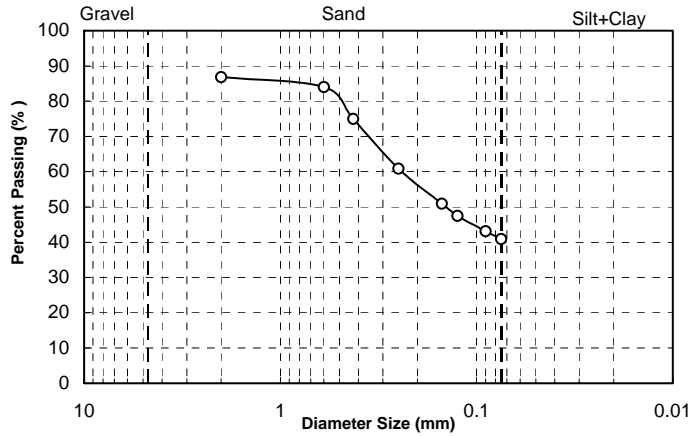


Figure A-8 Results of Gradation Analysis (Borehole BH-2, Continued)

## Grain Size Distribution

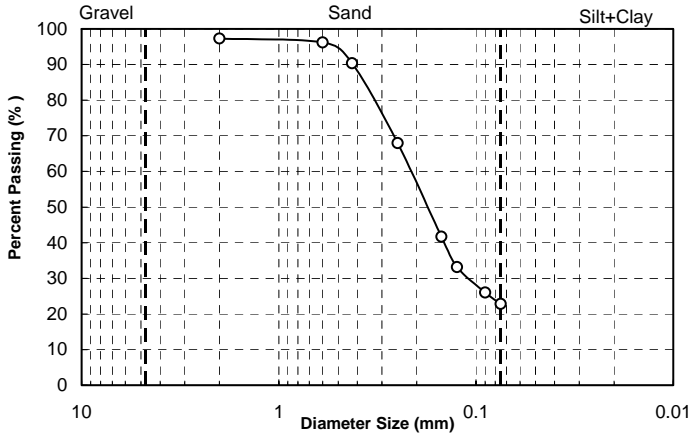
Location : East Campus  
 Borehole : BH-2  
 Sample No : S-12 (Bottom)  
 Depth : 18.29-18.75 m

Sieve No.	Sieve Size (mm)	Passing %
# 10	2.000	86.8
# 30	0.600	84.0
# 40	0.425	75.0
# 60	0.250	60.9
# 100	0.150	50.9
# 120	0.125	47.5
# 170	0.090	43.2
# 200	0.075	40.9
USCS	SC	



Location : East Campus  
 Borehole : BH-2  
 Sample No : S-13 (Bottom)  
 Depth : 19.81-20.27 m

Sieve No.	Sieve Size (mm)	Passing %
# 10	2.000	97.3
# 30	0.600	96.2
# 40	0.425	90.3
# 60	0.250	67.9
# 100	0.150	41.7
# 120	0.125	33.2
# 170	0.090	26.0
# 200	0.075	22.8
USCS	SM	



Location : East Campus  
 Borehole : BH-2  
 Sample No : S-14  
 Depth : 21.33-21.79 m

Sieve No.	Sieve Size (mm)	Passing %
# 10	2.000	98.4
# 30	0.600	97.3
# 40	0.425	93.7
# 60	0.250	87.4
# 100	0.150	81.8
# 120	0.125	79.2
# 170	0.090	74.0
# 200	0.075	71.3
USCS	CL	

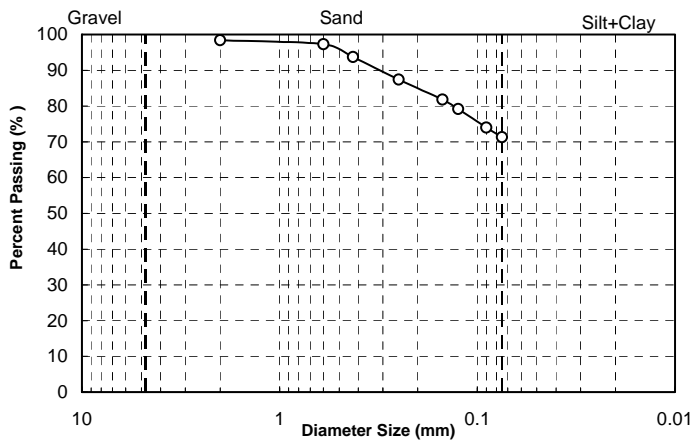


Figure A-9 Results of Gradation Analysis (Borehole BH-2, Continued)

## Grain Size Distribution

Location : East Campus  
 Borehole : BH-2  
 Sample No : S-15  
 Depth : 22.86-23.32 m

Sieve No.	Sieve Size (mm)	Passing %
# 10	2.000	98.8
# 30	0.600	94.6
# 40	0.425	83.1
# 60	0.250	64.4
# 100	0.150	54.4
# 120	0.125	51.4
# 170	0.090	47.6
# 200	0.075	45.9
USCS	SC	

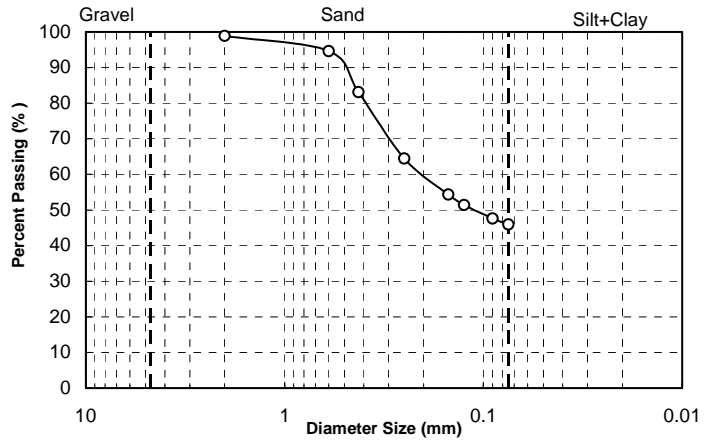


Figure A-10 Results of Gradation Analysis (Borehole BH-2, Continued)

## **APPENDIX B**

THIS PAGE LEFT BLANK

Table B.1 Summary of Soil Properties at Charter School Site

Sample No.	Depth (m)	Dry Density (kN/m <sup>3</sup> )	Moisture Content (%)	Cohesion (kN/m <sup>2</sup> )	Angle of Friction (Degree)	Penetration Resistance (Blows/ft)
SB 1-3	0.61	16.8	17.5			50/8"
SB 1-5	1.22	16.9	14.6			50/8"
SB 1-6	2.74	17.1	14.2			50/6"
SB 1-7	4.27					50/5"
SB 1-8	5.79	16.8	19.0			50/5"
SB 1-9	7.32					50/6"
SB 1-10	8.84					50/5"
SB 1-11	10.36	16.5	20.6			50/4"
SB 2-3	1.22	17.9	9.8			50/4"
SB 2-5	2.74					50/4"
SB 2-6	4.27	18.0	9.7			50/5"
SB 2-7	5.79					50/4"
SB 2-8	7.32	15.8	8.5			50/4"
SB 3-3	1.22					50/5"
SB 3-4	2.74	17.9	9.5			50/5"
SB 3-5	4.27					50/6"
SB 3-6	5.79	17.3	8.9			50/4"
SB 4-1	1.22	17.2	8.8			--
SB 5-1	0.61	19.0	10.0			50/4"
SB 5-2	4.27	16.7	18.6			50/5"
SB 5-3	5.79					50/5"
SB 5-4	7.32	16.2	18.5			50/4"
SB 6-1	1.22	18.1	9.9	40.7	31	--
SB 6-2	2.74	17.6	10.8	52.7	30	50/4"
SB 6-3	4.27					50/5"
SB 6-4	5.79	18.4	12.7			50/6"
SB 6-5	7.32					50/6"
SB 7-1	0.61	18.5	11.0			50/7"
SB 7-3	1.22	18.3	8.3			50/3"
SB 7-4	2.74					50/4"
SB 7-5	4.27					50/4"
SB 7-6	5.79	16.7	18.6			50/4"
SB 7-7	7.32					50/4"
SB 7-8	8.84	17.7	17.1			50/4"
SB 7-9	10.36					50/3"
SB 7-10	11.89	15.9	9.1			50/2.5"
SB 8-1	1.52	19.1	7.2			50/5"
SB 8-2	3.05					50/3"
SB 8-3	4.57	16.7	8.6			50/4"
SB 8-4	6.10					50/4"
SB 8-5	7.62					50/3"
SB 9-2	0.61	19.2	10.0			50/7"
SB 9-4	1.52	18.3	7.9			50/4"
SB 9-6	3.05					50/4"
SB 9-7	4.57	16.6	8.8			50/4"
SB 9-8	6.10					50/4"
SB 9-9	7.62	15.9	7.5			50/3"
SB 10-1	1.52	17.8	12.0			50/5.5"
SB 10-2	3.05					50/4"
SB 10-3	4.57	17.2	9.3			50/4"
SB 10-4	6.10					50/4"
SB 11-3	1.52					50/3.5"
SB 11-4	3.05					50/4"
SB 11-5	4.57					50/4"
SB 11-6	6.10					50/4"

Note: Extracted from GEOCON (1998). *Geotechnical Investigation–Charter School Site, University of California, San Diego, August 1998.*

Table B.2 Summary of Soil Properties at East Campus Utilities Plant Test Site

Sample No.	Depth (m)	Dry Density (kN/m <sup>3</sup> )	Moisture Content (%)	Cohesion (kN/m <sup>2</sup> )	Angle of Friction (Degree)	Penetration Resistance (Blows/ft)
1-3	1.52	17.0	6.6			50/3"
1-4	1.83	17.8	10.6	33.5	32	--
1-5	3.05	18.7	7.2			50/5"
1-7	4.57	14.6	11.6			50/5"
1-8	6.10	15.4	8.0			50/5"
1-9	7.62					50/6"
1-11	9.14	16.2	7.4			50/6"
3-1	0.00	16.9	5.5			50/3"
3-3	1.52	17.7	6.0			50/5"
3-5	3.05	16.7	9.3			78/10"
3-7	4.57	16.5	8.3			89/10"
3-8	6.10					50/5"
4-1	0.00	17.0	6.0	14.4	32	70
4-3	2.13	14.1	8.4			81/10"
4-5	3.05	15.4	6.6			50/6"
4-7	4.57	15.3	7.7			50/6"
4-8	6.10					50/6"
5-1	0.00	18.0	5.4			72/11"
5-3	2.13					88/9"
5-4	3.05	18.5	7.9			95/9"
5-6	4.57	16.9	--			50/6"
5-7	6.10					50/5"

Note: Extracted from GEOCON (2000). *Geotechnical Investigation–UCSD East Campus Utilities Plant, University of California*, November 2000.

## **APPENDIX C**

THIS PAGE LEFT BLANK

Table C.1 Summary of Soil Properties at UCSD Cancer Center Building Project

Sample No.	Depth (m)	Dry Density (kN/m <sup>3</sup> )	Moisture Content (%)	Cohesion (kN/m <sup>2</sup> )	Angle of Friction (Degree)	Penetration Resistance (Blows/ft)
B1-5	3.05					91/9"
B1-7	4.57					50/5"
B1-8	6.10	15.3	15.3			50/5"
B1-10	9.14	15.6	15.7			50/5"
B1-11	10.67	13.0	6.2			50/5"
B1-12	12.19					50/5"
B1-13	13.72	17.3	17.3			50/5"
B1-14	15.24	17.6	9.5	35.9	34	50/3"
B2-6	4.57					50/5"
B2-8	6.10					50/4"
B2-9	7.62	17.8	16.6			50/4"
B2-10	9.14	16.6	15.7	52.7	33	50/6"
B2-11	10.67	17.0	18.1			50/4"
B2-13	12.19	16.4	21.3			88/7"
B2-15	13.72					50/4"
B2-16	15.24	19.2	12.6			50/2"
B3-2	1.52					50/6"
B3-3	3.05					77/9"
B3-4	4.57					77/8"
B3-6	6.10	15.7	15.7			50/6"
B3-7	7.62	16.6	20.1			50/6"
B3-9	9.14					75/10"
B3-11	10.67	14.9	13.4			50/6"
B3-12	12.19	16.5	17.6			50/6"
B3-13	13.72	17.5	7.5			50/6"
B3-15	15.24					50/4"
B4-2	1.52					73
B4-4	3.05					50/4"
B4-6	4.57					64
B4-7	6.10	17.3	19.9			50/5"
B4-9	7.62					50/6"
B4-10	9.14					50/6"
B4-11	10.67	15.6	8.9			50/5"
B4-12	12.19	15.7	7.9			50/5"
B4-13	13.72					50/6"
B4-14	15.24	17.0	17.3			50/6"

Note: Extracted from GEOCON (2000). *Geotechnical Investigation–UCSD Cancer Center Building Project No. 3245, University of California, San Diego, October 2000.*

Table C.1 Summary of Soil Properties at UCSD Cancer Center Building Project (Cont'd)

Sample No.	Depth (m)	Dry Density (kN/m <sup>3</sup> )	Moisture Content (%)	Cohesion (kN/m <sup>2</sup> )	Angle of Friction (Degree)	Penetration Resistance (Blows/ft)
B5-3	3.05					68
B5-5	4.57	17.4	15.5			50/4"
B5-6	6.10	17.1	19			84/7"
B5-7	7.62					50/4"
B5-9	9.14	16.1	20			82/9"
B5-10	10.67	14.6	7.9			50/4
B5-11	12.19					50/5
B5-12	13.72	16.5	19.3			82/8"
B5-13	15.24					50/5"
B6-3	3.05					50/6"
B6-4	4.57					50/4"
B6-6	6.10	16.5	8.9			50/4"
B6-7	7.62	15.9	10.9			50/3"
B6-8	9.14	17.1	19.2			96/10"
B6-10	10.67	17.1	11.8			50/4"
B6-11	12.19	14.9	9.3			50/4"
B7-3	4.57					50/6"
B7-5	6.10	16.0	9.1			50/6"
B7-6	7.62	16.2	8.4			50/6"
B7-7	9.14					50/6"
B7-8	10.67	14.1	28.1			80/10"
B7-9	12.19	16.9	17.8			50/5"
B8-2	1.52					50/5"
B8-3	3.05					50/5"
B8-4	4.57					75/9"
B8-5	6.10	16.2	7.9			50/6"
B8-6	7.62	16.2	7.7			50/6"
B8-7	9.14					50/3"
B8-9	10.67	16.2	21.5			50/4"

Note: Extracted from GEOCON (2000). *Geotechnical Investigation–UCSD Cancer Center Building Project No. 3245, University of California, San Diego, October 2000.*

Table C.2 Summary of Soil Properties at UCSD EBU 3 and EBU 4 Site

Sample No.	Depth (m)	Dry Density (kN/m <sup>3</sup> )	Moisture Content (%)	Cohesion (kN/m <sup>2</sup> )	Angle of Friction (Degree)	Penetration Resistance (Blows/ft)
B1-3	3.05	16.5	17.9	50.3	33	91
B1-4	4.57	16.3	16.8			98
B1-5	6.10	16.8	20.0			100
B2-2	3.05	15.3	20.8			87
B2-3	4.57	15.7	19.3			100
B2-4	6.10	16.1	20.9	40.7	20	89
B2-5	7.62	17.2	17.3			100
B2-6	9.14					100
B3-2	3.05	16.1	18.0			100
B3-3	4.57	15.4	13.1			100
B3-4	6.10	15.2	15.1			100
B4-3	3.05	17.1	19.6			89
B4-4	4.57	16.0	19.0			87
B4-5	6.10					88
B4-6	7.62	16.9	18.2			80
B4-7	9.14	16.8	19.8			100
B5-3	3.05	16.1	21.3			100
B5-4	4.57	17.3	19.5			89
B5-5	12.19	16.0	18.6			100

Note: Extracted from GEOCON (2000). *Geotechnical Investigation–UCSD EBU 3A, 4A, 3B and 4B, University of California, San Diego, November 2000.*

Table C.3 Summary of Soil Properties at Gilman Drive Parking Structure Site

Sample No.	Depth (m)	Dry Density (kN/m <sup>3</sup> )	Moisture Content (%)	Cohesion (kN/m <sup>2</sup> )	Angle of Friction (Degree)	Penetration Resistance (Blows/ft)
B1-1	0.61	18.0	14.4			27
B1-2	1.52	15.1	23.8			37
B1-4	3.05	16.6	22.8			42
B1-5	4.57	16.2	21.4			52
B1-6	6.10	16.2	21.4			52/6"
B1-7	7.62	16.4	20.3			58/6"
B1-8	9.14					58/6"
B3-3	1.52	17.6	12.4			54
B3-4	3.05	17.2	11.2			73
B3-6	6.10	17.3	7.7			65/6"
B3-8	9.14					60/6"
B3-9	12.19					50/6"
B4-3	1.52	17.5	9.7			39
B4-5	3.05	17.4	11.5			97/10"
B4-7	6.10					53/6"

Note: Extracted from GEOCON (1998). *Geotechnical Investigation–Gilman Drive Parking Structure, University of California, San Diego, September 1998.*

## REFERENCES

- Alizadeh, M. (1969). "Lateral load tests on instrumented timber piles." *Performance of Deep Foundations, ASTM STP 444*, 379-394.
- Alizadeh, M., and Davisson, M. T. (1970). "Lateral load test on piles-Akansas river project." *J. Soil Mech. and Found. Div.*, ASCE, 96(5), 1583-1604.
- American Petroleum Institute (API) (1987). "Recommended practice for planning, designing, and constructing fixed offshore platforms." *API Recommended Practice 2A (RP-2A)*, 17<sup>th</sup> edn.
- Ashford, S. A., and Sitar, N. (1994). "Seismic response of steep natural slopes." *Report No. UCB/EERC-94/05*, College of Engineering, University of California, Berkley.
- Ashour, M., and Norris, G. (1998). "Lateral loading of a pile in layered soil using the strain wedge model." *J. Geotech. Engrg. Division*, ASCE, 124(4), 303-315.
- Ashour, M., and Norris, G. (2000). "Modeling lateral soil-pile response based on soil-pile interaction." *J. Geotech. Engrg. Division*, ASCE, 126(5), 420-428.
- ASTM Standard (1998), *Annual Book of ASTM Standards*, Vol. 04.09, West Conshohocken, PA, pp. 217-227.
- Banerjee, P. K., and Davies, T. G. (1978). "The behavior of axially and laterally loaded single pile embedded in non-homogeneous soils." *Geotechnique*, 21(3), 309-326.
- Banerjee, P. K., and Davies, T. G. (1979). "Analyses of some report case histories of laterally loaded pile groups." *Conf. Num. Methods in Offshore Piling*, I.C.E., London.
- Banerjee, S., Stanton, J. F., and Hawkins, N. M. (1987). "Seismic performance of precast concrete bridge piles." *J. of Structural Engineering*, ASCE, 113(2), 381-396.
- Barber, E. S. (1953). "Discussion to paper by S. M. Gleser." *ASTM, STP 154*, 94-101
- Bhushan, K., Lee, L. J., and Grime, D. B. (1981). "Lateral load tests on drilled pier in sand." *Preprint of the ASCE Annual Meeting*, St. Louis, Missouri, 114-131.
- Bowles, J. E. (1988). *Foundation Analysis and Design*. 4<sup>th</sup> Ed., McGraw-Hill, 1004 p.

- Bransby, M. F. (1999). "Selection of p-y curves for the design of single laterally loaded piles." *International Journal for Numerical and Analytical Methods in Geomechanics*, 23(15), 1909-1926.
- Brown, D. A., Shie, C. F., and Kumar, M. (1989). "p-y curves for laterally loaded piles derived from three dimensional finite element model." *Proc., 2<sup>nd</sup> Int. Symp., Numerical Models in Geomechanics, Niagra Falls, Canada*, New York, Elsevier Applied Sciences, 683-690.
- Budek, A. M. (1997). "The inelastic behavior of reinforced concrete piles and pile shaft," *UCSD Dissertation*, University of California, San Diego
- Budhu, M., and Davies, T. G. (1988). "Analysis of laterally loaded piles in soft clays." *Journal of Geotechnical Engineering*, 114 (1), 21-39.
- Caltrans (2000). *Caltrans Bridge Design Specifications*, State of California, Department of Transportation, July 2000.
- Carr, A. J. (1998). *RUAUMOKO Manual*. University of Canterbury, Dept. of Civ. Engrg., 225 p.
- Carter, D. P. (1984). "A non-linear soil model for predicting lateral pile response." *Report No. 359*, Civ. Engrg. Dept., University of Auckland, New Zealand.
- Chadwell, C. (1999). *UCFyber Cross Section Analysis Software for Structural Engineering*, Department of Civil and Environmental Engineering, University of California, Berkeley.
- Chai, Y. H., and Hutchinson, T. C. (1999). "Flexural strength and ductility of reinforced concrete bridge piles." Final Report to Caltrans for Contract Number 59Y500, *Report No. UCD-STR-99-2*, Dept. of Civil & Environmental Engineering, UC Davis, CA.
- Chopra, A.K. (1995). *Dynamics of Structures*. Prentice-Hall, Upper Saddle River, NJ, 729 p.
- Clough, G. W., Sitar, N., Bachus, R. C., and Rad, N. S. (1981). "Cemented sand under static loading." *J. Geotech. Engrg. Division*, ASCE, 107(6), 799-817.
- Cox, W. R., Reese, L. C., and Grubbs, B. R. (1974). "Field testing of laterally loaded piles in sand." *Proc. 6th Offshore Technology Conference, Paper 2079*, Houston, Texas, 459-472.

- Davies, T. G., and Budhu, M. (1986). "Non-linear analysis of laterally loaded piles in heavily overconsolidated clays." *Geotechnique*, 36, No.4, 527-538.
- Davisson, M. T., and Gill, H. L. (1963). "Laterally loaded piles in a layered soil." *J. Soil Mech. and Found. Div.*, ASCE, 89(3), 63-94.
- Davisson, M. T., and Salley, J. R. (1969). "Lateral load tests on drilled piers." *Performance of Deep Foundations, ASTM STP 444*, 68-83.
- Desai, C. S., and Appel, G. C. (1976). "3-D analysis of laterally loaded structures." *Proc., 2<sup>nd</sup> Int. Conf. on Numerical Methods in Geomechanics*, Blacksburg, ASCE, Vol. 1, 405-418.
- Dobry, R., and Gazetas, G. (1985). "Dynamic stiffness and damping of foundations by simple methods." *Vibration Problems in Geotechnical Engineering*, ed. G. Gazetas and E. T. Selig, ASCE, 77-107.
- Dordi, C. M., (1977). "Horizontally loaded piles in layered soils." *Proc. of Specialty Session 10, The Effect of Horizontal Loads on Piles due to Surcharge of Seismic Effects*, Ninth International Conference on Soil Mechanics and Foundation Engineering, Tokyo, 65-70.
- Dunnavant, T. W. (1986). "Experimental and analytical investigation of the behavior of single piles in overconsolidated clay subjected to cyclic lateral loads." *Ph.D. Dissertation*, University of Houston, Houston, Texas.
- Dunnavant, T. W., and O'Neill, M. W. (1985). "Performance analysis and interpretation of a lateral load test of a 72-inch-diameter bored pile in overconsolidated clay." *Report UHCE 85-4*, Dept. of Civ. Engrg., University of Houston, Texas, 57 p.
- Dunnavant, T. W., and O'Neill, M. W. (1989). "Experimental p-y curves model for submerged stiff clay." *J. Geotech. Engrg.*, ASCE, 115(1), 95-114.
- Elliot, W. J. (1988). *Geological Overview Investigation University of California, San Diego, East and West Campus, La Jolla, California*. dated May 20, 1988.
- Falconer, T. J., and Park, R. (1982). "Ductility of prestressed concrete piles under seismic loading." *Research Report No. 82-6*, Department of Civil Engineering, University of Canterbury, New Zealand.
- Gazetas, G. (1984). "Seismic response of end-bearing single piles." *Soil Dynamics and Earthquake Engrg.*, 3(2), 82-93.

- Gazetas, G. (1991). "Foundation vibrations." *Foundation Engineering Handbook* edited by Fang, H. Y., Second Edition, Van Nostrand Reinhold, New York, 553-593.
- GEOCON (1986). *Soil Investigation Report for UCSD – East Campus, San Diego, California*, dated February 1986.
- GEOCON (1998). *Geotechnical Investigation–Charter School Site, University of California, San Diego*, August 1998.
- GEOCON (1998). *Geotechnical Investigation–Gilman Drive Parking Structure, University of California, San Diego*, September 1998.
- GEOCON (2000). *Geotechnical Investigation–UCSD EBU 3A, 4A, 3B and 4B, University of California, San Diego*, November 2000.
- GEOCON (2000). *Geotechnical Investigation–UCSD East Campus Utilities Plant, University of California*, November 2000.
- GEOCON (2000). *Geotechnical Investigation–UCSD Cancer Center Building Project No. 3245, University of California, San Diego*, October 2000.
- Georgiadis, M. (1983). "Development of p-y curves for layered soils." *Proc. of the Conference on Geotechnical Practice in Offshore Engineering*, ASCE , 536-545
- Hetenyi, M. (1946). *Beams on Elastic Foundations*. University of Michigan Press, Ann Arbor, Michigan.
- Hsu, T. C. C. (1993). *Unified Theory of Reinforced Concrete*. CRC Press, Inc. Florida.
- Hudson, D. E. (1964). "Resonance testing of full-scale structures." *J. Engrg. Mech. Div.*, ASCE, 90(3), 1-19.
- Ikeda, S., Tsubaki, T., and Yamaguchi, T. (1982). "Ductility improvement of prestressed concrete piles." *Transaction of the Japan Concrete Institute*, vol. 4, 531-538.
- Ismael, N. F. (1990) "Behavior of laterally loaded bored piles in cemented sands." *J. Geotech. Engrg.*, ASCE, 116(11), 1678-1699.
- Janoyan, K., Stewart, J.P., and Wallace, J.W. (2001). "Analysis of p-y Curves from Lateral Load Test of Large Diameter Drilled Shaft in Stiff Clay." *Proceedings 6th Caltrans Workshop on Seismic Research*, Sacramento, CA.

- Khadilkar, B. S., Chandrasekaran, V. S., and Rizvi, I. A. (1973). "Analysis of laterally loaded piles in two-layered soils." *Proc. 8<sup>th</sup> International Conference on Soil Mechanics and Foundation Engineering*, Moscow, Vol. 21, 155-158.
- Kooijman, A. P. (1989). "Comparison of an elastoplastic quasi three-dimensional model for laterally loaded piled with field tests." *Proc. of the III International Symposium, Numerical Models in Geomechanics (NUMOG III)*, Niagara Falls, Canada, Elsevier Applied Science: New York: 675-682.
- Kuhlemeyer, R. L. (1979). "Static and dynamic laterally loaded floating piles." *J. Geotech. Engrg. Div.*, ASCE, 105(2), 289-304.
- Ling, L. F. (1988). "Back analysis of lateral load tests on piles." *Report No. 460*, Civ. Engrg. Dept., University of Auckland.
- Little, R. and Briaud, J. (1988). "Full-scale cyclic lateral load tests on six single piles in sand," *Research Report 5640 to the U.S. Army Engineer Waterways Experiment Station*, Texas A&M University, College Station.
- Long, J. H. and Reese, L. C. (1984). "Testing and analysis of two offshore piles subjected to lateral load." *Laterally Loaded Deep Foundations: Analysis and Performance*, ASTM SPT 835, Langer, J. A., Mosely, E. and Thompson, C. (eds). Philadelphia, 214-228.
- Matlock, H. (1970). "Correlations for design of laterally loaded piles in soft clay." *Proc., 2<sup>nd</sup> Annu. Offshore Technology Conf., Paper No. OTC 1204*, Houston, Texas, 577-594.
- Matlock, H. and Reese, L. C. (1960). "Generalized solutions for laterally loaded piles." *J. Soil Mech. and Found. Div.*, ASCE, 86(5), 63-91.
- McClelland, B., and Foch, J. A. Jr. (1958). "Soil modulus for laterally loaded piles," *Trans.*, ASCE, 123, 1049-1063.
- McNulty, J. F. (1956). "Thrust loading on piles." *J. Soil Mech. and Found. Div.*, ASCE, 82(2), paper 940, 1-25.
- Meyer, B. J., and Reese, L. C. (1979). "Analysis of single piles under lateral loading." *Research Report 244-1*, University of Texas at Austin, December 1979, 155 p.
- Meyerhof, G. G. (1956). "Penetration tests and bearing capacity of cohesionless soils." *J. Soil Mech. and Found. Div.*, ASCE, 82(1), 1-19.

- Mindlin, D. (1963). "Force at point in the interior of a semi-infinite solid," *Physics*, 7, 195-202
- Morison, C. S. (1986). "A lateral load test of a full-scale pile group in sand." *Thesis*, University Texas at Austin.
- Muguruma, H., Watanabe, F., and Nishiyama, M. (1987). "Improving the flexural ductility of pretensioned high strength spun concrete piles by lateral confining of concrete." *Proc. of the Pacific Conference on Earthquake Engineering*, vol. 1, Wairakei, New Zealand, 385-396.
- Naik, T. R., and Peyrot, A. (1976). "Analysis and design of laterally loaded piles and caissons in a layered soil system." *Methods of Structural Analysis, Proc. of the National Structural Engineering Conference*, ASCE, Madison, Wisconsin, Vol. II, 589-606.
- Naramore, S. A. and Feng, F. Y. (1990). "Field tests of large diameter drilled shafts part I-lateral loads." *Report No. FHWA/CA/SD-88/02*, California Department of Transportation.
- National Instrument Corporation (1998). *LabVIEW User Manual*, v. 5, Austin, Texas.
- O'Neill, M. W., and Dunnivant, T. W. (1984). "A study of effect of scale, velocity, and cyclic degradability on laterally loaded single piles in overconsolidated clay." *Report UHCE 84-7*, Dept. of Civ. Engrg., University of Houston, Texas, 368 p.
- O'Neill, M. W., and Murchison, J. M. (1983). "An evaluation of p-y relationships in sands." A report to the American Petroleum Institute." *PRAC 82-41-1*, University of Houston, Texas.
- Pam, H. J., Park, R., and Priestley, M. J. N. (1988). "Seismic performance of prestressed concrete piles and pile-pile cap connection." *Research Report 88-3*, Department of Civil Engineering, University of Canterbury, New Zealand.
- Peck, R. B, Hanson, W. E., and Thornburn, T. H. (1974). *Foundation Engineering*, 2<sup>nd</sup> Ed., John Wiley and Sons, New York.
- Pender, M. J. (1993). "Aseismic pile foundation design analysis." *Bull. NZ Nat. Soc. for Earthquake Engrg.*, 49-160.
- Poulos, H. G. (1971). "Behavior of laterally loaded piles: I – single piles," *J. Soil Mech. and Found. Div.*, ASCE, 97(5), 771-731.

- Poulos, H. G. (1973). "Analysis of piles in soil undergoing lateral movement," *J. Soil Mech. and Found. Div.*, ASCE, 99(5), 391-406.
- Poulos, H. G., and Davis, E. H. (1980). *Pile Foundation Analysis and Design*. John Wiley, New York.
- Poulos, H. G., and Hull, T. S. (1989). "The role of analytical mechanics in foundation engineering." *Found. Engrg., Current Principals and Practices*, ASCE 2, 1578-1606.
- Priestley, M. J. N., Seible, F., and Calvi, G. M. (1996). *Seismic Design and Retrofit of Bridges*, John Wiley&Sons, Inc., New York.
- Randolph, M. F. (1981). "The response of flexible piles to lateral loading." *Geotechnique*, 31(2), 247-259.
- Reese, L. C., Cox, W. R., and Koop, F. D. (1974). "Analysis of laterally loaded piles in sand," *Proc. 6th Offshore Technology Conference, Paper 2080*, Houston, Texas, 473-483.
- Reese, L. C., Cox, W. R. and Koop, F. D. (1975). "Field testing and analysis of laterally loaded piles in stiff clay." *Proc., 7th Offshore Technology Conf., Paper No. OTC 2321*, Houston, Texas, 671-690.
- Reese, L. C., and Matlock, H. (1956). "Nondimensional solutions for laterally loaded piles with soil modulus assumed proportional to depth." *Proc. of the VIII Texas Conference on Soil Mechanics and Foundation Engineering*, University of Texas, Austin.
- Reese, L. C., and Van Impe, W. F. (2001). *Single Piles and Pile Group under Lateral Loading*. A. A. Balkema, Rotterdam, 463 p.
- Reese, L.C., Wang, S. T., Isenhower, W. M., and Arrellaga, J. A. (2000). *Computer Program LPILE Plus Version 4.0 Technical Manual*, Ensoft, Inc., Austin, Texas.
- Reese, L. C., and Welch, R. C. (1975). "Lateral loading of deep foundation in stiff clay." *J. Geotech. Engrg. Div.*, ASCE, 101(7), 633-649.
- Saxena, S. K., and Lastrico, M. (1978). "Static properties of lightly cemented sand." *J. Geotech. Engrg. Div.*, ASCE, 104(12), 1449-1465.
- Sitar, N. (1990). "Seismic response of steep slopes in weakly cemented sands and gravels." *Proceedings, H. Bolton Seed Memorial Symposium*, Vol. II, 67-82.

- Spillers, W. R., and Stoll, R. D. (1964). "Lateral response of piles." *J. Soil Mech. and Found. Div.*, ASCE, 90(6), 1-9.
- Stevens, J. B., and Audibert, J. M. E. (1979). "Re-examination of p-y curve formulation." *Proc. Of the XI Annual Offshore Technology Conference*, Houston, Texas, OTC 3402, 397-403.
- Taylor, R. L. (1998). *FEAP—A Finite Element Analysis Program Version 7.1*, Department of Civil and Environmental Engineering, University of California at Berkeley.
- Terzaghi, K. (1955). "Evaluation of coefficients of subgrade reaction." *Geotechnique*, 5(4), 297-326.
- Trochanis, A. M., Bielak, J., and Christiano, P. (1991). "Simple model for analysis of one or two piles, *J. Geotech. Engrg.*, ASCE, 117 (3), 448-466.
- Tucker, L. M., and Briaud, J. (1988). "Analysis of the pile load test program and dam 26 replacement project." *Research Report 4690F*, Texas A&M University, College Station.
- University of Florida (1996). *User's Manual for FLORIDA-PIER Program*, Dept. of Civil Engineering, University of Florida, Gainesville.
- Van Laak, P., and Elgamal, A.-W. (1991). "RPI eccentric mass in-situ shaker." *Tech Rep.*, Department of Civil Engineering, Rensselaer Polytechnic Institute, Troy, N.Y.
- Vesic, A. S. (1961). "Beam on elastic subgrade and the Winkler hypothesis." *Proc., 5<sup>th</sup> Int. Conf. Soil Mech. and Found. Engrg.*, Paris, Vol. 1, 845-850.
- Wang, S. and Reese, L. C. (1993). "COM624P-Laterally loaded pile analysis program for the microcomputer, version 2.0." *FHWA-SA-91-048*, U.S. DOT, Federal Highway Administration.
- Welch, R. C., and Reese, L. C. (1972). "Laterally loaded behavior of drilled shafts." *Research Report 3-5-65-89*, Center for Highway Research, University of Texas, Austin.
- Winicki, L. A., and Zienkiewicz, O. C. (1979). "Plastic (or visco-plastic) behavior of axisymmetric bodies subjected to non-symmetric loading – semi-analytical finite element solution3" *Int. J. Numerical Methods in Engrg.*, Vol. 14, 1399-1412.

Winkler, E. (1867). "Die lehre von elasticzitat and festigkeit (on elasticity and fixity)."  
*Prague*, 182 p.

Wolf, J. P. (1985). *Dynamic Soil-Structure Interaction*. Prentice-Hall, Englewood Cliffs,  
N.J., 466 p.

THIS PAGE LEFT BLANK